RHEINISCHE FRIEDRICH–WILHELMS–UNIVERSITÄT
BONN

Stellar populations in gravitationally bound systems

Dissertation

zur

Erlangung des Doktorgrades (*Dr. rer. nat.*)

der

Rheinischen Friedrich–Wilhelms–Universität, Bonn

vorgelegt von
Tereza JEŘÁBKOVÁ
aus
Prag, Tschechien

Bonn 2020

Angefertigt mit Genehmigung der Mathematisch-Naturwissenschaftlichen Fakultät
der Rheinischen Friedrich–Wilhelms–Universität Bonn

1. Referent: Prof. Dr. Pavel Kroupa
2. Referent: Prof. Dr. Karl Menten
Tag der Promotion: 12.08.2020
Erscheinungsjahr: 2020

RHEINISCHE FRIEDRICH–WILHELMS–UNIVERSITÄT BONN

Abstract

by Tereza Jerabkova

for the degree of

Doctor rerum naturalium

The understanding of how, which, where and when stars form provides important information for the vast majority of astronomical fields. Star-formation has a complex multi-scale physical nature. Stars form in dense sub-parsec regions of molecular clouds, and since the very early stages of their life, their destiny is linked to the complex interplay between magneto-hydro-radiation-transfe-dynamics, stellar evolution and stellar dynamics. At the same time, star-forming regions are inevitably coupled to the galactic gravitational potential and as such are affected by tides and shears. This poses a computational challenge for theoretical investigations pushing technical feasibility to its limit in terms of computational time and the required spatial resolution. Nowadays, front-end facilities allow us to obtain detailed observations of nearby (up to 500pc from the Sun) star-forming regions. While such regions allow us to sample near-to-uniform environmental conditions in terms of cloud density, mass and metallicity, they do not allow us to investigate how star formation proceeds in the full range of diverse environmental conditions that can be found in local galaxies and at all redshifts where the stellar population cannot be resolved. Thus, despite a large and fruitful community effort in this field, we are still lacking a complete and coherent picture of how stars and star-clusters form.

This thesis investigates the physics of star-formation and stellar populations combining theoretical modeling with observations on multiple scales from resolved star-forming regions in the Milky Way through to stellar populations in galaxies reaching to cosmic star-formation. The discovery, my confirmation and theoretical explanation of the existence of three stellar populations in the Orion Nebula Cluster is a clear example of the impact and crucial role played by the stellar dynamics on star and star-cluster formation. Furthermore, the thesis presents the discovery, made possible with the advent of the Gaia space mission, of large scale co-eval filaments of star formation, a new fact posing novel viable constraints for theories of star-formation. Individual star-forming regions (in molecular cloud cores forming at least a few binary stellar systems) are used as building blocks of galaxy-wide stellar populations using the Integrated Galactic Initial Mass Function (IGIMF) theory. The publicly availible code, GalIMF, has been co-developed within this thesis to synthesise stellar populations of whole galaxies. This allowed me to compute, for the first time, a large grid of the empirically driven variable galaxy-wide stellar initial mass function for direct comparison with observations. This model and the associated code were

used, for example, to construct the cosmic star-formation history with a variable stellar-initial mass function.

The research presented in this thesis was published in four refereed publications led by its author and six refereed publications to which the author provided signicantly. This thesis as a whole presents a multi-scale and multi-technique contribution to star-formation and stellar populations and opens novel and original routes for future research.

RHEINISCHE FRIEDRICH–WILHELMS–UNIVERSITÄT BONN

Abstrakt

von Tereza Jerabkova

für den Grad von

Doctor rerum naturalium

Das Verständnis, wie, welche, wo und wann sich Sterne bilden, liefert wichtige Informationen für die überwiegende Mehrheit der astronomischen Forschungsfelder. Die Sternentstehung hat eine komplexe physikalische Natur auf mehreren Ebenen. Sterne bilden sich in dichten Sub-Parsec-Regionen in Molekülwolken, und ihr Schicksal ist, seit den sehr frühen Stadien ihres Lebens, verbunden mit dem komplexen Zusammenspiel von Sternentwicklung, Sternendynamik, Magneto-hydro-dynamik und Strahlentransport. Gleichzeitig sind sternbildende Regionen zwangsläufig gekoppelt zum galaktischen Gravitationspotential und werden als solches von Gezeiten und Scheren beeinflusst. Dieses stellt eine rechnerische Herausforderung für theoretische und numersische Untersuchungen dar. Modernste Einrichtungen ermöglichen es heutzutage, detaillierte Beobachtungen von nahe gelegenen (bis zu 500 pc entfernte) Sternentstehungsregionen zu erhalten. Solche Regionen erlauben es uns, nahezu einheitliche Umweltbedingungen in Bezug auf Wolkendichte, Masse und Metallizität zu untersuchen. Aber, sie erlauben es uns nicht zu untersuchen, wie die Sternentstehung in sehr abweichenden Bereichen abläuft, also unter physikalischen Bedingungen, die in lokalen Galaxien und bei allen Rotverschiebungen zu finden sind. Trotz großer und fruchtbarer Gemeinschaftsanstrengungen auf diesem Gebiet fehlt immer noch ein vollständiges und kohärentes Bild davon, wie sich Sterne und Sternhaufen bilden.

Diese Arbeit untersucht die Physik der Sternentstehung. Sie kombiniert die theoretische Modellierung mit Beobachtungen auf mehreren Skalen in der Milchstraße und in anderen Galaxien, bis hin zur kosmischen Sternentstehung. Die Entdeckung, Bestätigung und theoretische Erklärung der Existenz von drei Stern-Populationen im Orionnebel-Haufen sind ein klares Beispiel für die Auswirkungen der Stellardynamik bei der Stern- und Sternhaufenbildung. Darüber hinaus präsentiert diese Arbeit die Entdeckung, welche Anhand der Gaia Daten möglich wurde, von großflächigen und gleichaltrigen Filamenten der Sternentstehung. Dieses wirft wichtige Fragen für die Sternentstehung auf.

Einzelne sternbildende Regionen werden als Bausteine für galaxienweite Sternpopulationen benutzt unter Verwendung der IGIMF-Theorie (der "Integrated Galactic Initial Mass Function" Theorie). Das öffentlich verfügbare Computerprogramm, GalIMF, wurde in dieser Arbeit mitentwickelt. Dieses Programm ermöglicht es erstmals, ein großes Raster von Simulationen zu berechnen, mit einer empirisch gesteuerten variablen galaxienweiten stellaren Anfangsmassenfunktion, die direkt mit Beobachtungen vergleichbar sind. Dieses Modell und

das zugehörige Programm wurde beispielsweise verwendet, um die kosmische Sternentstehungsgeschichte mit einer variablen Stern-Anfangsmassenfunktion zu konstruieren.

Die in dieser Arbeit vorgestellten Forschungsergebnisse wurden veröffentlich in vier referierten Erstauthorpublikationen und in sechs referierten Veröffentlichungen, zu denen der Autor einen wichtigen Beitrag geleistet hat. Diese Arbeit als Ganzes präsentiert einen mehrskaligen und multitechnischen Beitrag zur Sternentstehung und zu Sternpopulationen und eröffnet neue und originelle Wege für die zukünftige Forschung.

Dark is the night without stars above
No matter why they're not there
Dark would be the world without love
And without those who dare

The author

To all those who dare ...

Acknowledgements

I would like to express my sincere special appreciation to my supervisor, Prof. Dr. Pavel Kroupa, without who's support, motivation, guidance and the tremendous amount of time spend correcting my texts and discussing science, this thesis could not have been written. I wish to show my gratitude to my second thesis supervisor, Prof. Dr. Karl Menten. I am thankful for useful discussion and a number of inspiring references, for interesting comments and suggestions.

While spending two years of my PhD at European Southern Observatory in Garching I whole-heartedly appreciated the support and mentoring through my ESO supervisor Dr. Giacomo Beccari. That has been very important for the success of this thesis and my scientific development. I would like to extend this gratitude to ESO's Dr. Henri J. Boffin, who read more than enough of my paper drafts and proposals - I value our collaboration greatly. I am also grateful to Dr. Eric Emsellem for all the support and interesting interactions and also for the exciting opportunity to learn more about the MUSE instrument while being part of a spontaneous collaboration. I wish to thank to my fellow mentor Dr. Carlo F. Manara and to show my gratitude to Prof. Dr Glenn van de Ven for motivation and inspiring discussions. I would like to recognize the constant optimism, presence of and the many discussions with Dr. Michael Hilker, and also thank to all of the others that contributed to making ESO such a lively place.

I would like to pay my special regards to Dr. Alexandre Vazdekis: thank you for the large number of all-day long fruitful discussions and always positive and motivating attitude. My thanks also belong to all the staff at the GRANTECAN telescope, especially to Dr. Antonio L. Cabrera Lavers and to Dr. Stefan Geier. I wish to thank Dr. David Jones for all the help with my stay at La Palma.

I would like to express my immense gratitude to Dr. Petr Kabath, for all the possibilities that he's provided for me during my carer, without which I might not even have started my PhD in the first place. I am indebted to Moritz Haslbauer for investing lots of his personal time to help me conquering formal aspects of PhD thesis submission and also to Prof. Dr. Simon Stellmer and Prof. Dr. Hubert Shorle for being part of my thesis committee.

Last but not least I wish to thank to all the people I haven't named, the always smiling guards at the entrances to the institutes that always lifted my spirit, Mama Lauda at Jocky's Treff in Garching, my always understanding family and friends all over the world, joke-making bus drivers, El cafe de don Manuel in La Palma and all of my amazing collaborators, that have been always encouraging me. Without you and without my dog Mistr this would have been way harder if even possible.

Outside, the Sun shines over empty streets void of their usual crowds and adorns the colors of the houses in the hills, occasionally the wind blows and clouds pass by in an aeroplane-free sky. An ordinary day? It has been like this for more than three weeks. An ordinary day.

Thank you, La Palma, the island with volcanoes, smiles, bananas and telescopes - it has been a great pleasure and privilege to be finishing my thesis here.

Contents

Chapter 1

Star-formation and stellar populations as a central research problem

"Stars are the 'atoms' of the Universe, and the problem of how stars form is at the nexus of much of the contemporary astrophysics" (McKee and Ostriker, 2007).
Indeed, what stars form, whether massive or not, and how many of them – that is in principle the stellar initial mass function (IMF) and its normalisation – affects the majority of astronomical fields. It sets the cosmic baryonic cycle, the production of chemical elements in the Universe, it affects the formation and evolution of galaxies and is important also on the smallest scales of the formation of planets and dust. Star-formation is a complex physical problem exhibiting itself on multiple scales, from sub-parsec dense regions of molecular clouds (MC) to cosmic volumes spanning 12 orders magnitude in spacial scales ($10^{11} - 10^{23}$cm, $\approx 10^{-8} - 10^{4}$pc) (Shu, Adams, and Lizano, 1987). Shu, Adams, and Lizano (1987) also point out that star-formation processes span over a similar range of magnitudes in mass, ranging from $10^{-1}\,M_{\odot}$ to $10^{11}\,M_{\odot}$.

As a consequence, studies that have been focusing on how stars form usually restrict themselves on a particular scale or introduce clear scale divisions. For example the paramount review on star-formation by Shu, Adams, and Lizano (1987) discussed mainly star-formation processes on molecular cloud scales. Another example can be found in the newer review by McKee and Ostriker (2007), in which the authors introduce a scale division in the form of "microphysics" and "macrophysics" of star-formation. In their definition the macrophysics of star-formation describes formation from star-clusters to galaxies and microphysics aims to understand the formation of individual and binary stars. They also outline several open questions, some of which are already raised by Shu, Adams, and Lizano (1987). The fact that a number of the questions put forward more than three decades back are still actively discussed today only demonstrates how difficult it is to understand how stars form.

Let me lay out several of these still standing research questions that are among the most relevant for this thesis, and possibly in general as well.
What are the initial conditions of star-formation and how do proto-stars accreate their mass? Do massive stars form with different initial conditions than low mass stars? Is the formation of stars and of star clusters affected by the properties of their birth environment such as the metallicity or mass density?
Along the same lines, let me share a question raised by Phil Myers: *"How does nature make hundreds of stars in an area smaller than one parsec in one million years with stellar masses following the IMF from a complex network of filaments, clumps and*

cores?" [Phil Myers' talk [1], VLMS Conference, October 2011]
These questions are directly addressing the microphysics of star-formation. However, stars are not isolated objects in the Universe, they are part of galaxies and are inevitably coupled to the larger scales of star-forming regions and galaxies as such. *What is the role of tides and shears driven by the galactic gravitational potential? How different is star-formation in the Milky Way relative to other distant galaxies?*

McKee and Ostriker (2007) compare their review to the classical review of Shu, Adams, and Lizano (1987) and point out that much changed in the 20 years of research in the field of star-formation. Perhaps one of the main advances they mention is the increase of knowledge on turbulence in the interstellar medium and its effect on the macrophysics of star-formation. Interestingly, Elmegreen and Scalo (2004) pointed out that a viable theory describing interstellar matter (ISM), that is a description similar to what is believed today, was outlined already by von Weizsäcker (1951). In that work it is proposed that the ISM is described as cloudy objects that exhibit a hierarchical structure due to shock waves interactions triggered by large scale supersonic turbulence fed by differential galactic rotation and dissipating on small scales due to viscosity. Turbulence is a physical term originating in fluid dynamics addressing the non-laminar regime of a fluid flow that results in non-linearities on spatial and temporal scales. Turbulence presents some difficulties in mathematical/physical terms and it does not posses enough degrees of freedom to be treated as a statistical ensemble (Elmegreen and Scalo, 2004). While it is possible to study turbulent flows in hydrodynamical fluids in laboratories, the ISM exhibits very different physical parameters and can also be self-gravitating. One of the key evidences manifesting that molecular clouds are turbulent is an analysis done by Larson (1981). The author presents data for 54 molecular clouds, the measurements revealing them to be essentially gravitationally bound, and shows that velocity dispersion vs. size follows a power-law relation. This is a similar relation to the Kolmogoroff law for subsonic turbulence. The observations done by the Infrared Astronomical Satellite (IRAS) exploring interstellar "cirruses" and dark clouds revealed their internal complexity (not accessible in visible wavelengths) and motivated a large body of research in astronomy dedicated to the turbulence of the ISM (McKee and Ostriker, 2007).

Now it is 2020, that is 12 years since the review of McKee and Ostriker (2007). If I am to highlight the biggest advance in the field, then it's unambiguously the establishment of star-formation in filaments. While most stars form in molecular cloud over-densities (containing at least a few stars), thus in embedded star clusters (Lada and Lada, 2003), the filamentary structure of molecular clouds is an important newly recognised aspect of the process (André, Di Francesco, Ward-Thompson, Inutsuka, Pudritz, and Pineda, 2014).

Filaments in molecular clouds have been indicated by optical images almost a hundred a years ago (Barnard, 1927; Lynds, 1962, e.g.), and one of the first studies discussing the formation and fragmentation of these structures was published by Schneider and Elmegreen (1979). The authors use Palomar Observatory Sky Survey and Whiteoak extension data together with additional literature sources to investigate visible dust clouds. They describe that these clouds show elongated structures and signs

[1] link:https://www.eso.org/sci/meetings/2011/vlms2011/talks/Myers.pdf

of integral fragmentation into globule-like beads. Schneider and Elmegreen (1979) introduced the name globular filaments. In the same publication it is argued that the globular filaments are indeed filaments and not flattened sheets created by differential Galactic acceleration as suggested by Disney and Hopper (1975). The main arguments are that the observed orientations of the filaments is not always parallel to the Galactic plane as implied by Disney and Hopper (1975) and the physical properties of observed filaments (small sizes, large densities) not being susceptible to the effect of galactic tides. Zinnecker (1991) suggests that filamentary geometry may play a key role in the fragmentation process and elaborates this in detail for the case of the formation of low-mass T Tauri binary stars. Myers (2009) wrote that "*star-forming clouds have long been known to be 'filamentary'*" and notices a new feature of multiple filaments radially emerging from a central hub that has a larger density. It is also noted that more active star-forming regions tend to have more hubs with on average larger densities – this is the first mentioning of the frequent modern association of young stellar groups/clusters with dense hubs.

A revolution in this field came with ESA's[2] *Herschel* satellite, which is emphasized by a comprehensive review of André, Di Francesco, Ward-Thompson, Inutsuka, Pudritz, and Pineda (2014). The authors not only review observational efforts in the field of star-formation in filaments, but also theoretical and computational endeavors in the field. The conclusions are formulated as a question, *"Toward a new paradigm for star formation?"*, and present a scenario according to which prestellar cores form in two steps. The first step is the formation of filaments in molecular clouds, possibly driven by dissipation of kinetic energy in large-scale MHD flows. The role of turbulence on these scales is not clear, but could contribute to the process. As a second step, the 0.1 pc wide filaments fragment into individual prestellar cores as they are dense enough and gravitationally unstable.

The next significant contribution on this topic came from (sub)mm observations (e.g. IRAM, APEX, ALMA). Highlighting the ALMA/IRAM study by Hacar, Tafalla, Forbrich, et al. (2018) they were being able to resolve structures in molecular clouds on 0.009pc scales. Their study reveals internal substructures within the massive filament located in the Orion star-forming region. These structures are called fibers, they are spatially organized and form dense bundles with multiple hub-like associations. Interestingly, the authors noticed that there is a significant increase of the surface number density of fibers as a function of the total mass per-unit-lenght in filamentary clouds and identify this as a difference between low and high mass star-formation. Plunkett, Fernández-López, Arce, Busquet, Mardones, and Dunham (2018) used ALMA to study young star-forming regions and found evidence for primordial mass segregation, pre-stellar object clustering and the concentration of the higher-mass sources near to the dense gas at the cluster center as previously reported (Kirk and Myers, 2011). These findings are in line with the above findings of Hacar, Tafalla, Forbrich, et al. (2018) as well as the ALMA study done by Joncour, Duchêne, Moraux and, and Motte (2018) that found stellar NESTs[3]/clusterings located at intersections of filaments. Larger scales (up to several hundred parsecs) have been explored within the

[2]European Space Agency
[3]NEST stands for Nested Elementary STructures

APEX/ATLASGAL survey (Li, Wyrowski, Menten, and Belloche, 2013; Li, Urquhart, Leurini, et al., 2016; Gong, Li, Mao, et al., 2018) showing that gaseous filaments can span up to such lengths. Similar structures are also visible in nearby galaxies thanks to the Spitzer Space Telescope (Elmegreen, Elmegreen, and Efremov, 2018; Elmegreen and Elmegreen, 2019).

Retrospectively, the filamentary structures of molecular clouds and the fact that stars form in these filaments, were not predicted by any theory of star-formation. It is an observation-driven advancement of the field and as such it questions the predictive power of our present theoretical investigations. *Did astronomy/astrophysics and our current knowledge become too complex for us to be able to provide theoretical predictions? If this is the case, are we dependent on observations and new/bigger telescopes in order to advance?* This might well be the case, as for example the thorough review on massive star formation by Zinnecker and Yorke (2007) emphasise the importance of future observations in order to learn more about how massive stars form, see their Chapter 8.

In the above paragraphs two pillar topics in the theory of star-formation and stellar populations are mentioned - the presence of turbulence in the ISM and the filamentary structure of molecular clouds. Interestingly, both turbulence and filamentary structures have been suggested decades before they became widely studied in the astronomical community. There is still long a way to go in order to understand the interplay between turbulence and filaments in molecular clouds and many open questions remain to be answered. One of the perhaps most important ones is the concept and origin of the initial mass function (IMF) of stars, already mentioned in the text above. As the stellar IMF is also the scope of several chapters in this thesis the next section is devoted to this topic.

1.1 The stellar initial mass function as a needed theoretical concept

The stellar initial mass function, $\xi(m)$, is the number of stars, $\mathrm{d}N$, (born) in the mass interval m, $m + \mathrm{d}m$. It is often written as

$$\frac{\mathrm{d}N}{\mathrm{d}m} = \xi(m)\,. \tag{1.1}$$

Before describing the importance of the stellar IMF for stellar populations and star-formation, let's mention some of its historical context. The stellar IMF as such has been established by Salpeter (1955), in a just seven-page long paper titled "The Luminosity Function and Stellar Evolution". Salpeter connected quantum mechanics with stellar astronomy and used the new (at that time) physics of nuclear processes in stars (e.g. the Bethe-Salpeter equation). The concept, that has just been understood in the 1950's, of stars forming, evolving and dying is applied. Salpeter used the observed luminosity function of stars in the Solar neighborhood and applied and estimated luminosity-stellar mas relation to construct the present day mass function of stars on the main sequence. However, since he realized that stars evolve and die, Salpeter provided statistical corrections for the stars already evolved away from the main sequence. This

resulted in the first formulation of the stellar initial mass function (IMF) *and* the concept of an IMF being formulated as a statistical distribution function as this was the only way how to provide estimates of already evolved stars in the old Galactic population. *From today's perspective this scientific contribution presents an immense jump forward for astrophysics. It bridges together different scientific fields and provides a result still in use today. If Edwin Salpeter would not have written this paper, a large fraction of modern astrophysics could not have been done.*

At this moment, it's time to get back to the question, why the stellar IMF presents a basic concept in star-formation and stellar populations? It is because we can only learn a certain amount of information about the Universe/star clusters/galaxies from observations and the stellar IMF allows us to explore beyond these limitations. The main limitations are: 1) With a given observational technique one can only observe a certain mass range of stars (often only indirectly via integrated light), especially for distant galaxies. One example is the emission in Balmer lines in star-forming galaxies due to ionizing radiation from young massive stars – this observation provides constraints on the massive stars, and it's difficult to constrain the associated lower stellar mass content. Another example are absorption features present in spectra of old elliptical galaxies emitted by low mass stars (with masses bellow a Solar mass). In this case only the stellar mass of stars within this mass range can be constrained. *We need to use the stellar IMF to estimate the total mass in all stars, assuming their mass distribution follows a stellar IMF.* 2) Stars evolve with time, on a time-scales from only few Myr for the most massive ones, to the age of the Universe itself for the sub-solar stars. *We use the stellar IMF to infer what stars formed initially, since we can only observed the stellar population when it is already evolved. These are concepts according which stellar IMF was first formulated by Salpeter (1955).*

In order to explore the baryonic cycle, star-formation rate or total baryonic mass, we need the stellar IMF to correct for stars we cannot see and stars that already evolved. Thus, while star-formation is a central astrophysical research problem, the stellar IMF is without any doubt it's necessary ingredient.

Since the importance of the stellar IMF has been clearly stated just above, it needs to be mentioned that the stellar IMF doest not exist in nature, as pointed out in the review by Kroupa, Weidner, Pflamm-Altenburg, et al. (2013). In order for the stellar IMF to be observable, all stars would have to form in an infinitesimally small time interval. However, this is not the case in the Universe and therefore it is not possible to actually empirically measure the stellar IMF. The stellar IMF is thus a mathematical construct, but a very useful and needed one, allowing us to model stellar populations and interpret observations.

While the definition introduced by Salpeter (1955), see eq. (1.1), has been kept, the stellar IMF has changed since then as shown in Fig. 1.1. The Salpeter IMF was updated for a larger magnitude range, taking into account more processes, such as stellar brightening during main-sequence evolution, the changing disk scale height with stellar age and also improved stellar mass-luminosity data by Miller and Scalo (1979). Zinnecker (1984) suggests a Monte Carlo model of star-formation accounting for the Miller and Scalo (1979) IMF shape while providing testable predictions, as any theory/model should, on black dwarf IMF and frequency distribution of the orbital periods of binary stars. Later Scalo (1986) used a better constrained luminosity function newly account-

ing for a dip around $M_V = 7$, see upper left panel of Fig. 1.1. Further advances came with the work that included unresolved multiple stars, Lutz–Kelker and Malmquist biases and pre-main-sequence dimming and main-sequence brightening (Kroupa, Tout, and Gilmore, 1993). Remarkably, it was shown that the subtle features in the stellar luminosity function have physical justification and are driven by a convective structure within late-type stars (Kroupa, Tout, and Gilmore, 1990). In 1991 they, for the first time, accounted for unresolved multiple-stars (Kroupa, Tout, and Gilmore, 1991). This combined together with the results of Massey, Johnson, and Degioia-Eastwood (1995) led to the formulation of the canonical IMF by Kroupa (2001),

$$\xi(m_\star) = \begin{cases} k_1 m^{-1.3} & 0.08 \leq m_\star/M_\odot < 1.0\,, \\ k_2 m^{-2.3} & 1.00 \leq m_\star/M_\odot \leq 120\,. \end{cases} \tag{1.2}$$

This formulation is considered being a benchmark IMF describing initial stellar population in MW star-forming regions. The canonical IMF is essentially indistinguishable from the later reformulation of the IMF as a log-normal function for low-mass stars (Chabrier, 2003).

Since the shape of the stellar IMF in the Solar neighborhood has been well established (Kroupa, 2001; Chabrier, 2003), the field has shifted to discuss the dependence of the stellar IMF on the environment. In addition, questions revising the original assumption by Salpeter (1955) making the stellar IMF a probability density function have been arising. *A point to emphasize, if the stellar IMF is a universal probability density function then it is scale and environment independent. However, if it is not universal and/or a probability density function then its definition and usage must take into account spatial and time dimensions (Kroupa and Jerabkova, 2018).*

Let me take, once again, a historical perspective on how the research evolved. The observational results in the early 1990's that the nearby pre-main sequence populations of stars have a significantly higher binary fraction than the Galactic field population observed around the Sun prompted Kroupa (1995a) and Kroupa (1995b) to suggest that most stars form as binary systems in (embedded) clusters. The notion that star formation takes place in the dense molecular cloud cores as groups of stars, i.e. in embedded clusters, which emerge from the cloud through dispersal of the remnant gas and therewith build-up the Galactic field population, allowed Kroupa (2002b) to show, by integrating over all recently formed embedded clusters, that the Galactic disk thickness may be related to the SFR of the Galaxy thereby suggesting a novel origin of the thick Galactic disk. This concept of using embedded clusters as the fundamental building blocks for a galaxy (Kroupa, 2005) was further developed by Kroupa and Weidner (2003b) who demonstrated that the galaxy-wide IMF is not the same as the IMF in embedded clusters, even if the latter is invariant. This led to the establishment of the integrated-galaxy-wide IMF (IGIMF) theory and to the first formulation of the SFR-dependent IGIMF by Weidner and Kroupa (2005). The different degree of dynamical processing of binary populations in embedded clusters of different masses (low-mass embedded cluster leaving the initial binary population largely unchanged, while massive embedded clusters destroy a large fraction of the initial binary population) allowed Marks and Kroupa (2011) to synthesise galactic-field binary populations by integrating over all embedded clusters recently formed, with the prediction that dwarf irregular and massive elliptical galaxies should have a high and small field binary

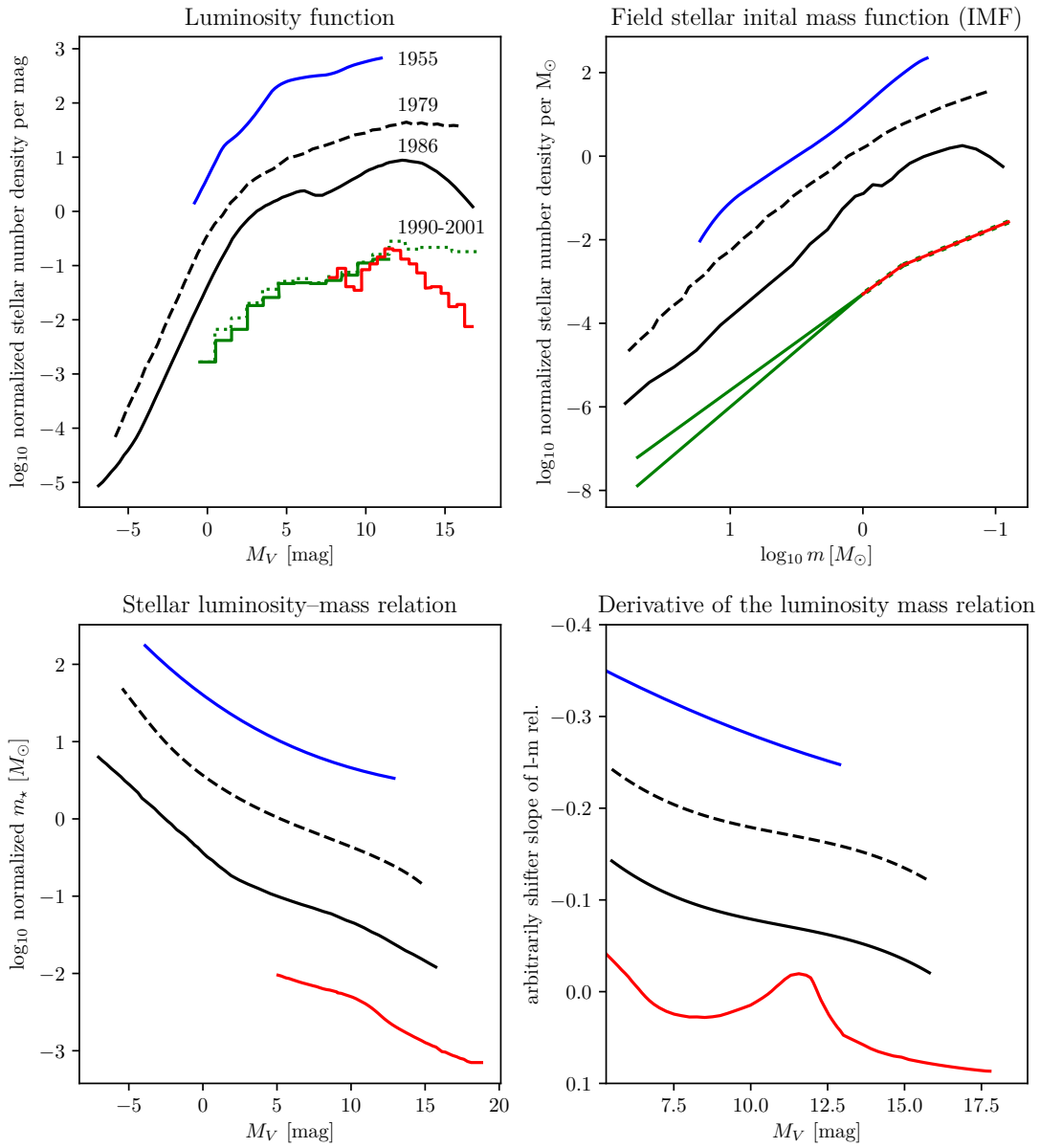

Figure 1.1: IMF-based properties for different IMF formulations with time: Salpeter IMF (blue), Miller & Scalo IMF (dashed black), Scalo IMF (solic black) and Kroupa IMF (green and red). **a)** Luminosity function, $\Psi(M_V)$, dotted green is for ground-based trigonometric parallaxes and solid green for space-based parallaxes, solid red histogram is using photometric paralllaxes. **b)** IMF, $\xi(m)$, red is for $m < 1\,M_\odot$, green for $m > 1\,M_\odot$, Scalo IMF being the lower line and the Sapeter-Massey IMF the upper line. **Bottom panels** show the stellar mass-luminosity relation (c) and its derivative (d). All curves are shifted vertically arbitrarily to demonstrate their differences. Figure and caption adapted from Kroupa and Jerabkova (2019).

fraction, respectively (the Milky Way having the intermediate value of about 50 per cent). Underlying this work is the implied concept that the observed invariance of the IMF in the Galaxy implies an invariant initial binary population, formulated as the "universality hypothesis" by Kroupa (2011). This would be understandable to be a result of physical processes that led to star formation being largely similar in the Milky Way.

The concept that stars form in embedded clusters thus became a powerful method for calculating various properties of Galactic-field populations. Potentially one of the most important results of this ansatz is the discovery that all star-forming galaxies have the same gas-consumption time-scale of about 2.5 Gyr, independent of their mass (Pflamm-Altenburg and Kroupa, 2009b).

1.2 Thesis structure

This thesis is a composition of four refereed publication of which the author of this thesis is the first author and one chapter based on several publications to which the author contributed significantly.

The above introduction provides the general context of the thesis, that is, it explains the importance and complexity of star-formation and its basic or related concepts, as is for example the stellar initial mass function.

Chapter 2 is based on the work by Jeřábková, Kroupa, Dabringhausen, Hilker, and Bekki (2017) titled "The formation of UCDs and massive GCs: Quasar-like objects to test for a variable stellar initial mass function". In this chapter, properties of high-redshift proto-globular clusters and progenitors of ultra-compact dwarf galaxies are discussed. It also provides predictions for the upcoming James Web Space Telescope. As mentioned above astronomy is a data driven science and thus these future observations might be necessary in order to advance our understanding of stellar populations in massive cluster-like stellar systems.

Chapter 3 is based on Jeřábková, Hasani Zonoozi, Kroupa, et al. (2018) with the title "The Impact of metallicity and star formation rate on the time-dependent, galaxy-wide stellar initial mass function". This thesis clarifies, for the first time, the importance of using the terminology "stellar IMF", "galaxy-wide IMF" and the "composite IMF" (for stellar populations in several clusters or complex regions). It also shows how we expect the stellar galaxy-wide IMF to evolve with time and allows future readers to use simple corrections in order to consider variable versus universal stellar IMFs.

Chapter 4 with the title "When the tale comes true: multiple populations and wide binaries in the Orion Nebula Cluster" by Jerabkova, Beccari, Boffin, et al. (2019) confirms the presence of the unexpected multiple stellar populations in the Orion Nebula Cluster (ONC). The ONC formed via three short bursts of star-formation each lasting approximately one Myr. The discovery that star-formation happened in the ONC via multiple short bursts questions our understanding of star cluster formation. Do the observed bursts of star-formation in the ONC represent a characteristic way in which stars form?

Chapter 5 is based on Jerabkova, Boffin, Beccari, and Anderson (2019) with the title "A stellar relic filament in the Orion star forming region." This work reports the

discovery of a long (90pc) thin (about 10pc) co-eval stellar structure in the Orion star-forming region. The structure is too young to be of tidal origin and thus it is concluded that the coeval stellar filament is likely a relic of star formation in a molecular cloud filament. Based on this it is named the *Orion relic filament*.

Chapter 6 is based on several papers to which the thesis author made significant contributions. It emphasises the overall work done during this thesis in the field of star-formation and stellar populations and demonstrates applications of the presented work in future research.

In this thesis the observationally well established finding that stars form in groups of at least a few binaries in the densest cores of molecular cloud cores is used and developed further in terms of linking these embedded clusters to the galaxy-wide properties. My newly found result, which is a central part of this thesis, that the embedded clusters are parts of molecular cloud filaments which emerge as coeval populations of stars in fossil relics spanning more than a hundred pc in length once the gas has dispersed, allows me to take the first explorative steps in generalising the IGIMF theory with the concept of the IGIMF being an operator, thus not limiting it to be based only on embedded clusters as the fundamental building blocks of galaxies.

To conclude the introduction chapter, this thesis, as star-formation exhibits itself in nature, documents studies of stellar populations on multiple scales and using multiple techniques from theory to observations and suggests the importance of building bridges between related fields in astronomy in order to advance our understanding.

Chapter 2

The formation of UCDs and massive GCs: Quasar-like objects to test for a variable stellar initial mass function

---

This chapter is based on the publication Jeřábková, Kroupa, Dabringhausen, Hilker, and Bekki (2017) with the same title "The formation of UCDs and massive GCs: Quasar-like objects to test for a variable stellar initial mass function". Only minor changes concerning formatting were made in order to present it as a chapter in the thesis.

Abstract: *The stellar initial mass function (IMF) has been described as being invariant, bottom-heavy, or top-heavy in extremely dense starburst conditions. To provide usable observable diagnostics, we calculate redshift dependent spectral energy distributions of stellar populations in extreme starburst clusters, which are likely to have been the precursors of present day massive globular clusters (GCs) and of ultra compact dwarf galaxies (UCDs). The retention fraction of stellar remnants is taken into account to assess the mass to light ratios of the ageing starburst. Their redshift dependent photometric properties are calculated as predictions for James Webb Space Telescope (JWST) observations. While the present day GCs and UCDs are largely degenerate concerning bottom-heavy or top-heavy IMFs, a metallicity- and density-dependent top-heavy IMF implies the most massive UCDs, at ages <100 Myr, to appear as objects with quasar-like luminosities with a 0.1-10% variability on a monthly timescale due to core collapse supernovae.*

2.1 Introduction

The question of whether the stellar IMF varies systematically with the physical conditions is a central problem of modern astrophysics (Elmegreen, 2004; Bastian, Covey, and Meyer, 2010; Kroupa, Weidner, Pflamm-Altenburg, et al., 2013). If it does vary, we would expect the largest differences in the most extreme starbursts conditions (e.g. Larson, 1998). Where are the most extreme starburst conditions in terms of star formation rate densities to be found, with the constraint that their present-day remnants are observable allowing detailed observational scrutiny of their present-day stellar populations? Given the present-day masses ($> 10^5\,M_\odot$) and present-day half-light radii ($1 - 50\,\mathrm{pc}$) globular clusters (GCs) and in particular ultra compact dwarf galaxies

(UCDs) are promising candidates (Mieske, Hilker, and Infante, 2002; Chilingarian, Cayatte, and Bergond, 2008; Brodie, Romanowsky, Strader, and Forbes, 2011, present-day half mass radius). For example a $10^7\,M_\odot$ present-day UCD with a half-light radius of 20 pc would likely have had a mass of $10^8\,M_\odot$ or and a radius of a few pc when a Myr old (Dabringhausen, Fellhauer, and Kroupa, 2010).

Ultra-compact dwarf galaxies (UCDs) have been discovered by Hilker, Infante, Vieira, Kissler-Patig, and Richtler (1999) and Drinkwater, Jones, Gregg, and Phillipps (2000). There is no unique definition of what a UCD is, but what is generally meant by a UCD is a stellar system with a radius between a few and 100 pc, and a dynamical mass of $10^6\,\mathrm{M}_\odot \lessapprox M_{dyn} \lessapprox 10^8\,\mathrm{M}_\odot$. Absolute magnitudes of UCDs lie roughly between $-10 \gtrapprox M_V \gtrapprox -16\,\mathrm{M_V}$, where the higher value corresponds to an old and low mass UCD (similar to ω Cen), while the lower value is more characteristic for a fairly young and/or massive UCDs (like W3). The most massive known old UCDs have magnitudes of $M_V \approx -14$. The presence of UCDs has been reported also in other galaxy clusters, e.g. Virgo (Drinkwater, Gregg, Couch, et al., 2004), Coma (Price, Phillipps, Huxor, et al., 2009), Centaurus (Mieske, Hilker, Jordán, Infante, and Kissler-Patig, 2007), Hydra I (Misgeld, Mieske, Hilker, Richtler, Georgiev, and Schuberth, 2011), Perseus (Penny, Forbes, and Conselice, 2012) or in massive intermediate-redshift clusters (e.g. Zhang and Bell, 2017). The existence of systems with properties of UCDs was discussed already by Kroupa (1998) based on the observations of star cluster complexes in the Antennae galaxies.

2.1.1 UCD formation and the categorization issue

The origin and evolution of UCDs is still a matter of debate (e.g. Côté, Piatek, Ferrarese, et al., 2006; Hilker, 2009; Brodie, Romanowsky, Strader, and Forbes, 2011) and up until today several possible formation scenarios have been proposed: (A) UCDs are the massive end of the distribution of GCs (e.g. Mieske, Hilker, and Infante, 2002; Forbes, Lasky, Graham, and Spitler, 2008; Murray, 2009; Dabringhausen, Kroupa, and Baumgardt, 2009; Chiboucas, Tully, Marzke, et al., 2011; Mieske, Hilker, and Misgeld, 2012; Renaud, Bournaud, and Duc, 2015), (B) UCDs are merged star cluster complexes (Kroupa, 1998; Fellhauer and Kroupa, 2002b; Fellhauer and Kroupa, 2002a; Brüns, Kroupa, Fellhauer, Metz, and Assmann, 2011), (C) UCDs are the tidally stripped nuclei of dwarf galaxies (Oh, Lin, and Aarseth, 1995; Bekki, Couch, and Drinkwater, 2001; Bekki, Couch, Drinkwater, and Shioya, 2003; Drinkwater, Gregg, Hilker, et al., 2003; Goerdt, Moore, Kazantzidis, Kaufmann, Macciò, and Stadel, 2008; Pfeffer and Baumgardt, 2013). (D) UCDs are remnants of primordial compact galaxies (Drinkwater, Gregg, Couch, et al., 2004).

Murray (2009) showed that the structure of the visible matter is not consistent with UCDs being objects dominated by non-baryonic dark matter halos. This is supported by a detailed study of one of the most massive UCDs (Frank, Hilker, Mieske, Baumgardt, Grebel, and Infante, 2011). Based on the Millenium II cosmological simulation, Pfeffer, Griffen, Baumgardt, and Hilker (2014) show that the formation of UCDs as tidally stripped nuclei of dwarf galaxies can account only for about 50 per cent of observed objects with mass $> 10^7\,M_\odot$, for masses $> 10^6\,M_\odot$ this drops to approximately 20 per cent (Pfeffer, Hilker, Baumgardt, and Griffen, 2016). And earlier Thomas,

Drinkwater, and Evstigneeva (2008) showed that the tidally stripped nucleus scenario fails to reproduce UCDs located in the outer parts of the Fornax cluster. Based on these results we focus on scenarios (A) and (B) which are both suggesting that UCDs are the high-mass end of star cluster-like objects, formed most likely during massive starbursts (Weidner, Kroupa, and Larsen, 2004; Schulz, Pflamm-Altenburg, and Kroupa, 2015; Schulz, Hilker, Kroupa, and Pflamm-Altenburg, 2016) at higher redshift, where compact starbursts are indeed observed (Vanzella, Calura, Meneghetti, et al., 2017; Glazebrook, Schreiber, Labbé, et al., 2017).

2.1.2 Aim of this work

In this contribution we aim to quantify how extreme star formation environments may appear at high redshifts, where the most intense starbursts likely have occurred. We therefore concentrate on the progenitors of present-day UCDs and GCs (i.e. their young counterparts at high redshift), which however, have not been knowingly observationally confirmed yet. We construct stellar population models using the PEGASE[1] (Fioc and Rocca-Volmerange, 1997) code to suggest possible photometric diagnostics to provide observational predictions for upcoming missions such as the James Webb Space Telescope (JWST). The underling question for this work is: Can a systematic variation of the stellar IMF in ultra-massive starburst clusters be confirmed in the very extreme starbursts at a high redshift using JWST?

This paper is structured as follows: The first section is devoted to the introduction of the topic. Section 2 describes the methods we use. Section 3 focuses on results and Section 4 and 5 contain discussions and conclusions, respectively.

2.2 Methods

We compute properties of UCDs and UCD progenitors assuming that they have formed according to scenario (A), i.e. by monolithic collapse. In such a case we expect that the first UCDs were formed alongside the formation of early massive galaxies ($\approx 0.5\,\mathrm{Gyr}$ after the Big Bang). Results obtained according to scenario (A) can be used to discuss and constrain also scenario (B), which is the formation of UCDs through mergers of cluster complexes. Since here we assume that GCs are low mass UCDs, we use unified notations for GCs and UCDs as UCDs from here on.

2.2.1 Parametrization of the UCDs

For quantifying our approach, we consider UCDs with the following properties: the UCD's initial stellar mass, $M_{UCD} \in [10^6, 10^9]\,\mathrm{M}_\odot$, redshift, $z \in 0, 3, 6, 9$, corresponding, respectively, to ages from the Big-Bang $\approx$ 13.5, 2.1, 0.9, 0.6 Gyr as demonstrated in Fig. 3.6. For the redshift computations we use the standard ΛCDM cosmology with Planck estimates, $\Omega_m \approx 0.308$, $\Omega_\Lambda \approx 0.692$, $H_0 \approx 67.8\,\mathrm{kms}^{-1}\mathrm{Mpc}^{-1}$ (Planck Collaboration, Ade, Aghanim, et al., 2016; Planck Collaboration, Adam, Aghanim, et al., 2016).

[1] www.iap.fr/pegase

Other parameters are metallicity, [Fe/H] $= -2$ and 0, and the stellar initial mass function (IMF).

2.2.2 The stellar IMF

We describe the stellar IMF as a multi-power law,

$$\xi(m_\star) = \begin{cases} k_1 m^{-\alpha_1} & 0.08 \leq m_\star/M_\odot < 0.50\,, \\ k_2 m^{-\alpha_2} & 0.50 \leq m_\star/M_\odot < 1.0\,, \\ k_2 m^{-\alpha_3} & 1.00 \leq m_\star/M_\odot \leq 120\,, \end{cases} \tag{2.1}$$

where

$$\xi(m_\star) = \mathrm{d}N/\mathrm{d}m_\star\,, \tag{2.2}$$

is the number of stars per unit of mass and k_i are normalization constants which also ensure continuity of the IMF function. As a benchmark we use the IMF α values derived from the Galactic star forming regions by Kroupa (2001), where $\alpha_1 = 1.3$ and $\alpha_2 = \alpha_3 = 2.3$, here denoted as CAN IMF (canonical IMF).

A larger α_1 than the canonical value leads to a bottom heavy IMF. A bottom-heavy IMF is also described by a single Salpeter slope $\alpha = \alpha_1 = \alpha_2 = \alpha_3 = 2.3$, which has been shown to lead to slightly elevated M/L_V values (Dabringhausen, Hilker, and Kroupa, 2008; Mieske and Kroupa, 2008) relative to the CAN IMF. Throughout this paper we will call this IMF the SAL IMF (Salpeter IMF). An even more bottom-heavy IMF, which might be necessary for explaining the observed M/L_V values around 10 and higher, was suggested by van Dokkum and Conroy (2010) for massive elliptical galaxies, due to features observed in their spectra (but see Smith and Lucey (2013)). This IMF is here referred to as the vDC IMF, and is characterised by an IMF slope $\alpha = \alpha_1 = \alpha_2 = \alpha_3 = 3.0$. A dependency of α on star-cluster-scale star-formation density and metallicity is currently not known. Chabrier, Hennebelle, and Charlot (2014) suggest increased turbulence to account for a bottom-heavy IMF in dense star forming regions. However, further theoretical work (Bertelli Motta, Clark, Glover, Klessen, and Pasquali, 2016; Liptai, Price, Wurster, and Bate, 2017) casts doubts on this. This issue clearly needs further research.

The other option how to explain the observed M/L_V ratios is a top-heavy IMF (Dabringhausen, Kroupa, and Baumgardt, 2009). The top-heavy IMF has an empirical prescription which establishes the slope of the heavy-mass end, α_3, over the interval of masses $(1, 120)\,\mathrm{M}_\odot$ as a function of metallicity, [Fe/H], and birth density of the embedded star cluster, ϱ_{cl}. The lower stellar masses ($< 1.0\,\mathrm{M}_\odot$) are in our formulation here distributed according to the CAN IMF. The relation for α_3 by Marks, Kroupa, Dabringhausen, and Pawlowski (2012) is,

$$\alpha_3 = \begin{cases} 2.3 & \text{if } x < -0.87\,, \\ -0.41x + 1.94 & \text{if } x \geq -0.87\,, \end{cases} \tag{2.3}$$

where

$$x = -0.14[Fe/H] + 0.99 \log_{10}\left(\frac{\varrho_{cl}}{10^6 M_\odot pc^{-3}}\right). \tag{2.4}$$

IMF	Top-heavy MKDP	Canonical CAN	Bott.-heavy SAL	Bott.-heavy vDC
α_1	1.3	1.3	2.3	3.0
α_2	2.3	2.3	2.3	3.0
α_3	0.6 – 2.3	2.3	2.3	3.0

Table 2.1: This table summarizes the IMF variations used in this paper. The α-coefficients are defined by Equation 3.4. The MKDP IMF depends on the initial stellar mass of the system according to Equation 2.3.

		MKDP IMF				CAN IMF	
		[Fe/H] = -2		[Fe/H] = 0			
M_{UCD} [M$_\odot$]	R_{cl} [pc]	α_3	$10^5 N_{\rm massive}$	α_3	$10^5 N_{\rm massive}$	α_3	$10^5 N_{\rm massive}$
10^6	0.6	1.61	0.2	1.73	0.2	2.3	0.1
10^7	0.8	1.37	2.4	1.48	2.4	2.3	1.1
10^8	1.1	1.12	23.2	1.23	23.8	2.3	10.9
10^9	1.5	0.87	213.8	0.99	222.7	2.3	109.1
10^{10}	2.0	0.62	1943.1	0.74	2032.6	2.3	1091.2

Table 2.2: This table presents values of the initial radii of the embedded star clusters, R_{cl}, (Marks and Kroupa, 2012), α_3 values, see Eq. (2.3) and the number of massive stars $N_{\rm massive} = N(m_\star > 8M_\odot)$ computed as a function of initial stellar mass, $M_{UCD} = M_{ecl}$, and metallicity. For comparison, we also show $N(m_\star > 8M_\odot)$ for the CAN IMF. The predicted values of the embedded cluster/UCD initial radii, R_{cl}, are small. However due to stellar and dynamical evolution UCDs expand by approximately a factor of 10 (Dabringhausen, Fellhauer, and Kroupa, 2010). We use the R_{cl} values as an empirical extrapolation from GCs and therefore at UCD scales departures are possible.

These relations have been obtained from a multi-dimensional regression of GC and UCD data. To calculate the birth density, ϱ_{cl}, we use the empirical relation from Marks and Kroupa (2012), where the half-mass radii of embedded clusters follow

$$R_{cl}/pc = 0.1(M_{ecl}/M_\odot)^{0.13}\,, \tag{2.5}$$

where M_{ecl} is the stellar mass. The total density (gas + star) , ϱ_{cl}, for a star formation efficiency, ε, is given by

$$\varrho_{cl} = \frac{3M_{ecl}}{4\varepsilon\pi R_{cl}^3}\,. \tag{2.6}$$

Further-on, we assume a star formation efficiency $\varepsilon = 0.33$ (e.g. Megeath, Gutermuth, Muzerolle, et al., 2016; Banerjee, 2017) and refer to the IMF derived using these relation as the MKDP IMF. The α_3 and half-mass radii R_{cl} are listed in Table 2.2. Theoretical arguments for the IMF becoming top-heavy with increasing density, temperature and decreasing metallicity of the star-forming gas cloud have been described by Larson (1998), Adams and Laughlin (1996), Dib, Kim, and Shadmehri (2007), and Papadopoulos (2010).

All the IMFs considered here are summarized in Table 2.1.

2.2.3 PEGASE parameters

The above parametrizations are used as input values to the PÉGASE time dependent stellar population synthesis code[2] (Fioc and Rocca-Volmerange, 1997) and we compute the time evolution of various quantities, such as the total luminosity, $L_{\rm UCD}$, number of massive stars ($m_\star > 8\,{\rm M}_\odot$), $N_{\rm mass}$, and also observable properties: the redshifted time-evolution of the SEDs, color-color diagrams, color-magnitude diagrams and we investigate in detail the M/L_V values. Besides the values considered here for the initial stellar mass, metallicity and redshift of the UCDs (M_{UCD}, [Fe/H], z), we use the following values to compute the PÉGASE models: a conservative value $\eta = 0.05$ for fraction of binaries producing supernovae Ia (e.g. Maoz, 2008, where $\eta \in (0.05, 0.4)$), zero inclination, no galactic winds and no in-fall matter, no metallicity evolution (this would require a more complicated time dependent IMF prescription and a star-formation history). We take into account nebular emission and we assume no extinction since it can be corrected based on various assumptions in the further interpretation of our models. It is, however, worth mentioning that young and intermediate-age massive clusters in the local universe seem to be gas- and dust-free very early on (e.g. Bastian and Strader, 2014; Longmore, 2015). The star formation history is assumed to have a shape of a step function with a non zero value for the first 5 Myr. We will compare this with the instantaneous starburst case which has the same parameters apart from all stars forming at the same time.

2.2.4 Calculating mass to light ratios

To evaluate the dynamical mass, M, and luminosity in the V band, L_V, several assumptions are made: (i) We assume that the UCDs are gas free during the whole period of their evolution, which means that our predictions are only valid for pure stellar populations. (ii) Mass loss from the UCDs is only through stellar evolution in the from of ejected gas. We assume that all stars are kept in the system and no stars are lost by dynamical evolution of the UCDs. Stellar loss due to dynamical evolution is an important process (e.g. Balbinot and Gieles, 2017) which is, however, significant only for systems with initial stellar mass $\lessapprox 10^6\,M_\odot$ (Lamers, Gieles, Bastian, Baumgardt, Kharchenko, and Portegies Zwart, 2005; Schulz, Hilker, Kroupa, and Pflamm-Altenburg, 2016; Brinkmann, Banerjee, Motwani, and Kroupa, 2017). The reason is that for large stellar mass, $\gtrapprox 10^6\,M_\odot$, the tidal radius in a Milky-Way galaxy potential is $\gtrapprox 100$ pc for Galactocentric distances $\gtrapprox$ few kpc such that the vast majority of stars remain bound. This is consistent with using equation (5) from Lamers, Gieles, Bastian, Baumgardt, Kharchenko, and Portegies Zwart (2005) which, after integration, gives an upper limit for tidal stellar mass loss over a Hubble time $\approx 10^3\,M_\odot$ independent of initial mass. (iii) Effect of loss of dark remnants (neutron stars and black holes) on the estimate of the dynamical mass for the vDC, SAL and CAN IMF is negligible to the value of the M/L_V ratio (for the CAN IMF dark remnants contribute only few per cent of the UCD mass). However, in the MKDP IMF case, where dark remnants contribute a substantial fraction to the total mass of the system, the amount of dark remnants kept is not negligible any more. The actual fraction of dark remnants kept in a system

[2] www.iap.fr/pegase

is still being discussed. Mainly because to study remnant ejections, close dynamical encounters in a system are important on a Hubble time scale (Banerjee, 2017). Such studies are extremely CPU intensive for systems as massive as UCDs. On the other hand, Peuten, Zocchi, Gieles, Gualandris, and Hénault-Brunet (2016) and Baumgardt and Sollima (2017), constrain the retention fraction of dark remnants in lower mass GCs, which allows us to deduce implications for UCDs.

2.2.4.1 Retention fraction of dark remnants

The mass-to-light ratios of UCDs depend on the retention fraction of stellar remnants within the system once the progenitor stars die. In order to assess the possible range of retention fractions we assume that white dwarfs (WDs) receive no kicks upon the death of their progenitor stars such that all WDs remain bound to the system. A star more massive than $8\,M_\odot$ explodes as a type II supernova or implodes leaving either a neutron star or a stellar black hole. The kicks these receive during such violent events due to the asymmetry of the explosion or implosion are uncertain. Large natal kicks will lead to the loss of most such remnants from the system.

We estimate the retention fraction by assuming that 10 per cent of all neutron stars and black holes are retained in a globular cluster with a mass of $10^5\,M_\odot$. This is a conservative assumption as Baumgardt and Sollima (2017) and Peuten, Zocchi, Gieles, Gualandris, and Hénault-Brunet (2016) constrain the retention fraction to be less than about 50 per cent for globular clusters (GCs) based on a detailed study of their observed mass segregation. With this normalisation condition, and assuming two possible radius-mass relations for GCs and for UCDs, we can estimate the likely values of the retention fraction of stellar remnants (neutron stars and black holes) as a function of birth system mass, M. One possibility for the $R(M)$ relation is to assume the observed radii of clusters (typically about 3 pc) and of UCDs (Eq. (4) in Dabringhausen, Hilker, and Kroupa, 2008). The other possibility is to assume that the stars die in their birth systems before these expand (Dabringhausen, Fellhauer, and Kroupa, 2010) due to residual gas expulsion and stellar evolution driven mass loss with the $R(M)$ relation constrained by Marks & Kroupa (2012, their eq. 7). Given the $R(M)$ relation, we assume that remnants are lost if their speed after the kick is larger than the central escape velocity. We assume the systems to be Plummer models and that the kick velocities follow a Maxwell-Boltzmann distribution (MBD) with velocity dispersion $\sigma_{\rm kick}$.

Fig. 2.1 shows the resulting MBD for the two assumed $R(M)$ relations. The adopted normalisation condition forces the MBD to be narrow with a small $\sigma_{\rm kick} = 24\,{\rm km/s}$ for the present-day radii of clusters and UCDs, while applying the birth radii a larger $\sigma_{\rm kick} = 61\,{\rm km/s}$ results. Despite the two different values, the resulting retention fractions, defined for the present purpose as the fraction of remnants with a speed smaller than the central escape speed, are very similar. This is shown in Fig. 2.2 from which it also follows that the retention fraction increases steeply with system mass such that for $M > 10^6\,M_\odot$ the retention fraction can be assumed to be near to 100 per cent, if the normalisation condition applied here holds. We also plot the retention fraction for distributions with larger $\sigma_{\rm kick}$ values, namely 100, 300 and 500 km/s. Given these results it is reasonable to assume that the retention fraction of UCDs with birth masses larger

than $10^7\,M_\odot$ is close to 100%. Indirect evidence suggesting possible large retention fraction in UCDs are recent findings of super massive black holes (SMBHs) in UCDs (e.g. Seth, van den Bosch, Mieske, et al., 2014; Ahn, Seth, Brok, et al., 2017), see Sec. 2.4.3. Nevertheless, we still investigate the effect of smaller retention fractions on the M/L_V values to allow us to see the maximum impact the assumed IMF can potentially have.

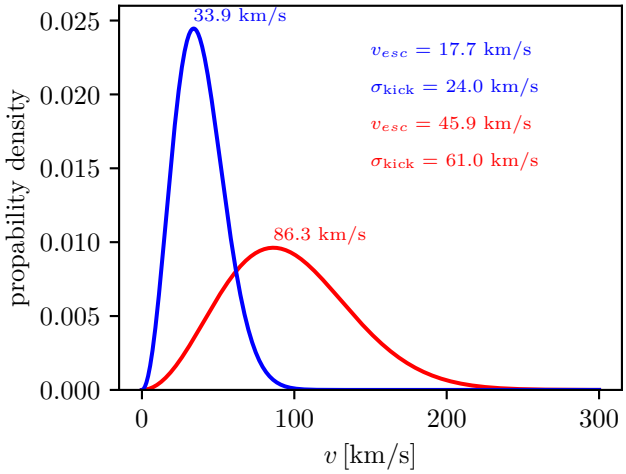

Figure 2.1: The distribution function of speeds of dark stellar remnants. We use the conservative estimate that only 10% of dark remnants are kept in $10^5\,M_\odot$ system due to SN kicks. We constrain the SN kick velocity distributions assuming it has a Maxwell-Boltzman shape for birth radius (Marks and Kroupa, 2012, red curve) and for present day radius (3 pc for GCs and for the UCDs we use the mass-radius relation from Dabringhausen, Hilker, and Kroupa (2008), their Eq. 4, blue curve. The peak velocity, $\sigma_{\rm kick}$ and v_{esc} values are stated.

2.2.5 Limitations of the models

We note here three possible limitations to the models introduced above:

1. Effects of binaries
   The majority of stars form in binaries (e.g. Marks, Kroupa, and Oh, 2011; Thies, Pflamm-Altenburg, Kroupa, and Marks, 2015). Mass transfer and mergers can rejuvenate stellar populations leading to significantly more UV radiation even after a few Gyr (Stanway, Eldridge, and Becker, 2016, BPASS code). Since here we focus on the IR region mostly and on systems younger than 100 Myr, it is likely that our conclusions are not affected strongly if binary-star evolution is taken into account, but it is nevertheless important to check that in the future.

2. Multiple populations
   It is well established that GCs have multiple stellar populations (e.g Renzini, D'Antona, Cassisi, et al., 2015, review). This may be true for UCDs as well. Future SED modeling has a potential to address how and if these can be observed

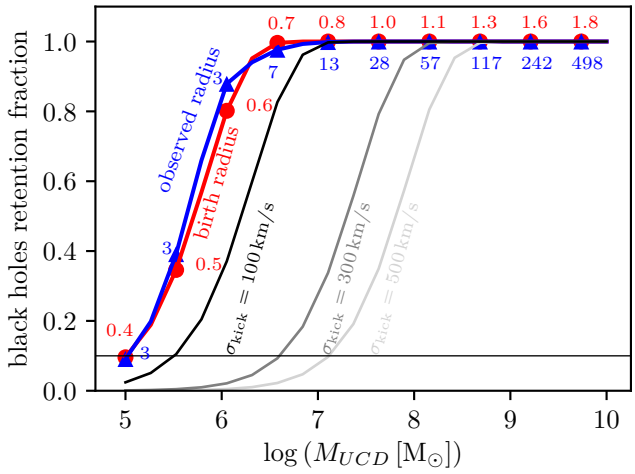

Figure 2.2: The retention fraction of dark remnants as a function of system mass if we assume that the main mechanism of dark remnants ejection are SN kicks with a Maxwell-Boltzman kick velocity distribution shown in Fig. 2.1. We assumed two different mass-radius relations (red and blue curves, as in Fig. 2.1), radii for each mass being written next to the corresponding points and a normalisation described in the text. In black and gray colors we plot retention fractions if a larger kick velocity dispersions are assumed. In this case we use the mass-radius relation from Marks and Kroupa (2012).

in young systems at high redshift. But we caution that binary stellar evolution (Item 1 above) may lead to degeneracies.

3. Statistical importance
   Large statistical samples may be needed to ascertain a systematic variation of the IMF with physical conditions Dabringhausen, Hilker, and Kroupa (2008), Dabringhausen, Kroupa, and Baumgardt (2009), and Dabringhausen, Kroupa, Pflamm-Altenburg, and Mieske (2012).

2.3 Results

For the grid of chosen parameters we construct a time grid (1-10 Myr with 1 Myr step, 10-100 Myr with 10 Myr steps, 100-1000 Myr with 100 Myr steps and 1-13 Gyr with 1 Gyr steps) of SEDs which contain all the light information from the source necessary for the construction of other observables. This SED data set will be published together with this paper. For more details (e.g comparison of the PEGASE code and the StarBurst99–code (Leitherer, Schaerer, Goldader, et al., 1999) with description of the evolution of SEDs with time and dependency on redshift) see Appendix 2.6.

In the next subsections we describe important results.

2.3.1 Evolution of the bolometric luminosity with time

To demonstrate how luminous progenitors of UCDs could have been, we compute the bolometric luminosity, L_{bol}, as a function of time. The $L_{bol}(t)$ dependency is shown

QSO	z	M_V	M_I	RQ/RL
0923+201	0.193	-24.6	-24.28	RQ
2344+184	0.138	-23.6	-23.80	RQ
1635+119	0.147	-23.1	-22.39	RQ
1012+008	0.185	-24.3	-25.39	RQ
1004+130	0.241	-25.7	-24.90	RL
1020-103	0.197	-24.2	-24.35	RL
2355-082	0.211	-23.0	-23.71	RL

Table 2.3: This table presents quasar (QSO) data, the first column is the QSO identification, z is the redshift, M_V and M_I are absolute magnitudes and RQ/RL labels the QSO as being radio quiet (RQ) or radio loud (RL). We have not found any publication or catalogue presenting both, the absolute magnitudes in the V filter, M_V, and I filter M_I. Therefore, the data in the table use the catalogue by Souchay, Andrei, Barache, et al. (2015) containing the M_I values. The M_V values are taken from Dunlop, Taylor, Hughes, and Robson (1993) and Dunlop, McLure, Kukula, Baum, O'Dea, and Hughes (2003).

in Fig. 2.3. The bench mark initial mass is $M_{UCD} = 10^8\,M_\odot$. For the cases of the CAN, SAL and vDC IMF the L_{bol} values are proportional to M_{UCD}. The MKDP IMF is a function of M_{UCD} and therefore we plot $L_{bol}(t)$ also for $M_{UCD} = 10^7$ and $10^9\,M_\odot$. The main difference between different MKDP IMFs (for different M_{UCD}) is the slope of the luminosity as a function of time. For a more top-heavy IMF, the decrease of the luminosity with time is steeper.

There are several noticeable features in this figure: (i) for the MKDP IMF, UCDs with initial stellar mass $M_{UCD} \gtrapprox 10^8\,M_\odot$ are as bright as quasars (Dunlop, Taylor, Hughes, and Robson, 1993; Dunlop, McLure, Kukula, Baum, O'Dea, and Hughes, 2003; Souchay, Andrei, Barache, et al., 2015) for the first few 10^7 yr. [3] This is mainly due to the presence of a large number of O and B stars ($10^6 - 10^7$) in the system. Due to stellar evolution and core collapse supernova explosions these UCDs will be variable on a time scale of months. As already suggested by Terlevich and Boyle (1993) such objects might be confused with quasars, especially for example in large photometric surveys. (ii) After less than a 100 Myr, a strong degeneracy between the IMF and M_{UCD} appears. That is for different M_{UCD} and different IMFs similar luminosities comparable to those of observed UCDs occur. (iii) The metallicity is a second order effect.

2.3.2 Time evolution of the M/L_V ratio

The PEGASE output allows us to evaluate the mass-to-light (M/L_V) ratios in arbitrary photometric filters since with the time evolution the code keeps information about the current stellar mass, mass in black holes and neutron stars and also about the gas (non consumed initial gas and the gas ejected by stars). Since the vDC or SAL (bottom-heavy) IMFs do not depend on the initial UCD mass, neither does the M/L_V ratio.

[3] We use low-redshift quasars because for these we were able to find bolometric luminosities, but also absolute magnitudes in the V and I band. Note however that high redshift quasars show very comparable luminosities as shown for example by Mortlock, Warren, Venemans, et al. (2011).

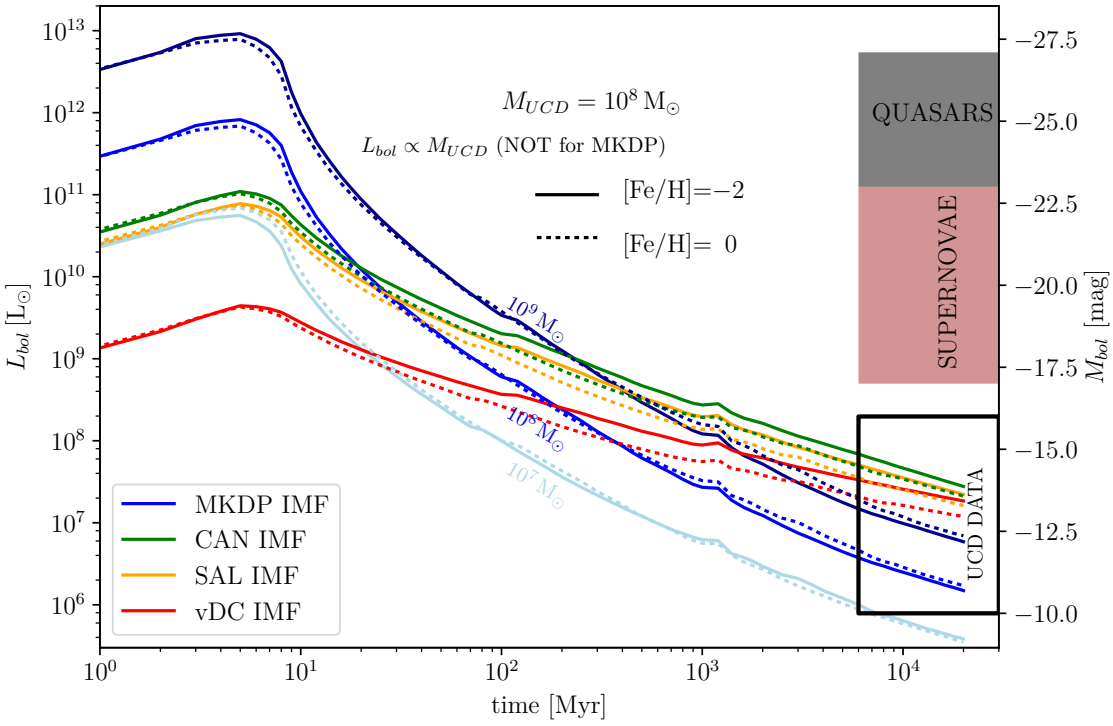

Figure 2.3: The time evolution of the bolometric luminosity for different IMFs. The MKDP IMF changes with the initial mass of the UCD and does not scale linearly with its mass. In contrast the vDC, SAL or CAN IMFs have UCD-mass independent slopes and scale proportionally with M_{UCD}. The grey panel shows the typical luminosities of quasars (Dunlop, Taylor, Hughes, and Robson, 1993; Dunlop, McLure, Kukula, Baum, O'Dea, and Hughes, 2003; Souchay, Andrei, Barache, et al., 2015) and the brown panel shows the luminosity-span for the peak luminosities supernovae (Gal-Yam, 2012; Lyman, Bersier, James, et al., 2016) which might cause luminosity variations in L_{bol} of UCDs younger than about 50 Myr according to SNe rates.

The situation is different for the MKDP IMF and we therefore plot the time evolution of the M/L_V ratio for different initial masses in Fig. 2.4.

2.3.2.1 M/L_V ratio variations

The results show that largest differences in M/L_V ratios are evident in the first $\approx$ 100 Myr, which is the age corresponding to the time when the most massive stars evolve into dark remnants, see Fig. 2.4 where we can also see the effect of the retention fraction of remnants on the M/L_V values. For later times degeneracy among the data appears: the UCDs formed with a MKDP IMF are equally or less bright than the UCDs with a CAN or SAL IMF formed with the same initial mass. Even the M/L_V ratios might become indistinguishable at times older than $\approx$ 100 Myr for different IMFs within the observational and metallicity uncertainties.

Using the same models, we construct the dependence of M/L_V on L_V for different

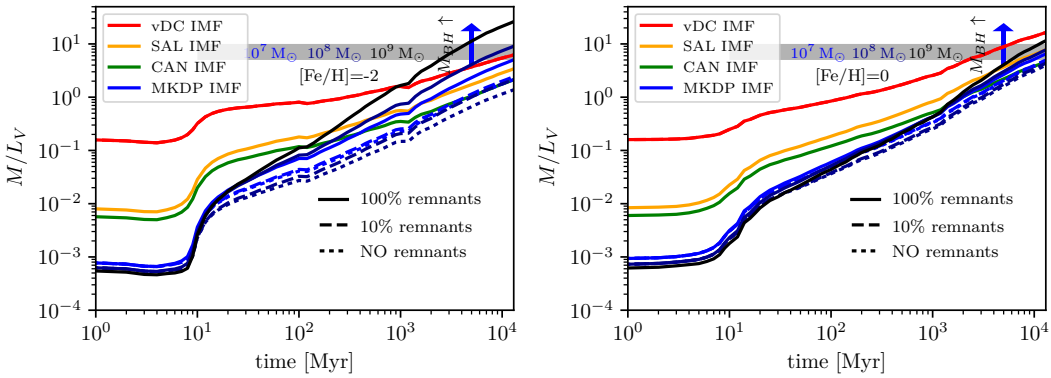

Figure 2.4: The time evolution of M/L_V for all IMFs considered (vDC, SAL, CAN, MKDP). We assume that the system is gas free and that neither stars nor remnants are leaving (the dashed lines show the change of the M/L_V value if only certain fractions of remnants are kept). The upwards pointing blue arrow demonstrates that if we would assume more massive remnants (e.g. due to implosion directly to a BH without a SN explosion) then this would lead to larger values of M/L_V. The models are computed for the case of $M_{UCD} = 10^9\,M_\odot$, however, results are mass independent. The only exception is the MKDP IMF, which depends on initial object mass, M_{UCD}, and also contains a large fraction of mass in high mass stars, and is plotted for $M_{UCD} = (10^9, 10^8, 10^7\,M_\odot$, bottom to top) and different fractions of remnants kept (100%,10%,0%). **Left panel:** The evolution for [Fe/H]=-2. **Right panel:** The evolution for [Fe/H]=0. The grey band indicates the span of the observed present day M/L_V values, approximately 5-10 for the majority of UCDs (Mieske, Dabringhausen, Kroupa, Hilker, and Baumgardt, 2008; Dabringhausen, Kroupa, and Baumgardt, 2009). The scales are identical for both panels.

evolutionary times (Fig. 2.5). To construct these plots, we assumed the set of initial UCD masses to be 10^7, 10^8, $10^9\,M_\odot$. As is clear from the comparison of the panels in Fig. 2.5, the metallicity has a large effect on the M/L_V values.

2.3.3 The supernova rates

The SNe II rate (Lonsdale, Diamond, Thrall, Smith, and Lonsdale, 2006; Anderson, Habergham, and James, 2011) can be a very good indicator of the IMF as one can see in Fig. 2.6. According to the standard stellar evolutionary tracks, employed here, every star more massive than $8\,M_\odot$ ends as a supernova explosion. However this may not be the case always. As the metallicity varies it may occur that a star of a given mass may implode and create a black hole directly without any explosion (see e.g. Pejcha and Thompson, 2015) and therefore our theoretical prediction represents the upper limit to the SN II rate.

It is important to point out that the SN rate depends on the star formation history of a system. If the whole system is formed during an instantaneous starburst the peak SNII rate might by a factor of 10 higher than in the case of constant star formation over a period of 5 Myr. On the other hand if the star formation is more extended then the period of high SNII rate lasts longer.

Considering the luminosities of SNe (Gal-Yam, 2012; Lyman, Bersier, James, et al.,

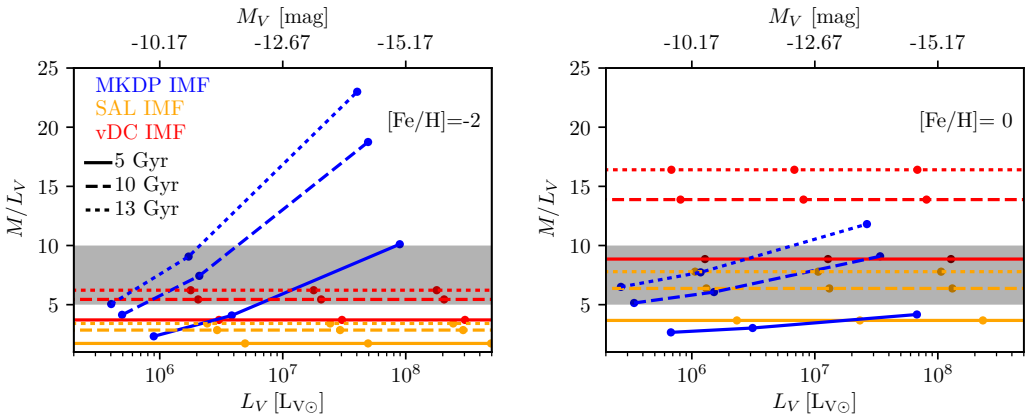

Figure 2.5: M/L_V as a function of L_V for three different times 5, 10, 13 Gyr. The case of the MKDP IMF is not constant since the MKDP IMF is a function of initial mass. The plotted curves assume all remnants are kept, if only some fraction is kept the M/L_V values would become smaller accordingly. There are two horizontal axes, the one on the top of the plots shows corresponding values of the absolute magnitude in the rest-frame V-band. The observed values of M/L_V for UCDs are in the interval from approximately 5 to 10 with few values spanning up to a 15 (Mieske, Hilker, and Infante, 2002) which are demonstrated by the grey band. The points plotted on the curves mark luminosities and M/L_V values for UCDs starting with initial mass of $10^9, 10^8$ and $10^7\,M_\odot$. **Left panel:** [Fe/H]=-2 and **right panel:** [Fe/H]=0.

2016), in Fig. 2.3 it is shown that at the later phases, >10 Myr, the SNe can reach up to 10% of the UCD's total flux for the MKDP IMF and $10^9\,M_\odot$ initial mass (for smaller initial masses SN II explosions will be more pronounced) and therefore might be detectable as photometric fluctuations on the scales of months.

To compute the SN Ia rate we adopt a conservative fraction, $\eta = 0.05$, of intermediate-mass stars that eventually explode as SNe Ia. According to Maoz (2008) $\eta = 0.02 - 0.4$. We use $\eta = 0.05$ also because it is a default value of this parameter and therefore our results will be likely comparable with other studies. The η value affects the estimates of the number of SNe Ia and also of the ejecta (Thielemann, Nomoto, and Yokoi, 1986; Greggio and Renzini, 1983; Matteucci and Greggio, 1986). The computed rates are plotted in Fig. 2.6. Using a value as large as $\eta = 0.4$ (Maoz, 2008, upper value) would imply an eight times larger SN Ia rate. The other results, such as the luminosities or M/L_V values, are not affected by the value of η. Since different values of η do not change the mass distribution of stars.

2.3.4 Time evolution of the β_{UV} slope

The β_{UV} slope is defined here as the slope of the fitted linear function to the logarithmically scaled SED, expressed in units of $\mathrm{ergs}^{-1}\mathrm{cm}^{-2-1}$, in a wavelength interval (1350,3500)Å in the rest frame of the observed object, as shown in Fig. 2.11 in the Appendix.

We computed β_{UV} for the complete set of our SEDs (Fig. 2.7). The β_{UV} values have been determined for objects down to $10^5\,M_\odot$ at high redshifts (up to $z = 6$) (Vanzella,

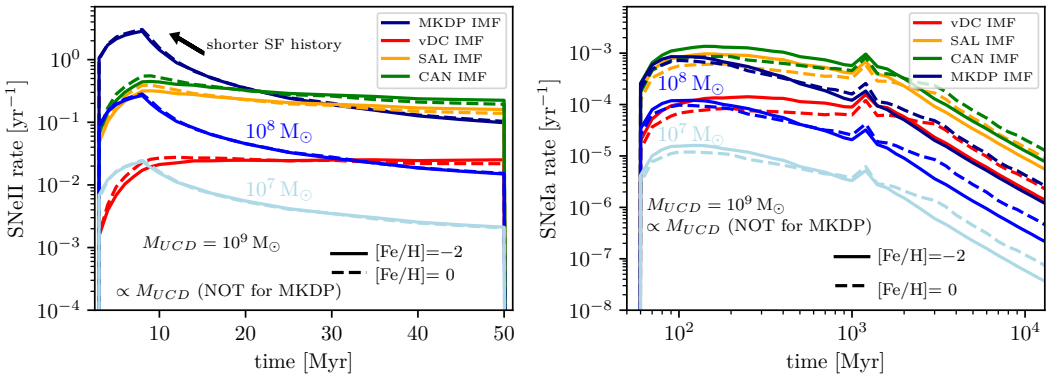

Figure 2.6: **Left panel:** The SNe II rate as a function of time, for a constant star formation history over a period of 5 Myr. In the instantaneous starburst case the SNeII rate may be up 10× higher at ages < 10 Myr. We show the case of the vDC, SAL, CAN, MKDP IMFs. Since only the MKDP IMF does not scale linearly with initial stellar mass, M_{UCD}, we show also the lines for $M_{UCD} = 10^7$ M$_\odot$ and 10^8 M$_\odot$, for the other IMFs we chose to plot only 10^9 M$_\odot$. The arrow indicates that the peak of the SN II rate shifts to the left and upwards for a star-formation history which is shorter than 5 Myr. **Right panel:** The SNe Ia rate as a function of time. We show the case of the vDC, SAL, CAN, MKDP IMFs. Since only the MKDP IMF does not scale linearly with initial stellar mass, M_{UCD}, we show also the lines for $M_{UCD} = 10^7$ M$_\odot$ and 10^8 M$_\odot$, for the other IMFs we chose to plot only 10^9 M$_\odot$.

Calura, Meneghetti, et al., 2017) and therefore might allow very useful additional constraints on the IMF and the age estimates. The β_{UV} values are metallicity sensitive and do have a generally increasing trend with age. The dependence on the IMF is stronger for objects younger than 10 Myr and at low metallicity, $\beta_{UV}^{MKDP} \approx -2.1$, $\beta_{UV}^{vDC} \approx -2.6$ at age 1 Myr for [Fe/H]=-2. At an age of 200 Myr, these values evolve to $\beta_{UV}^{MKDP} \approx -1.3$, $\beta_{UV}^{vDC} \approx -1.1$.

At a high redshift it may not always be possible to obtain a spectrum of a UCD. In such a case we can obtain photometric fluxes in at least two filters and use these to approximate the β_{UV} slope. For $z = 3$ one could, for example, use the JWST NIRCam instrument with filters F070W and F115W. For $z = 6$ and $z = 9$ it is possible to use the same instrument but with filters F090W, F200W and F115W, F300M, respectively.

2.3.5 The color-magnitude and the color-color diagrams

Other observables which can be computed from the SED and for standard filters and are provided by PEGASE are various colors and magnitudes. The time evolution of our objects is shown in the V vs $V - I_c$ diagram for comparison with other work (e.g. Evstigneeva, Drinkwater, Peng, et al., 2008). This is done for the MKDP IMF in Fig. 2.8 and for the CAN, SAL and vDC IMFs in Fig. 2.9. As expected we can see the increasingly strong degeneracy with time that makes it hard to distinguish the metallicity, initial mass or the IMF.

The color-color diagram has the advantage of having differences in magnitudes on both axis and therefore in a way subdues the information about the absolute values and

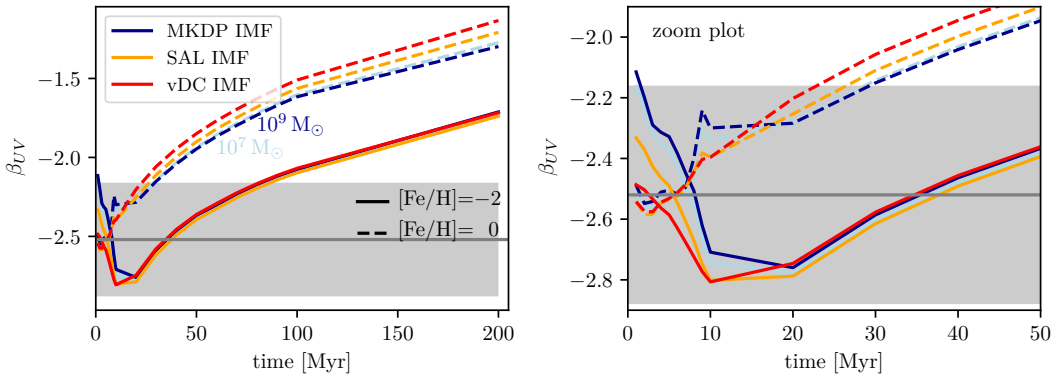

Figure 2.7: Time evolution of the β_{UV} values fitted over the wavelength interval (1350,3500)Å to the SEDs in the rest frame of the observed object in units ergs^{-1}cm^{-2-1}. The β_{UV} slope is M_{UCD} independent, but not for the case of the MKDP IMF for which we plot the case of $M_{UCD} = 10^7\,M_\odot$ and $10^9\,M_\odot$. **Left panel:** The time evolution of the β_{UV} slope over the time period of 200 Myr. **Right panel:** The zoom-in plot covers the first 50 Myr. The grey band shows the measurement from Vanzella, Calura, Meneghetti, et al. (2017) for their object GC1.

enhances the differences in spectral shapes and features. As is shown in Fig. 2.12 we chose to use the standard filters J, K and N. The N filter is almost identical to F1000W on the MIRI instrument on the JWST. The J and K filters cover a similar range as the F115W and F200W filters on NIRCam on the JWST. The results presented here assume transmission functions corresponding to their filters to be given by the rectangular regions shown in Fig. 2.13. These filters possess several useful characteristics, (i) even for a redshift of value 9 they are still in the spectral range covered by the PEGASE SEDs and therefore we do not introduce any additional errors by using the extrapolated range of the SEDs, (ii) J, K and N cover large parts of the SEDs and therefore are good representatives of an overall shape, and (iii) the N filter is still in the well described region where we do not expect large discrepancies from model to model and therefore also in real measurements as can be seen in Fig. 2.14.

2.3.6 Predictions for JWST

The first question which we need to ask is whether UCD progenitors are bright enough to be detected and if so up to which redshift. To quantify this we use the upcoming James Webb Space Telescope (JWST) as a benchmark. To cover the here computed wavelength region by PEGASE, the most suitable instrument is NIRCam in imaging mode, in total covering the region from 0.6 to 5 μm. To probe also longer wavelengths we compute predictions also for the MIRI instrument in imaging mode.

All predictions we make are for the UCDs with an initial stellar mass of $10^8\,M_\odot$, we use the CAN IMF as the standard and consider also the MKDP IMF. For the NIRCam instrument we use as a setup sub arrays FULL, readout DEEP8, groups 10, integration 1, exposures 5. This results in a total exposure time of 10149 s. For the MIRI instrument the parameters are: subarrays FULL, readout FAST, groups 100, integration 1, exposures 36, resulting in a similar exposure time of 10090 s. The predictions for the

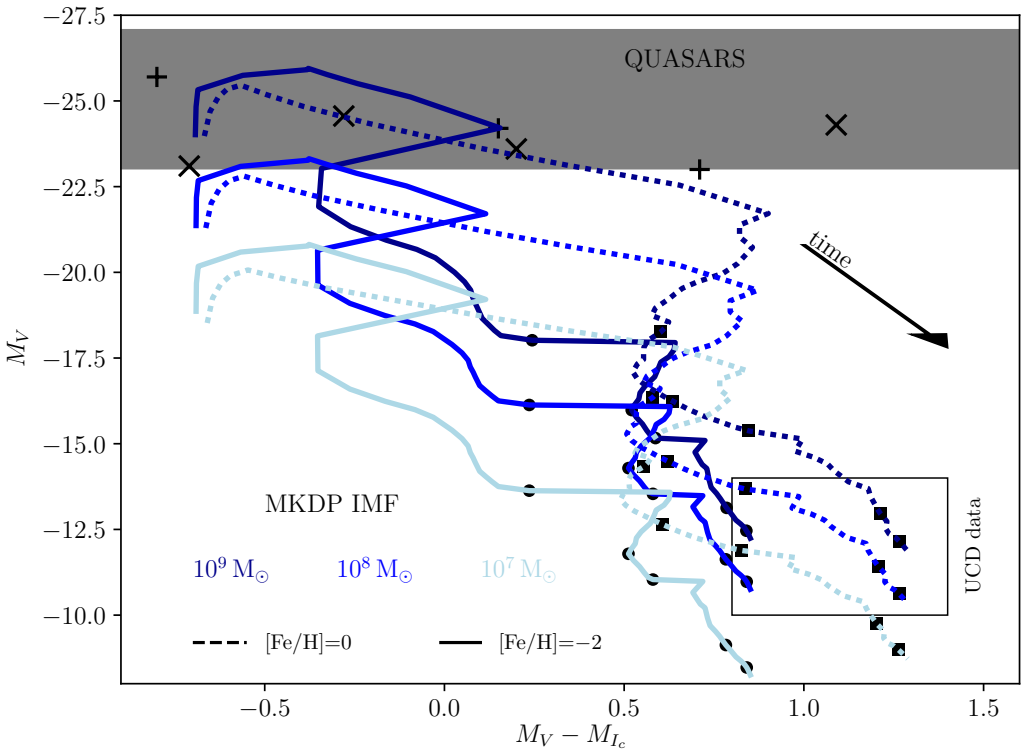

Figure 2.8: The color-magnitude diagram showing M_V as a function of $V - I_c$ (in the UCD rest frame) which are photometric filters directly computed by PEGASE. We consider 10^7, 10^8, 10^9 M$_\odot$ as initial stellar masses, and metallicity values $[Fe/H] = -2, 0$. Here we show only the results for the MKDP IMF plotted together with the quasar data (black cross and plus markers, cross for radio quiet and plus for radio loud quasars) from Dunlop, Taylor, Hughes, and Robson (1993), Dunlop, McLure, Kukula, Baum, O'Dea, and Hughes (2003), and Souchay, Andrei, Barache, et al. (2015). The data are compiled in Table 2.3. The CAN IMF, SAL IMF and vDC IMF are shown in Fig. 2.9. The arrow indicates the time evolution for the UCD models, the black filled circles and squares mark evolutionary time, from left to right: 100 Myr, 500 Myr, 1 Gyr, 5 Gyr, 10 Gyr for [Fe/H]=-2 and 0 dex. The rectangular region indicates where the majority of observed UCDs are located (e.g. Evstigneeva, Drinkwater, Peng, et al., 2008). Since UCDs have a different metallicity, we do not plot individual data points.

JWST telescope are summarized in Table 2.4. The general conclusion is that UCD progenitors are detectable using JWST photometry with a ≈ 3h exposure time with promising values of S/N, as already suggested for GCs progenitors by Renzini (2017).

2.4 Discussion

2.4.1 Where to look

The star-formation rate density typically peaks near the centre of a galaxy. This is evident in interacting galaxies (Joseph and Wright, 1985; Norman, 1987; Wright, Joseph, Robertson, and Meikle, 1988; Dabringhausen, Kroupa, Pflamm-Altenburg, and

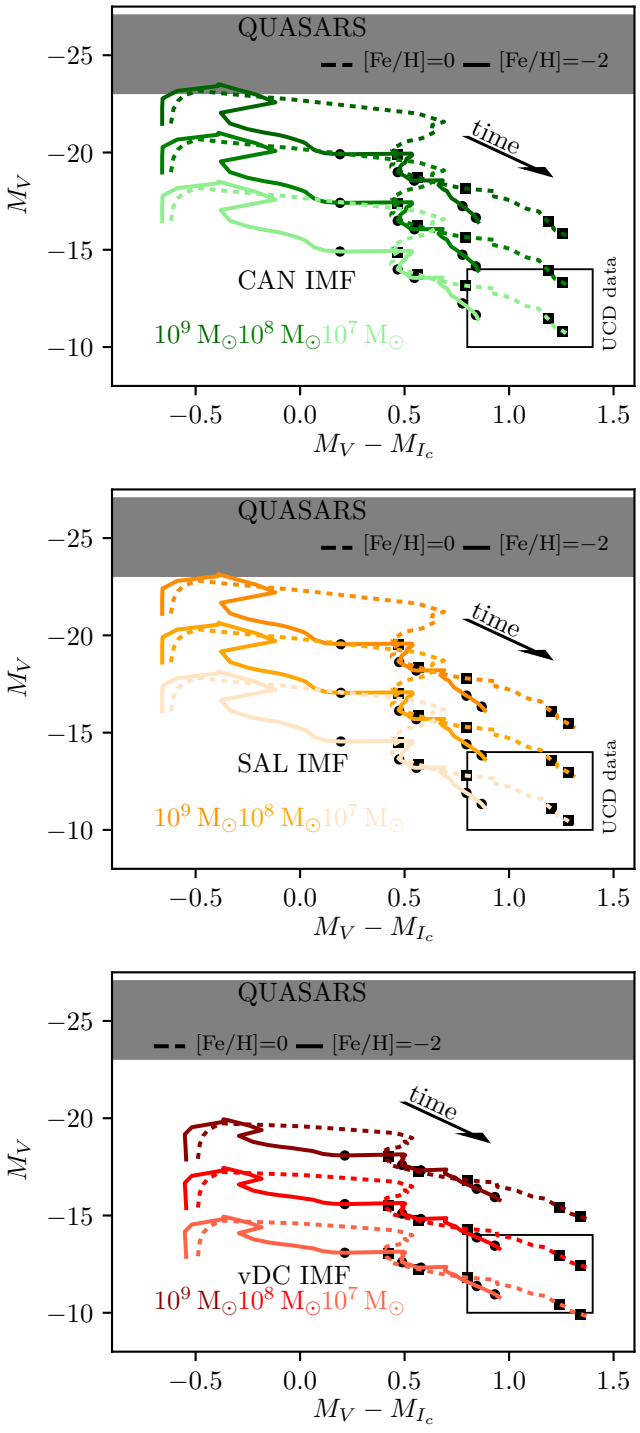

Figure 2.9: As Fig. 2.8 but for the CAN IMF **top panel**, the SAL IMF **middle panel** and the vDc IMF **bottom panel**.

instr.	filter	z	S/N CAN	S/N MKDP
NIRCam	F115W	3	47	194
NIRCam	F200W	3	47	215
NIRCam	F480M	3	7	52
MIRI	F1000W	3	0.4	4
NIRCam	F115W	6	14	76
NIRCam	F200W	6	15	83
NIRCam	F480M	6	2	16
MIRI	F1000W	6	0.1	1
NIRCam	F115W	9	6	36
NIRCam	F200W	9	7	42
NIRCam	F480M	9	1	7
MIRI	F1000W	9	0.06	0.5

Table 2.4: This table shows the predictions for different filters of the JWST telescope. All values are computed for an initial stellar mass of $10^8\,M_\odot$ and for reference the CAN IMF and the MKDP IMF are considered. The S/N values can be reached within a total integration time of ≈ 3 hours. See Sec. 2.3.6 for more details.

Mieske, 2012), while in self-regulated galaxies the distribution of star-formation-rate density may be more complex as a result of converging gas flows, e.g. at the intersection points between a disk and bar. Generally though, central regions are the most active in star-formation activity in star-forming galaxies. That the most massive clusters form near the centres of galaxies where the SFR-density is highest is evident in various starbursting galaxies (Ferrarese and Merritt, 2002; Dabringhausen, Kroupa, Pflamm-Altenburg, and Mieske, 2012), in our Galaxy (Stolte, Hußmann, Morris, et al., 2014) and also in young-cluster surveys of individual galaxies (Pflamm-Altenburg, González-Lópezlira, and Kroupa, 2013a). Simulations of star-forming galaxies led to the same result (Li, Gnedin, Gnedin, Meng, Semenov, and Kravtsov, 2017). Observationally it has been shown that the most massive clusters form preferentially in galaxies with the highest SFR (Weidner, Kroupa, and Larsen, 2004; Randriamanakoto, Escala, Väisänen, et al., 2013). We can therefore consider the following overall process: In the process of the formation of massive galaxies, star formation would have been spread throughout the merging proto-galactic gas clumps. The most massive clusters, the proto-UCDs, would be forming in the deepest potential wells of these, but would decouple from the hydrodynamics once they become stellar systems. As the proto-galaxies merge to form the massive central galaxies of galaxy clusters, many of such formed UCDs would end up on orbits about the central galaxy, possibly with the most massive UCDs within and near the centre of the galaxy.

We can therefore expect that the most massive UCDs, those that formed monolithically (i.e. according to formation scenario A), are to be found in the innermost regions of forming central-dominant galaxies at a high redshift. Such galaxies have been deduced to form on a timescale of and within less than a Gyr of the Big Bang with SFRs larger than a few $10^3\,M_\odot$/yr (Recchi, Calura, and Kroupa, 2009). Under more benign conditions, i.e. when the system-wide SFR is smaller as in later interacting galaxies or

the formation of less massive elliptical galaxies within a few Gyr of the Big Bang, UCDs may form also but are more likely to be the mergers of star-cluster complexes. Cases in point are the Antennae galaxies where such young complexes are evident (Kroupa, 1998; Fellhauer and Kroupa, 2002b) and the Tadpole galaxy (Kroupa, 2015).

Therefore, the best place to search for very massive UCDs is in the inner regions of extreme starbursts at very high redshift. Forming elliptical galaxies and bulges may also host young massive UCDs. If it were possible to observationally remove the gas and dust obscuration, then such systems are likely to look like brilliantly lit Christmas trees.

2.4.2 Which IMF is to be expected if the formation scenario (A) or (B) is realized?

If monolithic collapse (scenario A) applies, then according to Marks, Kroupa, Dabringhausen, and Pawlowski (2012) and Dabringhausen, Kroupa, Pflamm-Altenburg, and Mieske (2012) top-heavy MKDP IMFs are expected, which in turn led to larger M/L_V values at old ages (Fig. 2.4 and 2.5). At young ages such objects can be as bright as quasars (Fig. 2.3).

In the case of the formation of UCDs from merged cluster complexes (scenario B), the IMF in each sub-cluster would be closer to the canonical IMF. The IMF of a whole object would thus be less top-heavy (e.g. Pflamm-Altenburg, Weidner, and Kroupa, 2009; Weidner, Kroupa, Pflamm-Altenburg, and Vazdekis, 2013; Fontanot, De Lucia, Hirschmann, Bruzual, Charlot, and Zibetti, 2017; Yan, Jerabkova, and Kroupa, 2017), leading to smaller M/L_V ratios at old ages (Fig. 2.4 and 2.5). They are significantly less luminous than monolithically formed objects with MKDP IMFs (Fig. 2.3). Therefore the realization of both scenarios (A) and (B) in reality may lead to a spread of M/L_V values for present day UCDs, which may be comparable to the observed spread.

In the case of a bottom-heavy IMF one might expect similar behaviour, that is, if a UCD is created by a monolithic starburst the IMF may be more bottom-heavy than in the case of merged cluster complexes. Thus, for monolithically formed objects the M/L_V ratios are large at all ages (Fig. 2.4) while they would be sub-luminous for their mass (Fig. 2.3).

All these different IMF cases can be distinguished best when the objects are younger than 100 Myr as their luminosities and colours will be most different (Fig. 2.8, Fig. 2.9). Particularly useful observable diagnostic are provided by the color-color plots (Fig. 2.12) and the slope of the SED (Fig. 2.7).

2.4.3 The implications of observed M/L_V–ratios

The elevated M/L_V ratios observed for some UCDs can be caused by three, partially interconnected scenarios: (1) a variation of the IMF (top-heavy or bottom-heavy), (2) the presence of a super-massive black hole (SMBH), and (3) the presence of non-baryonic dark matter. Point (3) is directly connected to formation scenario (D) which is, as already mentioned, disfavoured for UCDs. As shown above, the variable IMF, scenario (1), can explain the observed elevated M/L_V values. The mass of a SMBH in scenario (2) required to explain the observed M/L_V values, needs typically to be 10-

15% of the present day UCD mass (Mieske, Frank, Baumgardt, Lützgendorf, Neumayer, and Hilker, 2013). The presence of SMBHs with such masses is indeed suggested or observationally confirmed at least for a few UCDs (e.g. Seth, van den Bosch, Mieske, et al., 2014; Janz, Forbes, Norris, et al., 2015; Ahn, Seth, Brok, et al., 2017).

To address which scenario (variation of IMF, (1), or presence of SMBH, (2)) is responsible for the elevated M/L_V values in different formation scenarios is not straightforward. In the case of formation scenario (C), where UCDs are tidally stripped nuclei, there is an observational connection with the presence of SMBHs. Graham and Spitler (2009) found that the existence of a SMBH in a galactic nuclear cluster is indeed frequently the case. However, since the exact formation mechanism of SMBHs is still discussed, it is not possible to constrain the IMF of UCDs formed by scenario (C). On the other hand, even though in formation scenarios (A) and (B), where UCDs are cluster-like objects and where the variable IMF is introduced to explain observed M/L_V values, the existence of a SMBH cannot be excluded. The SMBH can potentially be formed as a merger of dark remnants (Giersz, Leigh, Hypki, Lützgendorf, and Askar, 2015, Kroupa, et al., in prep.). If a standard IMF is assumed, the mass of dark remnants (BHs and neutron stars) represent approximately only 2% of the present day mass of a system. For a top-heavy IMF this fraction can be significantly higher.

2.5 Conclusions

We investigated if observations with upcoming observatories, with an emphasis on predictions for the JWST, may be able to discern the formation and evolution of UCDs assuming that they are cluster-like objects which form by (A) single monolithic collapse or (and) (B) by the merging of cluster complexes. The primary area of interest is to find observable diagnostics which may allow us to assess how the stellar IMF varies with physical conditions. The extreme starbursts, which massive GCs and UCDs must have been at a high redshift, may be excellent test beds for this goal. For this purpose we compute the time-dependent evolution of SEDs for different physical parameters and mainly for different IMFs. We test the top-heavy IMF, as parametrised by Marks, Kroupa, Dabringhausen, and Pawlowski (2012), which predicts a top-heavy IMF for the case of scenario (A) and an IMF closer to the canonical IMF in the case of scenario (B). The bottom-heavy IMFs are implemented as a single power law function with a slope -2.3 (Salpeter) and -3 (van Dokkum and Conroy, 2010).

The main conclusions concerning the formation scenario for UCDs and the stellar IMF variability can be summarized within five main points:

- The retention fraction of stellar remnants is near to 100% for systems with birth masses larger than $10^7\,M_\odot$.
- We show that if UCD progenitors younger than $\approx 100\,\mathrm{Myr}$ are observed, their stellar IMF can be constrained and therefore also the formation scenario by obtaining achievable measurements (e.g. absolute luminosity and supernova rate or an appropriate combination of colors and the value of β_{UV}). UCD progenitors most likely located at redshifts 3-9 have not been observed yet, however according to our predictions we should be able to detect them even with current telescopes as they would appear like point sources with high, quasar-like

luminosities. Computed exposure times for chosen JWST MIRI and NIRCam instruments are presented.

- We also discuss degeneracies which start appearing at ages $> 50\,\mathrm{Myr}$ as massive stars evolve into dark remnants and we reveal which information and constraints we can obtain from present day UCDs. That is, the object's luminosity with a top-heavy IMF starts to be comparable with a UCD of the same (or even smaller) initial mass but with a canonical or bottom-heavy IMF. Therefore, within observational uncertainties, these cases might be indistinguishable on color-magnitude or color-color diagrams. Even M/L_V becomes degenerate, however for the majority of cases we should be able to separate a vDC IMF from the rest if the metallicity of the UCD is constrained reasonably well.

- If UCDs were formed with a top-heavy IMF ($\alpha_3 < 2.3$ with the most extreme case considered $\alpha_3 = 0.6$) their progenitors are extreme and very different from Galactic star formation regions. The UCD progenitors with initial stellar masses of $\approx 10^9\,\mathrm{M}_\odot$ would contain $\approx 10^7$ O stars in a region spanning not more than a few pc. This drives a tremendous luminosity, very high SN II rates and also poses the further question as to how the strong radiation field influences the state and evolution of other stars and thus the IMF especially at the low-mass end (e.g. Kroupa and Bouvier, 2003).

- Interestingly, we have found evidence that some of the observed quasars have photometric properties of very young UCD models with top-heavy IMFs. This may suggest that some quasars at high redshift may actually be very massive UCDs with ages $< 10\,\mathrm{Myr}$. This needs further study though, e.g. by quantifications of SEDs. One method to help identifying true UCDs with top-heavy IMFs would be to monitor their luminosities. Since core-collapse supernovae will be common in such systems, exploding at a rate of more than one per year, the luminosity of such a UCD ought to show increases by $\approx 0.1 - 10$ per cent (depending on a star formation history, IMF and initial stellar mass) over a time-scale of a few months up to a few dozen times a year. Young UCDs should thus be time-variable.

- Groups of very young UCDs, if found at high redshift, may be indicating the assembly of the inner regions of galaxy clusters (see also Schulz, Hilker, Kroupa, and Pflamm-Altenburg, 2016): the assembly time-scale is $10^2\,\mathrm{Myr}$, being of the order of the dynamical time-scale. The seeds of the most massive galaxies in the center of galaxy clusters probably had a very clustered formation of UCD-mass objects that created today's giant ellipticals and brightest cluster galaxies. Thus, during the assembly of the inner region of galaxy clusters we would expect generations of quasar-like UCDs, each with a high luminosity and life-time of about $10\,\mathrm{Myr}$, forming such that the overall life-time of the UCD-active epoch would be about $10^2\,\mathrm{Myr}$. This is comparable to the life-time of quasars, adding to the above noted similarity in photometric properties.

- The majority of ultra-massive very young UCDs, which look comparable to quasars, are therefore likely to form in the central region of the starbursts from which the present-day central dominant elliptical galaxies emerge. But such

UCDs will not be observable today as they are likely to sink to the centres of the elliptical galaxies through dynamical friction (Bekki, 2010).

To gain more firm conclusions individual cases of observed UCDs need to be considered taking all observational constrains into account. To disentangle degeneracies which arise mainly with age, new data reporting UCDs younger than $\approx 100\,\mathrm{Myr}$ are needed. We would like to emphasize here that no such objects have been observationally confirmed yet knowingly.

Acknowledgements: *We thank the referee and Holger Baumgardt for useful comments which helped to improve this manuscript. TJ was supported by Charles University in Prague through grant SVV-260441 and through a stipend from the SPODYR group at the University of Bonn. TJ, PK a KB thank the DAAD (grant 57212729 "Galaxy formation with a variable stellar initial mass function") for funding exchange visits. We would like to acknowledge existence of Python (G. van Rossum, Python tutorial, Technical Report CS-R9526, Centrum voor Wiskunde en Informatica (CWI), Amsterdam, May 1995). Except from standard Python libraries we used pyPegase from Colin Jacobs. We also acknowledge discussions with Christopher Tout and many useful contributions seen during the ImBaSe 2017 conference in Garching.*

2.6 Appendix: Additional figures and procedures

To make the text of the main paper more continuous we present a selection of the figures in this Appendix.

At first we would like to present here redshift as a function of time from the Big-Bang. Even though this plot is elementary it is not straightforward to find it in other literature in this format. We marked the redshift-time points which are relevant for this study.

In addition, since the PEGASE SED's minimal wavelength is ≈ 1000 , and because at higher redshifts ($z \gtrapprox 6$) this region contributes to the standard optical filters, we extrapolate the computed SEDs at smaller wavelengths using a black-body approximation. Not to add an additional uncertainty to our results, we do not use the extrapolations for making any predictions or conclusions, but strictly as a demonstration of an approximate trend.

As a consistency check and also as a basic estimation of the difference between different stellar population codes we computed the same set of SEDs with the StarBurst99–code (Leitherer, Schaerer, Goldader, et al., 1999) online library. The results are plotted in Fig. 2.14 showing agreement in the general characteristic of the SED and in the time evolution. The maximum differences, estimated only in the region which is computed by PEGASE without extrapolating, reach a factor of a few and are expected since different stellar evolutionary tracks are used in both codes. These differences represent the minimal uncertainty which needs to be considered if our results are compared with observations.

The time evolution of SEDs for the MKDP IMF is plotted in Fig. 2.15 in comparison to the CAN IMF. The same time evolution for the vDC and SAL IMFs is plotted in Fig. 2.16 and Fig. 2.17. The wavelength shift and dimming proportional to the inverse square of luminosity distance with redshift is shown in Fig. 2.13.

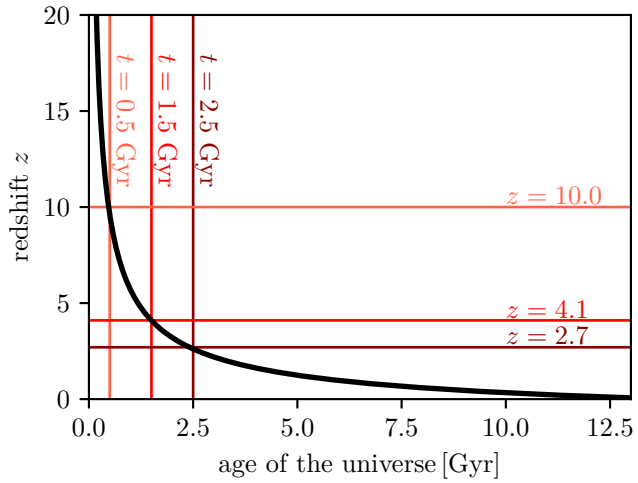

Figure 2.10: Redshift z as a function of time from the Big-Bang (age of the Universe) adopting for this study the standard ΛCDM cosmology with Planck parameters, see Sec. 2.2.1.

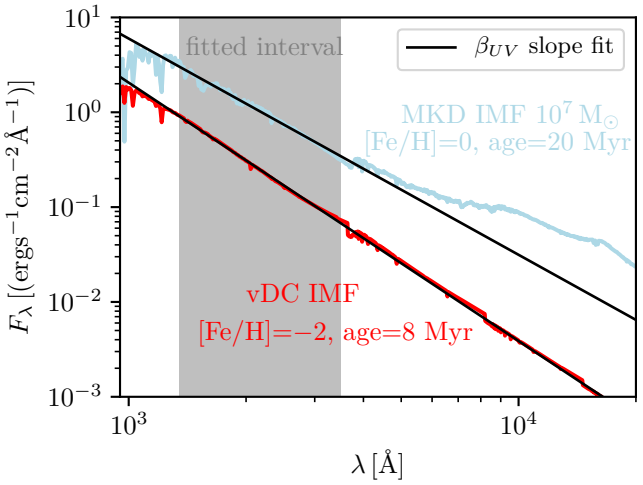

Figure 2.11: The fit to a SED in the gray shaded region shows the slope β_{UV} for two different UCDs with different age, the same mass $10^7\,M_\odot$ and different metallicity. We can see that in the gray region the spectra have a smooth shape and therefore it is possible to fit this part by a linear function to obtain a good estimate of β_{UV}. See Sec. 2.3.4 for more details.

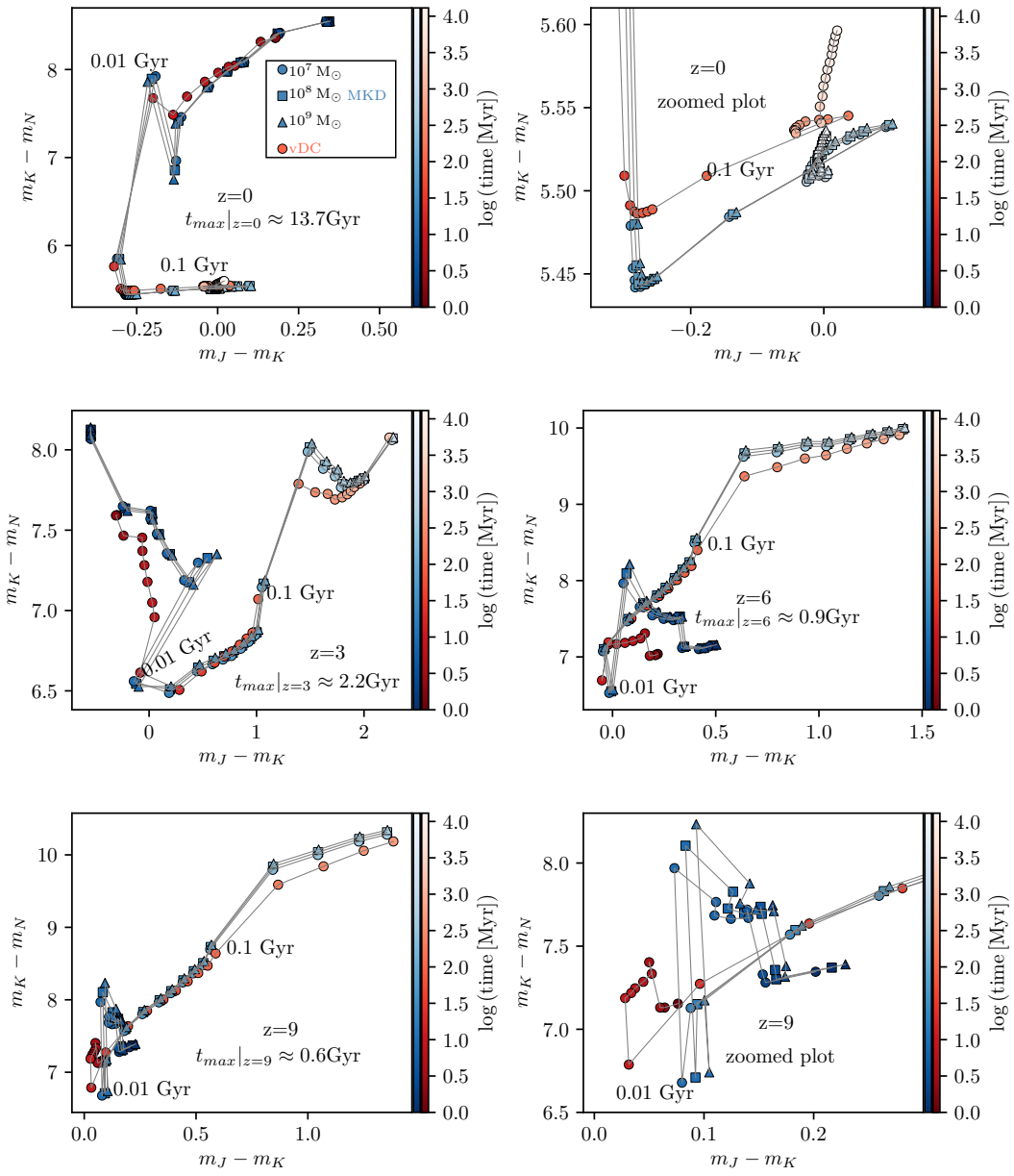

Figure 2.12: The color-color diagram made for standard filters J, K and N approximated here by rectangular boxes in Fig. 2.13 showing the comparison of the vDC IMF and the MKDP IMF for different initial UCD masses, M_{UCD}. Since according to the ΛCDM cosmological model the upper limit to the age of the universe is $t_{\max} \approx 13.7\,\mathrm{Gyr}$, we plot only ages consistent with this constraint on a corresponding redshift (here values are plotted at a redshift of 0, 3, 6 and 9). The age evolution is shown by a color scale which is the same for all plots.

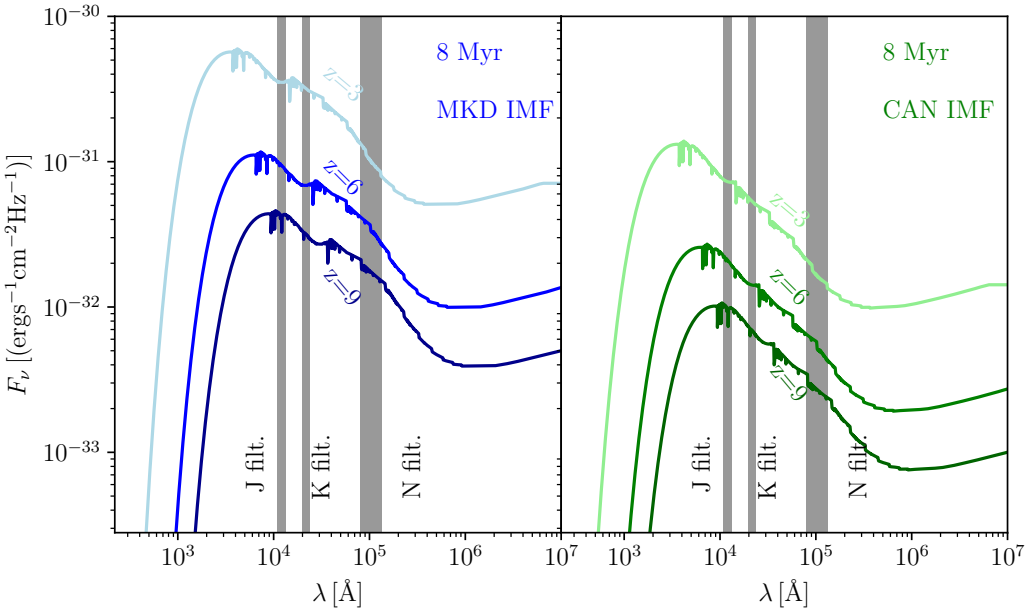

Figure 2.13: This plot shows SEDs of 8 Myr old UCDs at different redshifts. For this purpose we arbitrary chose the SED of an 8 Myr old stellar population with metallicity [Fe/H]=-2 and corrected the spectrum for the wavelength shift and luminosity fainting with luminosity distance for redshifts 3, 6 and 9. **Left panel:** shows the SEDs of the MKDP IMF and the **right panel** shows the those for the CAN IMF. The photometric filters, here approximated by rectangular profiles as shaded vertical regions, are shown. The J, K and N filters are used in the color analysis of the data.

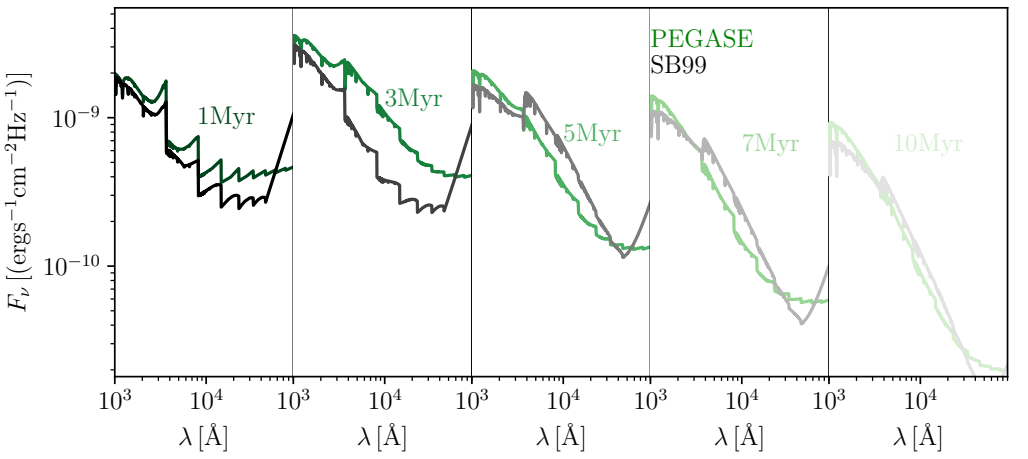

Figure 2.14: Time evolution of SEDs for a $10^9\,M_\odot$ system normalized to the distance of 10 pc for the Salpeter IMF slope $\alpha = 2.35$ within the mass range $(1{,}100)M_\odot$ and metallicity $Z = 0.001$. We compare computed PEGASE models and downloaded SB99 models with the same parameters. The SEDs are normalized to the distance of 10 pc. Note that the stellar mass range used here has been adopted only for this comparison for computational ease.

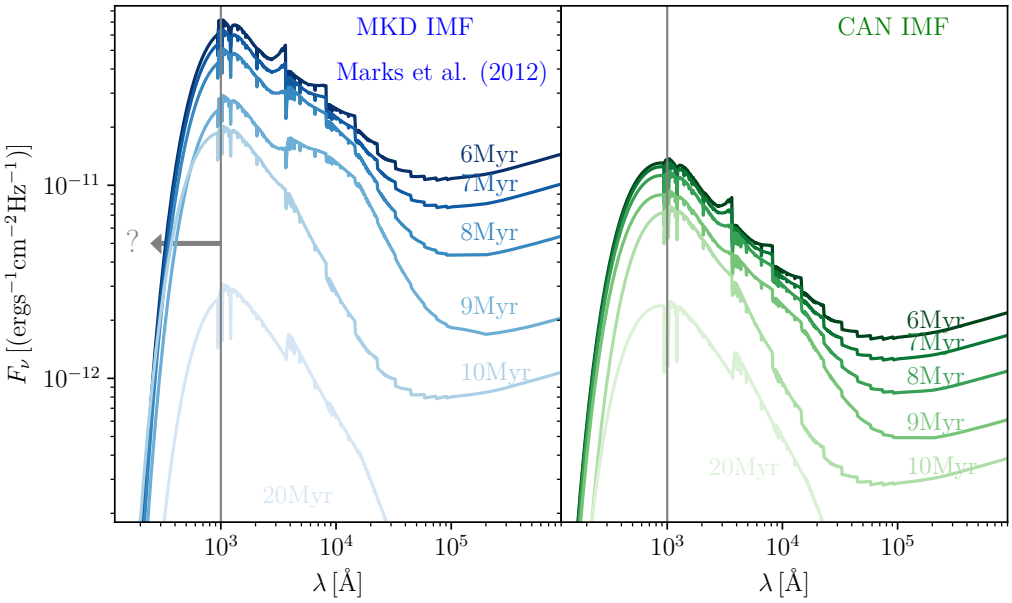

Figure 2.15: PEGASE time evolution of SEDs for [Fe/H]=-2 and a representative initial stellar mass of 10^7 $M_\odot$ as if it is at a distance of 10 pc. Since we assume that the star formation lasts for 5 Myr we start with the SED at 6 Myr to avoid overlapping of lines. **Left panel:** The evolution for the MKDP IMF. **Right panel** The evolution for the CAN IMF. The region below a wavelength of $\approx$ 1000 (marked by arrow and question mark) is the black-body approximation. The PEGASE code does not predict values in this region, for more details see the text.

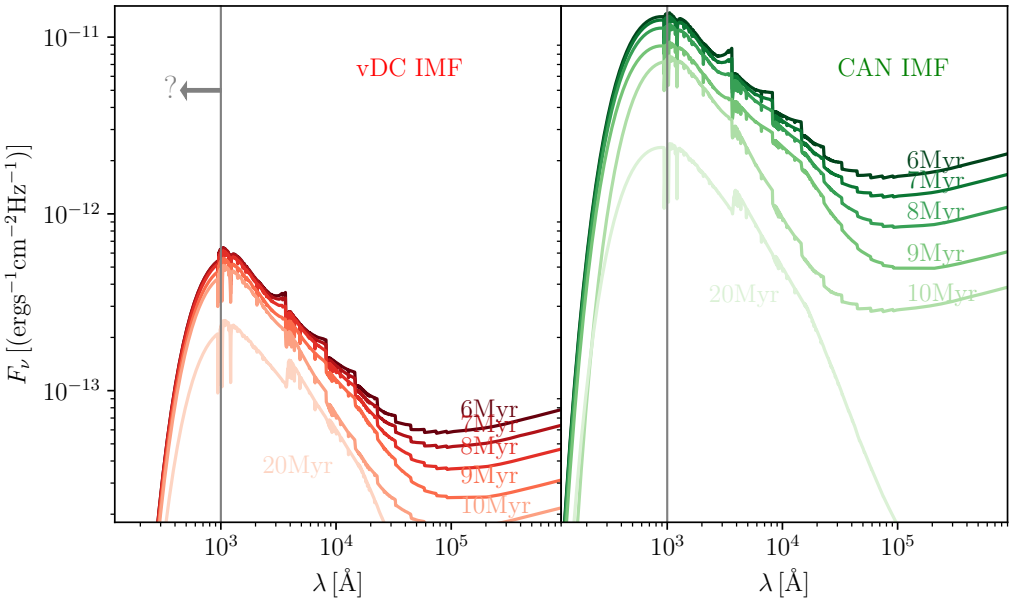

Figure 2.16: As Fig. 2.15 but for the vDC IMF (**left panel**), with the CAN IMF (**right panel**, identical to Fig. 2.15) is shown here as a benchmark.

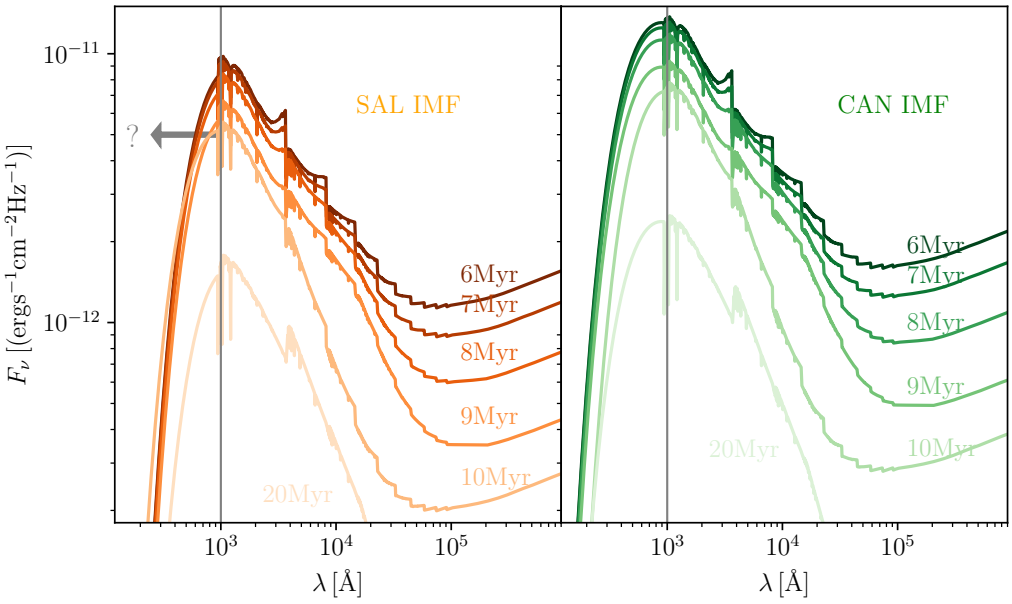

Figure 2.17: As Fig. 2.15 but for the SAL IMF (**left panel**), with the CAN IMF (**right panel**, identical to Fig. 2.15) is shown here as a benchmark.

Chapter 3

Impact of metallicity and star formation rate on the time-dependent, galaxy-wide stellar initial mass function

This chapter is based on the publication Jeřábková, Hasani Zonoozi, Kroupa, et al. (2018) with the same title "Impact of metallicity and star formation rate on the time-dependent, galaxy-wide stellar initial mass function". Only minor changes concerning formatting were made in order to present it as a chapter in the thesis.

Abstract: *The stellar initial mass function (IMF) is commonly assumed to be an invariant probability density distribution function of initial stellar masses. These initial stellar masses are generally represented by the canonical IMF, which is defined as the result of one star formation event in an embedded cluster. As a consequence, the galaxy-wide IMF (gwIMF) should also be invariant and of the same form as the canonical IMF; gwIMF is defined as the sum of the IMFs of all star-forming regions in which embedded clusters form and spawn the galactic field population of the galaxy. Recent observational and theoretical results challenge the hypothesis that the gwIMF is invariant. In order to study the possible reasons for this variation, it is useful to relate the observed IMF to the gwIMF. Starting with the IMF determined in resolved star clusters, we apply the IGIMF-theory to calculate a comprehensive grid of gwIMF models for metallicities,* $[\mathrm{Fe/H}] \in (-3, 1)$*, and galaxy-wide star formation rates (SFRs),* $\mathrm{SFR} \in (10^{-5}, 10^{5})\,\mathrm{M_\odot/yr}$*. For a galaxy with metallicity [Fe/H]*< 0 *and SFR*$> 1\,M_\odot/yr$*, which is a common condition in the early Universe, we find that the gwIMF is both bottom light (relatively fewer low-mass stars) and top heavy (more massive stars), when compared to the canonical IMF. For a SFR* $< 1\,\mathrm{M_\odot/yr}$ *the gwIMF becomes top light regardless of the metallicity. For metallicities* $[\mathrm{Fe/H}] > 0$ *the gwIMF can become bottom heavy regardless of the SFR. The IGIMF models predict that massive elliptical galaxies should have formed with a gwIMF that is top heavy within the first few hundred Myr of the life of the galaxy and that it evolves into a bottom heavy gwIMF in the metal-enriched galactic centre.*

3.1 Introduction

The stellar initial mass function (IMF) is a theoretical representation of the number distribution of stellar masses at the births of stars formed in one star formation event.

The IMF is often described as $\xi_\star(m) = \mathrm{d}N/\mathrm{d}m$, where $\mathrm{d}N$ is the number of stars formed locally[1] in the mass interval m to $m+\mathrm{d}m$. The IMF can be mathematically expressed conveniently in the form of a multi-power law with indices $\alpha_1^{\rm can} \approx 1.3$ for stars in the mass range $0.1 - 0.5\,M_\odot$ and $\alpha_2^{\rm can} \approx 2.3$ for stars more massive than $0.5\,M_\odot$. The fact that this canonical stellar IMF is an invariant probability density distribution function of stellar masses is usually considered to be a null hypothesis and a benchmark for stellar population studies (e.g. Selman and Melnick, 2008; Kroupa, Weidner, Pflamm-Altenburg, et al., 2013; Offner, Clark, Hennebelle, et al., 2014; Jeřábková, Kroupa, Dabringhausen, Hilker, and Bekki, 2017; Kroupa and Jerabkova, 2018).

The detailed form of the IMF is relevant for almost all fields related to star formation, thus it has important implications for the luminous, dynamical, and chemical evolution of stellar populations. In studies of both Galactic and extragalactic integrated systems, an IMF needs to be assumed to derive star formation rates (SFRs) by extrapolating from massive stars that always dominat luminosities. The IMF is therefore a fundamental entity entering directly or indirectly into many astrophysical problems (e.g. Kroupa, 2002a; Chabrier, 2003; Bastian, Covey, and Meyer, 2010; Kroupa, Weidner, Pflamm-Altenburg, et al., 2013; Offner, Clark, Hennebelle, et al., 2014; Hopkins, 2018). Observational studies of nearby star-forming regions suggest that stars form in dense cores inside molecular clouds (Lada and Lada, 2003; Lada, 2010; Kirk and Myers, 2011; Gieles, Moeckel, and Clarke, 2012; Kirk and Myers, 2012; Megeath, Gutermuth, Muzerolle, et al., 2016; Stephens, Gouliermis, Looney, et al., 2017; Ramírez Alegría, Borissova, Chené, et al., 2016; Hacar, Alves, Tafalla, and Goicoechea, 2017; Lucas, Rybak, Bonnell, and Gieles, 2018) usually following the canonical stellar IMF (e.g. Kroupa, 2002a; Chabrier, 2003; Bastian, Covey, and Meyer, 2010; Kroupa, Weidner, Pflamm-Altenburg, et al., 2013).

The canonical stellar IMF is derived from observations of field stars and nearby star-forming regions that form stars in local over-densities called embedded star clusters or correlated star formation events (CSFEs), which are approximately 1 pc across and form a population of stars on a timescale of 1 Myr (Kroupa, Weidner, Pflamm-Altenburg, et al., 2013; Yan, Jerabkova, and Kroupa, 2017 and references therein). The molecular clouds as a whole are not self-gravitationally bound in the majority of cases (Hartmann, Ballesteros-Paredes, and Bergin, 2001; Elmegreen, 2002; Elmegreen, 2007; Ballesteros-Paredes, Klessen, Mac Low, and Vazquez-Semadeni, 2007; Dobbs, Burkert, and Pringle, 2011; Lim, Sung, Bessell, et al., 2018). However, their complex filamentary substructures on sub-parsec scales can be locally gravitationally bound and also gravitationally unstable (Hacar, Alves, Tafalla, and Goicoechea, 2017; Hacar, Tafalla, and Alves, 2017), which may set the initial conditions for the formation of stars. Star formation happens in correlated dense regions of molecular gas, which have intrinsic physical connections instead of being distributed randomly inside molecular clouds (e.g. Joncour, Duchêne, Moraux and, and Motte, 2018). For practical purposes we refer to these CSFEs as embedded clusters. For the computations of gwIMF only the stellar census matters. Nevertheless the initial conditions in star-forming regions are relevant to interpret observations of stellar populations in galaxies. The CSFEs and embed-

[1] We note that we use "local" to mean a small region in a galaxy and in this case an embedded-cluster-forming molecular cloud core. It is not the solar neighbourhood.

ded clusters are potentially dynamically very active (Kroupa and Boily, 2002; Kroupa, 2005; Oh, Kroupa, and Pflamm-Altenburg, 2015a; Oh and Kroupa, 2016a; Brinkmann, Banerjee, Motwani, and Kroupa, 2017)[2] . Thus they spread their stars out through the star-forming regions and later to the galactic field very quickly within fractions of a Myr. Therefore, the dynamical processes on a star cluster scale need to be taken into account to obtain a physically correct picture of young stellar populations and of their distribution.

Increasing observational evidence suggests that star formation is a self-regulated process rather than a purely stochastic process (Papadopoulos, 2010; Kroupa, Weidner, Pflamm-Altenburg, et al., 2013; Kroupa, 2015; Yan, Jerabkova, and Kroupa, 2017; Lim, Sung, Bessell, et al., 2018; Plunkett, Fernández-López, Arce, Busquet, Mardones, and Dunham, 2018). The idea that the star formation efficiency of embedded clusters is found, both observationally and theoretically, to be less than 30-40 per cent (Adams and Fatuzzo, 1996; Lada and Lada, 2003; Lada, 2010; Hansen, Klein, McKee, and Fisher, 2012; Machida and Matsumoto, 2012; Federrath, Schrön, Banerjee, and Klessen, 2014; Federrath, 2015; Megeath, Gutermuth, Muzerolle, et al., 2016) supports self-regulation. The gravitational collapse of an embedded-cluster forming cloud core leads to star formation that heats, ionizes, and removes gas from the core. This may be one reason why a relation between a most massive star and an embedded cluster mass might exist (Weidner, Kroupa, and Bonnell, 2010).

For nearby resolved star-forming regions, the IMF can be understood as describing a single star formation event happening on a physical scale of about 1 pc and beyond this scale the molecular gas is gravitationally unstable and would form individual embedded clusters or small groups of stars. However, it is non-trivial to calculate the IMF of an unresolved stellar population, for example, of a whole galaxy because it contains many stellar clusters formed at different times. The galaxy-wide IMF (gwIMF) is, on the other hand, the sum of all the IMFs of all star-forming regions belonging to a given galaxy (e.g. Kroupa and Weidner, 2003a; Weidner, Kroupa, Pflamm-Altenburg, and Vazdekis, 2013; Kroupa, Weidner, Pflamm-Altenburg, et al., 2013; Yan, Jerabkova, and Kroupa, 2017, see also Fig. 3.1). Assuming that the canonical IMF is a universal probability density distribution function, the shape of the gwIMF should be equal to that of the canonical IMF. On the other hand, if the gwIMF differs from the canonical IMF, then the canonical IMF cannot be universal and/or it cannot be described as a stationary probability density distribution function.

Therefore, a fundamental question naturally arises: Is the stellar IMF a universal probability density distribution function (Kroupa, Weidner, Pflamm-Altenburg, et al., 2013)? An overabundance of low-mass stars ($< 1\,M_\odot$) with respect to the canonical stellar IMF is called a *"bottom-heavy"* IMF and a deficit of low-mass stars is a *"bottom-light"* IMF. For the massive stars ($> 1\,M_\odot$), an overabundance or deficit of stars relative to the canonical IMF results in a *"top-heavy"* and a *"top-light"* IMF, respectively. Studies of globular clusters, ultra-compact dwarf galaxies, and young massive clusters have suggested that in a low metallicity and high gas-density environment

[2]The Nbody star cluster evolution computations available on youtube, "Dynamical ejection of massive stars from a young star cluster" by Seungkyung Oh based on Oh, Kroupa, and Pflamm-Altenburg (2015a) and Oh and Kroupa (2016a), demonstrate how dynamically active the binary-rich very young clusters are in dispersing their stars to relatively large distances.

the stellar IMF may become top heavy (e.g Dabringhausen, Kroupa, and Baumgardt, 2009; Dabringhausen, Kroupa, Pflamm-Altenburg, and Mieske, 2012; Marks, Kroupa, Dabringhausen, and Pawlowski, 2012; Zonoozi, Haghi, and Kroupa, 2016; Haghi, Khalaj, Hasani Zonoozi, and Kroupa, 2017; Kalari, Carraro, Evans, and Rubio, 2018; Schneider, Sana, Evans, et al., 2018), while being bottom heavy in metal-rich ($Z > Z_{\odot}$) environments (Kroupa, 2002a; Marks and Kroupa, 2012). Such bottom-heavy IMFs have been found in the centre of nearby elliptical galaxies, where the metallicities are higher than $Z_{\odot}$ (van Dokkum and Conroy, 2010; Conroy, van Dokkum, and Villaume, 2017). The progenitors of elliptical galaxies, on the other hand, have been suggested to have had top-heavy gwIMFs based on the evolution of their chemical composition (Matteucci, 1994; Vazdekis, Peletier, Beckman, and Casuso, 1997; Weidner, Kroupa, Pflamm-Altenburg, and Vazdekis, 2013; Ferreras, Weidner, Vazdekis, and La Barbera, 2015; Martín-Navarro, 2016). Top-heavy gwIMFs are often found in galaxies with high SFRs (Gunawardhana, Hopkins, Sharp, et al., 2011; Fontanot, De Lucia, Hirschmann, Bruzual, Charlot, and Zibetti, 2017; De Masi, Matteucci, and Vincenzo, 2018; Zhang, Romano, Ivison, Papadopoulos, and Matteucci, 2018; Fontanot, La Barbera, De Lucia, Pasquali, and Vazdekis, 2018; Fontanot, De Lucia, Xie, Hirschmann, Bruzual, and Charlot, 2018), while top-light gwIMFs are evident in galaxies with low SFRs (e.g. Lee, Gil de Paz, Tremonti, et al., 2009; Meurer, Wong, Kim, et al., 2009; Watts, Meurer, Lagos, Bruzzese, Kroupa, and Jerabkova, 2018). The new method of tracing the variation of the gwIMF using observations of CNO isotopes in the molecular ISM with ALMA is interesting in this context and shows highly consistent results with the gwIMF theory (Papadopoulos, 2010; Romano, Matteucci, Zhang, Papadopoulos, and Ivison, 2017; Zhang, Romano, Ivison, Papadopoulos, and Matteucci, 2018). All this work suggests that gwIMF is not in a constant form and that it deviates from the canonical IMF, depending on star formation activity. These new findings challenge the idea that the IMF is a universal probability density distribution function.

We study the variation of the gwIMF using the integrated galaxy-wide IMF (IGIMF) theory (Kroupa and Weidner, 2003a; Kroupa, Weidner, Pflamm-Altenburg, et al., 2013; Yan, Jerabkova, and Kroupa, 2017). In this theory, the model of the gwIMF, i.e. the IGIMF, is constructed by summing (i.e. integrating) the IMFs of all star formation events in the whole galaxy at a given time. This results in a dependency of the gwIMF on the galaxy-wide SFR and metallicity and therefore also on the time.

With this contribution we investigate the full range of IGIMF variation. The novel aspect is the incorporation of the metallicity dependence of the IMF, as deduced by Marks, Kroupa, Dabringhausen, and Pawlowski (2012) based on a stellar-dynamical study of evolved globular clusters, which also took into account constraints from ultra-compact dwarf galaxies by Dabringhausen, Kroupa, and Baumgardt (2009), Dabringhausen, Fellhauer, and Kroupa (2010) and Dabringhausen, Kroupa, Pflamm-Altenburg, and Mieske (2012). These constraints on how the IMF varies with local physical conditions are independent from any variation of the gwIMF deduced from observation. Thus, if the observed variation of the gwIMF can be accounted for with these IMF variations then this will play an important role in the convergence of our understanding of stellar populations over cosmic time.

Section 2 defines and clarifies terminology used in the paper. Section 3 explains the IGIMF theory and its implementations. In Section 4, we present our results by

introducing a parametrized grid of gwIMFs. The implications include the evolution of the gwIMF in elliptical galaxies, quantifying the correction factors for Hα-based SFR estimators, the case of the Leo P dwarf galaxy and its very low SFR and massive star population, the baryonic Tully-Fisher relation (BTFR), and ultra-faint dwarf (UFD) galaxy satellites. In Sec. 5 additional discussion is provided and Sec. 6 contains the conclusions. We emphasize that this is the first time that a full grid of IGIMFs, with dependency on the galaxy-wide SFR and galaxy metallicity, has been made available.

3.2 Terminology

In the manuscript we frequently use four acronyms referring to the stellar initial mass function, i.e. IMF, cIMF, gwIMF, and IGIMF. The IMF represents the stellar initial mass function of stars formed during one star formation event in an initially gravitationally collapsing region in a molecular cloud (timescale $\approx$ 1 Myr, spatial scale $\approx$ 1 pc), that is in an embedded cluster. The cIMF represents the sum of the IMFs over a larger region, such as whole T Tauri and OB associations or even a larger part of a galaxy. The gwIMF is the initial stellar mass function of newly formed stars in a whole galaxy formed over a timescale $\delta t \approx 10$ Myr (see Sec. 3.3.2) and can be inferred from observations or can be computed. The IGIMF is the theoretical framework that allows us to compute the gwIMF. For clarity the acronyms are summarized in Tab. 3.1. We use the term cIGIMF to refer to a theoretical formulation of the cIMF within the IGIMF framework. Once the region of interest is bigger than several molecular clouds (about $>$ 100 pc) the timescale δt would not change since the lifetime of molecular clouds is about 10 Myr.

We emphasize that it is important to distinguish between the IMF, cIMF, and gwIMF. This is because only if the star formation process is stochastically invariant, in the sense that once stars begin to form then the mass of the star is not related to the local physical conditions, will the IMF be an invariant probability density distribution function. If however, the mass of the born star (which assembles to within about 95 per cent of its main-sequence value within about 10^5 yr, Wuchterl and Tscharnuter, 2003; Duarte-Cabral, Bontemps, Motte, Hennemann, Schneider, and André, 2013) depends on the local conditions, then the IMF is not an invariant probability density distribution function. If the physical conditions in a embedded-cluster-forming molecular cloud core differ from those in another molecular cloud core, then the distribution of stellar masses also differ. The recent ALMA observation of an extremely young embedded cluster shows the millimetre sources to be nearly perfectly mass-segregated, suggesting that local physical conditions are probably very important in determining which stars form (Plunkett, Fernández-López, Arce, Busquet, Mardones, and Dunham, 2018). A variation of the IMF with physical conditions has been expected from basic theory (see e.g. the discussion in Kroupa, Weidner, Pflamm-Altenburg, et al., 2013), but resolved observations of star-forming regions in the Local Group have been indicating that the variations, if they exist, are not detectable (Kroupa, 2001; Kroupa, 2002a; Bastian, Covey, and Meyer, 2010).

Thus, if the IMF is not an invariant probability density distribution function, then the sum of two star-forming events is not the same as a larger event with the same

Acronym	Explanation
IMF	stellar initial mass function of stars formed during one star formation event in an initially gravitationally bound region
cIMF	the sum of the IMFs over larger regions within a galaxy
gwIMF	initial stellar mass function of *newly* formed stars in a whole galaxy
IGIMF	theoretical framework that allows us to compute the gwIMF
cIGIMF	cIMF computed withing IGIMF framework
caninvgwIMF	gwIMF is invariant and equal to the invariant canonical stellar IMF

Table 3.1: Initial mass function acronyms summary. This table summarizes the acronyms and variables used in this paper to characterize initial stellar masses of stellar populations over different scales. As *newly* we assume the timescale $\delta t = 10\,\mathrm{Myr}$ (Sec. 3.3.2) in this text. We note that the conservative benchmark or null hypothesis to compare models with is the assumption that gwIMF=stellar IMF, assuming in this particular case that the stellar IMF is an invariant scale-free probability density distribution function. That is, in this case gwIMF is referred to as the canonical invariant gwIMF (caninvgwIMF) case. We also note that "local" is used throughout this text to mean a small region in a galaxy. It is not the solar neighbourhood.

number of stars. The composite and galaxy-wide IMF in this case differs from the IMF. An explicit observational example of this is reported for the Orion A cloud by Hsu, Hartmann, Allen, et al. (2012). The physical and empirical evidence thus suggests that the gwIMF should vary. The alternative, benchmark conservative model is to treat the IMF as a scale-free invariant probability density distribution function and to set gwIMF=stellar IMF taking into account the appropriate normalization. This conservative hypothesis is referred to as the caninvgwIMF hypothesis according to which gwIMF is equal in form to the invariant canonical stellar IMF.

3.3 Methods

The IGIMF theory is based on several assumptions that are described below in detail. We consider possible variations resulting in several different formulations that are all considered in this work. The assumptions, or axioms, are also detailed in Recchi and Kroupa (2015).

In a nutshell, the IGIMF theory spatially integrates over the whole galaxy by summing the local galactic star-forming regions to obtain the gwIMF (of the newly formed stellar population) in a given time interval δt (see Sec. 3.3.2). Two approaches exist: In this work (as well as in Yan, Jerabkova, and Kroupa, 2017), the first approach is used according to which the galaxy is treated as one unresolved object in which the integration over all freshly formed embedded clusters is performed without taking into account their spatial position and individual chemical properties. In this IGIMF approach the gwIMF is calculated at a particular time assuming all embedded clusters

Acronym	Physical meaning
m	integration ($\int$) variable for stellar mass
$m_{\rm max}$	$\int$ upper limit for stellar mass
$m_{\rm min}$	$\int$ lower limit for stellar mass
m	stellar mass
M	$\int$ variable for stellar mass of EC
$M_{\rm max}$	$\int$ upper limit for stellar mass of EC mass
$M_{\rm min}$	$\int$ lower limit for stellar mass of EC mass
$M_{\rm ecl}$	stellar mass of EC
$M_{\rm ecl,max}$	most massive EC mass
$M_{\rm cl}$	mass of the pre-cluster molecular cloud
SFR	galaxy-wide SFR

Table 3.2: Physical meanings of acronyms and model parameters. This table summarizes the used variables in this paper, which are the same as in Yan, Jerabkova, and Kroupa (2017). We note embedded cluster as EC in the table.

have the same metallicity. The second, spatially resolved approach has also been pioneered (Pflamm-Altenburg and Kroupa, 2008a) and in principle allows the embedded clusters to have different metallicities.

In both approaches, the IMF in an individual embedded cluster follows the empirical parametrization from mostly nearby (Galactic) observations of resolved stellar populations and varies with initial volume gas density of the embedded-cluster-forming cloud core or clump and its metallicity (Marks, Kroupa, Dabringhausen, and Pawlowski, 2012; Marks and Kroupa, 2012). The cosmological principle is assumed in that the physical variations and associated IMF variations apply to the early Universe as well. That is, we assume that embedded clusters with the same mass, metallicity, and density yield the same IMF independent of at which redshift they are found. The integration over the freshly formed IMFs results in a gwIMF that varies with SFR and metallicity. In the IGIMF theory, gwIMF variations are driven by the physics of the embedded cluster scales. An important aspect of the IGIMF is therefore that it is automatically consistent with the stellar populations in star clusters.

The calculations presented in this work deal with the first approach and are mainly based on the publicly available python module GalIMF (Yan, Jerabkova, and Kroupa, 2017) in which the implementation of the IGIMF theory is described in more detail. An equivalent FORTRAN package is also available (Hasani Zonoozi, Mahani, and Kroupa, 2018, https://github.com/ahzonoozi/GWIMF). Throughout this text we use log or $\log_{10}$ independently and always refer to the decimal logarithm.

3.3.1 Star-forming regions in a galaxy

Observational evidence shows that star formation is always concentrated in small (sub-parsec scale), dense ($> 10^3\,{\rm cm}^{-3}$) and massive H2 cores within molecular clouds (Tafalla, Myers, Caselli, Walmsley, and Comito, 2002; Wu, Evans, Shirley, and Knez, 2010; Joncour, Duchêne, Moraux and, and Motte, 2018). We refer to the star-forming cloud cores as correlated star formation events (CSFEs). Depending on their density

(and thus mass), these CSFEs form from a few binaries to millions of stars. For practical purposes they can be called embedded clusters or clumps (Lada and Lada, 2003; Lada, 2010; Gieles, Moeckel, and Clarke, 2012; Megeath, Gutermuth, Muzerolle, et al., 2016; Kroupa, Jeřábková, Dinnbier, Beccari, and Yan, 2018) even though the definition of star cluster is neither precise nor unique (Bressert, Bastian, Gutermuth, et al., 2010; Ascenso, 2018). For example, the low- and high-density star formation activity in the Orion A and B molecular clouds is organized in such CSFEs (fig. 8 in Megeath, Gutermuth, Muzerolle, et al., 2016). The important point, however, independent of whether these CSFEs are called embedded clusters or just stellar groups or NESTS (Joncour, Duchêne, Moraux and, and Motte, 2018) is that these form a co-eval (within a few 0.1 Myr) population of stars that can be described using the stellar IMF. For simplicity we refer to the newly formed stellar groups and CSFEs as embedded clusters.

A visualization of a newly formed stellar population is shown as a sketch in Fig. 3.1 in which the right panels illustrate how different individual star-forming regions can be. The massive cluster containing many O stars most likely survive as an open cluster (Kroupa, Aarseth, and Hurley, 2001; Brinkmann, Banerjee, Motwani, and Kroupa, 2017). Low-mass embedded clusters or groups, on the other hand, dissolve quickly owing to loss of their residual gas (Brinkmann, Banerjee, Motwani, and Kroupa, 2017) and energy-equipartition driven evaporation (Binney and Tremaine, 1987; Heggie and Hut, 2003; Baumgardt and Makino, 2003). Examples of this range of embedded clusters can be seen in Orion (Megeath, Gutermuth, Muzerolle, et al., 2016), each having spatial dimensions comparable to the molecular cloud filaments and the intersection thereof (André, Revéret, Könyves, et al., 2016; Lu, Zhang, Liu, et al., 2018).

In general the sum of outflows and stellar radiation compensate the depth of the gravitational potential of the embedded cluster and individual protostars such that star formation in the embedded clusters is feedback regulated. Indeed, observational evidence shows that the majority of gas is expelled from massive star-forming cores (e.g. in Orion A and B the star formation efficiency is less than about 30 per cent per embedded cluster, Megeath, Gutermuth, Muzerolle, et al., 2016). Observations of outflows from embedded clusters document this in action (Whitmore, Zhang, Leitherer, Fall, Schweizer, and Miller, 1999; Zhang, Fall, and Whitmore, 2001; Smith, Stassun, and Bally, 2005; Qiu, Zhang, Beuther, and Yang, 2007; Qiu, Zhang, Megeath, et al., 2008; Qiu, Zhang, and Menten, 2011). Magnetohydrodynamical simulations (Machida and Matsumoto, 2012; Bate, 2014; Federrath, Schrön, Banerjee, and Klessen, 2014; Federrath, 2015; Federrath, 2016) also led to the same result. Well-observed CSFEs, for example, the Orion nebula cluster, Pleiades, NGC3603, and R136, span a stellar mass range from a few 10 to a few $10^5\,M_\odot$ in stars. Their dynamics can be well reproduced in N-body simulations with a star formation efficiency ≈ 33 per cent, 10 km/s gas expulsion, and 0.6 Myr for the typical embedded phase (Kroupa and Bouvier, 2003; Kroupa, Aarseth, and Hurley, 2001; Banerjee and Kroupa, 2013; Banerjee and Kroupa, 2014; Banerjee and Kroupa, 2015; Banerjee, 2017).

Observations suggest that even T Tauri associations lose their residual gas on a timescale of about a Myr (Neuhäuser, Frink, Röser, et al., 1998), which is supported by magnetohydrodynamic radiative transfer simulations by Hansen, Klein, McKee, and Fisher (2012). Given the loss of about two-thirds of the binding mass, embedded clusters expand by a factor of three to five owing to the expulsion of most of their gas

such that embedded clusters with a stellar mass smaller than about $10^4\,M_\odot$ lose more than 60 per cent of their stars; the rest re-virialize to form longer lived low-mass open clusters (Brinkmann, Banerjee, Motwani, and Kroupa, 2017). This implies that embedded clusters that are typical in molecular clouds become unbound within less than a Myr, forming stellar associations if multiple embedded clusters spawn from one molecular cloud (e.g. also Lim, Sung, Bessell, et al., 2018). The observed properties of OB associations are further established by stars being efficiently ejected from their embedded clusters (Oh, Kroupa, and Pflamm-Altenburg, 2015b; Oh and Kroupa, 2016b). Interesting in this context is that a recent study was able to identify a complex expansion pattern consisting of multiple expanding substructures within the OB association Scorpius-Centaurus using Gaia data (Wright and Mamajek, 2018, e.g. their Fig 11).

3.3.2 Assumptions

1. Embedded cluster initial mass function (ECMF)

The embedded cluster initial mass function (ECMF) represents the population mass distribution, $\xi_{\rm ecl}$, of the birth star cluster, which was formed in one formation timescale throughout a galaxy (δt, see Paragraph 2 below). In the present IGIMF implementation, based on the available data (Yan, Jerabkova, and Kroupa, 2017 and references therein), it is assumed that the ECMF is represented by a single power law with a slope β as a function of galactic SFR,

$$\xi_{\rm ecl}(M_{\rm ecl},{\rm SFR}) = \begin{cases} 0, & M \leq M_{\rm ecl,min}\,, \\ k_{\rm ecl} M^{-\beta({\rm SFR})}, & M_{\rm ecl,min} \leq M_{\rm ecl} < M_{\rm ecl,max}({\rm SFR})\,, \\ 0, & M_{\rm ecl,max}({\rm SFR}) \leq M_{\rm ecl}\,, \end{cases} \tag{3.1}$$

where $M_{\rm ecl,min} = 5\,M_\odot$ is the lower limit of the mass in stars of the embedded cluster (Kirk and Myers, 2012; Kroupa and Bouvier, 2003), $M_{\rm ecl,max}$ is the upper limit for the stellar mass of the embedded cluster because it is computed within the IGIMF theory (see Schulz, Pflamm-Altenburg, and Kroupa, 2015; Yan, Jerabkova, and Kroupa, 2017), and $k_{\rm ecl}$ is a normalization constant. If $\mathrm{d}N$ is the number of embedded cluster with masses in stars between $M_{\rm ecl}$ and $M_{\rm ecl} + \mathrm{d}M_{\rm ecl}$ values, then $\xi_{\rm ecl} = \mathrm{d}N_{\rm ecl}/\mathrm{d}M_{\rm ecl}$.

The detailed shape of the ECMF might be different from the assumption of a single power law (e.g. Lieberz and Kroupa, 2017), however such a change can be easily incorporated into the IGIMF framework and is not expected to cause significant differences from the results presented in this work. The dependence of β on SFR is described by the relation (Weidner, Kroupa, and Larsen, 2004; Weidner, Kroupa, and Pflamm-Altenburg, 2013; Yan, Jerabkova, and Kroupa, 2017),

$$\beta = -0.106 \log_{10} {\rm SFR} + 2\,. \tag{3.2}$$

This description implies that galaxies undergoing major starbursts produce top-heavy ECMFs. Observational data suggest that the ECMF may not be a probability density distribution function (Pflamm-Altenburg, González-Lópezlira, and Kroupa, 2013b).

2. Formation timescale of the stellar population

In a galaxy, in which stars are being formed over hundreds of Myr to many Gyr, it

is important to establish the duration, δt, over which the interstellar medium spawns a complete population of embedded clusters. This timescale allows us to compute the total stellar mass, $M_{\rm tot}$, formed within δt as the integral over the ECMF over all embedded cluster masses,

$$M_{\rm tot} = {\rm SFR} \cdot \delta t \,. \tag{3.3}$$

Solving this integral yields $M_{\rm ecl,max}({\rm SFR})$.

We set $\delta t = 10$ Myr for several reasons. The timescale for galaxy-wide variations of the SFR is $\approx$ few 100 Myr (Renaud, Famaey, and Kroupa, 2016). $\delta t \approx 10\,$Myr corresponds to the timescale over which molecular clouds are forming stars (Egusa, Sofue, and Nakanishi, 2004; Egusa, Kohno, Sofue, Nakanishi, and Komugi, 2009; Fukui and Kawamura, 2010; Meidt, Hughes, Dobbs, et al., 2015) and to the survival/dissolution timescale of giant molecular clouds (Leisawitz, 1989; Padoan, Pan, Haugbølle, and Nordlund, 2016; Padoan, Haugbølle, Nordlund, and Frimann, 2017). In addition, it has been shown that the $\delta t \approx 10\,$Myr timescale predicts the $M_{\rm ecl,max} - {\rm SFR}$ relation within the IGIMF concept consistent with observational data (Weidner, Kroupa, and Larsen, 2004; Schulz, Pflamm-Altenburg, and Kroupa, 2015; Yan, Jerabkova, and Kroupa, 2017). It is to be emphasized that this timescale of $\delta t \approx 10\,$Myr is neither the pre-main-sequence stellar evolution nor the stellar evolution timescale. Essentially, $\delta \approx 10\,$Myr is the free-fall time of bound regions of molecular clouds and the time cycle over which the interstellar medium of a galaxy spawns new populations of embedded clusters. It is evident in the offsets between Hα and CO spiral arms (Egusa, Sofue, and Nakanishi, 2004; Egusa, Kohno, Sofue, Nakanishi, and Komugi, 2009).

3. Stellar IMF

We describe the stellar IMF as a multi-power-law function,

$$\xi_\star(m) = \begin{cases} k_1 m^{-\alpha_1} & m_{\rm min} \leq m/M_\odot < 0.50\,, \\ k_2 m^{-\alpha_2} & 0.50 \leq m/M_\odot < 1.00\,, \\ k_2 m^{-\alpha_3} & 1.00 \leq m/M_\odot < m_{\rm max}\,, \end{cases} \tag{3.4}$$

where

$$\xi_\star(m) = {\rm d}N_\star/{\rm d}m \tag{3.5}$$

is the number of stars per unit of mass and k_i are normalization constants that also ensure continuity of the IMF, $m_{\rm min} = 0.08\,M_\odot$ is the minimum stellar mass used in this work, the function $m_{\rm max} = {\rm WK}(M_{\rm ecl}) \leq m_{\rm max*} \approx 150\,M_\odot$ is the most massive star in the embedded cluster with stellar mass $M_{\rm ecl}$ (the $m_{\rm max} - M_{\rm ecl}$ relation, Weidner and Kroupa, 2006), and $m_{\rm max*}$ is the empirical physical upper mass limit of stars (Weidner and Kroupa, 2004; Figer, 2005; Oey and Clarke, 2005; Koen, 2006; Maíz Apellániz, Walborn, Morrell, Niemela, and Nelan, 2007). Stars with a higher mass are most likely formed through stellar dynamically induced mergers (Oh and Kroupa, 2012; Banerjee, Kroupa, and Oh, 2012).

We assume that star formation is feedback self-regulated and thus we implement the $m_{\rm max} = WK(M_{\rm ecl})$ relation based on observational data (Weidner and Kroupa, 2006; Kirk and Myers, 2012; Weidner, Kroupa, and Pflamm-Altenburg, 2013; Ramírez

Alegría, Borissova, Chené, et al., 2016; Megeath, Gutermuth, Muzerolle, et al., 2016; Stephens, Gouliermis, Looney, et al., 2017; Yan, Jerabkova, and Kroupa, 2017) assuming no intrinsic scatter (Weidner, Kroupa, and Bonnell, 2010; Weidner, Kroupa, and Pflamm-Altenburg, 2013). Despite the newer data (e.g. Ramírez Alegría, Borissova, Chené, et al., 2016; Stephens, Gouliermis, Looney, et al., 2017) supporting the existence of such an $m_{\rm max} - M_{\rm ecl}$ relation, future investigations of the interpretation and true scatter in this relation will be useful.

As a benchmark we use the canonical IMF α_i values derived from Galactic star-forming regions by Kroupa (2001), where $\alpha_1 = 1.3$ and $\alpha_2 = \alpha_3 = 2.3$ (the Salpeter–Massey index or slope, Salpeter, 1955; Massey, 2003). These are mostly based on in-depth analysis of star counts (Kroupa, Tout, and Gilmore, 1993) as well as young and open clusters for $m \leq 1\,M_\odot$ and on the work of Massey (2003) for $m > 1\,M_\odot$. The relation for α_3, derived by Marks, Kroupa, Dabringhausen, and Pawlowski (2012) (see erratum Marks, Kroupa, Dabringhausen, and Pawlowski, 2014), is

$$\alpha_3 = \begin{cases} 2.3 & \text{if } x < -0.87\,, \\ -0.41x + 1.94 & \text{if } x \geq -0.87\,, \end{cases} \tag{3.6}$$

where

$$x = -0.14[\mathrm{Fe/H}] + 0.99 \log_{10}\left(\frac{\varrho_{cl}}{10^6 M_\odot pc^{-3}}\right), \tag{3.7}$$

where ϱ_{cl} is the total density (gas and stars) of the embedded cluster (Marks, Kroupa, Dabringhausen, and Pawlowski, 2012),

$$\varrho_{cl} = 3M_{cl}/4\pi r_h^3\,, \tag{3.8}$$

where M_{cl} is initial cluster mass including gas and stars and r_h is its half mass radius (Marks and Kroupa, 2012). The density of the stars is expressed as $\rho_{\rm ecl} = 3\,M_{\rm ecl}/(4\pi\, r_h^3)$. We assume a star formation efficiency 33% and thus the mass of the embedded cluster in stars, M_{ecl}, is $M_{ecl} = M_{cl} \cdot 0.33$. To estimate the value of the density, ϱ_{ecl}, we adopt the relation from Marks and Kroupa (2012), $r_h/\mathrm{pc} = 0.1 M_{ecl}^{0.13}$, where M_{ecl} has units of $M_\odot$. In addition the relation $\log_{10}\varrho_{ecl} = 0.61\log_{10} M_{ecl} + 2.08$ allow us to formulate the relation between ϱ_{cl} and M_{ecl} as $\log_{10}\varrho_{cl} = 0.61\log_{10} M_{ecl} + 2.85$. This allows us to compute α_3 once the metallicity and mass of star cluster is known. From the original formulation of Eq. 3.7 by Marks, Kroupa, Dabringhausen, and Pawlowski (2012) it is possible to combine the assumptions on the cluster mass and radius to formulate the concise equation

$$x = -0.14[\mathrm{Fe/H}] + 0.6 \log_{10}\left(\frac{M_{ecl}}{10^6 M_\odot}\right) + 2.83\,. \tag{3.9}$$

We note that Eq. 3.9 conveniently uses only the star cluster initial stellar mass, M_{ecl}, and the metallicity of the embedded cluster as input parameters.

In addition in Kroupa (2002a) and Marks, Kroupa, Dabringhausen, and Pawlowski (2012) an empirical relation for the dependence of α_i, $i = 1, 2$, on [Fe/H] is suggested, i.e.

$$\alpha_i = \alpha_{ic} + \Delta\alpha[\mathrm{Fe/H}]\,, \tag{3.10}$$

	α_1	α_2	α_3
IGIMF1	1.3	2.3	2.3
IGIMF2	1.3	2.3	Eq. (3.6)
IGIMF3	Eq. (3.10)	Eq. (3.10)	Eq. (3.6)

Table 3.3: IGIMF implementations via local variations. This table summarizes the variations of the stellar IMF resulting in different IGIMFs implemented in this work. The α_i coefficients are defined in Eq. (3.4). We note that the model IGIMF1 assumes the IMF to be the invariant canonical form and corresponds to the original formulation of the IGIMF theory (Kroupa and Weidner, 2003a; Weidner and Kroupa, 2006) before evidence for the variation of the stellar IMF was quantified, the model IGIMF2 assumes that only the upper end of the IMF varies with density and metallicity, while the model IGIMF3 assumes the IMF varies over all stellar masses.

where $\Delta\alpha \approx 0.5$ and α_{ic} are the respective slopes of the canonical IMF. This equation is based on a rough estimate by Kroupa (2002a) for stellar populations in the Milky Way (MW) disc, the bulge, and globular clusters spanning a range of about [Fe/H]$= +0.2$ to ≈ -2. Beyond this range the results are based on an extrapolation. This is also true for the validity of Eq. 3.6, which is based on Galactic field populations and a dynamical analysis of globular clusters and ultra-compact dwarf galaxies.

We note that we use [Fe/H] as a metallicity traces and thus these relations might be re-calibrated to use more robust full metallicity, Z, using self-consistent chemical evolution codes.

3.3.3 IGIMF formulation

Based on the assumptions detailed above we can describe the stellar IMF for the whole galaxy, $\xi_{\rm IGIMF}$, as a sum of all the stars in all embedded clusters formed over the time $\delta t = 10\,$Myr,

$$\xi_{\rm IGIMF}(m, {\rm SFR}, [{\rm Fe/H}]) \quad = \quad \int_0^{+\infty} \xi_\star(m, M, [{\rm Fe/H}]) \xi_{\rm ecl}(M, {\rm SFR}) {\rm d}M \,, \quad (3.11)$$

where $\xi_{\rm ecl}$, the IMF of embedded clusters, is described by Eq. 3.1 and the stellar IMF is given by Eq. 3.4, Eq. 3.6, and Eq. 3.10.

Eq. 3.11 represents the general recipe for constructing gwIMF from local stellar IMFs that appear within a galaxy within the time interval δt. Three versions of the IGIMF are calculated (IGIMF1, IGIMF2, IGIMF3); the properties of each are tabulated in Table 3.3.

3.4 Results

3.4.1 IGIMF grid

Together with this publication we provide the IGIMF grid in electronic form. That is, for each value of the galaxy-wide SFR and [Fe/H] that is in the computed set we provide the gwIMF (calculated as the IGIMF) in the mass range from 0.08 to 120 $M_\odot$.

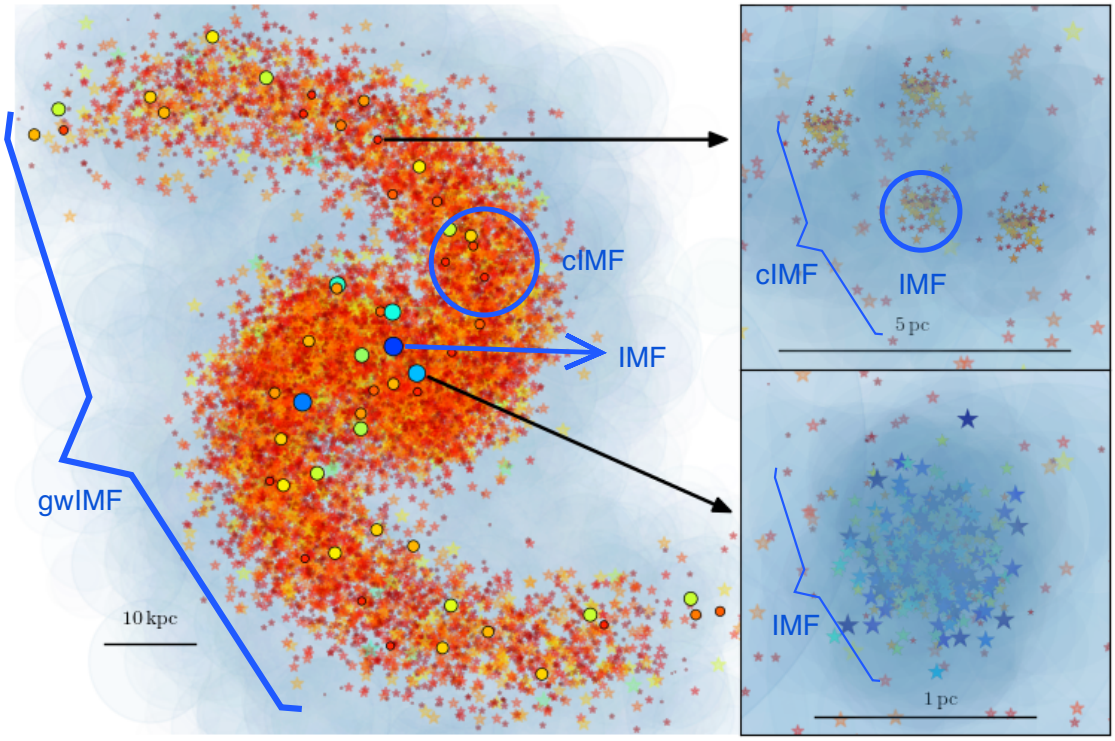

Figure 3.1: Schematic showing a late-type galaxy. Its field population is represented by red and orange stars. The newly formed stellar population is indicated by coloured circles that represent CSFEs (embedded star clusters). The colours and sizes of symbols scale with stellar/cluster mass. The acronyms from Tab. 3.3 are shown here with examples. **Right bottom panel:** A young massive embedded cluster, which will most likely survive and contribute to the open star cluster population of the galaxy. **Right top panel:** Young embedded cluster complex composed of a number of low-mass embedded clusters, which will evolve into a T Tauri association once the embedded clusters expand after loss of their residual gas and disperse into the galaxy field stellar population.

This grid can be readily truncated at $100\,M_\odot$. The IGIMF is tabulated as the stellar mass bin in one column and the other three columns contain IGIMF values in the form of IGIMF1/2/3 summarized in Tab. 3.3. The mass range is the same for the whole parameter space for easier implementation into any code and potential interpolation within the grid. The IGIMF is normalized to the total stellar mass, $M_{\rm tot}$ (Eq. 3.3), produced in $\delta t = 10\,{\rm Myr}$, $\int_{m_{\rm min}}^{m_{\rm max}} m \cdot \xi_{\rm IGIMF}\,{\rm d}m = M_{\rm tot}$.

A representative selection from the grid is shown in Fig. 3.2 in which we can see variations of the gwIMF over the large span of parameters. The panels on the left show that for low SFR the gwIMF is top light. That is, we expect a deficit of high-mass stars in comparison to the canonical IMF and that the mass of the most massive star in a galaxy varies with metallicity because of the IMF-metallicity dependence. For a SFR of $1\,M_\odot$/yr, which is approximately the SFR of the MW, the gwIMF is very close to but slightly steeper than the canonical IMF above a few $M_\odot$ (Scalo, 1986;

Mor, Robin, Figueras, and Lemasle, 2017; Mor, Robin, Figueras, and Antoja, 2018). Therefore the IGIMF is always consistent with the MW and local star formation regions and automatically fulfills this test every theory of IMF variations needs to pass. For larger SFR values the gwIMF becomes top heavy, that is relatively more massive stars form than would be given by the canonical IMF. The IGIMF1 formulation that does not implement IMF variations, but only the $m_{\rm max} - M_{\rm ecl}$ relation, does not show any variations at SFR $\geq 1 M_\odot$/yr. This is essentially the IGIMF version calculated by Kroupa and Weidner (2003a) before the constraints on IMF variations discussed above had become evident. The IGIMF3 formulation, which implements the full variations of the IMF with density and metallicity, can result in bottom-heavy gwIMFs at metallicities [Fe/H] > 0 and bottom-light gwIMF for [Fe/H] < 0 independent of SFR. For SFR $< 1 M_\odot$/yr the gwIMF becomes top light independent of metallicity. For SFR $> 1 M_\odot$/yr gwIMF becomes top heavy and this effect becomes stronger for [Fe/H] < 0.

All the scripts used here are uploaded to the galIMF scripts (https://github.com/Azeret/galIMF) such that the galIMF module can be self-consistently implemented into any chemical evolution code.

A compact quantification of the changing shape of the IGIMF for different assumptions can be achieved by calculating the mass ratios in multiple stellar mass bins. To see how relevant low-mass stars are to the total mass budget formed in $\delta t = 10\,$Myr, the F_{05} parameter (Weidner, Ferreras, Vazdekis, and La Barbera, 2013) is defined as

$$F_{05} = \frac{\int_{m_{\rm min}}^{0.5\,M_\odot} m \cdot \xi_{\rm IGIMF}\,{\rm d}m}{M_{\rm tot}}\,. \tag{3.12}$$

This quantifies the fraction of stellar mass in stars less massive than $0.5\,M_\odot$ relative to the total initial stellar mass. The dependency of F_{05} on the SFR and metallicity is shown in Fig. 3.3 for the different IGIMF formulations. Values $F_{05} > 0.25$ indicate bottom-heavy IGIMFs. Values of $F_{05} > 0.6$ are required to match IMF-sensitive spectral features in elliptical galaxies (La Barbera, Ferreras, Vazdekis, et al., 2013; Ferreras, Weidner, Vazdekis, and La Barbera, 2015). Such large F_{05} values would not lead to very high dynamical mass-to-light ratios as the resulting IGIMF is not significantly steeper than the canonical IMF for $m < 0.5\,M_\odot$. This is very important because an IGIMF with a single Salpeter power-law index over all stellar masses would lead to unrealistically high dynamical mass-to-light ratios (see Ferreras, La Barbera, de la Rosa, et al., 2013).

Similarly, the mass fraction of stars with $m < 0.4\,M_\odot$ relative to the present-day stellar mass (in all stars less massive than $0.8\,M_\odot$) is defined as

$$F_{04/08} = \frac{\int_{m_{\rm min}}^{0.4\,M_\odot} m \cdot \xi_{\rm IGIMF}\,{\rm d}m}{\int_{m_{\rm min}}^{0.8\,M_\odot} m \cdot \xi_{\rm IGIMF}\,{\rm d}m}\,. \tag{3.13}$$

This constitutes an approximation to a stellar population that is about 12 Gyr old. This parameter, plotted in Fig. 3.4, informs the bottom heaviness of the present-day stellar population ignoring stellar remnants. Furthermore, the parameter

$$F_8 = \frac{\int_{8.0\,M_\odot}^{m_{\rm max}} m \cdot \xi_{\rm IGIMF}\,{\rm d}m}{M_{\rm tot}} \tag{3.14}$$

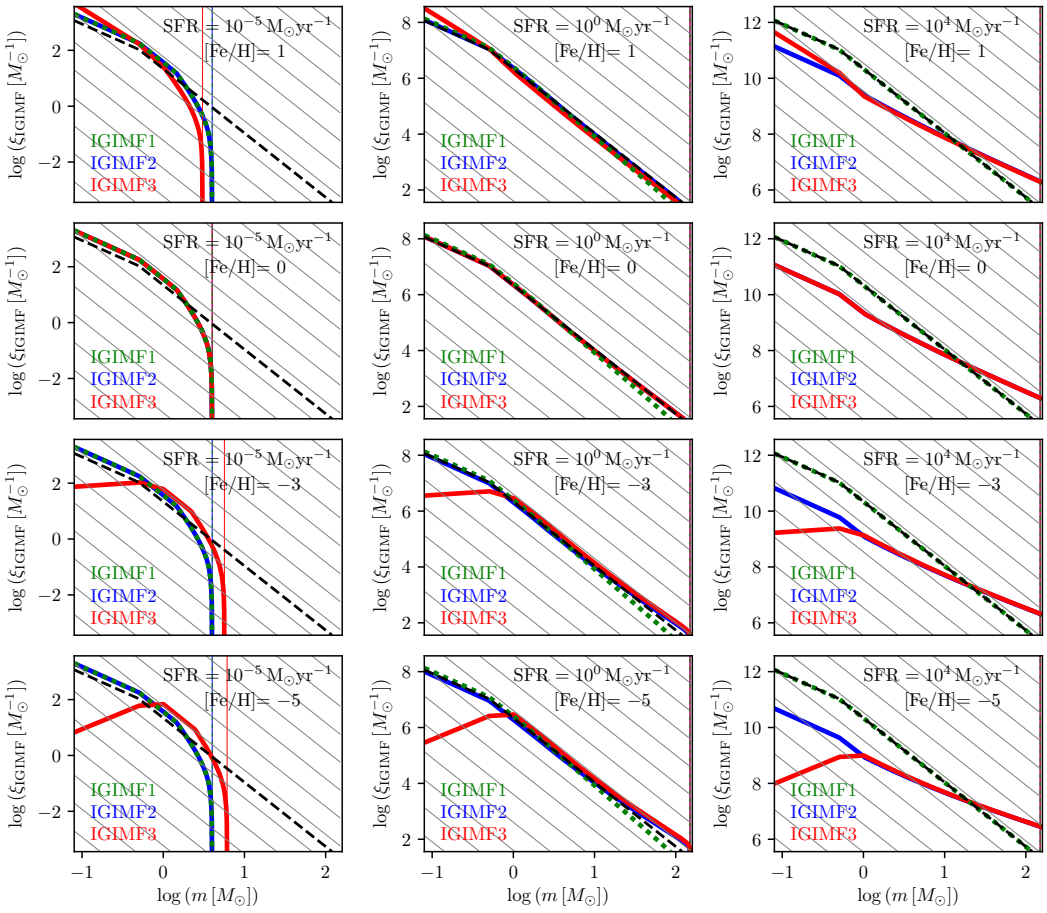

Figure 3.2: Selection of IGIMF models representing the overall characterization of the IGIMF grid published in electronic form with this work. The metallicity used in this figure is [Fe/H] = $1, 0, -3, -5$ from top to bottom; the SFR = $10^{-5}, 10^{0}, 10^{4}\,\mathrm{M_\odot/yr}$ from left to right. All IMF models are normalized to the total stellar mass formed over $\delta t = 10\,\mathrm{Myr}$ to make the comparison with the canonical IMF (black dashed line in each panel) quantitative. To compare the slope variations we plot the Salpeter-Massey slope, $\alpha = 2.3$, as a grey-line grid in each plot.

is the mass fraction of stars more massive than $8.0\,M_\odot$ relative to the total initial stellar mass formed in 10 Myr, $M_{\rm tot}$ and indicates the degree of top heaviness of the IGIMFs (Fig. 3.5).

3.4.2 Evolution of gwIMF of an elliptical galaxy and its chemical evolution

The presented IGIMF grid, or the script using galIMF to produce the grid, can be readily implemented into galaxy chemical evolutionary codes to obtain a self-consistent gwIMF evolution with time. To show that the IGIMF approach is promising in this regard, we created a burst star formation history (SFH) that approximately resembles the formation of an elliptical galaxy with a total mass in all stars formed of $10^{12}\,M_\odot$.

Its present-day roughly 12 Gyr old counterpart would according to the present results (Fig. 3.6) have a mass of about $2 \times 10^{11}\,M_\odot$ in main-sequence stars. The [Fe/H] enrichment, a prescribed function of time used in this work solely for the purpose of demonstration, is shown in the top panel in Fig. 3.6. For each $\delta t = 10\,\mathrm{Myr}$ epoch the IGIMF is computed for the given SFR and [Fe/H] value. The bottom set of panels show the evolution of the IGIMF. In this example, the gwIMF is top heavy at high SFR and becomes bottom heavy during the metal-rich phase of the evolution. That is, the stellar population, as described by this IGIMF, can produce rapid α element enrichment in a fast first phase and can also potentially produce an overabundance of low-mass stars mainly in the most metal-rich centre. This is because it is plausible that star formation may continue near the centre in the high-density metal-enriched gas, which has the shortest cooling time in this region.

The IGIMF grid is now ready to be implemented into various chemo-dynamical codes to be tested against data in a self-consistent way.

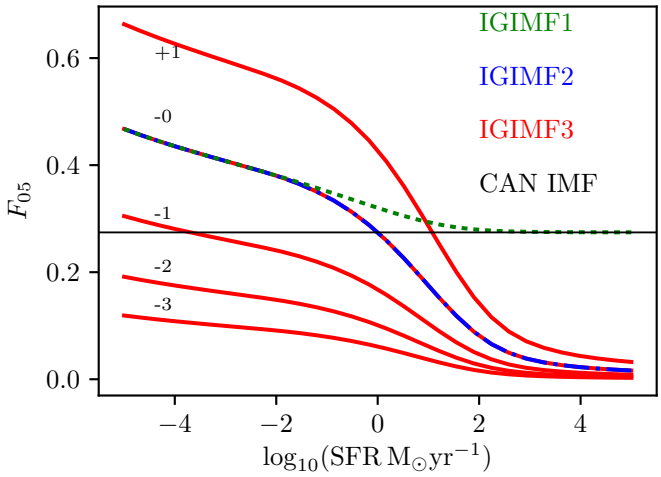

Figure 3.3: Mass fraction formed in $\delta t = 10\,\mathrm{Myr}$ in stars less massive than $0.5\,M_\odot$ relative to the total initial mass in the IGIMF models (Eq. 3.12) is shown in dependence of the SFR and [Fe/H]. The canonical IMF is depicted as the horizontal black line ($F_{05} \approx 0.25$). We note that the IGIMF1 and IGIMF2 models lead to F05 values as if the gwIMF were bottom heavy in comparison with the canonical IMF. However this is due to the normalization caused by the IGIMF being top light for low SFRs ($< 1 M_\odot/\mathrm{yr}$).

3.4.3 Correction to SFR–Hα relation

Given the gwIMF varies with the SFR and metallicity of a galaxy, it is expected that any observational tracer of this SFR needs to take this into account. In the following we distinguish between the true physical SFR of a galaxy (i.e. the actual mass per unit time that is being converted to stars) versus the observationally derived SFR (e.g. $\mathrm{SFR_K}$ in Eq. 3.15 below); the derived SFR requires a tracer such as the Hα flux that is often used to measure the SFR subject to an assumption concerning the shape of the gwIMF. This measure works in principle by counting the number of photons

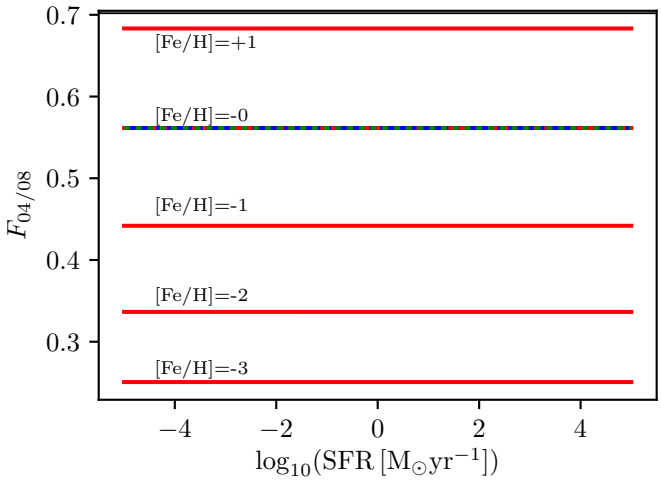

Figure 3.4: Mass fraction formed in $\delta t = 10\,\mathrm{Myr}$ in stars less massive than $0.4\,M_\odot$ relative to the total present-day stellar mass formed in $\delta t = 10\,\mathrm{Myr}$ in the IGIMF models (Eq. 3.13) shown in dependence of the SFR and [Fe/H]. The canonical IMF is depicted as the horizontal black line ($F_{04/08} \approx 0.7$), as are the IGIMF1 and IGIMF2 models as these are metallicity independent. The present-day stellar population is assumed to contain only stars less massive than $0.8\,M_\odot$, ignoring remnant masses. The fractions are constant because these IGIMF models do not depend on the SFR for stars with $m < 1\,M_\odot$.

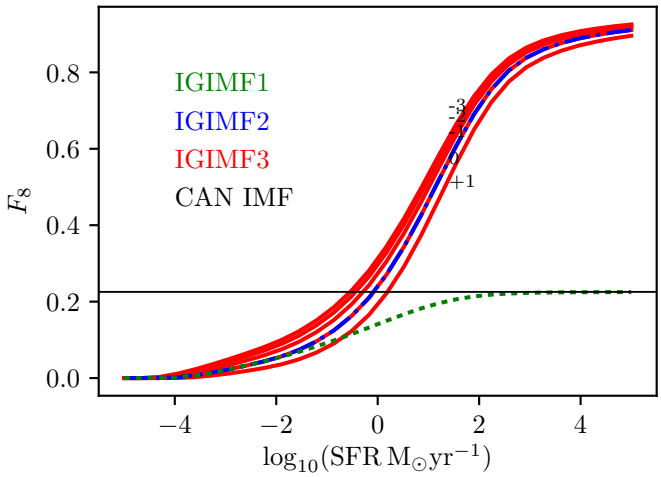

Figure 3.5: Mass fraction formed in $\delta t = 10\,\mathrm{Myr}$ in stars more massive than $8.0\,M_\odot$ relative to the total initial mass in the IGIMF models (Eq. 3.14) shown in dependence of the SFR and [Fe/H]. The canonical IMF is depicted as the horizontal black line ($F_{80} \approx 0.22$).

emitted from recombining hydrogen atoms such that each recombination accounts for an ionizing event, thereby the Hα flux is a measure of the flux of ionizing photons. We obtain a measure of the number of massive stars that have formed by measuring the Hα flux. We can calculate the total amount of mass converted to stars by assuming an IMF.

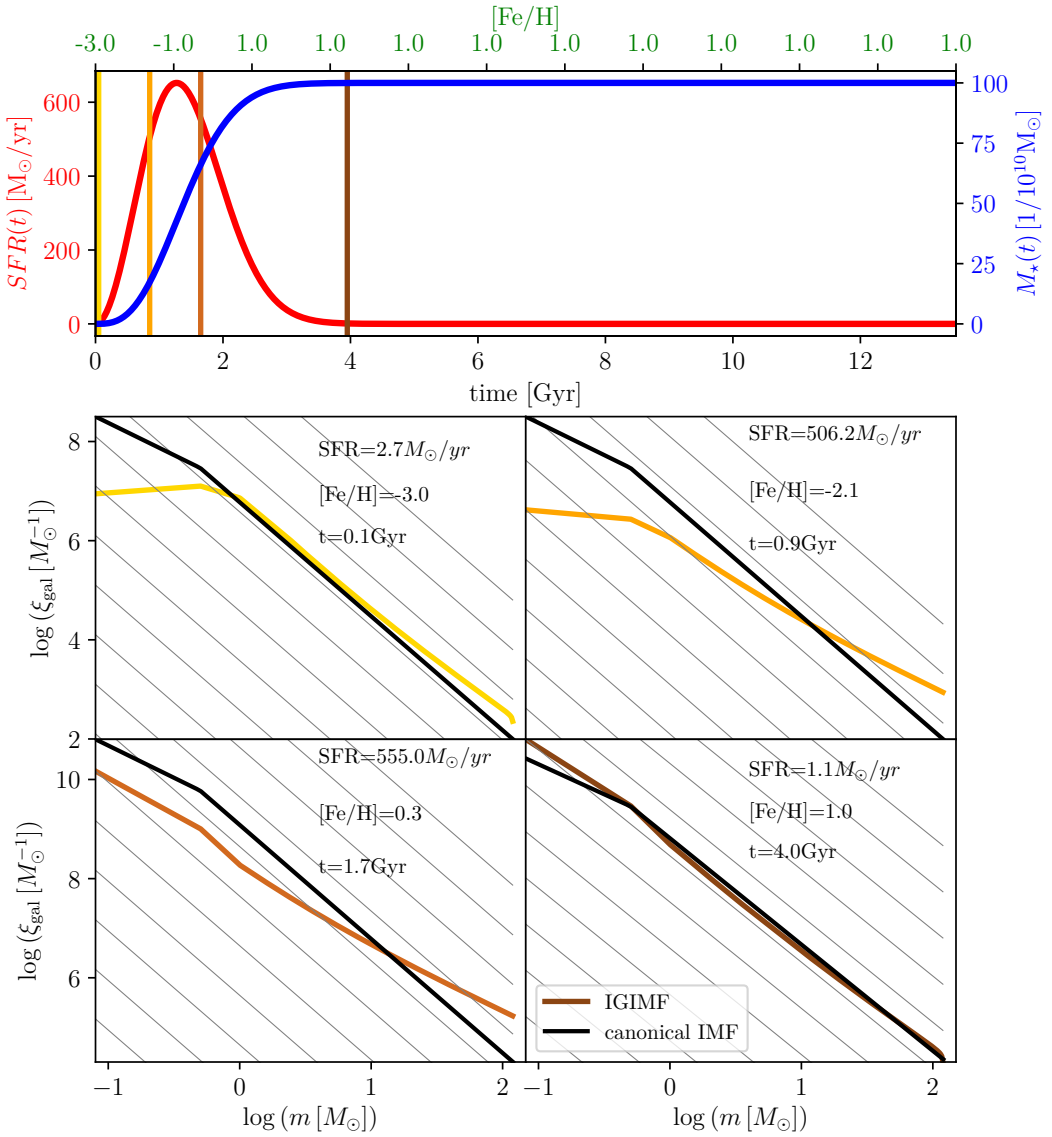

Figure 3.6: Example of IGIMF evolution with time, plotting only the IGIMF3 model. **Top panel:** The prescribed evolution of the SFR with time (red solid curve, left y-axis), that is the SFH, stellar mass build-up with time (blue solid curve, right y-axis) , and the metallicity evolution (upper x-axis). This example serves to show a typical evolution and therefore the curves were synthetically created. This example of how a $10^{12}\,M_{\odot}$ elliptical galaxy assembles over about 1 Gyr is consistent with downsizing (Recchi, Calura, and Kroupa, 2009), but due to stellar evolution the stellar mass of this galaxy is $2 \times 10^{11}\,M_{\odot}$ after 12 Gyr. Using the IGIMF grid, the same principle can be applied self-consistently in a chemo-dynamical code. In addition the four vertical lines represent the chosen time snapshots shown in the bottom panels. **Bottom panels:** Four IGIMF plots at the chosen times (see top panel), showing how the IGIMF can potentially evolve throughout elliptical galaxy assembly. Shown is the top-heavy phase, but also the bottom-heavy phase during the metal-rich part of the evolution.

A widely used relationship between the galaxy-wide SFR and the measured integrated Hα flux of a galaxy is given by Kennicutt (1998, his Eq. (2)),

$$\mathrm{SFR_K}/(M_\odot \mathrm{yr}^{-1}) = 7.9 \cdot 10^{-42} L(\mathrm{H}\alpha)/(\mathrm{ergs} \cdot \mathrm{s}^{-1}) \,, \tag{3.15}$$

which is derived based on a single power-law IMF having a Salpeter slope (Salpeter, 1955) in the mass range (0.1, 100) $M_\odot$ assuming solar metallicity. Therefore this relation needs to be corrected for any IMF variation and metallicity, as has already been done previously (e.g. Lee, Salzer, Impey, Thuan, and Gronwall, 2002; Lee, Gil de Paz, Tremonti, et al., 2009; Pflamm-Altenburg, Weidner, and Kroupa, 2007).

For low SFR $\lessapprox 1\,M_\odot$/yr and under the assumption that the universal IMF is a probability density distribution function (the Kennicutt $\mathrm{SFR_K}$–Hα relation; Eq. 3.15), we note that large fluctuations in the measured SFRs would be obtained when applied to star-forming systems constrained by an ECMF with $M_{min} < m_{max}$. The average SFR would also be biased to smaller values because the galaxy would typically lack massive stars. Such a bias can be larger than 0.5 dex for $\log_{10}(SFR/(M_\odot/\mathrm{yr})) \lessapprox -4$, assuming $M_{min} = 20\,M_\odot$ owing to the combination of stochastic effects and the ECMF constraint (e.g. Silva, Fumagalli, and Krumholz, 2014). The Appendix 3.7 contains a brief comparison between the IGIMF theory and the SLUG Silva, Fumagalli, and Krumholz (2014) approach.

In this work corrections of the SFR–Hα function are presented in the full IGIMF (IGIMF1 and IGIMF3) framework for the first time. We note that the IGIMF2 model yields the same results as the IGMF3 model for solar metallicity and that the IGIMF1 model is metallicity independent. But a metallicity dependence enters into all IGIMF models due to the metallicity dependency of stellar evolution. For this purpose the galIMF module is linked with the PEGASE stellar population synthesis code (Fioc, Le Borgne, and Rocca-Volmerange, 2011, see also Fioc and Rocca-Volmerange, 1999 for an astro-ph documented manual) taking advantage of the PyPegase python wrapper[3]. The Hα flux is computed by PEGASE directly from the ionizing photons. Even though it is possible to introduce, for example, dust as an absorber, we do not use any additional parameters in our computations. The PEGASE code is structured such that it does not allow the input IMF or gwIMF to vary during the computation. In our application the gwIMF however varies with the SFR. Thus we limited our simulations to those with a constant SFR and metallicity over the timescale $\delta t = 10\,\mathrm{Myr}$. The gwIMF computed by the IGIMF theory is a continuous function that is approximated by multi-slope power-law functions, which are translated to an input file for PEGASE. In practice, we use four slopes to describe the calculated IGIMF: i.e. a power-law fit to each of the four mass ranges $0.08 - 0.5\,M_\odot$, $0.5 - 1.0\,M_\odot$, $1 - 0.8 m_{max}\,M_\odot$, $0.8 m_{max} - 150\,M_\odot$. This four-segment power-law description provides an excellent approximation to the full IGIMF over all stellar masses. Nevertheless, it would be better if the full numerical form of the IGIMF can be used for such calculations with PEGASE in the future; PEGASE does not currently enable an IMF to be read in as a data file but requires the IMF to be defined as power-law sections.

This allows us to calculate the Hα flux as an output from the PEGASE code for a chosen gwIMF and metallicity and thus to quantify the SFR–Hα relations for the

[3] https://github.com/coljac/pypegase

SFR–Hα– relation					
IGIMF	[Fe/H]	d	c	b	a
IGIMF1	0	$7.123 \cdot 10^{1}$	$-5.45819 \cdot 10^{0}$	$1.1949 \cdot 10^{-1}$	$-7.0 \cdot 10^{-4}$
IGIMF1	-2	$1.038596 \cdot 10^{2}$	$-7.98057 \cdot 10^{0}$	$1.838 \cdot 10^{-1}$	$1.25 \cdot 10^{-3}$
IGIMF3	0	$2.8893 \cdot 10^{0}$	$-4.6408 \cdot 10^{-1}$	$4.1 \cdot 10^{-4}$	$2.2 \cdot 10^{-4}$
IGIMF3	-2	$2.394696 \cdot 10^{1}$	$-2.2008 \cdot 10^{0}$	$4.623 \cdot 10^{-2}$	$-1.7 \cdot 10^{-4}$
correction factor					
IGIMF1	-2	$4.724408 \cdot 10^{1}$	$-1.59889 \cdot 10^{0}$	$-1.15 \cdot 10^{-3}$	$-2.91 \cdot 10^{-4}$
IGIMF1	0	$3.200615 \cdot 10^{1}$	$-3.0079 \cdot 10^{-1}$	$-3.690 \cdot 10^{-2}$	$6.15 \cdot 10^{-4}$
IGIMF3	-2	$6.504733 \cdot 10^{1}$	$-3.2008 \cdot 10^{0}$	$4.623 \cdot 10^{-2}$	$-1.74 \cdot 10^{-4}$
IGIMF3	0	$4.398965 \cdot 10^{1}$	$-1.46407 \cdot 10^{0}$	$4.1 \cdot 10^{-4}$	$2.2 \cdot 10^{-4}$

Table 3.4: Coefficients of the fits of eq. (3.16) to the SFR–Hα relations and to the correction factor; see Fig. 3.7. The fits and precision of the coefficients gives values of the log of the SFR with precision of approximately 0.1 dex.

metallicity dependent formulation of the IGIMF. From this the correction for each metallicity with respect to the Kennicut $\mathrm{SFR_K}$–Hα relation can be computed.

The solar-metallicity SFR–Hα relations are shown in the left panel of Fig. 3.7, and the sub-solar metallicity case is shown in the right panel. In addition to the Kennicutt $\mathrm{SFR_K}$–Hα relation and the IGIMF1,3 relations, we show the empirical correction of this relation proposed by Lee, Gil de Paz, Tremonti, et al. (2009) based on far ultraviolet (FUV) non-ionizing continuum and Hα nebular emission, which deviates from the Kennicutt $\mathrm{SFR_K}$–Hα relation and is closer to the IGIMF relation.

For the purpose of general use of the corrected relations in Fig. 3.7, the IGIMF SFR–Hα relations are represented with third order polynomials,

$$\log_{10}(\mathrm{SFR_{IGIMF,i}}/(M_\odot \mathrm{yr}^{-1})) = ax^3 + bx^2 + cx^1 + d\,, \tag{3.16}$$

where $i = 1, 3$ and $x = \log_{10}(L_{\mathrm{H}\alpha}/(\mathrm{ergs} \cdot \mathrm{s}^{-1}))$. The polynomial coefficients for different metallicities and for the IGIMF1,3 models are summarized in Tab. 3.4. The sub-solar values are consistent with the results of Boquien, Buat, and Perret (2014).

The correction factor (Fig. 3.7) is calculated as follows:

$$\text{correction factor}(\mathrm{H}\alpha) = \frac{\mathrm{SFR_{IGIMF,i}}(L_{\mathrm{H}\alpha})}{\mathrm{SFR_K}(L_{\mathrm{H}\alpha})}. \tag{3.17}$$

3.4.3.1 The case of the Leo P galaxy

Leo P is a late-type dwarf galaxy approximately at a distance of 1.6 Mpc, which has a metallicity [Fe/H]≈ -1.8 and an Hα flux, $L_{H\alpha} = 5.5 \cdot 10^{36}\,\mathrm{ergs} \cdot \mathrm{s}^{-1}$. This flux comes from one HII region powered by one or two stars with individual masses of $m \approx 25\,M_\odot$ (e.g. McQuinn, Skillman, Dolphin, et al., 2015).

We use the measured Hα flux as a star formation indicator with the newly developed SFR indicators of Sec. 3.4.3. Table 3.5 summarizes the computed SFRs based on different assumptions. The masses of the most massive star and second-most massive star are calculated for the IGIMF1 and IGIMF3 models (IGIMF2 is indistinguishable from IGIMF3; see also Yan, Jerabkova, and Kroupa, 2017) using the values of the

SFR derived from the observed Hα luminosity. The most massive star has a mass of $23 - 26\,M_{\odot}$, the second most massive star has a mass in the range $16 - 20\,M_{\odot}$. That is, according to the IGIMF theory, the $\mathrm{SFR}_{\mathrm{IGIMF,i}}$ of Leo P would be significantly larger than the standard value, $\mathrm{SFR}_{\mathrm{K}}(L_{\mathrm{H}\alpha})$, being consistent with the presence of the observed massive stars in Leo P. The SLUG approach (see Appendix 3.7) also implies a larger true SFR than given by the standard value (fig. 3 in Silva, Fumagalli, and Krumholz, 2014).

The message to be taken away from this discussion is that when the Hα flux is used as a star-formation indicator to test the IGIMF theory the appropriate Hα SFR relation also needs to be employed. Pflamm-Altenburg, Weidner, and Kroupa (2007) already emphasized that there is a physical limit to the SFR if a galaxy forms a single star only at a given time (their Eq. 16); these authors also pointed out that distant late-type dwarf galaxies are likely to have Hα-dark star formation. In the limit where only few ionizing stars form, the UV-flux derived SFRs are more robust and these are indeed consistent with the higher SFRs as calculated using the IGIMF1 formulation. This is shown explicitly in fig. 8 of Lee, Gil de Paz, Tremonti, et al. (2009), who compared UV- and Hα-based SFR indicators for dwarf galaxies for which the original IGIMF formulations (IGIMF1, which did not include the IMF variation of Marks, Kroupa, Dabringhausen, and Pawlowski, 2012) remain valid. We add a note of caution that part of the discrepancies between the H$\alpha-$ and UV-based SFR indicators may be influenced by several physical effects, such as the different gas phases (such as the diffuse inoized gas present in galaxies), photon leakage from HII regions, gas, and dust abundance. Calzetti (2013) and also for example Kennicutt and Evans (2012) provide a more detailed discussion of various SFR tracers and their interrelations.

McQuinn, Skillman, Dolphin, et al. (2015) constructed the optical colour-magnitude diagram (CMD) for Leo P in order to infer its SFH and assumed the invariant canonical IMF for this purpose, i.e. the authors assumed the caninvgwIMF hypothesis of Table 3.1. An issue worthy of future study is to quantify the degeneracies between the shape of the gwIMF and the derived SFH. Unfortunately, the implementation of a variable gwIMF into the time-dependent scheme that would allow the self-consistent modelling of the SFH while reproducing the full CMD has not been done for the IGIMF theory yet. Knowing the $\mathrm{SFR}_{\mathrm{IGIMF,i}}$ within the IGIMF theory using the Hα flux allows us to discuss possible effects in the CMD and the whole low-mass stellar population in the galaxy, as is touched upon in the next section.

3.4.3.2 Implications for the BTFR and the CMD:

Given the higher SFRs in the IGIMF theory produced by the top-light gwIMF, the positions of Leo P and other dwarf galaxies in the BTFR (McGaugh, Schombert, Bothun, and de Blok, 2000; Lelli, McGaugh, and Schombert, 2016) need be considered as a consistency check. That is, if there is substantial dark star formation it might alter the total mass of the galaxy, assuming an age.

This problem is relevant also for the dark matter problem and notably for Milgromian gravitation (MOND; Milgrom, 1983; Famaey and McGaugh, 2012). The application of the IGIMF theory to dwarf galaxies has already shown (Pflamm-Altenburg and Kroupa, 2009b) that the build-up times of the observed stellar populations (as

SFR–Hα relation	$\log_{10}(\mathrm{SFR}/(M_\odot/\mathrm{yr}))$
Kennicutt (1998)	-4.4
Lee, Gil de Paz, Tremonti, et al. (2009)	-3.2
CAN IMF, [Fe/H]=0	-4.6
CAN IMF, [Fe/H]=-2	-4.9
IGIMF1, [Fe/H]=0	-2.8
IGIMF1, [Fe/H]=-2	-3.0
IGIMF3, [Fe/H]=0	-2.8
IGIMF3, [Fe/H]=-2	-3.2

Table 3.5: The SFR of Leo P based on the observed Hα flux. We note the more than one order of magnitude difference in the calculated SFR between the IGIMF models and the invariant IMF models. The Lee, Gil de Paz, Tremonti, et al. (2009) value is derived assuming their purely empirical correction to the Kenniutt relation (reached without an underlying model for an IMF variation), which is consistent with the IGIMF models in the regime $-4 < \log_{10}(L_{H\alpha}/(10^{41}\mathrm{erg\,sec}^{-1})) < 0$. To form a single massive star with a main-sequence mass of $25\,M_\odot$ over 10^5 yr (Wuchterl and Tscharnuter, 2003; Duarte-Cabral, Bontemps, Motte, Hennemann, Schneider, and André, 2013), a $\mathrm{SFR} = 25/10^5\,M_\odot/\mathrm{yr} = 10^{-3.60}\,M_\odot/\mathrm{yr}$ is needed over this time, but a dwarf galaxy would be forming other stars as well, such that the SFRs calculated using the IGIMF theory are consistent with the existence of such a star in Leo P.

assessed using the luminosity) is well accounted for within less than a Hubble time (see their Figs.10 and 11), solving the problem according to which such galaxies need longer than a Hubble time to form their stellar content if the SFR was not significantly larger in the past. Applying the IGIMF theory to dwarf galaxies therefore does not change their baryonic masses, it merely shortens their gas-consumption timescale (Pflamm-Altenburg and Kroupa, 2009b) and allows them to form stellar populations within a Hubble time. The BTFR therefore remains untouched.

For the case of Leo P, the known extent and baryonic matter in Leo P and the flat (non-rising) part of the rotational curve are prone to uncertainty and therefore more observational data are required (Giovanelli, Haynes, Adams, et al., 2013) to constrain the position of Leo P in the BTFR.

Another consistency test is to study if the observed CMD of Leo P can be reproduced within the IGIMF theory. This needs further work and it is to be noted that the central stellar population is similar to a canonical stellar population; for example, in the IGIMF theory the central embedded cluster that formed the two $25\,M_\odot$ stars is, by construction, canonical for solar metallicity. A detailed calculation and comparison with the observed CMD needs to resort to the local IGIMF formulation (Sec. 3.5.1) that allows the spacial integration of stellar populations within a galaxy (Pflamm-Altenburg and Kroupa, 2008b).

3.4.4 Ultra-faint dwarf galaxies

Recent measurements with the Hubble Space Telescope by Gennaro, Tchernyshyov, Brown, et al. (2018) of UFD satellite galaxies, as an extension of the study by Geha, Brown, Tumlinson, et al. (2013), have suggested a possible gwIMF variation in these galaxies in the stellar-mass range $(0.4 - 0.8\,M_\odot)$. The authors, however, mentioned that a larger data sample is needed to improve the reliability of the presented results.

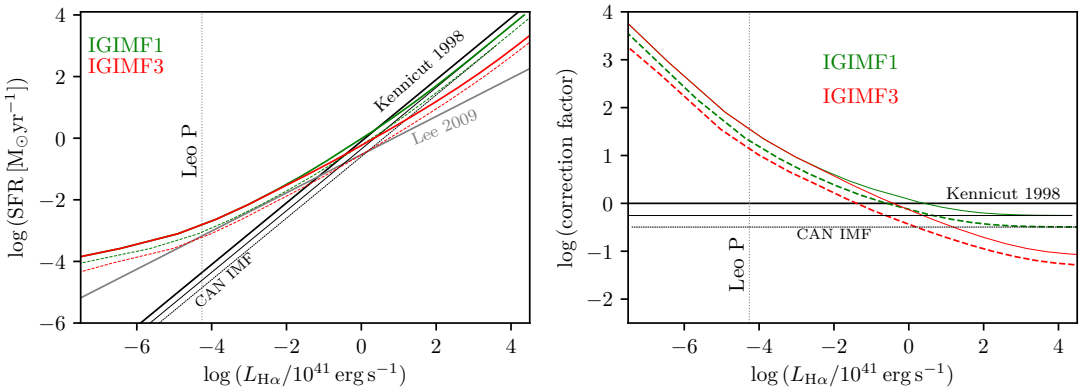

Figure 3.7: **Left panel:** SFR–Hα relation. The IGIMF version in comparison with the empirical power laws proposed by Kennicutt (1998) and Lee, Gil de Paz, Tremonti, et al. (2009). The red and green solid lines are IGIMF1/3 computed for solar metallicity [Fe/H]$= 0$ and the dashed lines represent the case of sub-solar metallicity, [Fe/H]$= -2$. **Right panel:** Corrections to the Kennicutt $\mathrm{SFR_K}$–Hα relation (Eq. 3.17). The true (IGIMF) SFRs are divided by the Kennicutt value. The Hα flux of LeoP is shown by the vertical dotted line in both panels. For example, from the left panel it is evident that the IGIMF1,3 models yield values of the SFR that are consistent with the presence of massive stars in the Leo P galaxy. The two panels show that dwarf galaxies with Hα fluxes near 10^{36} erg/s have a SFR that is more than 100 times larger than that suggested by the Kennicutt relation (Eq. 3.15), while massive or profusely star-forming galaxies with H$\alpha \approx 10^{44}$ erg/s have SFRs that can be 10–100 times smaller than given by the traditional Kennicutt relation. As for the left panel the solid lines indicate solar metallicity [Fe/H]$= 0$ and the dashed lines indicate [Fe/H]$= -2$.

In this work we use the gwIMF variations derived by Gennaro, Tchernyshyov, Brown, et al. (2018) as an illustrative case to show how the gwIMF variations can constrain the stellar IMF on star cluster scales using the IGIMF approach. But in order to draw more robust conclusions and firmer constraints on the low-mass end of the IMF slopes (α_1, α_2) further measurements in such objects are required.

Fig. 3.8 shows inferred and measured values by Gennaro, Tchernyshyov, Brown, et al. (2018) in comparison with the canonical IMF and IGIMF formulations as defined in Sec. 3.3.3. Gennaro, Tchernyshyov, Brown, et al. (2018) assumed that the gwIMF can be reprsented by a single power-law form to derive the slope of the gwIMF in the mass range $0.4 - 0.8\,M_\odot$. To be able to compare these measurements with the two-part power law in the IGIMF parametrization, we compute the single power-law fit to the IGIMF/canonical IMF in the same mass range. We can see that the IGIMF predictions do not describe the Gennaro, Tchernyshyov, Brown, et al. (2018) data well although the general trend is reproduced. The local IMF variations used in this work to calculate the IGIMF models are based on an extrapolation from data values in the range [Fe/H] $\in$ (-0.5,0) (Kroupa, 2001; Marks, Kroupa, Dabringhausen, and Pawlowski, 2012). Based on this new observation of the gwIMF in the low-mass regime at metallicities in the range [Fe/H] $\in$ (-3,-2), a refinement of Eq. (3.10) may be needed, i.e.

$$\alpha_{1,2}^{\mathrm{cor}} = \alpha_{1c,2c} + \Delta\alpha^{\mathrm{cor}}\,([\mathrm{Fe/H}] + 2.3)\ , \tag{3.18}$$

where $\Delta\alpha^{\mathrm{cor}} \approx 2.5$. For [Fe/H]$> -2.3$ the canonical IMF would be valid in this formulation. It may be possible to identify a systematic variation of the local IMF for low-mass

stars with additional data that cover a larger metallicity range and test the robustness of these results given the uncertainties. Any such new constraints must, however, be consistent with the observationally derived stellar mass functions in present-day GCs.

As a caveat we note that additional factors affect the empirically determined present-day mass function power-law index in UFDs. For example, the fraction of unresolved multiple systems may be different in the dwarfs as it depends on the dynamical history of the population (Marks and Kroupa, 2012; Marks, Kroupa, Dabringhausen, and Pawlowski, 2012). Also, the final deduced index may be affected by the formation of the stellar population in embedded clusters that expel their residual gas, leading to expanding low-mass stellar populations that may be lost from a weak UFD potential. This process is exaggerated if the embedded clusters formed mass segregated (Haghi, Zonoozi, Kroupa, Banerjee, and Baumgardt, 2015). In addition to this the gwIMF slopes of Gennaro, Tchernyshyov, Brown, et al. (2018) are sensitive to the mass of the lowest stellar mass that is measured and to the form of the gwIMF that is assumed. In Gennaro, Geha, Tchernyshyov, et al. (2018), these authors used a two-part power-law gwIMF for the case of the Coma Berenices UFD finding a smaller variation with respect to the MW.

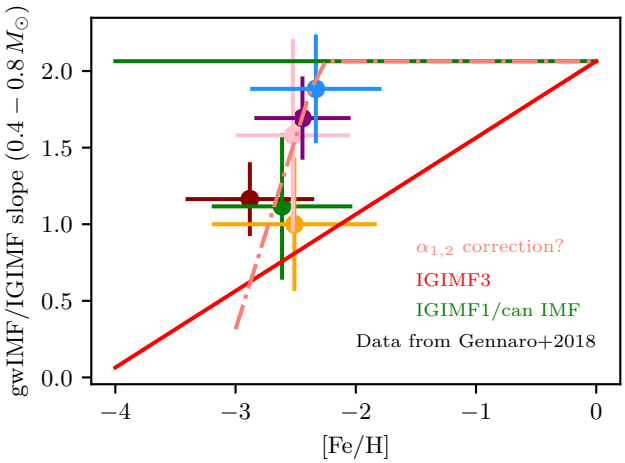

Figure 3.8: Variable gwIMF in the stellar mass regime $(0.4 - 0.8\,M_\odot)$ for 6 UFDs shown by the coloured points from Gennaro, Tchernyshyov, Brown, et al. (2018). The IGIMF1 models (given by two slopes $\alpha_1 = 1.3$ and $\alpha_2 = 2.3$) are represented by the horizontal green line. These have the same effective invariant slope as the canonical IMF in this mass regime. The IGIMF3 metallicity-dependent effective slope based on Eq. 3.10 is shown in red. These data may indicate the necessity for a different dependency of the $\alpha_{1,2}$ indices on metallicity than represented by Eq. 3.10. This different dependency is indicated by the orange dot-dashed line (Eq. 3.18).

3.5 Discussion

3.5.1 Local or regional cIMF

The gwIMF variation is parametrized within the IGIMF framework with global galaxy properties, namely the total SFR and the average metallicity. As an output we obtain the total stellar population formed in 10 Myr without any information about its spatial distribution in a galaxy. In reality, however, the gas density and metallicity varies spatially and therefore a mathematical formulation of the cIMF (Tab. 3.1), which takes into account the local gas surface density and metallicity at some position within the galaxy, is needed. A cIGIMF version has been formulated by Pflamm-Altenburg and Kroupa (2008a, the 'local' IGIMF). These authors applied the IGIMF1 formulation and assumed the disc galaxy to be subdivided into radial annular bins within each of which the local IGIMF is calculated subject to the constraint that the galaxy has an exponential radial structure and the gas and SFR densities are related. This work showed that the radial Hα cut-off and extended UV discs can be explained naturally within the IGIMF framework because in the outskirts the gas density is low. This leads to a low SFR density, low-mass embedded clusters, and thus a deficit of ionizing stars, while intermediate-mass stars form there. In addition, the cIGIMF results in metallicity gradients, as are suggested to be present for example in elliptical galaxies (McConnell, Lu, and Mann, 2016), and provides a description for low surface-brightness galaxies (LSBGs) having low gas surface densities (Pflamm-Altenburg, Weidner, and Kroupa, 2011). Based on the cIGIMF calculation, LSBGs form preferentially low-mass stars with a deficit of high-mass stars relative to the canonical IMF even though the global SFR can be high and the IGIMF would predict that massive stars will be formed. We plan to include a mathematically and physically consistent cIGIMF description in the next version of the galIMF code originally developed by Yan, Jerabkova, and Kroupa (2017).

3.5.2 Changes to IMF variations within IGIMF framework

As formulated in this work, the IGIMF implements several empirical relations such as the star-mass function of embedded clusters, its variation, the correlation between the birth radius and mass of the embedded clusters, and local IMF variations with the physical conditions in the star-forming cloud core. Since these are empirically derived not covering all possible physical values (extreme SFRs and metallicities are not accessible in the Local Universe for example), the IGIMF prescription applied in this work can be improved with time. That is, obtaining better data or data from environments not yet probed on a galactic scale and on larger scales can be used to infer local IMF variations. This has been shown in this paper for the case of UFD measurements from Gennaro, Tchernyshyov, Brown, et al. (2018) (see Fig. 3.8 and Eq. 3.18) in contrast to the original empirical extrapolation from MW data described by Eq. 3.10.

Any proposed changes can be readily implemented into the galIMF code (Yan, Jerabkova, and Kroupa, 2017) and further tested. However any local IMF variations need to match the canonical IMF for a SFR comparable to that of the MW and an average MW metallicity as well as the present-day mass functions observed in globular

clusters, open clusters, and embedded clusters as a necessary constraint on any viable IMF theory.

3.6 Conclusions

For the first time a grid of gwIMFs computed within the IGIMF framework with SFR and metallicity dependence is presented, together with its implementation into the galIMF module and an equivalent FORTRAN code. This allow us to trace the variations of gwIMFs for different galaxies assuming that the physics driving the gwIMFs comes from local star-forming regions. The main contributions of this work can be summarized as follows:

- The attached IGIMF grid with the parameter-span SFR $\in (10^{-5}, 10^{4})$ and [Fe/H] $\in (-5, 1)$ presents the gwIMF normalized to the total stellar mass formed in 10 Myr episodes, M_{tot} = SFR $\times$ 10Myr; the individual stars always have the same range of masses (from 0.08 to 120 $M_{\odot}$) for an implementation into galaxy-evolution (e.g. chemo-dynamical evolution) codes and also for a possible interpolation in the grid.

- The overall variation of the gwIMF is as follows: (1) The gwIMF can become top light even if the shape of the local stellar IMF is invariant (IGIMF1 version). This can been explained with a demonstrative example: 1000 star clusters with a mass of $10\,M_{\odot}$ would have a top-light stellar population in comparison to a monolithically formed star cluster of $10^4\,M_{\odot}$ because stars more massive than $10\,M_{\odot}$ would exist only in the latter case (Yan, Jerabkova, and Kroupa, 2017). This statement is basically independent of metallicity and reflects the fact that there is a maximum stellar mass that forms in a given cluster because of the $m_{\rm max} = WK(M_{\rm ecl})$ relation. Also the upper limit for the most massive star cluster to be formed in a galaxy depends on galactic properties (Johnson, Seth, Dalcanton, et al., 2017). The top-light IGIMF appears to be in good agreement with gwIMF measurements in nearby dwarf galaxies (Lee, Gil de Paz, Tremonti, et al., 2009; Watts, Meurer, Lagos, Bruzzese, Kroupa, and Jerabkova, 2018). The above demonstrative example is actually found in nature (Hsu, Hartmann, Allen, et al., 2012; Hsu, Hartmann, Allen, et al., 2013). (2) The gwIMF, as expected, is close to the canonical IMF for a SFR near $1\,{\rm M}_{\odot}$/yr and solar metallicity and becomes top heavy with increasing SFR above that value. (3) Interestingly, for sub-solar metallicity the gwIMF can be bottom light and for super-solar metallicity bottom heavy (according to the IGIMF3 parametrization which includes the full metallicity and density variation of the stellar IMF). This might be reflected in the cores of elliptical galaxies.

- We present the possible time evolution of the gwIMF for the case of a monolithic (starburst) formation of an elliptical galaxy showing the potential to explain observed features: high α element abundances implying a short formation timescale, high metallicity implying a top-heavy gwIMF during this short assembly time, and an overabundance of low-mass stars indicating a metal-rich formation epoch in which the gwIMF is bottom heavy.

- As a consequence of the variable gwIMF the majority of standard and widely used stellar-population correlations used to estimate galaxy properties need to be recomputed and re-interpreted correctly. This is because assumptions concerning the IMF enter into many of these correlations. This is shown using the SFR–Hα relation. Assuming the IGIMF theory to be the correct description it follows that the SFR is underestimated for galaxies with a low SFR and it is overestimated for galaxies with high SFRs, by up to several orders of magnitude, if the standard Kennicutt $\mathrm{SFR_K}$–Hα relation is used. We present the appropriate correction factors (Fig. 3.7). The Leo P galaxy, often mentioned as posing a significant problem for the IGIMF theory because for the estimated SFR stars as massive as $25\,M_\odot$ should not be forming in this galaxy, is shown to be well reproduced using the IGIMF theory. This is because in the literature the Kennicutt $\mathrm{SFR_K}$–Hα relation is incorrectly applied when star cluster masses are smaller than the most massive stars, i.e. when $M_{min} < m_{max}$. In this case the ensemble of freshly formed star clusters contain low-mass clusters within which the IMF cannot be sampled to the most massive stars in the case of the IMF being a constrained probability distribution as in the SLUG approach (Appending 3.7). This implies a systematic deficit of massive stars in the whole ensemble. This produces a biased result when the Kennicutt relation is extrapolated to low $H\alpha$ fluxes, that is when $SFR_K \lessapprox 10^{-4} M_\odot/\mathrm{yr}$ because the Kennicutt relation assumes all star formation events to always have a fully sampled IMF (da Silva, Fumagalli, and Krumholz, 2012). This is naturally corrected for in the IGIMF theory such that the observed galaxy (e.g. Leo P) behaves physically correctly (see Fig.3.7).
- The data by Gennaro, Tchernyshyov, Brown, et al. (2018) for UFD galaxies have suggested a possible variation of the low-mass IMF for stars in the mass range (0.4-0.8 $M_\odot$) and metallicity in the range ([Fe/H]$= -3$ to -2). The IMF variations over this mass range and metallicity range have not been constrained empirically and only an extrapolation has been applied in this work (Kroupa, 2001; Marks, Kroupa, Dabringhausen, and Pawlowski, 2012, see Eq. 3.10). The IGIMF theory is used to translate the observed galaxy-wide variation to a possible variation of the IMF and therewith to possibly improve the formulation of the local IMF variation in this stellar mass range and at low metallicity ([Fe/H] $= -3$ to -2). The newly suggested variation (see Eq. 3.18 and Fig. 3.8) shows how gwIMF measurements can help constrain star formation on star cluster scales, but we note the caveats discussed in Sec. 3.4.4.

The IGIMF theory which is, by construction, consistent with MW data, has now demonstrated its general potential in allowing the computations of gwIMFs from local empirical stellar IMF properties; this theory also has the ability to improve our understanding of how the IMF varies in embedded clusters. It is ready to be implemented into chemo-dynamical codes and to be tested with more data. First implementations of the IGIMF theory into self-consistent galaxy formation and evolution simulations have been achieved (Bekki, 2013; Ploeckinger, Hensler, Recchi, Mitchell, and Kroupa, 2014). The implications of the IGIMF theory for the gas-depletion and stellar-mass build-up timescales of galaxies are significant (Pflamm-Altenburg and Kroupa, 2009b); many other galaxy-evolution problems are potentially resolved naturally (Pflamm-Altenburg,

Weidner, and Kroupa, 2011). The SFR correction factors shown in Fig. 3.7 need to be applied to the traditional Kennicutt values and, in general, entail significantly larger true SFRs for low-mass, star-dominated populations in dwarf galaxies with a general shift to significantly smaller true SFRs for massive star-forming galaxies. These correction factors (Eq. 3.17) led to a change of the slope of the galaxy main sequence (Speagle, Steinhardt, Capak, and Silverman, 2014), which will be addressed in an upcoming contribution. Finally, the occurrence of Hα-dark star formation may significantly affect the cosmological SFR (Pflamm-Altenburg, Weidner, and Kroupa, 2007).

Acknowledgements: *The authors acknowledge the exceptionally useful and comprehensive comments from an anonymous referee. We also thank to ESO visitor programme for supporting AV and PK during their stay. We thank Frederico Lelli for useful discussions and comments to the manuscript. AV acknowledges support from grant AYA2016-77237-C3-1-P from the Spanish Ministry of Economy and Competitiveness (MINECO). AHZ acknowledges support from Alexander von Humboldt Foundation through a Research Fellowship. The discussions and the provided references by Neal Evans are also acknowledged.*

3.7 Appendix: The stochastically lighting up galaxies

The stochastically lighting up galaxies (SLUG) approach (Silva, Fumagalli, and Krumholz, 2014) is an alternative to the newer IGIMF formulation; this alternative approach implements star formation basically using principles from a first formulation of the IGIMF theory (Kroupa and Weidner, 2003a; Weidner and Kroupa, 2005; Weidner and Kroupa, 2006). In SLUG, a galaxy is constructed by first drawing the masses of star clusters. These star clusters are then filled up with stars by randomly choosing from an IMF until the cluster mass is reached (Silva, Fumagalli, and Krumholz, 2014, their Sec. 2.1). Therefore this is not fully random sampling but mass-constrained sampling instead (Weidner and Kroupa, 2006). This means that it is impossible to have a $100\,M_\odot$ star in a $80\,M_\odot$ star cluster, for example. The SLUG approach therefore is along the original IGIMF approach, which fundamentally rests on the notion that the stellar population in a galaxy is formed in star clusters and thus constitutes conditional stochasticity (Kroupa and Weidner, 2003a; Weidner and Kroupa, 2006). We note however that the SLUG approach differs from the current IGIMF formulations by not explicitly accounting for the $m_{\rm max} - M_{\rm ecl}$ relation since each cluster is assumed to be populated randomly by stars subject to the mass constraint.; the published IGIMF work fulfils this constraint. Whether there is a physical function $m_{\rm max} = WK(M_{\rm ecl})$ is thus an important problem to continue to study. The SLUG approach therefore does not comprise pure stochastic sampling from a gwIMF, which would yield no deficit in ionizing stars on average for galaxies with low SFRs (Pflamm-Altenburg, Weidner, and Kroupa, 2009). Instead, in SLUG (as in a original form of the IGIMF theory), a deficit comes about because of the mass constraint on the stars within a cluster imposed by the masses of the star clusters. The SLUG approach is thus a useful tool for comparison with the IGIMF theory as applied in this work; the IGIMF method is deterministic because it is related to the concept that star formation is strongly feedback self-regulated, by imposing the additional condition (in addition to the cluster mass $M_{\rm ecl}$) that the

$m_{\rm max} - M_{\rm ecl}$ relation be obeyed. We also note that similar ideas to those underlying the IGIMF theory have been considered by Vanbeveren (1982).

Chapter 4

When the tale comes true: multiple populations and wide binaries in the Orion Nebula Cluster

---

This chapter is based on the publication Jerabkova, Beccari, Boffin, et al. (2019) with the same title "When the tale comes true: multiple populations and wide binaries in the Orion Nebula Cluster". Only minor changes concerning formatting were made in order to present it as a chapter in the thesis.

Abstract: *Context: Recently published high-quality OmegaCAM photometry of the 3x3 deg around the Orion Nebula Cluster (ONC) in r, and i filters revealed three well-separated pre-main sequences in the color-magnitude diagram (CMD). The objects belonging to the individual sequences are concentrated toward the center of the ONC. The authors concluded that there are two competitive scenarios: a population of unresolved binaries and triples with an exotic mass ratio distribution, or three stellar populations with different ages (≈ 1 Myr age differences). Aims: We use Gaia DR2 in combination with the photometric OmegaCAM catalog to test and confirm the presence of the putative three stellar populations. We also study multiple stellar systems in the ONC for the first time using Gaia DR2. Methods: We selected ONC members based on parallaxes and proper motions and take advantage from OmegaCAM photometry that performs better than Gaia DR2 photometry in crowded regions. We identify two clearly separated sequences with a third suggested by the data. We used Pisa stellar isochrones to estimate ages of the stellar populations with absolute magnitudes computed using Gaia parallaxes on a star by star basis. Results: 1) We confirm that the second and third sequence members are more centrally concentrated toward the center of the ONC. In addition we find an indication that the parallax and proper motion distributions are different among the members of the stellar sequences. The age difference among stellar populations is estimated to be 1-2 Myr. 2) We use Gaia proper motions and other measures to identify and remove as many unresolved multiple system candidates as possible. Nevertheless we are still able to recover two well-separated sequences with evidence for the third one, supporting the existence of the three stellar populations. 3) Due to having ONC members with negligible fore- or background contamination we were able to identify a substantial number of wide binary objects (separation between 1000-3000 au) and with relative proper motions of the binary components consistent with zero. This challenges previously inferred values that suggested no wide binary stars exist in the ONC. Our inferred wide-binary fraction is $\approx 5\%$. Conclusions: We confirm the three populations correspond to three separated episodes of star formation. Based on this result, we conclude that star formation is not happening in a single burst in this region.*

In addition we identify 5% of wide-binary stars in the ONC that were thought not to be present.

4.1 Introduction

Young star clusters (YSC) with resolved populations are ideal objects for studying and constraining star and star cluster formation. Most of the theoretical and observational works devoted to the study of YSCs seem to agree that their (pre-)stellar population, still embedded in the pristine molecular cloud, is mostly coeval with an intrinsic age spread of $\approx 0.5 - 1$ Myr and a physical size of ≈ 1 pc (e.g Zinnecker, McCaughrean, and Wilking, 1993; Lada and Lada, 2003; Pfalzner, 2011; Marks and Kroupa, 2012; Getman, Kuhn, Feigelson, Broos, Bate, and Garmire, 2018).

However, many authors report on the presence of an age spread up to several Myr in YSCs (Palla and Stahler, 2000; Cargile and James, 2010; Cignoni, Tosi, Sabbi, et al., 2010; Reggiani, Robberto, Da Rio, Meyer, Soderblom, and Ricci, 2011; Bell, Naylor, Mayne, Jeffries, and Littlefair, 2013; Balog, Siegler, Rieke, et al., 2016; Getman, Feigelson, Kuhn, Bate, Broos, and Garmire, 2018). Whether the measured age spreads are real and, hence, related to the physics at play during the early stages of the formation of the stars in clusters (Larson, 2003; Pflamm-Altenburg, Weidner, and Kroupa, 2007; Pflamm-Altenburg and Kroupa, 2009a; Klassen, Pudritz, and Kirk, 2017) or related to inaccurate evaluation of the impact of observational biases related to differential extinction, stellar variability and complex physical processes like episodic accretion (Baraffe, Chabrier, and Gallardo, 2009; Da Rio, Robberto, Soderblom, et al., 2010; Jeffries, Littlefair, Naylor, and Mayne, 2011) – is still an open debate.

Recently, Beccari, Petr-Gotzens, Boffin, et al. (2017, hereafter B17) reported on the detection of three well separated sequences of pre-main sequence (PMS) stars in an optical color-magnitude diagram (CMD) of an area of ~ 1.5 deg radius centered on the Orion Nebula Cluster (ONC). The stars belonging to the three sequences, while being all centered around the Trapezium area, show a different spatial distribution with the apparently oldest (and most populous) population being more spatially spread around the center of the ONC with respect to the youngest one which shows an increasing concentration toward the center. The authors discussed the possibility that differential extinction and/or a population of unresolved binaries might be at the origin of such an observational feature in their CMD. The effect of differential reddening is safely excluded by the fact that the three populations show an identical distribution of visual extinction. While binaries are certainly present as unresolved sources, B17 demonstrated that in order to reproduce the separation in the color distribution of the populations, they require a mass-ratio distribution heavily skewed toward equal mass binaries. While such a population of binaries could not be safely excluded using the data in hand, B17 stressed that it would still imply an exotic population of binaries never observed before in a cluster. In addition, if unresolved binaries or triples were the reason for the discrete sequences in the CMD, then this would contradict that the binary sequence in this assumption is the most concentrated, because binaries are more easily broken up in denser environments (Kroupa, 1995a). Supported by recent results from infrared spectroscopy from Da Rio, Tan, Covey, et al. (2016), they concluded

that a real difference in age is most likely at the origin of the presence of three populations in the CMD. The populations of PMS stars in the ONC were thus formed in bursts of star formation separated in age by ≈ 1 Myr. We note that the projection effect (i.e., the emergence of apparent unresolved binaries in the inner region due to projection) is larger in the inner region of the ONC and this could conceivably fake a more centrally concentrated younger population. The stellar number density at the center is $4.7 \times 10^4\,\mathrm{stars/pc^3}$ (McCaughrean and Stauffer, 1994) which implies an average projected separation between two stars at the densest place of about 6000 AU. The resolution of our survey (OmegaCAM and GAIA DR2) is a couple of 100 AU such that the occurrence of an unresolved line-of-sight (non-physical) binary is sufficiently small to be ignored.

Kroupa, Jeřábková, Dinnbier, Beccari, and Yan (2018) proposed a theoretical explanation in support of multiple-bursts of star formation in the ONC, which has been further investigated by Wang, Kroupa, and Jerabkova (2018). In summary, (1) the formation of a first generation, fueled at the hub of inflowing molecular filaments, is truncated by the feedback of massive stars formed as a part of the first generation; (2) these massive stars are stellar-dynamically ejected and as a consequence the inflow of gas still present in surrounding filaments is restored; (3) the next generation of stars forms. This process can be repeated until either the ionizing stars are not ejected or the filamentary gas reservoir is exhausted or destroyed. The model well predicts the spatial distribution of the three populations as described in B17.

In this paper we use the Gaia DR2 (Gaia Collaboration, Brown, Vallenari, et al., 2018) in combination with OmegaCAM photometry to safely isolate the ONC stellar population from fore- or background objects and to confirm or discard the detection of multiple sequences in the optical CMD. The impact of unresolved binaries will be studied in detail. If the presence of multiple populations in the ONC is confirmed, the case of the ONC may represent a fruitful testing site for theoretical models of star cluster formation including the potentially important process of its stellar-dynamical modulation. In addition we take advantage of the Gaia spatial resolving power and analyze apparent multiple system candidates using isolated (that is, with negligible fore- or background contamination) ONC star members only. Such a study is possible for the first time thanks to Gaia.

The manuscript is structured as follows: In Sect 4.2 we introduce our data sets, then we apply selection criteria to obtain ONC members (Sect 4.3). Using this sample we recover the sequences found by B17 and discuss their properties in Sect 4.4. The study of the binary stars allowed by Gaia is described in Sect 4.5, followed by a discussion and the conclusions in Sect 4.6.

4.2 Data sets

4.2.1 The Gaia data

We used the python Astroquery package (Ginsburg, Robitaille, Parikh, et al., 2013) to retrieve the Gaia DR2 data (Gaia Collaboration, Brown, Vallenari, et al., 2018)

from the Gaia science archive [1]. We downloaded all the objects detected by Gaia that are within a radius of three degrees on the sky from the ONC (R.A.≈ 83.75 deg, Dec ≈ -5.48 deg, 1 deg on the sky corresponds to ≈ 7 pc at the ONC distance of 400 pc) without any additional filtering. The data sample contains 278,444 targets, of which 12% have parallaxes measured with a relative error of 10% or smaller, while 15% do not have a measured parallax. The data sample is dominated by faint stars, with only 43% stars being brighter than 19 mag in the Gaia G-band.

We note that Gaia DR2 photometry in BP and RP filters is not suitable to study the dense and still in-gas embedded regions as the ONC. We follow the Gaia DR2 quality data check in the Appendix 4.7 and Sect 4.3.3 to study Gaia DR2 photometric capabilities on our data set and conclude that for our analysis it is necessary to use additional photometric data.

4.2.2 The OmegaCAM catalog

We acquired a new set of deep multi-exposures with OmegaCAM, attached to the 2.6-m VST telescope in Paranal, with the aim of increasing the photometric accuracy toward the faintest region of the optical CMD shown in B17. We surveyed a 3×3 deg area around the center of the ONC using the r and i filters, that is, the same bands as adopted in B17. In particular we acquired 10×25s exposures in both filters for each pointing under the proposal 098.C-0850(A), PI Beccari. As in B17, the whole data reduction process (from removal of detector signatures to the extraction and calibration of stellar magnitudes) was carried out at the Cambridge Astronomical Survey Unit (CASU). We downloaded the astrometrically and photometrically calibrated single band catalogs from the VST archive at CASU[2]. We used a large number of stars in common with the AAVSO Photometric All-Sky Survey (APASS) to correct for possible residual offsets in r and i magnitudes between each single exposures. We finally require that a single object should be detected in at least seven out of ten images both in the r and i band in order to be accepted as a real star. Since the error on individual stellar sources is very small (see Fig. 4.2), the average of the magnitudes measured in each individual frame was adopted as stellar magnitude while the standard error was used as the associated photometric error. The final catalog includes 93846 objects homogeneously sampled in r and i bands down to $r \approx 21-22$ mag on an 3×3 deg area around the cluster's center.

4.2.3 The initial catalog

We used the C^3 tool from Riccio, Brescia, Cavuoti, Mercurio, di Giorgio, and Molinari (2017) in order to identify the stars in common between the OmegaCAM and the Gaia catalog. C^3 is a command-line open-source Python script that, among several other options, can cross-match two catalogs based on the sky positions of the sources. We used the C^3 *best* matching option and circular selection region with a radius of 50 arcsec that is used for sky partition. We found 84022 targets in common between the Gaia and the OmegaCAM data. The majority of targets that are in the OmegaCAM catalog

[1] http://gea.esac.esa.int/archive/
[2] http://casu.ast.cam.ac.uk/vstsp/

but not in the Gaia one are faint ($r \gtrapprox 21$) and blue objects ($r - i \lessapprox 1.2$). We note that we also loose a fraction of objects in the most crowded regions, like the center of the ONC (see Appendix 4.7). Hereafter we refer to the Gaia DR2 *and* OmegaCAM cross-matched catalog as the initial catalog.

4.3 The ONC members with Gaia

As described in the previous section, our initial catalog includes optical photometry from OmegaCAM and astrometric informations from Gaia DR2 for objects in the range of mag $12 \lesssim r \lesssim 20$ within 3×3 deg around the center of the ONC. We now propose a roadmap which allows users to fully exploit the potential offered by the Gaia DR2 astrometric information in efficiently disentangling the stellar populations of a cluster from field objects in the CMD. Such a strategy is adopted here to specifically identify and study the PMS population(s) in the ONC, but we are confident that such criteria can be applied to perform similar studies of stellar populations in close-by young clusters.

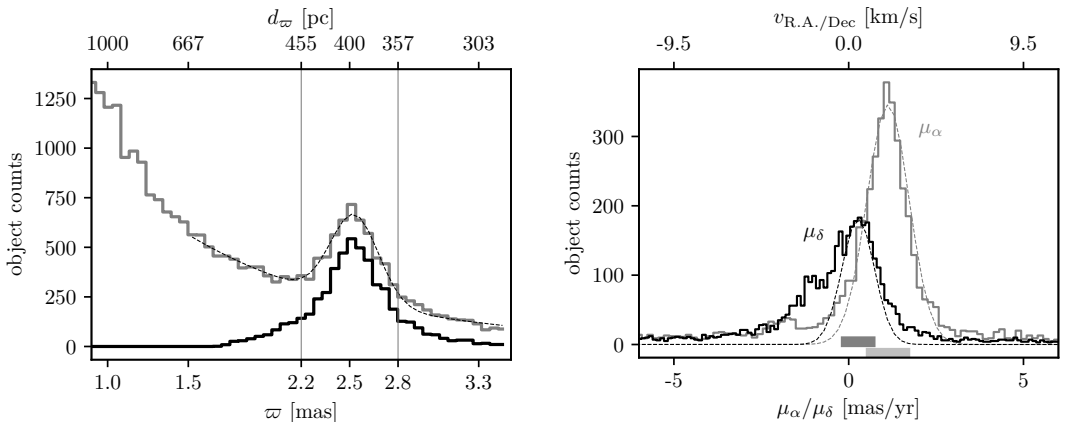

Figure 4.1: **Left panel:** distribution of the parallax, ϖ, of all the objects in the initial catalog (gray histogram) and the bona fide ONC members selected with C1 (black histogram; see Sect. 4.3). The dashed line show the Gaussian fit to the distribution of parallaxes of the stars in the initial catalog. The vertical line indicates the $\pm 2\sigma$ distance from the peak of the distribution at ≈ 2.52. The top horizontal axis shows corresponding values, d, in parsecs using $d[\mathrm{pc}] = 1/(\varpi[\mathrm{mas}] \cdot 10^{-3})$, valid for those objects that have small relative errors (Gaia Collaboration, Brown, Vallenari, et al., 2018). **Right panel:** Distributions of the R.A. and Dec proper motions (gray and black histograms, respectively). To select the objects that have proper motions consistent with the bulk of the ONC we fit each distribution with a Gaussian function shown by dashed lines. The gray horizontal bars indicate the 1σ range of the respective fit. The top axis shows the values of the proper motions in km/s, calculated assuming a distance of 400 pc.

4.3.1 Constraining the reliable ONC members: Parallax selection - C1

We first use the parallaxes provided by Gaia DR2 to reliably identify ONC members. We show as gray histogram in Fig. 4.1 the distribution of the parallaxes ϖ for all the stars belonging to our initial catalog. The stellar population belonging to the ONC is easily recognized through a well defined peak at $\varpi_{\rm peak} \approx 2.5$ mas corresponding to a distance $d \approx 400$ pc, in full agreement with previous estimates of the ONC distance (e.g., Menten, Reid, Forbrich, and Brunthaler, 2007). This plot already witnesses the unprecedented opportunity offered by the Gaia-DR2 catalog to safely identify and hence study the details of the stellar populations in clusters.

In order to isolate the ONC members, we performed a fit to the parallax distribution (dashed line in Fig. 4.1) using a Gaussian function in combination with an exponential function. The latter is appropriate to describe the fore- or background sources. The fit shows a peak at

$$\varpi_{\rm ONC} = 2.52 \pm 0.15\,{\rm mas}\,,$$

where the uncertainty is 1-σ of the Gaussian fit. Note that with σ we here indicate the uncertainty related to the Gaussian fit while elsewhere in the paper we indicate as σ_{ϖ} the error associated to the value of ϖ as given in the Gaia catalog. To ensure that we only keep the best candidates, we retain as bona fide members all the objects whose parallax falls in the range defined by $\pm 2\sigma$ distance from the peak of the distribution (that is 2.22 and 2.82 mas – the vertical lines in Fig. 4.1). In addition, only the targets having a relative parallax error within 10% are considered as this ensures good quality of the astrometric solution (see also Gaia Collaboration, Brown, Vallenari, et al., 2018). The final selection criterion C1 is purely based on the parallaxes and is defined as:

$$2.22 - 3\sigma_{\varpi} \leq \varpi \leq 2.82 + 3\sigma_{\varpi} \,\texttt{and}\, \sigma_{\varpi}/\varpi \leq 0.1\,, \tag{4.1}$$

where σ_{ϖ} is the uncertainty on each single parallax given in Gaia DR2.

The black solid line in Fig. 4.1 shows the distribution of the parallaxes of the 4988 stars selected using the parallax filtering C1 (Eq. 5.1). We include the stellar population in a ≈ 100 pc region from the ONC along the line of sight. Such a region is somehow larger than the physical extension of the ONC star forming region on the sky (e.g., B17 or our Fig. 4.8). We note, however, that having 10% uncertainty in parallax at the distance of the ONC results in ≈ 40 pc uncertainty on the distance inferred from the parallax.

By adopting the criterion C1 (Eq. 5.1), we uniquely rely on the use of parallaxes, implying that targets with available optical photometry from OmegaCAM but not having precise enough cataloged parallaxes are not considered. Such objects are usually faint or are residing in crowded fields, like the ONC center. In addition multiple or close by objects for which a single star's astrometric solution was not found would also lack cataloged astrometric parameters. We stress here that 12% of the stars in the initial photometric catalog do not have parallaxes. This fraction is reduced to 4% if we only consider objects that are in the CMD position occupied by the young stellar population of the ONC.

4.3.2 Constraining the reliable ONC members: Proper motion selection - C2

As previously mentioned, by adopting the C1(Eq. 5.1) criterion we isolate the stars in a region with a depth of ≈ 100 pc around the ONC. Since this area is much larger than the expected physical size of the ONC (Hillenbrand, 1997a), it is not unexpected that the use of the C1(Eq. 5.1) criterion alone does not fully filter out fore- or back-ground objects. Since the stars belonging to a given cluster do in general show similar values of proper motions ($\mu_{\alpha,\delta}$), we can use the $\mu_{\alpha,\delta}$ available from Gaia DR2 to further constrain the ONC membership of the stars selected with the C1(Eq. 5.1) criterion. We show in the right panel of Fig. 4.1 the distributions of μ_α and μ_δ (gray and black histograms, respectively) of all the stars in the C1(Eq. 5.1) selected data set.

It is interesting to note that the distributions of $\mu_{\alpha,\delta}$ are not Gaussian. The histograms show a prominent main peak together with one or more sub-peaks populating the wings of the distributions. Such sub-peaks might be indicative of a system of subclusters or streams located in the vicinity of the main cluster and likely born out of the same molecular cloud. We will investigate this interesting possibility and the detailed nature of such sub-peaks in a forthcoming work, while here we only focus on the main population of the ONC star cluster. To further isolate the bona fide ONC members we hence fit a Gaussian function to the main peaks only. The two Gaussian functions are shown as dashed lines in the right panel of Fig. 4.1 with peaks at

$$\begin{aligned} \mu_\alpha^{\rm ONC} &= \ \ 1.1 \pm 0.6\,{\rm mas/yr}, \\ \mu_\delta^{\rm ONC} &= \ \ 0.3 \pm 0.5\,{\rm mas/yr}. \end{aligned} \tag{4.2}$$

These values are consistent with the ones derived by Kuhn, Hillenbrand, Sills, Feigelson, and Getman (2018) for the inner most 378 selected members, $\mu_{\alpha\star}^K = 1.51 \pm 0.11\,{\rm mas\,yr^{-1}}$, $\mu_\delta^K = 0.5 \pm 0.12\,{\rm mas\,yr^{-1}}$. The selection criterion $n\sigma$ C2 is defined in the PM space and allows us to include only the stars whose PM in R.A. and in Dec fall inside a $n\sigma$ range as follows,

$$\begin{aligned} \mu_\alpha^{\rm ONC} - n\sigma_{{\rm F}\,\mu_\alpha} \leq \mu_\alpha \leq +\mu_\alpha^{\rm ONC} + n\sigma_{{\rm F}\,\mu_\alpha}\,, \\ \mu_\delta^{\rm ONC} - n\sigma_{{\rm F}\,\mu_\delta} \leq \mu_\delta \leq +\mu_\delta^{\rm ONC} + n\sigma_{{\rm F}\,\mu_\delta}\,, \end{aligned} \tag{4.3}$$

where $n\sigma_{{\rm F}\,\mu_\alpha}$ and $n\sigma_{{\rm F}\,\mu_\delta}$ are the number of σ values of the Gaussian to the $\mu_{\alpha,\delta}$ distributions, respectively. The 1-σ values denoted as $\sigma_{{\rm F}\,\mu_\alpha}$ and $\sigma_{{\rm F}\,\mu_\delta}$ are shown in the right panel of Fig. 4.1 as horizontal light and dark gray bars. Their estimated values are written in Eq. (4.2). While the combined use of the C1(Eq. 5.1) and C2(Eq. 4.3) criteria is quite powerful in removing fore- or backgrounds objects, it certainly also removes genuine ONC members. Still we stress here that such objects show PM properties that deviate from the main ONC populations. Such objects are likely binary systems with separations ≈ 0.1" − 0.4" or stars sitting in regions affected by severe crowding where the performance of Gaia degrades and the astrometric solution can be spurious (Arenou, Luri, Babusiaux, et al., 2018; Lindegren, Hernández, Bombrun, et al., 2018). In the first case, the use of C1 (Eq. 5.1), and even more so C2 (Eq. 4.3), very nicely serves one of the main goals of this study to verify the presence of multiple populations in the ONC reported by B17 (see Sec 4.3.3). In the second case, removing genuine

ONC stars that are mostly sitting in the center of the ONC where most of the stars belonging to the youngest population are found, might delete statistically significant kinematic signatures. Hence, the rigorous selection criteria adopted in this work might potentially weaken or even remove any signature of multiple sequences in the CMD. On the other hand, we are confident that, by applying these filters, if any signature of multiple populations is still observed, this would be a solid observational support toward the presence of multiple and sequential bursts of star formation in the ONC.

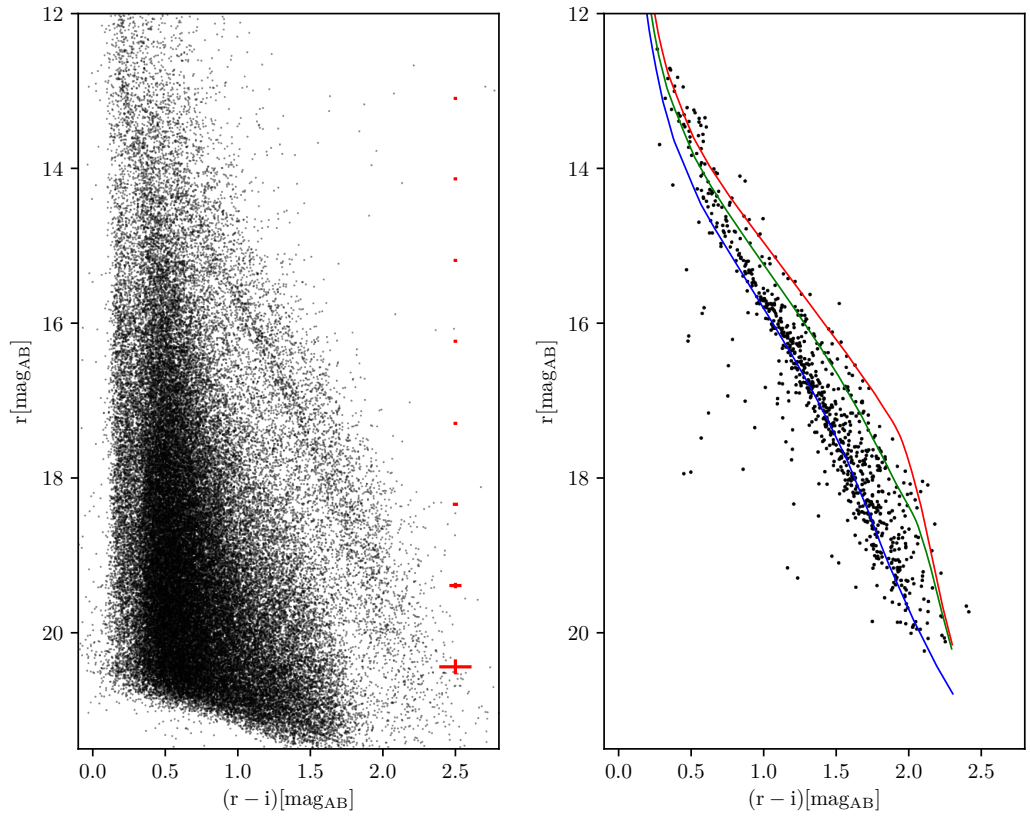

Figure 4.2: **Left panel:** CMD for the initial catalog. The red crosses show $3-\sigma$ color and magnitudes errors. **Right panel:** The CMD of the parallax and proper motion selected ONC members (criteria C1(Eq. 5.1) and 1σ C2(Eq. 4.3) and C3). The color lines are the best fitting isochrones from the Pisa stellar evolutionary model of the three populations.

4.3.3 Constraining the reliable ONC members: Gaia quality check - C3

There are several factors that can affect the accuracy of the astrometric and photometric parameters measured by the Gaia satellite (Lindegren, Hernández, Bombrun, et al., 2018; Evans, Riello, De Angeli, et al., 2018; Arenou, Luri, Babusiaux, et al., 2018). Among others, stellar crowding in a high density environment, faintness of the stars and stellar multiplicity are of particular interest for our work. Such effects are at the origin of the fact that for a number of objects observed with OmegaCAM, parallaxes

were not available or had too large uncertainty (C1; see above). The Gaia catalog offers several parameters that can be used to verify the quality of the measures associated to given objects (Arenou, Luri, Babusiaux, et al., 2018). In the following we describe a few parameters that are of particular interest for our work:

- Duplicated source criterion:
  The current version of the Gaia catalog cannot provide any reliable measurements for sources whose separation on the sky is lower than $0.4-0.5''$ (Lindegren, Hernández, Bombrun, et al., 2018; Arenou, Luri, Babusiaux, et al., 2018). Such objects are flagged in the Gaia-DR2 as duplicated sources (`duplicated_source == True`). Hence, it is immediately understandable that this parameter can be used to identify objects whose measurements are affected by high stellar density (crowding) or unresolved multiplicity. According to Arenou, Luri, Babusiaux, et al. (2018) the average separation among duplicated targets is $0.019''$, corresponding to ≈ 8 au at the distance of the ONC (≈ 400 pc). In summary, when we apply the criterion C3 we remove all the stars which appear with the `duplicated_source == True` in the Gaia catalog.

- Astrometric:
  Arenou, Luri, Babusiaux, et al. (2018) defined the following criterion:

$$u \leq 1.2 \max\left(1, \exp\left(-0.2(G-19.5)\right)\right), \tag{4.4}$$

  where $u = \sqrt{\chi^2/\nu}$, χ^2 = `astrometric_chi2_al` and ν = (`astrometric_n_good_obs_al` -5) suggesting that it can be used to check for spurious astrometric solutions. In the first panel of Fig. 4.10, the u parameter is shown as a function of the apparent Gaia G magnitude. The red dashed line shows Eq. (4.4) for the equal sign. Following the study of Arenou, Luri, Babusiaux, et al. (2018) we will reject from our study all objects whose value of u falls above this line.

The Duplicate source criterion together with the Astrometric criterion are called the C3 criterion. We show in the left panel of Fig. 4.2 the CMD of all the stars included in our initial catalog. In the right panel of the same figure we instead show the CMD of the 852 bona fide ONC stars selected using the C1 (Eq. 5.1) and 1σ C2 (Eq. 4.3) and C3 filtering criteria described above. The population of PMS stars belonging to the ONC is identified with unprecedented accuracy in our final catalog. A main population of PMS is clearly detected while a second parallel sequence is also clearly visible. We emphasize here that using the criteria C1+C2+C3 we already removed many unresolved binary systems.

As previously mentioned, the potential biases introduced by the filtering certainly affect the star counts in the very central part of the cluster because of the presence of stellar crowding and multiple systems. In the next section we will use the catalog of bona fide members to quantitatively investigate the presence of multiple sequences as reported in B17, and their relation to multiplicity. We stress here that the youngest (reddest) populations detected in B17 are also more concentrated toward the center of the cluster. Therefore the biases introduced by the C1(Eq. 5.1), C2(Eq. 4.3) and C3

criteria will certainly affect the statistical significance of the detection of the redder (and possibly younger) sub-populations.

4.4 Identification of multiple sequences in the CMD

In order to identify the presence of multiple and parallel sequences of PMS objects in the ONC, we applied the same approach as described in B17. First, we calculate the main ridge line of the bluest and most populated PMS population in the range of magnitudes $15.5 < r < 17$ (left panel of Fig. 4.3). We use the mean ridge line as reference in the $(r, r-i)$ CMD and we then calculate the projected distance in $r-i$ colors of each star from the reference line (see the central panel of Fig. 4.3). We show in the right panel of Fig. 4.3 the distribution of the perpendicular distances in color from the main ridge line, $\Delta(r-i)$. The black histogram shows the distribution of C1+1σC2+C3 selected data sample. To complement Fig. 4.3 that is showing projected distribution $\Delta(r-i)$ from the main ridge we show, on the request of the anonymous referee, a distribution in vertical distances from the main ridge line $\Delta(r)$, see Fig.4.4.

Clearly the distribution in color of the ONC members is described by at least two peaks with a gap in the middle. This feature fully confirms the observation in B17. As already noted by B17, the number of stars belonging to the third population (i.e., the reddest peak) is quite low. We would like to stress here once more that the use of the C1(Eq. 5.1), C2(Eq. 4.3) and C3 filtering preferentially removes stars located in crowded regions. We hence expect that our selection criteria mostly lower the number of stars in the reddest or youngest population that, according to B17 is the one that is most concentrated toward the ONC center.

We used three Gaussian functions (gray line in the figure) to fit the color distribution and in particular the three peaks. We then use these functions to select members belonging to each population. Given the fact that the second and third sub-populations are overall populated by a very low number of stars (54 and 15, respectively) we decided to proceed further with our analysis by dividing the ONC populations into an "old" and "young" population (respectively blue and orange bar in Fig. 4.3 and afterwards). Hence the stars belonging to the second and third peak are grouped and studied together.

In Fig. 4.5 we show the distribution on the sky of the two sub-populations (blue and orange points). The two-dimensional Kolmogorov-Smirnov test (Peacock, 1983; Fasano and Franceschini, 1987; Press, Teukolsky, Vetterling, and Flannery, 2007) done on the measured distribution suggests that the two populations are not extracted from the same parental population at $\approx 2.3\sigma$ level of significance. We would like to stress here that the data set shown in the figure suffers from severe incompleteness, especially in the central region, because of the Gaia DR2 loss of sensitivity in regions affected by stellar crowding. As extensively discussed by B17, the use of the OmegaCAM data-set alone (i.e., without applying the filtering used in this work) indicate the presence of a prominent concentration of all three populations toward he same center.

Gaia offers us the possibility to study, for the first time, the parallax distribution and the proper motions of the two sub-populations. We plot in Fig. 4.6 the histogram of

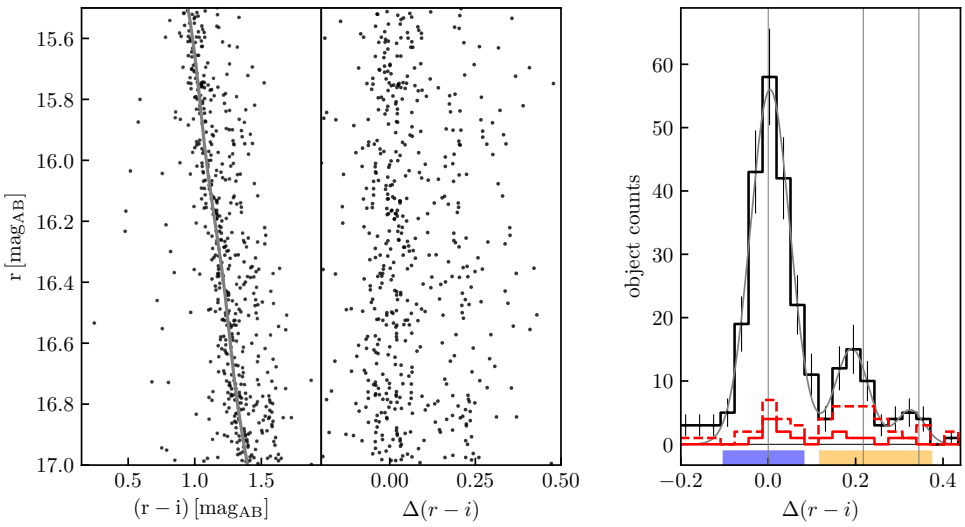

Figure 4.3: **Left panel:** CMD of the C1+C2-1σ+C3 selected data sample. The main ridge line is shown as a gray line. **Middle panel:** The CMD rotated along the slope of the main ridge line. **Right panel:** The histograms of the distances in color from the main ridge line. The black solid line corresponds to the data sample after applying all selection criteria (C1, C2 1-σ and C3). The vertical line at $\Delta(r-i)=0$ shows the position of the mean ridge line which serves as a reference line. It also represent the location of the single stars belonging to the main population of the ONC. The two vertical lines $\Delta(r-i)>0$ indicate the expected positions of the equal mass binary and triple systems, respectively. The red dashed histogram shows the unresolved binary stars from Tobin, Hartmann, Furesz, Mateo, and Megeath (2009). The solid-line red histogram shows the distribution of the unresolved binaries that passed the selection criteria (C1, C2 1-σ and C3).

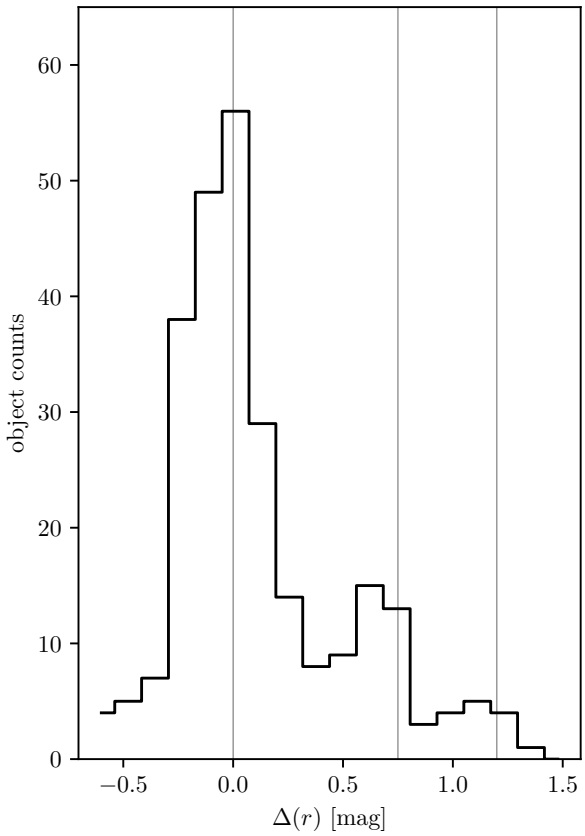

Figure 4.4: Complementary plot to Fig. 4.3 showing the distribution of magnitudes from the main ridge line instead of the perpendicular distance in color and magnitude that is on Fig. 4.3. We show the position of the main ridge line (at 0.0) as well as unresolved equal-mass binaries and equal-mass triples stars, using vertical lines. The positions of the three peaks relative to the main ridge line and equal-mass binaries or triples is quantitatively comparable to the Fig. 4.3.

the parallax (left panel) and proper motions (right panel) distributions of the blue and orange populations. The 2D KS test indicates that the proper motions of the blue and orange sub-populations are not extracted from the same parental population at only $\approx 1.3\sigma$. For the parallax distributions, which are 1D, the Anderson-Darling statistical test [3] indicates that they are not extracted from the same parental distribution at $\approx 2.3\sigma$ (see Alves and Bouy, 2012, for suggested line-of-sight complex distribution of stellar populations). Since the members of the ONC were selected such that they have the same proper motion values (see Sect 4.2.2) the potential difference in proper motions for the different populations might have been erased. However, it is the use of proper motions that offers the most reliable way to constrain the membership in the ONC with Gaia DR2 as the parallax uncertainties are still too large. The 2.3σ difference is thus suggestive but not conclusive evidence of a real difference in proper motions and needs to be investigated further with future releases of the Gaia catalog.

[3] implemented in the `scipy.stats` python package based on Scholz and Stephens (1987)

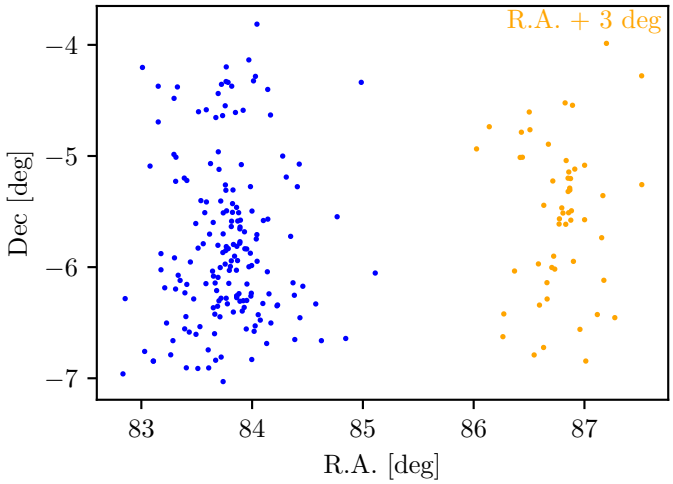

Figure 4.5: The R.A. - Dec distribution of the first and second sequence identified in Fig. 4.3. To compare on-the-sky distributions of the "old" and "young" sequences we use two-dimensional Kolmogorov-Smirnov test (Peacock, 1983; Fasano and Franceschini, 1987; Press, Teukolsky, Vetterling, and Flannery, 2007) resulting in $p = 0.01$ ($\approx 2.3\sigma$).

We used the Anderson-Darling test to explore the possibility that the comparison of the distributions of proper motions are not affected by different distributions in magnitudes among the different stellar populations. The test indicates that the distributions of magnitudes of the bluest population and the two reddest ones combined are extracted from parental populations which cannot be distinguished significantly ($p = 0.4$ for the magnitudes not to being drawn from the same parental distribution).

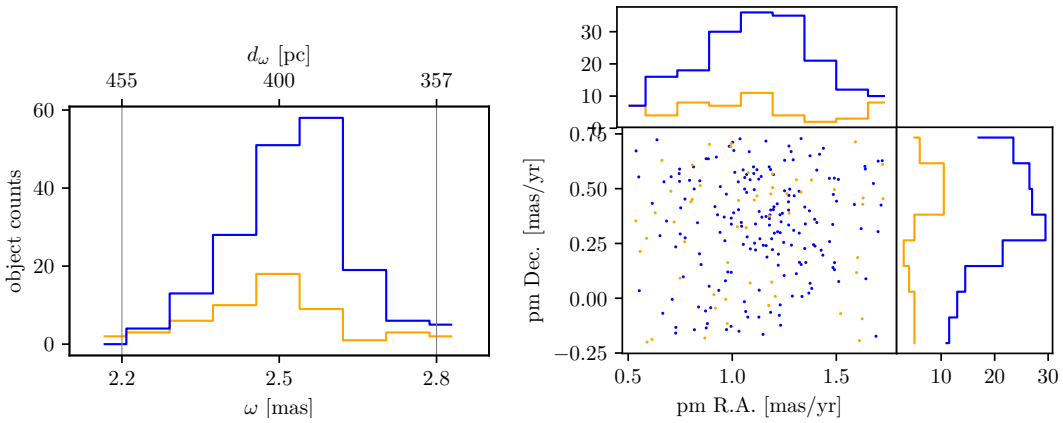

Figure 4.6: Left panel: distribution of the parallax, ϖ, of the identified main-ridge sequence (blue), second +third sequence (orange). The top horizontal axis shows corresponding values, d, in parsec using $d[\mathrm{pc}] = 1/(\varpi[\mathrm{mas}] \cdot 10^{-3})$, valid for those objects that have small relative errors (Gaia Collaboration, Brown, Vallenari, et al., 2018). Right panel: the R.A. and Dec proper motions with the histograms of projected distributions on the sides of the plot.

To summarize, the currently available data indicate that the ONC objects are gradually more centrally concentrated (proportionally to $\Delta(r - i)$) and suggest potential

differences in the parallax distributions between the sequences. Under the assumption that the bluer population is older with respect to the orange one (see B17) the current analysis indicate that the older population of the ONC might be closer to us with respect to the younger one. Both of these findings seems to support the hypothesis that a genuine difference in age is at the origin of the distribution in the CMD of the two sub-populations.

4.4.1 Multiple sequences in the ONC with binary star analysis

Here we would like to study the presence of unresolved multiple systems among the catalog used to obtain the histograms of Fig. 4.3. Ideally, the main ridge line of the main population (corresponding to $\Delta(r-i)=0$) represents the position of single stars. In reality single stars will have certain scatter due to intrinsic photometric uncertainty and possible age spreads.

Unresolved binary system will have a total magnitude in the range of the primary component up to being brighter by 0.75mag in the case of equal mass binaries. Thus the upper theoretical limit for $\Delta(r-i)$ of unresolved binaries is constructed by projecting the theoretical location on the CMD of the equal mass binary sequence along the main ridge line, as done for the observed stars. The same exercise can be done for the equal mass triple systems. The two gray vertical lines in the right panel of Fig. 4.3 represent the theoretical maximum values in $\Delta(r-i)$ of any unresolved binary and triple systems. But this is not realistically the case because the second and third peaks are too defined, since an age dispersion would soften the peaks if they were due to unresolved binaries and triples. That is, in order to explain the outlying systems through a small age spread, one would need an even more unnatural mass-ratio distribution than already excluded by B17. While it is possible that the objects falling in between the reference line at $\Delta(r-i)=0$ and the one indicating the position of multiples are indeed unresolved binaries, one should invoke a peculiar mass ratio distribution in order to reproduce the observed color distribution and the presence of a gap (see B17 for explicit calculations). The separation of the main ridge line and the second peak remain the same as in B17 and thus we do not repeat the calculations here. We would need to do exactly the same as in B17 with those same data, since the data used here are subject to, among other biases as stated above, the central incompleteness that certainly affects the shape of the distributions in $\Delta(r-i)$.

Tobin, Hartmann, Furesz, Mateo, and Megeath (2009) published a catalog of 135 spectroscopic binaries (SBs) in the ONC. All the SBs are recovered in our initial catalog. We show as a red dashed histogram in Fig. 4.3 the distribution in $\Delta(r-i)$ of the unresolved binary stars from Tobin, Hartmann, Furesz, Mateo, and Megeath (2009) falling in the magnitude range 15.5<r<17 (64 out of 135). Among the 64 unresolved binaries, 30 populate the $\Delta(r-i)$ range coincident with the bluest and oldest population of the ONC, while 34 are in the reddest peak. This sample allow us to test how efficient is our filtering methods in identifying unresolved multiple systems.

In fact we applied to the catalog of 64 unresolved binaries from Tobin, Hartmann, Furesz, Mateo, and Megeath (2009) and retrieved in our photometry the C1, C2 and C3 selection criteria. The distribution in the $\Delta(r-i)$ plane of the catalog of filtered binaries that survive to our selection criteria is shown as solid red line in the right panel

of Fig. 4.3. Only 16 stars out of the initial 64 (25%) passed our filtering. In particular, nine stars among the 30 objects populating the bluest (30%) peak remains undetected, while only seven among the reddest 34 systems passed our selection criteria (20%). This test demonstrates that our filtering method largely removes the unresolved binary stars, especially those that are in the position of the second peak (that is $q \gtrapprox 0.5$). So it indeed shows that our filtering method is able to remove binaries that are present in the second sequence. To confirm this we performed the following experiment: we define as the general population, the sample that has been parallax selected with a 3-sigma cut in proper motion, that is, we keep only the likely members of the regions (noting that such a sample is incomplete). For this general population the above-applied filtering keeps 60% of the stars belonging to the main peak (population one) and 40% of the stars belonging to the second and third peak – proving a) that the filtered number of targets is smaller for the general population data sample than for the binary star catalog by Tobin, Hartmann, Furesz, Mateo, and Megeath (2009), in agreement with the statement that the applied filtering is able to remove binary stars, and b) that the removed fraction of stars in the range where we expect unresolved binary or triple stars is higher, in line with the previous point a).

We note that the filtering removes a substantial fraction of multiple systems. In particular, Gaia cannot find astrometric solutions typically for binaries. The exact fraction of binaries filtered out by which of the criteria is however a non-trivial problem and cannot be quantified here as this would depend on detailed modeling of the space craft and the stellar population at the distance of the ONC, see for example Michalik, Lindegren, Hobbs, and Lammers (2014).

4.4.2 PMS isochrones

Stellar models have been computed using the most recent version of the Pisa stellar evolutionary code (see e.g., Tognelli, Prada Moroni, and Degl'Innocenti, 2011) described in detail in previous papers (see Randich, Tognelli, Jackson, et al., 2018; Tognelli, Prada Moroni, and Degl'Innocenti, 2018, and references therein). We simply recall the main aspects relevant for the present analysis. The reference set of models adopts a solar calibrated[4] mixing length parameter, namely $\alpha_{\rm ML} = 2.0$. However, for the comparison we also used a much lower value, namely $\alpha_{\rm ML} = 1.00$ (low convection efficiency models) which produces cooler models with inflated radii (see e.g., Tognelli, Degl'Innocenti, and Prada Moroni, 2012; Tognelli, Prada Moroni, and Degl'Innocenti, 2018). Evolutionary tracks of mass $\geq$1.20 $M_\odot$ have been computed adopting a core convective overshooting parameter $\beta_{\rm ov} = 0.15$, following the recent calibration of the Pisa models by means of the TZ Fornacis eclipsing binary (Valle, Dell'Omodarme, Prada Moroni, and Degl'Innocenti, 2017).

From the models (in the mass range 0.1-20 M_{sun}) we obtained isochrones in the age range [0.1, 100] Myr with a variable spacing in age (down to $\delta t = 0.1$ Myr), allowing for a very good age resolution. For the reference set of models we used [Fe/H]= +0.0, corresponding to an initial helium abundance $Y = 0.274$ and metallicity $Z = 0.013$

[4]Solar calibration is an iterative procedure to derive the initial metallicity, helium content and mixing length parameter needed to reproduce, at the age of the Sun, for a 1 $M_\odot$ model the Solar luminosity, radius and surface (Z/X) composition, within a tolerance of less than 10^{-4}.

given the Asplund, Grevesse, Sauval, and Scott (2009) solar heavy-element mixture.

We have converted the theoretical results into the OmegaCAM r and i absolute AB magnitudes using bolometric corrections we computed using a formalism similar to that described in Girardi, Bertelli, Bressan, et al. (2002), employing the MARCS 2008 synthetic spectra library (Gustafsson, Edvardsson, Eriksson, Jørgensen, Nordlund, and Plez, 2008), which is available for $T_{\rm eff} \in [2500, 8000]$ K, $\log g \in [-0.5, 5.5]$, and [Fe/H] $\in [-2.0, +0.5]$ completed with the Castelli and Kurucz (2003) models for $T_{\rm eff} > 8000$ K.

Next we compared the evolutionary models with the data in order to identify the best fitting isochrones for the observed PMS populations. This was performed by using the same Bayesian maximum likelihood technique described in Randich, Tognelli, Jackson, et al. (2018). Briefly, the method computes the distance of each star in the observational plane from a given isochrone extracted from our database. The square of the distance is used to define the likelihood of a single star. Then, the total likelihood is defined as the product of all the single star likelihoods.

The parameters to be recovered in this work are the age t and the reddening E(B-V). Thus, along with the grid in age, we also built up a fine grid in E(B-V). To derive the extinction in a given band (i.e., r and i) we adopted the Cardelli, Clayton, and Mathis (1989) extinction law by re-computing the extinction coefficients A_r/A_V and A_i/A_V for the OmegaCAM filters employed. In the following we have performed the parameters recovery under two assumptions: 1) the spread is caused by unresolved binary stars and 2) the spread is actually due to multiple populations.

In the first case, we derived the age and reddening running the recovery over the whole dataset, allowing for the presence of a binary sequence. We have imposed that the binary sequence has a fixed secondary-to-primary mass ratio $q = 0.8$ and 1. However, to achieve such a large separation as visible in the CMD, a value of $q = 1$ is preferred.

In the second case, that is, in case of multiple populations, we adopted another strategy. First, we selected the members belonging to each population (see Sect 4.4): the selection identified three populations. We imposed the constraint that all the three populations contained in our sample are affected by the same reddening, in agreement with B17.

Such a condition has been implemented in our recovery code in four steps. First, we obtained the total likelihood – which depends on the age and E(B-V) – for each population. Then, we marginalized over the age to obtain a likelihood which is a function of only E(B-V). This step produces the distribution of the possible E(B-V) for each population. We multiply the E(B-V) distributions obtained at the previous step (for each population), to obtain the E(B-V) distribution for the whole dataset under the assumption that the best E(B-V) is the same. Then, as the best E(B-V) of the whole dataset we chose the maximum of such a distribution. As a final step, we run again the recovery for each population, but using this value of E(B-V) as a prior (Gaussian prior), to derive only the age of each population.

In both cases, to obtain the confidence interval on t and E(B-V), we adopted a Monte Carlo simulation, that is, we perturbed independently each datum within its uncertainty range, to create a given number $N_{\rm pert} = 100$ of representations of the ONC population. For each representation we derived the age and reddening using the method discussed above, to obtain a sample of ages and reddening. Then, we defined the best value as the mid of the ordered sample (in t and E(B-V)) and the upper and

lower extreme of confidence interval as the 84th and 16th percentile of the distribution, respectively.
The best fitting parameters are,
$\mathrm{age_{pop1}} = 4.5^{+1.5}_{-1.2}$ Myr,
$\mathrm{age_{pop2}} = 2.1^{+0.5}_{-0.4}$ Myr and
$\mathrm{age_{pop3}} = 1.4^{+0.3}_{-0.2}$ Myr,
with E(B-V)=0.052±0.020 begin consistent with E(B-V) from B17. The corresponding χ^2 is $\chi^2 = 3.6$. The best fitting isochrones are shown in Fig. 4.2 (right panel).

4.4.3 The apparently old "scattered" objects in the CMD

After applying selection criteria C1(Eq. 5.1),1-σ C2(Eq. 4.3) and C3 we expect to be left with mainly ONC members which are PMS stars. However in right panel of Fig. 4.2 there is clearly a noticeable group of stars that do not appear to be PMS stars, that is, the objects are bluer than the majority of stars. Manara, Beccari, Da Rio, et al. (2013) studied two such objects in detail using broadband, intermediate resolution VLT X-shooter spectra combined with an accurate method to determine the stellar parameters and the related age of the targets. They show that the two selected stars are actually as young as the bulk of the ONC stars. They conclude that, if only photometry is used as an age estimator then especially for bands sensitive to the presence of accretion, like the here used r and i, several accreting objects may appear scattered from the bulk PMS population on the CMD. That is accretors are most likely the explanation for the presence of the blue-wards scattered points in the CMD. We will investigate these bluer targets in detail in a follow-up work (Beccari et al., in preparation).

4.5 Apparent binary and triple systems

In the previous section we investigated the impact of unresolved binaries on the detection of multiple populations among the PMS of the ONC. We are now interested in exploiting the potential of the Gaia DR2 catalog in combination with the OmegaCAM photometry to investigate resolved multiple systems. The seeing limited OmegaCAM photometry aims at resolving binaries having separations $\gtrapprox$ 0.7". While the resolution of Gaia DR2 is 0.4", Ziegler, Law, Baranec, et al. (2018) show that Gaia is only able to reliably recover all binaries down to 1.0" at magnitude contrast as large as 6 magnitudes.

One method to investigate resolved apparent binary candidates is to construct the so-called Elbow plot (e.g., Larson, 1995; Gladwin, Kitsionas, Boffin, and Whitworth, 1999). The method consists in calculating the distribution of the number density of observed targets (Σ) as a function of on-the-sky separation (θ). As shown in Gladwin, Kitsionas, Boffin, and Whitworth (1999) the presence of an elbow in the density distribution described above is caused by the presence of resolved binaries. In short, for each star in our catalog we divide the surrounding area of sky into a set of annuli, by drawing circles of radius θ_i centered on the star, with $\theta_i = 2\theta_{i-1}$ and $i \geq 1$. θ_0 is chosen

to be well below the smallest separation in the sample. Next we count the number of companion stars in each annulus and we calculate the $\Sigma(\theta)_i$ as follows,

$$\Sigma(\theta)_i = \frac{N_i}{\pi N_{\rm tot}(\theta_i^2 - \theta_{i-1}^2)}\,, \tag{4.5}$$

where N_i is the number of stars in the ith bin, $N_{\rm tot}$ is the total number of stars and $\theta = (\theta_i + \theta_{i-1})/2$ is the angular separation of measured sources.

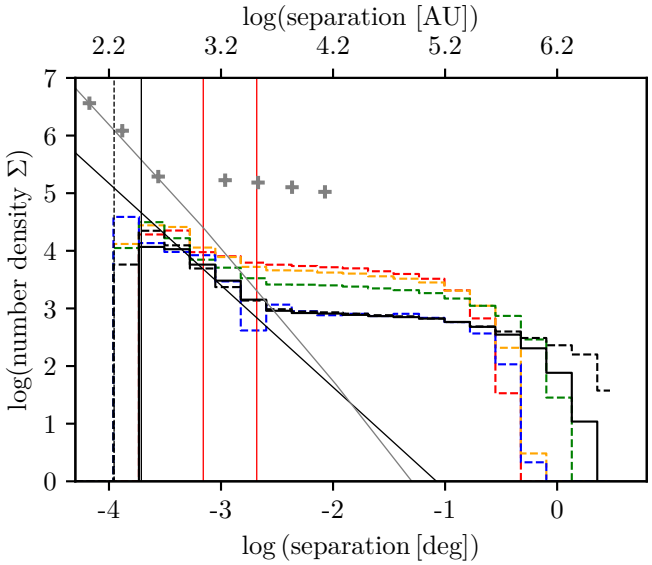

Figure 4.7: The Elbow plot showing the surface number density as a function of separation on the sky. The black dashed line shows the original Gaia data sample, the black solid line shows the cross-matched, that is, initial, catalog after the C1 and 2-σC2 are applied. We fit the elbow part of the diagram obtaining a slope value -1.7 ± 0.05. The gray data points and the DM slope are from Simon (1997) having a smaller field of view by using the HST. The gray line is the Duquennoy and Mayor (1991) distribution of binary stars of G-type primaries that has been reformulated to the number density Σ by Gladwin, Kitsionas, Boffin, and Whitworth (1999) (their eq. (5)). The vertical lines (from left to right) are the resolution limit of Gaia DR2, the resolution limit of OmegaCAM, respectively, the first red line shows $(1 \cdot 10^3$ au) as the definition of wide binaries, and the last line shows the start of the Elbow feature $(3 \cdot 10^3$ au). The color histograms are constructed for central circular regions (see Fig. 4.8) to see how the potential of detection of wide binaries changes with the chosen spatial region.

We show in Fig. 4.7 the Elbow plot as calculated using the stars sampled with the Gaia DR2 catalog alone (black dashed line) and Gaia DR2 cross-matched with the OmegaCAM catalog (black solid line). We applied the C1 and 2σC2 criterion to both catalogs. The C1 and 2σC2 criterion reduces significantly the contamination by objects not belonging to the ONC, but on the other hand keeps the data sample as complete as possible. The slope of the elbow is -1.70 ± 0.05 which suggests incomplete data sample toward smaller separations as slope values for complete samples in binary-devoted studies are ≈ -2 (Gladwin, Kitsionas, Boffin, and Whitworth, 1999). This is consistent with the recovery completeness found by Ziegler, Law, Baranec, et al. (2018) showing that Gaia DR2 is complete for multiple systems separated by at least 1 arcsec.

Prosser, Stauffer, Hartmann, et al. (1994) used the Hubble Space Telescope to probe the densest central region of the ONC and Simon (1997) then created the elbow plot. The data are plotted as gray crosses in Fig. 4.7. The difference between the results of Simon (1997) and our study is most likely caused by the different field of view, as Simon (1997) looked at the inner-most part of the ONC, as well as by the fact that using Gaia, we are able to successfully remove fore- or background contaminators.

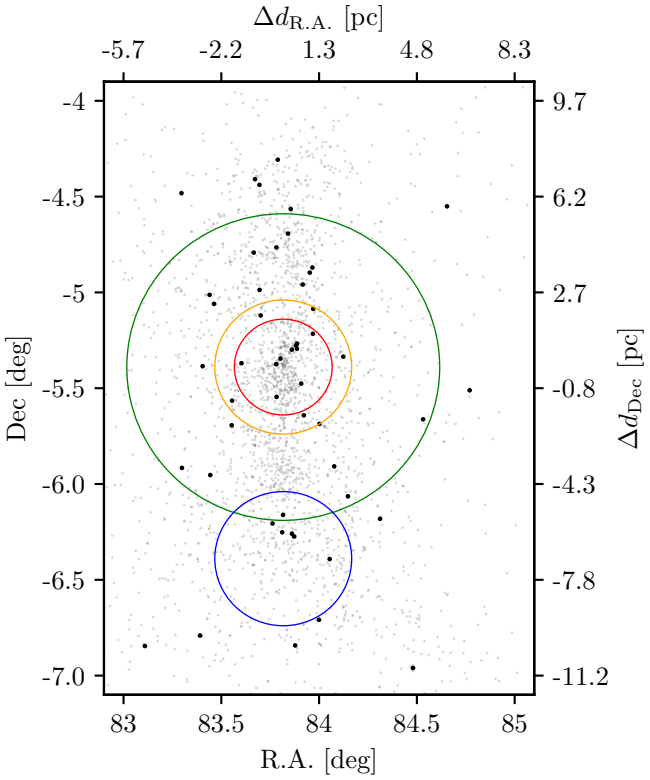

Figure 4.8: On-the-sky distribution of the wide (on-the-sky component separation between 1000 and 3000 au) binaries. Only one component of the binary star candidates is plotted. The red circle shows the region, 15 arcmin = 0.25 deg, investigated by Scally, Clarke, and McCaughrean (1999) who found only four candidates. The orange (radius of 0.35 deg) circle shows the region we selected to test how the Elbow plot depends on the investigated spatial scale. The green circle is the (1 deg) large testing region and the blue circle (radius 0.35 deg) is outside where the stellar density is lower.

From the Elbow plot we can see that the overabundance of stars, suggesting the presence of multiple systems, starts at $\approx$ 3000 au. Interestingly, Scally, Clarke, and McCaughrean (1999), based on a proper motion study, suggested that there should be no wide binaries with separations larger than 1000 au. Therefore we decided to investigate the indications of the presence of wide binaries (binaries with apparent separations larger than 1000 au) in our data in more detail.

To investigate the effect of crowding on the Elbow plot we divide the sampled region in four circular regions. Three of the regions are concentric and centered on the ONC center, where the stellar crowding is more severe and hence the completeness expected

to be lower. A fourth circle has been centered at 1 deg distance toward the south with respect to the ONC. Such region is located well in the outskirt of the cluster, where the stellar distribution is quite homogeneous and the stellar density very low. We show the location of the circles in the sky in Fig. 4.8 while in Fig. 4.7 we show with the same color code the Elbow plot only for objects within each circle. Clearly, the detection of wide binaries in the central region is challenged by most likely the high stellar density. The more we expand toward the external regions, the detection becomes more and more significant (see the blue line).

Next, we use parallax and proper motion cuts to minimize potential fore- or background contaminants (C1 and C2 but assuming 3σ tolerance as here we aim to remain as complete as possible). There are 86 candidates having apparent separation smaller than 3000 au as defined by the Elbow plot, and larger than 1000 au. Such pairs with separations between 1000 and 3000 au are our wide binaries candidates.

As additional criterion for two stars being a binary candidate we implement the relative proper motion criterion introduced by Scally, Clarke, and McCaughrean (1999). That is, we check the relative proper motions of all the candidates and require their value to be 0 within the $3\sigma_\mu$ proper motion uncertainty (the average uncertainty, σ_μ, is larger than the escape velocity from a system with 1000 au separation assuming Solar masses of both components). After this we have 60 wide binary candidates from which ten are in the inner 15 arcmin region used by Scally, Clarke, and McCaughrean (1999). Scally, Clarke, and McCaughrean (1999) found only four candidates in the very same region. All the binary star candidates fulfilling the separation and the pm criteria are listed in Tab. 4.A1 in the Appendix to this Chapter, including also binary candidates with separations smaller than 1000 au.

In Fig. 4.9 we construct the normalized binary fraction distributions defined as the number of binaries over the total number of objects, and compare it with the previous study of Duchêne, Lacour, Moraux, Goodwin, and Bouvier (2018). We extend the separation range of the Duchêne, Lacour, Moraux, Goodwin, and Bouvier (2018) study and find excess of wide binaries in comparison to Scally, Clarke, and McCaughrean (1999). We compare the central 15 arcmin around the ONC, that is, the same area studied by Scally, Clarke, and McCaughrean (1999), with the full region studied here and find comparable binary fraction.

The main reason why we are able to detect more of these wide apparent binary star candidates than Scally, Clarke, and McCaughrean (1999) is likely due to the fact that Gaia DR2 allows us, for the first time, to obtain a clean sample of the ONC region only. The contamination of other sources is otherwise too high. We note that due to the crowding at the very center - in the ONC - the detection of the wide pairs are more likely due to chance projections. Our findings are sharpened up by the proper motion study, nevertheless obtaining the 3D velocity information would provide an additional test.

4.5.1 Apparent triple systems

In the Gaia data sample, that is Gaia only catalog with C1 parallax cut and 2-σC2 proper motion cut, we identified five apparent triple systems and only one of these has component relative proper motions consistent with zero. To identify triple system

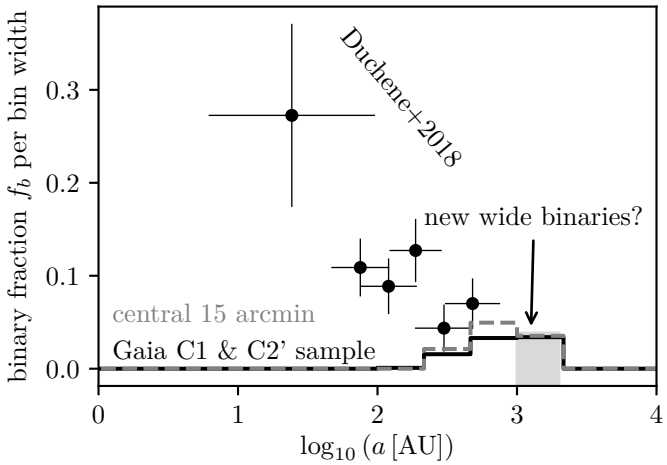

Figure 4.9: The plot shows the binary fraction, defined as the number of binaries over the total number of objects, normalized by the bin width. The black points are data for the ONC from Duchêne, Lacour, Moraux, Goodwin, and Bouvier (2018). The black histogram shows f_b for the spatially not constrained region, that is Gaia DR2 data with C1 and C2 selections. The gray dashed histogram shows the data only for the central part that is the same as in the study by Scally, Clarke, and McCaughrean (1999). The last bin showing wide binaries in the range 1000-3000 au represents newly discovered potential binaries that seemed to be absent (Scally, Clarke, and McCaughrean, 1999) (see Fig. 4.8). The limit 3000 au is motivated by the beginning of the elbow in Fig. 4.7.

candidates we at first identified the closest potential binary companion candidate and quantified the center of light of the candidate binary. We then find its closest neighbor. If the closest neighbor has a projected separation smaller than 3000 au (the maximal separation captured by our data) then the three neighbors are classified as an apparent triple star candidate. The identified candidates are summarized in Tab. 4.1.

4.6 Summary and conclusions

The ONC star forming region has been studied in detail using the data from Gaia DR2 in combination with deep OmegaCAM photometric data. We summarize our main findings bellow: Firstly, we used parallaxes and proper motions to separate the ONC stellar population from background and foreground contamination using Gaia DR2. Cross-matching with the OmegaCAM photometric catalog provides high-quality photometry in r and i filters. This fact turns to be critical in studying the properties of the stellar populations in the ONC as Gaia DR2 photometry does not provide reliable magnitudes in crowded regions (see Appendix 4.7). Using these data we are able to construct the CMD and detect two well separated PMSs with a suggestion for the existence of a third one, despite Gaia DR2 data being incomplete in the central high density regions where the members of the second and third sequences are mostly located.

To explore the effect of unresolved binary stars we applied filtering as thoroughly as possible. The adopted filtering criteria are able to remove basically all unresolved

ID1	ID2	ID3	a_1 (deg.)	a_2 (deg.)	G_1	G_2	G_3
3017367121346098944	3017367121333529984	3017367086986361216	0.26	1.97	17.2	15.5	16.8
3017244388347833728	3017244388350754816	3017244388350754944	0.40	1.76	14.9	16.7	15.4
3017242532924887936	3017242532921992320	3017242528629466624	0.42	1.24	15.0	14.6	17.8
3209528905960092160	3209528905962364160	3209528905962363904	0.49	1.11	17.5	15.4	14.3
3017135399259048704	**3017135394962860800**	**3017135394965152000**	**0.52**	**1.46**	**15.3**	**15.2**	**16.2**

Table 4.1: Identified apparent triple system candidates. The apparent triple system candidates identified based on the projected distance. Only the bottom-most line, the black one, fulfills the additional constraint of all putative companions having identical proper motions within 3-σ uncertainty range.

binary stars contributing to the second sequence. In order to probe the capability of our filtering criteria to isolate unresolved binaries, we identified in our catalog 64 unresolved binaries from Tobin, Hartmann, Furesz, Mateo, and Megeath (2009). We applied our filtering selection to these stars and demonstrate that we are able to safely identify and filter-out 80% of unresolved binaries.

We confirm the previous result of B17 that a single stellar populations with binaries (or triples) can not alone describe the observed distribution of stars in the CMD. Our study supports the hypothesis that the PMS population of the ONC is better described as three stellar populations with different ages. We use PMS models calculated using the Pisa stellar evolutionary code to find the best fitting isochrones describing the population on the CMD. We estimate an age difference of ~ 3 Myr between the youngest (~ 1.4Myr) and the oldest (~ 4.5Myr) stellar population. In line with B17 the youngest sequences appear to be more concentrated toward the ONC center with respect to the oldest population. We perform a series of statistical tests with the aim of identifying kinematic differences between the old and young stellar population (see Sect 4.4). We find a mild indication that the individual sequences might have different parallax distributions with the older population slightly closer to us along the line of sight with respect to the youngest one. While this result is in principle in line with the youngest population being still more embedded in the molecular clouds, we note that the uncertainties in the Gaia DR2 data are still too big to allow us to perform such a detailed study with solid statistical significance. More precise data (or additional data - like radial velocities) will be necessary to confirm these results.

Interestingly, even adopting a rigorous filtering strategy via accurate parallaxes and proper motions selection criteria, the stars belonging to the ONC seem to occupy a ≈ 100 pc region in the line-of-sight direction and ≈ 20 pc on the sky. Hence this study well extend behind the canonical size of the ONC star cluster, which is only few a pc large (Hillenbrand, 1997a). While it is well know that the Orion Nebula is in fact a complex star forming region, hosting several episodes of star formations, we stress here that the precision of the Gaia DR2 parallaxes implies, for a 10% relative error, a 40 pc uncertainty at the distance of the ONC.

Secondly, we use our final catalog of bona fide ONC member to study the population of apparent resolved multiple objects in the region. We analyze apparent multiple system candidates using the elbow plot. The position of the elbow suggests that wide binaries that we are able to capture have a separation of up to ≈ 3000 au (≈ 7 arcsec). However, this depends on the investigated region and becomes less clear in the dense ONC center. Thus we identify all the targets having a separation smaller than 3000 au and identical proper motions within the measurement uncertainty. This allows us to detect in total 91 targets out of which 60 have a separation between 1000 au and 3000 au. Scally, Clarke, and McCaughrean (1999) suggested that wide binaries (semi-major axis larger than 1000 au corresponding to an orbital period longer than $28,000$ yr for a system mass of $1.3\,M_{\odot}$) are largely absent from the ONC implying that ONC-like clusters cannot be at the origin of the majority of field stars. Here we have found evidence for a large population of wide binaries in the ONC with projected separation up to 3000 au, or an orbital period of $\approx 144,000$ yr for a system mass of $\approx 1 M_{\odot}$.

Using detailed stellar-dynamical models of the ONC (expanding, collapsing and dynamical equilibrium models) Kroupa, Petr, and McCaughrean (1999) showed that,

depending on the dynamical state of the ONC, wide binaries are expected to be present. Moreover, the way binary fraction varies radially can put new constraints on the dynamical state of the ONC. Evidence for the breakup of wide binaries after falling through the cluster has been found in the survey for optical binaries in the ONC by Reipurth, Guimarães, Connelley, and Bally (2007). Even more realistic N-body models have been computed by Kroupa (2001) who assumed the ONC to be post-gas expulsion, that is, to have just emerged from the embedded phase. These authors also show that the ONC ought to have a population of wide binaries depending on how concentrated the ONC was prior to the onset of the removal of the residual gas (compare the upper and lower panels in their Fig.10). Therefore, if there were no wide binaries, then the pre-gas-expulsion ONC would have corresponded to a model with a half-mass radius close to 0.2 pc, while the presence of wide binaries would require it to have been close to 0.45 pc. While firm conclusions cannot yet be reached on the dynamical state of the ONC, in particular also because the dynamical state of very young clusters with masses near to that of the ONC may be complex (Kroupa, Jeřábková, Dinnbier, Beccari, and Yan, 2018; Wang, Kroupa, and Jerabkova, 2018), this discussion shows the importance of surveying for binaries in the ONC and for correlating them with their ages, positions and motion vectors relative to the ONC.

Acknowledgements: *TJ thanks Hans Zinnecker and Pavel Kroupa for interesting and fruitful discussions and useful comments to the manuscript. In addition TJ acknowledges discussions with Josefa Großschedl and Stefan Meingast, who found important formatting error in the Tab. A.1. We thank Frédéric Arenou for clarification of the photometric excess parameter in the Gaia DR2 catalog. PGPM, ET and SD acknowledge INFN "iniziativa specifica TAsP". CFM acknowledges an ESO Fellowship. Based on observations collected at the European Southern Observatory under ESO program 098.C-0850(A).*

4.7 Appendix: Comparison of OmegaCAM photometry with Gaia DR2 photometry

In the following text we demonstrate that additional photometric data set is needed in dense region as ONC to be able to study the stellar populations. We follow Gaia DR2 release work by Arenou, Luri, Babusiaux, et al. (2018) and show that the photometric information in Gaia Gp and Rp filters gets affected by crowding and is not suitable for precise study. Arenou, Luri, Babusiaux, et al. (2018) introduced the photometric excess criterion,

$$1.0 + 0.015(G_{BP} - G_{RP})^2 < E < 1.3 + 0.06(G_{BP} - G_{RP})^2 \,,$$

where E is defined as the flux ratio in the three different Gaia passbands,

$$E = \frac{I_{BP} + I_{RP}}{I_G} \,. \tag{4.6}$$

The Gaia DR2 presents the photometric set in broad band photometric filters G, G_{BP} and G_{RP}. The photometry measurements suffer from significant systematic effects for the faint sources ($G \geq 19$), in crowded regions, nearby sources (such as multiple

systems) included. The G band is measured using the astrometric CCDs with a window of typical size of 12x12 pixels (along-scan x across-scan). However it is 60x12 pixels for the BP and RP spectral bands. Thus for a single isolated point-source the G band flux has a comparable value with the sum of the integrated fluxes from the BP and RP bands as expected from the bands' wavelength coverage. On the other hand, if the source is contaminated by a nearby source or it is extended so it is not fully covered by the G band window, then the G flux is not comparable with the sum of BP and RP fluxes (Gaia Collaboration, Prusti, de Bruijne, et al., 2016a). The photometric excess criterion described above can hence be used to check the accuracy of the photometry in the Gaia DR2 catalog (Gaia Collaboration, Brown, Vallenari, et al., 2018).

We show in Fig. 4.10 (third panel from the left) the distribution of the excess factor E as a function of $G_{BP} - G_{RP}$ color for the entire catalog (gray points) and for the stars selected using the criterion C1 (black points). The red dashed lines indicate the selection limits on this plane as defined using the equation from Arenou, Luri, Babusiaux, et al. (2018) and reported above. According to the E limits defined by Arenou, Luri, Babusiaux, et al. (2018), only the objects falling in between the two lines should be retained. In the last panel on the right of Fig. 4.10 we show the distribution of E as a function of R.A. Clearly, by filtering the data using such a parameter would completely exclude the central region of the ONC star forming region where the distribution of E clearly peaks. This is a direct consequence of the fact that the photometric magnitudes G_{bp} and G_{rp} of a given source available in the Gaia DR2 release can be affected by strong contamination by close-by (3.1 x 2.1 arcs^2, Evans, Riello, De Angeli, et al. (2018)) companions in regions affected by high stellar density. We hence decided to not use the E filtering in our analysis and to use the high quality optical photometry available through the OmegaCAM data.

To show the effect of crowding on the Gaia photometric filters directly we plot the comparison of the CMD for the Gaia photometry and the OmegaCAM one. For that we use the C1(eq.(5.1) selected data sample. In Fig. 4.11 we select the one degree region around the ONC for which we construct the CMD (black points). We do the same for only the inner region (central 0.2 deg) plotted using red points. We clearly see that the OmegaCAM photometry plots mainly PMS objects with no obvious difference between the black and red data point. Contrary to this, Gaia photometry in the bp and rp filters shows significant scatter and deviations from the PMS objects.

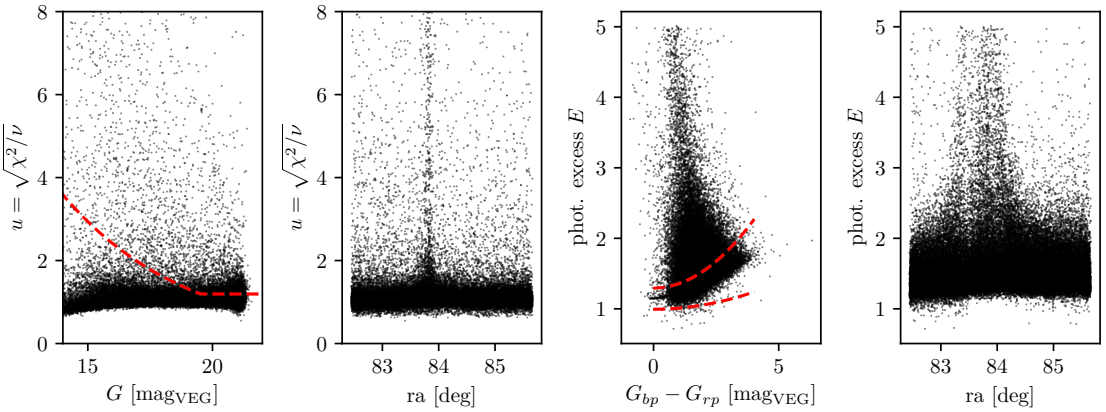

Figure 4.10: The black points are the data from the initial catalog. **First panel:** The astrometric u parameter as a function of G magnitude. The red dashed line is the u selection criterion from Arenou, Luri, Babusiaux, et al. (2018). **Second panel:** shows how this factor depends on R.A. The u parameter is affected by crowding in the central parts of the ONC. **Third panel:** shows the photometric excess, E, parameter as a function of the color in Gaia DR2 filters. The region between the dashed red lines shows the E selection criterion from Arenou, Luri, Babusiaux, et al. (2018). **Fourth panel:** shows E as a function of R.A. demonstrating that E and therefore Gaia DR2 photometry in bp and rp filters are significantly affected by crowding.

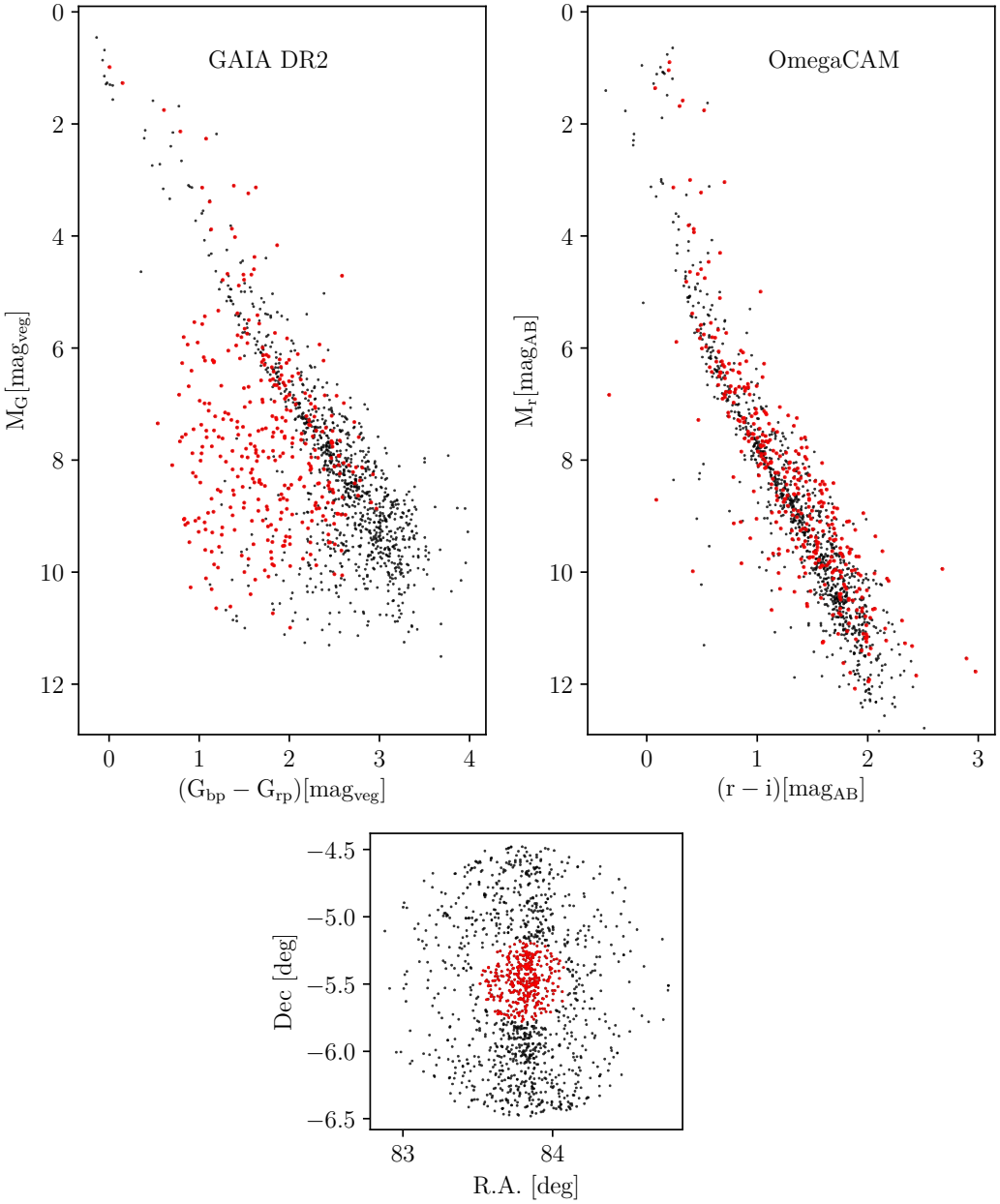

Figure 4.11: The black points are the C1 and 2-σ C2 selected objects. **Top panels:** CMD using Gaia photometric filters (left) and using OmegaCAM filters (right). The black points show the one-degree region from the ONC center and the red points the inner 0.2 degree region. Clearly, the Gaia photometry in bp and rp filters is affected by the central crowding. **Bottom panel:** The R.A. and Dec plot showing the one-degree region and the 0.2 degree central selection (red points).

ID1	ID2	$\log_{10}(a/\mathrm{au})$	sep./"	G1	G2
3209599721383025792	3209599721380315264	2.494	0.780	16.862	16.948
3209528523708699392	3209528528005247616	2.544	0.875	14.924	16.664
3016932397629080448	3016932401924820992	2.568	0.924	17.758	18.071
3017383201698509312	3017383201705272192	2.576	0.942	16.904	14.982
3017367121346098944	3017367121333529984	2.580	0.950	17.239	15.530
3017343310042814464	3017343310049098112	2.592	0.978	16.982	18.811
3215642671646074240	3215642671647475328	2.632	1.072	18.011	18.455
3017235901495548928	3017235901493475840	2.645	1.105	17.058	18.639
3016935867962755968	3016935872258388480	2.674	1.180	12.686	8.836
3016093543272153856	3016093543270824704	2.682	1.202	14.780	16.235
3017082244744312576	3017082240448693120	2.723	1.320	17.177	15.694
3016773827439214720	3016773827436894848	2.733	1.351	17.155	17.711
3017378803658760960	3017378803651996800	2.738	1.366	16.822	17.319
3209696061792962432	3209696066088278016	2.750	1.405	15.714	12.482
3216062272771926144	3216062272770760320	2.757	1.429	13.405	18.632
3016952502370440064	3016952502371760896	2.766	1.459	17.325	17.042
3016535684386060544	3016535680090105344	2.788	1.535	17.885	18.076
3017348257851409536	3017348257845029376	2.810	1.615	18.044	15.062
3017356602958232064	3017356607266117760	2.850	1.772	15.573	16.124
3209540313395426176	3209540309099093760	2.854	1.787	16.511	15.634
3016973290013463936	3016973285718581632	2.869	1.851	18.314	15.024
3017135399259048704	3017135394962860800	2.873	1.868	16.338	16.809
3209566667314795264	3209566663016374400	2.877	1.881	15.466	15.933
3210561587895715328	3210561587897894528	2.887	1.927	6.289	18.276
3216980983457421440	3216980979159662720	2.890	1.941	13.744	14.206
3017367293144786304	3017367293132202624	2.903	1.998	17.323	17.676
3017157595651831168	3017157595651831040	2.913	2.045	17.450	8.882
3017199548892295808	3017199548892295936	2.917	2.063	17.481	15.412
3017363582294579456	3017363582294579328	2.946	2.206	14.270	15.283
3016549492705111936	3016549497001135104	2.951	2.231	9.721	12.482
3016781356516442624	3016781356513940224	2.963	2.295	16.612	16.606
3209653597452614144	3209653597452613760	3.001	2.504	8.098	16.555
3209650883033326848	3209650883033326720	3.024	2.642	14.285	14.385
3209545845313264256	3209545845313264384	3.026	2.656	18.083	17.574
3016086740044032512	3016086740044032384	3.032	2.689	16.333	17.787
3209553866617873920	3209553866617873792	3.037	2.719	14.130	13.508
3016952326278137344	3016952330573066496	3.041	2.747	15.576	15.262
3209530276057350656	3209530280351892096	3.042	2.757	16.560	16.795
3209541412907075456	3209541412907075584	3.056	2.845	17.590	17.839
3017364303848916992	3017364303848916480	3.074	2.964	16.525	11.905
3017228273633491712	3017228273633491840	3.076	2.978	11.737	16.759
3017265244711916928	3017265244711916672	3.082	3.020	16.853	17.487
3016985281562139136	3016985281562139264	3.093	3.100	15.603	15.821
3016030493152341632	3016030493152341760	3.096	3.118	17.269	16.434
3016469060853517824	3016469056559465984	3.098	3.136	10.323	17.764

3016507303242247552	3016507303242247680	3.110	3.224	16.239	15.943
3209576528559565184	3209576528559728000	3.112	3.235	13.416	14.641
3017364441282354176	3017364436980916096	3.124	3.325	15.406	14.175
3017192608225149568	3017192608225149440	3.144	3.479	17.011	15.530
3023289881235865216	3023289876940144768	3.144	3.480	18.403	13.834
3017359562205002880	3017347811174480000	3.155	3.570	16.129	15.755
3017145707182344320	3017145707182344192	3.158	3.597	17.058	18.352
3017248786397358080	3017248786397531136	3.163	3.637	17.237	14.548
3017366468511064960	3017366468511064448	3.166	3.663	15.868	16.158
3017214869037692800	3017214873335520896	3.181	3.795	17.782	15.645
3209633290847280256	3209633290847279744	3.198	3.948	16.779	18.369
3017145638462872576	3017147111635948288	3.207	4.024	17.794	15.843
3209811652247750272	3209811647950503424	3.215	4.101	14.576	14.622
3209526844377985152	3209526844377984896	3.215	4.103	14.628	17.403
3017366640309747072	3017366640309746816	3.224	4.185	15.102	16.424
3209553576254369792	3209553576254369536	3.228	4.231	16.532	17.968
3017367391918079744	3017367396211298048	3.233	4.279	16.841	15.662
3016641370647772672	3016641370646103808	3.238	4.328	15.642	18.298
3023427522052064896	3023427560708065408	3.247	4.414	17.244	18.455
3016547710294461440	3016547710294461312	3.251	4.458	18.062	15.635
3017309981102805760	3017309912383329280	3.265	4.605	14.632	16.766
3209561371619512704	3209561375914929920	3.272	4.679	13.419	15.229
3017142752244845056	3017142752244845184	3.285	4.819	15.709	17.416
3017286479041796480	3017286479041796352	3.301	5.001	17.486	15.251
3016858975164012928	3016858975164013184	3.301	5.005	14.471	17.442
3014873940064089472	3014873944359395968	3.307	5.075	14.707	12.226
3209544024247187584	3209544024247187456	3.330	5.342	17.519	16.475
3017175462715836416	3017175462715713920	3.336	5.423	15.678	16.565
3017266962698857216	3017266958403468032	3.344	5.516	16.793	17.009
3209424795953358976	3209424795953358720	3.348	5.574	15.204	15.266
3016017264653139840	3016017230293401728	3.353	5.636	17.310	17.513
3017144538951245184	3017144538951245440	3.357	5.683	17.006	13.594
3017256757856824448	3017256753560684672	3.367	5.820	16.883	17.235
3209650608155686272	3209650608155686400	3.382	6.020	16.766	12.900
3016926045373231744	3016926045373231616	3.388	6.104	16.436	12.686
3015806124061283968	3015806119765504512	3.396	6.218	17.797	17.507
3017247515087034240	3017247515087033984	3.398	6.244	12.277	13.950
3017356435467423616	3017356469827161856	3.398	6.248	11.922	17.876
3016723803954896256	3016723803954896896	3.402	6.302	17.791	16.157
3017366537230536832	3017366537230535936	3.405	6.356	16.105	17.495
3016744037543326592	3016744041840721024	3.418	6.545	16.315	18.011
3209426582659553408	3209426578363441024	3.424	6.634	14.383	15.045
3209579449137299072	3209579444841918976	3.435	6.803	10.566	17.329
3017373203021508736	3017373203019748864	3.436	6.824	15.383	16.412
3209559864086618240	3209559791071547392	3.443	6.929	18.238	15.995
3017147661389569536	3017147661389568256	3.447	7.004	15.627	14.567

Table 4.A1: The apparent binary star objects up to 3000 au separation based on the Elbow plot, see Fig. 4.7. The selection was done on the projected separation and further filtered by the requirement that both components have an identical proper motion within the 3-σ uncertainty.

Chapter 5

A stellar relic filament in the Orion star forming region

This chapter is based on the publication Jerabkova, Boffin, Beccari, and Anderson (2019) with the same title "A stellar relic filament in the Orion star forming region". Only minor changes concerning formatting were made in order to present it as a chapter in the thesis.

Abstract: *We report the discovery of the oldest stellar substructure in the Orion star forming region (OSFR), the* Orion relic filament*. The relic filament is physically associated with the OSFR as demonstrated by Gaia DR2 photometry and astrometry, as well as targeted radial velocity follow-up observations of a bright sub-sample of proper-motion selected candidate members. Gaia DR2 parallaxes place the Orion relic filament in the more distant part of the OSFR, ≈ 430 pc from the Sun. Given its age, velocity dispersion, spatial extent, and shape, it is not possible for the Orion relic filament to have formed as a single stellar cluster, even taking into account residual gas expulsion. The relic filament is also too young to be a tidal stream, since Galactic tides act on much longer time scales of order 100 Myr. It therefore appears likely that the structure formed from a molecular cloud filament similar to Orion A in the OSFR and retained its morphology despite decoupling from its natal gas. Hence, the Orion relic filament bears witness to the short-lived evolutionary phase between gas removal and dispersion due to shears and tides, and provides crucial new insights into how stars are formed in molecular clouds.*

5.1 Introduction

The Orion star forming region (hereafter OSFR) is the closest active star forming site that is producing massive stars. Together with other two prominent OB associations, Sco-Cen and Per OB2, it lies on the Gould Belt of young stars (Lesh, 1968; de Zeeuw, Hoogerwerf, de Bruijne, Brown, and Blaauw, 1999), that feature a spatially complex structure (Zari, Hashemi, Brown, Jardine, and de Zeeuw, 2018). The Gould Belt of young stars spatially coincides with the structure known as the Lindblad Ring of HI (Lindblad, Grape, Sandqvist, and Schober, 1973) – the Sun lying at a galactocentric radius within the Lindblad Ring.

The OSFR is known to have been forming stars over the last 12 Myr producing in total around $10^4\,M_\odot$ in several clusters and sub-groups confined to approximately 100–200 pc[3]. It is one of the best-studied star forming region. Bally (2008) subdivides the OSFR into several groups based on sky distribution, distances, and ages: group 1a (8-12 Myr, 350 pc), 1b (3-6 Myr, 400 pc), 1c (2-6 Myr, 400 pc), 1d ($<$ 2 Myr,

420 pc) and λ Ori (< 5 Myr). The OSFR hosts an "integral-shaped filament" in the northern portion of the Orion A molecular cloud (Bally, Langer, Stark, and Wilson, 1987), within which the young Orion Nebula Cluster is forming (Hillenbrand, 1997b; Beccari, Petr-Gotzens, Boffin, et al., 2017). It is the largest molecular cloud/filament in the local neighbourhood (Großschedl, Alves, Meingast, et al., 2018).

Using Gaia (Gaia Collaboration, Prusti, de Bruijne, et al., 2016b) DR2 photometry and astrometry, OmegaCAM photometry and spectroscopy with Hermes on the Flemish 1.2-m Mercator telescope we report here the serendipitous discovery of an $\approx$ 17 Myr old, cigar-like ($\approx$ 90 pc long) structure that is clustered and distinct in proper motions and parallaxes. This newly found structure is the oldest stellar population linked to the ORSF and seems to represent the first case of a known stellar relic filament.

5.2 Observations and datasets

We used the python Astroquery package (Ginsburg, Robitaille, Parikh, et al., 2013) to retrieve the Gaia DR2 data (Gaia Collaboration, Brown, Vallenari, et al., 2018; Lindegren, Hernández, Bombrun, et al., 2018; Riello, De Angeli, Evans, et al., 2018; Evans, Riello, De Angeli, et al., 2018) from the Gaia science archive[1]. We downloaded all the objects detected by Gaia that are within a radius of fifteen degrees from the ONC (R.A.$\approx$ 83.75 deg., Dec ≈ -5.48 deg. – 1 deg on sky corresponds to $\approx$ 7 pc at the ONC distance of 400 pc) without any additional filtering. Hereafter, we will refer to this catalogue as the Gaia or the 15-degree catalogue. The size of the region described by the catalogue was made arbitrary, but is sufficiently large for the purpose of this study.

In this work we also used the photometric catalogue obtained via a set of deep multi-band images acquired with OmegaCAM (098.C-0850(A), PI: Beccari), a 1 deg^2 camera (Kuijken, 2011) attached to the 2.6-m VLT Survey Telescope (VST) at ESO's Paranal Observatory. The catalogue was used in Jerabkova, Beccari, Boffin, et al. (2019) to study the stellar population in a 3×3 degree area around the centre of the ONC in the r and i filters. While the details of the data-reduction procedure are described in Jerabkova, Beccari, Boffin, et al. (2019), here we recap that the data were reduced and calibrated by the Cambridge Astronomy Survey Unit[2], while a large number of stars in common with the AAVSO Photometric All-Sky Survey (APASS) were used to correct for any residuals in the photometric calibration. The OmegaCAM catalogue includes 93,846 objects homogeneously sampled in the r and i bands down to $r \approx 21 - 22$ mag (ABmag) over a 3×3 deg^2 area around the cluster's centre.

We used the C^3 tool (Riccio, Brescia, Cavuoti, Mercurio, di Giorgio, and Molinari, 2017) in order to identify the stars in common between the OmegaCAM and the Gaia catalogue. C^3 is a command-line open-source Python script that, among several other options, can cross-match two catalogues based on the sky positions of the sources. We found 84,022 targets in common between the Gaia and the OmegaCAM data. The majority of objects that are present in the OmegaCAM catalogue, but not in Gaia, are typically faint ($r \gtrapprox 21$) and blue ($r - i \lessapprox 1.2$).

[1] http://gea.esac.esa.int/archive/
[2] http://casu.ast.cam.ac.uk/vstsp/

We use Gaia DR2 parallaxes to separate members of the Orion star forming complex from fore- and background contaminators. Thus we apply a parallax selection criterion in the form

$$2.0 - 3\sigma_{\varpi} \leq \varpi \leq 3.0 + 3\sigma_{\varpi} \,\texttt{and}\, \sigma_{\varpi}/\varpi \leq 0.1\,, \tag{5.1}$$

where σ_{ϖ} is the uncertainty on the parallax as given in Gaia DR2. That is, we impose that the Orion candidate members are confined between distances of 333-500 pc from the Sun (e.g. Zari, Brown, and de Zeeuw, 2019). In addition, only the targets having a relative parallax error smaller than 10% are considered, to ensure a good quality of the astrometric solution (see also Gaia Collaboration, Brown, Vallenari, et al., 2018). Hereafter, we will refer to this catalogue as the "3x3 deg catalogue".

We convert the observed angular proper motions (mas/yr) to tangential velocities (km/s) by computing $v_{\mathrm{R.A.,Dec}}[\mathrm{km/s}] = \mu_{\mathrm{R.A.,Dec}}[\mathrm{mas/yr}] \cdot 4.74/\varpi[\mathrm{mas}]$. Such velocities are better suited to search for kinematically clustered structures in the OSFR than observed proper motions, since the spatial extent of the OSFR is a significant fraction of the distance to it ($\Delta d/d \approx 0.4$). Thus, converting to velocities resolves the distance degeneracy affecting observed proper motions in (mas/yr).

Since for the 15-degree catalogue we rely only on the Gaia DR2 photometry, we also impose a photometric quality filter, using the photometric excess criterion (Lindegren, Hernández, Bombrun, et al., 2018; Evans, Riello, De Angeli, et al., 2018; Arenou, Luri, Babusiaux, et al., 2018) defined as

$$1.0 + 0.015(G_{BP} - G_{RP})^2 < E < 1.3 + 0.06(G_{BP} - G_{RP})^2\,, \tag{5.2}$$

where E is defined as the flux ratio in the three different Gaia passbands,

$$E = \frac{I_{BP} + I_{RP}}{I_G}\,. \tag{5.3}$$

It is known that the Gaia DR2 photometry suffers from significant systematic effects in regions characterized by severe stellar crowding. This can be mitigated by using the criterion above. For more details, we refer to Jerabkova, Beccari, Boffin, et al. (2019).

5.2.1 Spectroscopic observations with Hermes

In order to verify that the group of stars discovered in proper motion space (see below) is kinematically bound, we derived the line-of-sight (radial) velocities. In January 2019, we selected 13 candidate member stars for spectroscopic follow-up with the goal of determining the third, radial, velocity component. The 13 objects observed were selected based on their clear membership indicated by the *Gaia* DR2 astrometry and photometry, as well as having a V-band magnitude brighter than ≈ 13.5 mag to be accessible via a 1m-class telescope.

The spectroscopic observations were carried out between 1 and 11 March 2019 using the high-resolution optical fibre-fed Echelle spectrograph *Hermes* mounted on the Flemish 1.2m Mercator telescope located on the Roque de los Muchachos Observatory on La Palma, Canary Island, Spain (Raskin, van Winckel, Hensberge, et al., 2011). All observations were carried out using the high-resolution fibre (HRF), which yields a spectral resolving power of $R \sim 85,000$ and the highest throughput. We selected

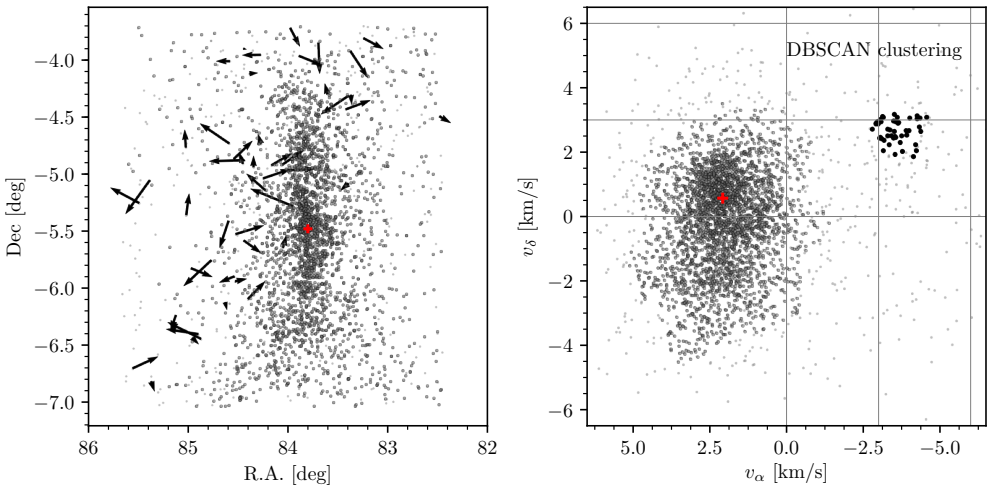

Figure 5.1: **Right panel:** Distribution of proper motions of the targets in the initial catalogue after parallax selection. The faint gray points show all targets, while the black and dark gray points were identified by the DBSCAN clustering algorithm as two distinct groups. The red point represents the peak value of the distribution of proper motions of the Orion Nebula Cluster (ONC) (Jerabkova, Beccari, Boffin, et al., 2019). The vertical gray lines are plotted for values of v_α of 0, -3 and -6 km/s. The horizontal gray lines are plotted for values v_δ of 0, 3 and 6 km/s. **Left panel:** The distribution of the targets on the sky with the same colour coding as in the right panel. The arrows indicate the proper motions of the black points after removing the mean value. The red cross indicates the position of the Orion Nebula Cluster for reference.

exposure times between 180 and 1800s, aiming for signal-to-noise (S/N) ratios of about 15 around $\lambda 5000 - 6000$ Å. The raw spectra were reduced using the dedicated *Hermes* reduction pipeline that carries out standard processing steps such as flat-fielding, bias corrections, order extraction, and cosmic clipping. A summary of our observations is available in Tab. 5.1.

The radial velocities were measured by cross-correlation with synthetic spectra, which were constructed at the same spectral resolution as the observations. Three synthetic spectra were used, depending on the brightness (i.e. the spectral type) of the target considered: a hot one ($T_{\rm eff}$ = 8000 K, $\log g$ = 4.), a solar model, and a cooler star ($T_{\rm eff}$ = 5000 K, $\log g$ = 4.5). The models were created with the software[3] `SPECTRUM v2.76` of R.O. Gray.

The measured radial velocities are listed in Tab. 5.1.

5.3 Discovery of the Orion Relic Filament

5.3.1 A group/cluster in proper motions

While investigating the three bursts of star formation in the Orion Nebula Cluster (ONC; Jerabkova, Beccari, Boffin, et al., 2019), using the OmegaCAM catalogue

[3] http://www.appstate.edu/~grayro/spectrum/spectrum.html

mentioned in Sec. 5.2, we noticed in proper motion space a distinct clump of stars that is well separated from the ONC. The sky distribution (R.A., Dec) and the proper motion distribution (v_α,v_δ) are plotted in Fig. 5.1 (left and right panel, respectively). We run the clustering algorithm using DBSCAN (Ester, Kriegel, Sander, and Xu, 1996) in a three-dimensional plane containing the two proper motions on sky and the parallax, and are able to identify and thus confirm the presence of two clear structures – the larger structure containing the Orion A stellar population (in gray) and a distinct clump (black) at $v_\alpha \approx -3.8$ km/s and $v_\delta \approx 2.5$ km/s, as seen in Fig. 5.1.

The objects belonging to the distinct clump form an elongated structure on the sky and do not overlap with Orion A. The parallax distribution peaks at a value corresponding to a distance of 430 pc (±20 pc), placing the objects from the clump further away from us than the ONC. In addition, the structure is co-eval in the colour-magnitude diagram (CMD), being older than the rest of the population in Orion A, as one can see in the left panel of Fig. 5.2. The cluster in proper motions was also seen by Zari, Brown, and de Zeeuw (2019) for Orion A region where co-evality was discussed (in the paper noted as group F and see also their group B8) and by Kounkel, Covey, Suárez, et al. (2018), but without further discussion or analysis.

5.3.2 Extent of the discovered feature

By inspecting the distribution of the stars on sky as shown on the left panel of Fig. 5.1 we cannot exclude that the newly discovered population extends beyond the area covered by the 3x3 deg catalogue. We hence decided to use the 15-degree catalogue with the aim to recover the structure on a wider area. It should be noted that the stellar populations in the OSFR is complex. In particular, if we consider a larger area than 3x3 deg, then in proper motion space, other populations from the region tend to blend in with the structure discovered in the 3x3 deg catalogue, making it much less prominent. In light of the OSFR's complexity and angular size, we apply two independent, proper-motion-based methods (S1 and S2, described below) to the 15-degree catalogue and check whether the clump can be successfully recovered.

S1) We select only the stars having parallaxes in the range $2.16 < \varpi < 2.48$ as defined by the stars in the clump in proper motions found in the 3x3 deg catalogue. This approach is lowering the contamination from the population of the OSFR at the distance where the objects belonging to the clump is expected. We then run DBSCAN on this sub-catalogue in the 3D space spanned by proper motions and parallax. The stars belonging to the new clump are successfully isolated. Their distribution on the sky and their CMD are shown in Fig. 5.3 (black points on the panels on the top left and second top row, respectively). Since the method S1 relies only on the clustering algorithm DBSCAN, we do additional checks of the physical properties not used in the clustering – radial velocities and the CMD. In addition, we introduce the method S2 that is clustering-independent.

S2) We consider all targets in the 15-degree catalogue that have proper motions in the circular region corresponding to the clump as derived from the 3x3 deg catalogue (that is, a radius of 1.0 km/s centred around v_α=-3.8 km/s,v_δ=2.5 km/s). The bottom panels of Fig. 5.3 show the target locations in Galactic coordinates as well as the CMD, parallax distribution, and any available radial velocity data of these targets in the 15-

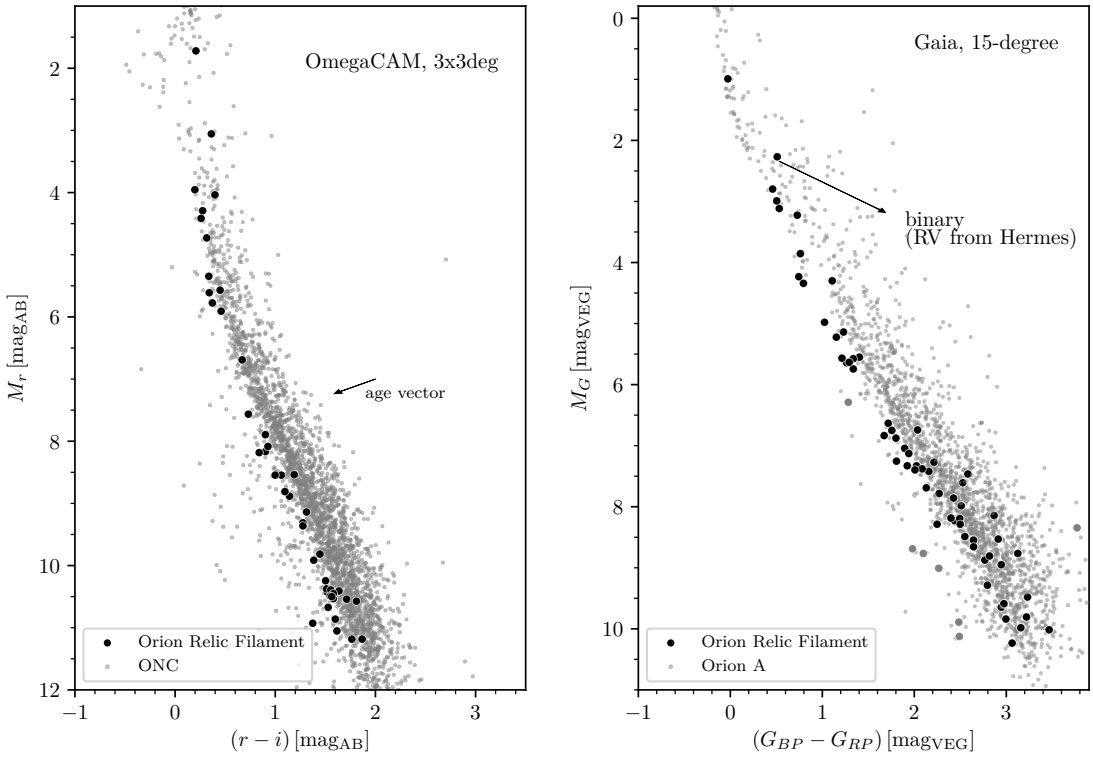

Figure 5.2: **Left panel:** Colour-absolute magnitude diagramme (CMD) of the $3 \times 3\,\mathrm{deg}^2$ catalogue using OmegaCAM r and i filters. Gaia parallaxes were used to compute the absolute magnitudes. The gray and the black points show the stars in the clusters identified in proper motions and parallax by the DBSCAN algorithm and shown in Fig. 5.1. **Right panel:** The CMD for the Gaia 15-degree catalogue using the Gaia photometric data. In gray, we see all the already known, stars identified in the catalogue with DBSCAN using on-the-sky distributions (see also Fig. 5.4 and Fig. 5.5). The black points correspond to the proper motion-selected group members in the the OmegaCAM catalogue – the Orion relic filament.

degree Gaia catalogue. By way of construction, the method S2 will lead to a much larger contamination from fore- and background stars, as clearly seen in the figure. These can be separated when using the CMD.

Using method S1 we can clearly isolate a clump of stars in proper motion as previously done in the 3x3 deg catalogue. The clump identified in the 15-degree catalogue is located at the same position as the original clump in the 3x3 deg catalogue, but is more extended, therefore bringing the values of proper motions of the members of the clump closer to those of the Orion A members plotted in Fig. 5.1. Using this selection we can confirm the presence of a coeval population of stars which extends well beyond the 3-degree area studied before. We note the recovered population's elongated, filamentary morphology in Galactic coordinates, whereas it is clearly clustered in proper motion space. The S1 method requires a significant cut in parallaxes in order to discern in the 15-degree Gaia data set the clump in proper motions that was detected in the 3x3 deg catalogue. Due to still large uncertainties of Gaia DR2 parallaxes (10% error is $\approx$ 40pc at the distance of the OSFR), the S1 method is not able to recover all the targets belonging to the structure by using S1 but only the subset of likely members.

Method S2 allows us to explore a larger region in parallax values. This method consistently reveals the presence of an over-density of stars on sky at the same position and with the same extent as for objects selected by method S1. The distribution on the CMD of the stars populating the elongated over-density (black points on the first and second lower row plot of Fig. 5.3) confirms that these stars are coeval. They are, however, younger than the sparse component (in gray on the same plots). Furthermore, the parallax distribution of such stars is statistically consistent with the distribution imposed via the S1 method (see the black histograms on the plots of the third column). The method S2 clearly introduces more contamination into the discovered structure from the field stars than method S1. On the other hand, the total extent of the structure is the same as for the method S1. That is, the extent seen can thus be considered real and the size of the catalog 15deg sufficient.

At the request of an anonymous referee we performed two additional tests of the robustness of method S1. The main principle of both is to randomly reshuffle proper motions in R.A and Dec independently while keeping other catalogue parameters intact and test what structures can be recovered by the clustering algorithm. Test one uses the same data set as in S1 and test two applies a cut in l and b to select the area around the discovered structure only. For test one, we reshuffled the proper motion values several times and were not able to find similar structures to the one we have detected. We note that even when a larger structure was found in the reshuffled proper motions, it never had a co-eval distribution in the CMD nor similar values of RVs. This means that the clustering algorithm is robust and the discovered structure is not a density fluctuation in proper motion space. For test two, we applied a cut in l and b as shown in the middle left panel of Fig. 5.A1 in the Appendix to this Chapter. The plot in the middle row right panel of Fig. 5.A1 shows that the cut in l and b described above clearly lowered the overall contamination, thereby increasing the apparent visibility of the clump in proper motions. However, the contamination from the OSFR is still too high to allow the DBSCAN algorithm to recover the discovered clump of stars. Thus, we further restricted the catalogue in parallax as shown in the bottom row of Fig. 5.A1. We were able at this point to fully recover the clump in proper motions using DBSCAN.

ID	R.A.	Dec.	G [mag]	$RV_{\rm Gaia}$ [km/s]	$RV_{\rm Hermes}$ [km/s]	Epoch (BJD-245854)	Exp. time [s]	comment
3216997407412184576	82.16820	-2.73367	9.14	–	+13.5 ± 2.6	4.33881	300	binary?
3016216856077986816	85.36432	-6.81766	10.46	–	−55.7 ± 4.1	4.3436	180	binary!
					−41.4 ± 4.1	9.35148	500	
3320525395058674176	86.46964	4.80873	10.93	–	+23.3 ± 2.7	5.34945	300	
3223717107084373504	83.51508	2.63526	11.18	+34.16 ± 1.50	+30.4 ± 2.0	5.35456	300	
3223574204932246016	83.16921	2.19963	11.30	–	+29.2 ± 1.8	4.34802	300	
3215983485892366848	83.47961	-3.15763	11.39	–	+17.5 ± 1.2	6.3657	600	binary?
3010622094238648320	84.39491	-10.11905	11.97	+50.94 ± 2.47	+50.1 ± 1.7	6.37477	700	binary?
3236001709982983680	82.10707	3.33701	12.39	–	+45.4 ± 1.7	5.3586 8	180	
3217571696079288320	83.59811	-1.36120	12.42	+25.15 ± 9.91	+28.9 ± 1.4	6.38637	1000	
					+28.1 ± 1.8	11.3871	1800	
3000057956459742720	96.68656	-12.56129	12.51	+1.31 ± 3.79	+3.0 ± 1.7	5.36791	900	binary?
3216096632510194176	84.04834	-2.74891	13.15	–	+28.3 ± 2.0	6.40058	1200	
3216974386386913280	83.57078	-1.93627	13.31	–	+27.4 ± 1.5	9.40488	1800	
3223703603706959360	83.51694	2.54048	13.39	–	+31.3 ± 1.5	4.35853	1200	

Table 5.1: List of the brightest members of the Orion relic filament followed up by spectroscopic measurements using the Hermes spectrograph on the Flemish 1.2m Mercator telescope. The targets are shown as black crosses in Fig. 5.4. When removing the targets with large RV variations, i.e. those that are likely close binaries, the velocity dispersion of our measurements is $\approx$ 4 km/s confirming the physical existence of the Orion relic filament.

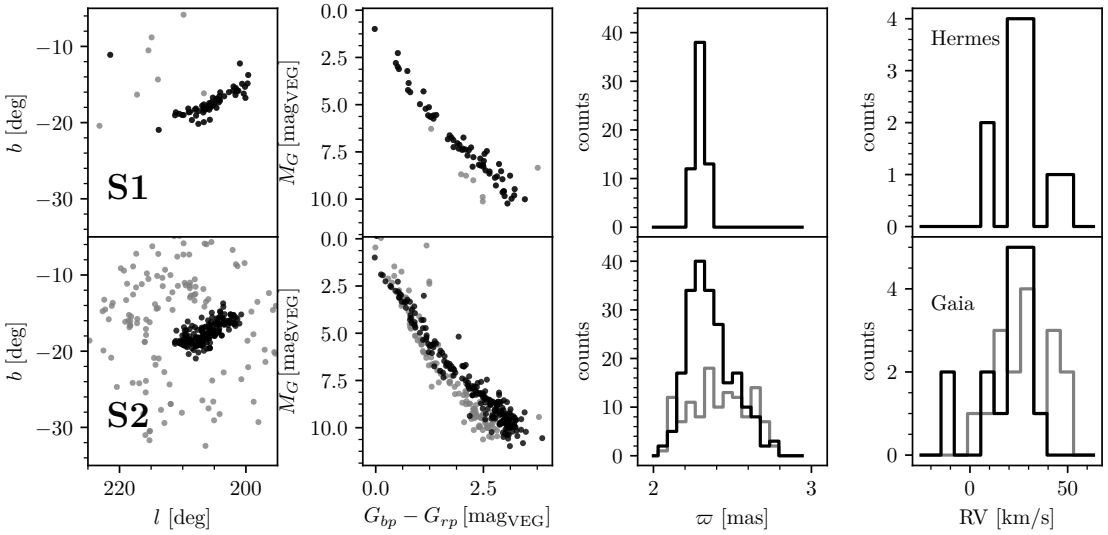

Figure 5.3: Distribution in the Galaxy (uttermost left) and in the colour-magnitude diagramme (second column) for the selection using either S1 (top) or S2 (bottom) – see text. The associated parallax distribution is show in the third column and the Hermes(top)/ Gaia(bottom) radial velocity distribution (right). The black points are those identified as members depending on the selection criterion, the gray points show non-members. We note that the CMD on the top panel shows the same data sample as right panel of Fig. 5.2, the CMD on the bottom panel contains fore-/back-round contaminators. The gray histograms for the bottom panels show distributions for targets that are not identified as members.

We then randomly re-shuffled the proper motion values, as done in test number one, and used DBSCAN to identify potential structures in proper motion space. We did not find a single case in which, after re-shuffling of proper motions, the identified structures by DBSCAN would be coeval or share similar radial velocity values. This further confirms the statistical strength of our results and our conclusions.

In summary, we successfully recover the new kinematic structure in the wider, 15-degree catalogue. We used two independent methods to recover the structure. For each method, we ensured that additional data – that were not used in the identification of the structure – are consistent with the existence of a coeval (CMD), kinematically unique (RVs), physical structure at the same distance (parallax distribution). On the sky, the identified stars resemble a 90-pc long filament, henceforth referred to as the *Orion Relic Filament*, which is older than Orion A, as indicated by the CMD.

5.3.3 Radial velocity measurements

The RV measurements based on the Hermes spectra (cf. Sec. 5.2.1, Tab. 5.1) agree to within the errors with Gaia mean velocities, where these are available from DR2. For two stars, we have had two measurements, separated by a few days. In one case, Gaia DR2 3016216856077986816, we have clearly identified a spectroscopic binary, as over a period of 5 days, the radial velocity varied by 14 kms^{-1}. The position in the colour-magnitude diagram of this star also confirms its binary nature. This star would have a mass of about 2 M$_\odot$ and such stars are known to be often in binary systems.

Given the mean radial velocity of the relic filament (see below), the minimum semi-amplitude of the radial velocity curve is at least 30 kms^{-1}, which implies a period above 10 days, but below $\approx$ 150 days. For the second star for which we had two epochs, Gaia DR2 3217571696079288320, we did not detect any significant radial velocity change. Moreover, the value we obtain is compatible with that determined by Gaia, and with the mean value for the velocity of the relic filament. Hence, there is no indication that this star is a spectroscopic binary.

We show on the right-hand panels of Fig. 5.3 the distribution of radial velocities from Gaia (lower panel) and Tab. 5.1 (upper panel). For the latter we exclude all outliers. It is immediately seen that the distribution of the radial velocities of the stars belonging to the filament and identified via S1 and S2 are consistent.

Using the Hermes radial velocities we derive a mean value of 26.1 ± 4.7 kms^{-1}, which is consistent with the peak value, 28 ± 2 kms^{-1}, of the Gaia RV distribution based on the selection method S2 (see right-most panels in Fig. 5.3). The dispersion is formally larger than the one seen in the proper motion space, but we note that it corresponds to only about twice the errors on our measurements (limited by the relatively low S/N of our spectra), so that it is most likely overestimated. There are four additional stars that have measured radial velocities which are different by more than 3-σ from the mean velocity. These are likely spectroscopic binaries or, alternatively, stars that have been ejected. We note that if we accept that these are binaries, we would have a fraction of binaries of 5/13= 38%, which is not unusual, especially as we are biased to the brightest objects in the filament, which could be brighter because of the presence of a companion.

5.3.4 Orion Relic Filament and Orion star forming region

The next step is to put the discovered Orion relic filament into the context of the OSFR. For this purpose we investigate further the 15-degree catalogue. First, we run the clustering algorithm DBSCAN on the entire catalogue in the 3D parameter space [R.A., Dec, ϖ] to select substructures in the OSFR. We identified 9 groups or clusters that are clearly visible as over-densities of stars on the sky. We plot them in Fig. 5.4, and in Galactic coordinates, in Fig. 5.5, together with the known bright stars and star clusters. These groups are used as reference stellar populations of the OSFR. Note that even though a much more detailed analysis of the OSFR could be done (for example, see Kounkel, Covey, Suárez, et al., 2018), we defer this to future work and here aim to define the reference populations.

The extent of the Orion relic filament is similar to that of the OSFR as shown in Fig. 5.4 and Fig. 5.5. The typical proper motions of its stars are offset from the OSFR members (see the right panel of Fig. 5.6). The distribution of parallaxes (Fig. 5.6) clearly reveals that the Orion relic filament is located in the most distant part of the OSFR.

In order to further characterise the relic filament, we derived the age of each star by comparing its position on the CMD with stellar isochrones. Given the extent of the stellar structure and the likely presence of a foreground molecular cloud, some degree of differential extinction can be expected. Following the approach described by Zari, Hashemi, Brown, Jardine, and de Zeeuw (2018) we use the interstellar extinction (A_G

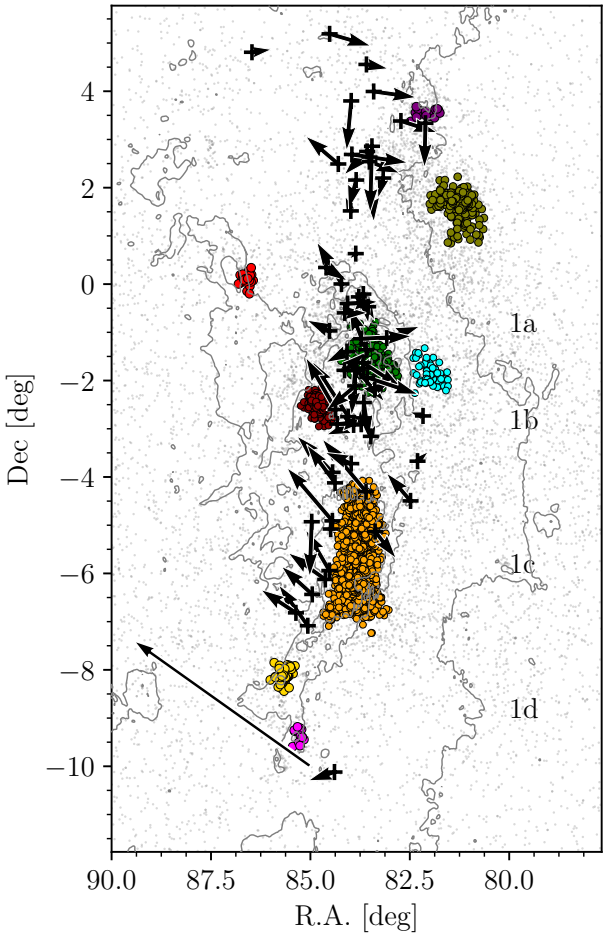

Figure 5.4: The OSFR and the identified clusters in R.A. and Dec. All data points in the Gaia DR2 catalogue having parallaxes in the interval [2–3] mas are plotted as gray points. We used the DBSCAN algorithm to identify clustering in space (b,l, ϖ) – the resulting core members of found groups are marked as colour points (see text for more details). The underling isocontours show IRAS 100 μm. The newly discovered old (17 Myr) structure is shown as black '+' symbols, while the black arrows show the proper motions in R.A. and Dec coordinates after removing the mean (indicated by the large black arrow). The division groups are listed in Tab. 5.2 and their names are placed on the right at the corresponding values of Dec.

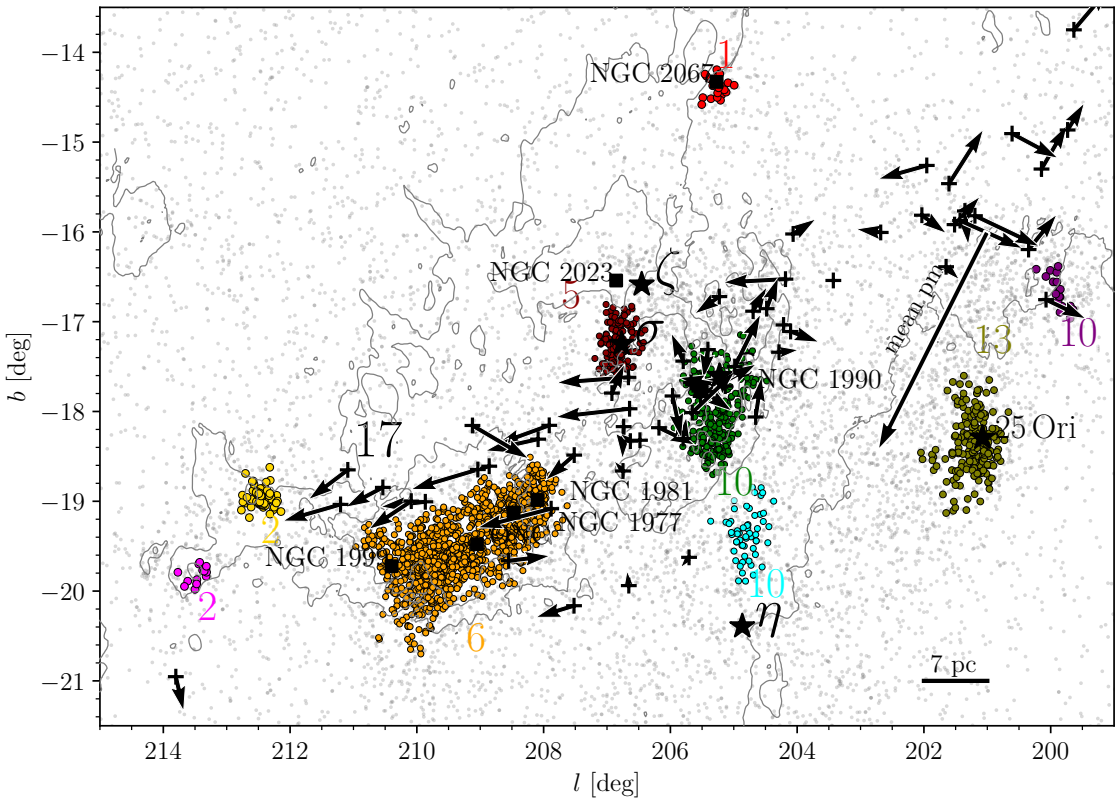

Figure 5.5: The Orion region in galactic coordinates, (l, b). All data points in the Gaia DR2 catalogue having parallaxes in the interval [2–3] mas are plotted as gray points. We used the DBSCAN algorithm to identify clustering in space (b,l, ϖ) - the resulting core members of found groups are marked as colour points with estimated age based on isochrone fitting (see text for details) written next to them. The known star clusters are marked as squares and bright stars as star symbol. The underling isocontour shows IRAS 100 μm. The newly discovered old (17 Myr) structure is shown as black '+' symbol, while the white arrows show the proper motions in Galactic coordinates after removing the mean (indicated by the large black arrow).

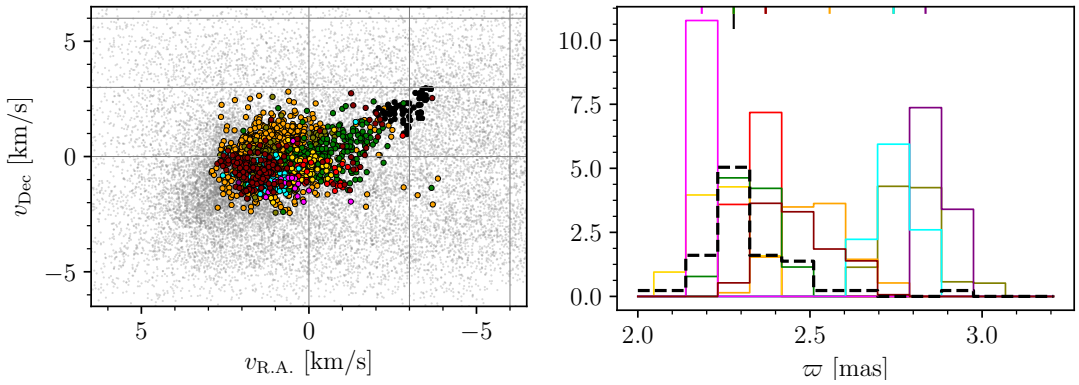

Figure 5.6: **Left Panel:** The proper motions in R.A. and Dec coordinates). Different colours correspond to the different groups identified in Fig. 5.5, while the black points are members of the Orion relic filament. The vertical gray lines are plotted for values of v_α of 0, -3 and-6 km/s. The horizontal gray lines are plotted for v_δ values of 0, 3 and 6 km/s. **Right Panel:** The parallax distributions for the different groups identified in Fig. 5.5, with the black histogram showing the parallax distribution of the Orion relic filament.

and $E(G_{PB}-G_{RP})$) available for the brightest stars in the Gaia DR2 catalogue to build a 3D extinction map. In short, we first bin the data in l, b and parallax space. For each cell we then calculate the mean and the standard deviation of A_G and $E(G_{PB}-G_{RP})$ using the measurements available in the given region. We consider such values as characteristic values describing the amount of extinction in a given bin which is then used to de-redden the magnitudes of each star located in the same bin (Fig. 5.7). This allows us to put all stars of a given cluster in a colour-magnitude diagramme and determine their age by comparing with stellar isochrones. For this purpose we acquire a grid of solar metallicity PARSEC isochrones (version 1.2S; Bressan, Marigo, Girardi, et al., 2012; Chen, Girardi, Bressan, Marigo, Barbieri, and Kong, 2014; Tang, Bressan, Rosenfield, et al., 2014; Chen, Bressan, Girardi, Marigo, Kong, and Lanza, 2015) with time steps of 0.1 Myr.

We run a least-square fitting routine to estimate the best age for each identified group in the OSFR and of the Orion relic filament. The errorbars on the best fitted age are estimated from the scatter of the points along the isochrones – the age corresponding to a $1-\sigma$ offset from the mean is used. The final ages and their uncertainties are quoted in Tab. 5.2 and the best fitting isochrones are shown in Fig. 5.8. We recover the ages for the groups of the OSFR as quoted Bally (2008). The Orion relic filament is older than the rest of the OSFR, or at the very least, given the uncertainties, among the oldest populations present in the region. Thus this results suggests that the Orion relic filament was the first star formation event in the OSFR and was then followed by the rest of the star formation activity in this region.

To summarise, the Orion relic filament is the oldest kinematically distinct structure in the vicinity of the OSFR. It is several Myr older than the oldest previously known regions, with which it overlaps in (l, b, ϖ) space (cf. Fig. 5.5).

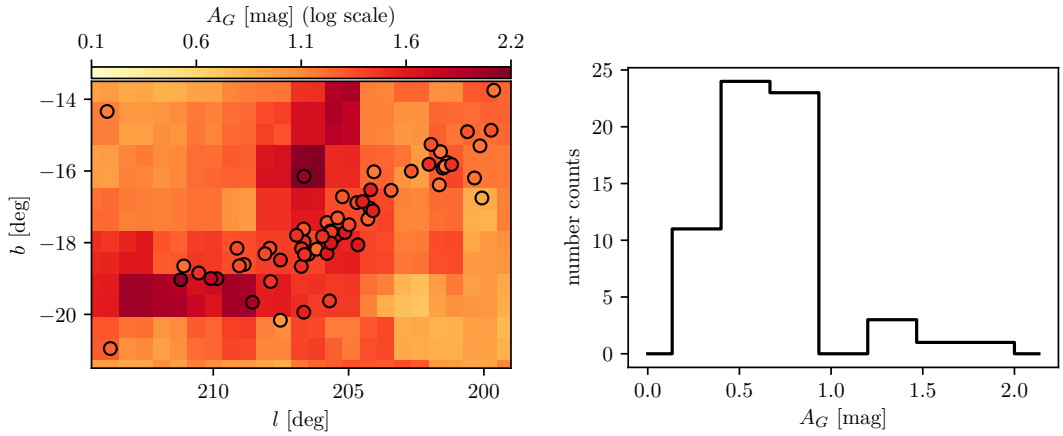

Figure 5.7: **Left Panel:** Extinction map for the parallax cut $2.25 < \varpi < 2.40$, corresponding to the location of the Orion relic filament. The plotted points are the members of the Orion relic filament, with the grid boxes being colour-coded based on the computed values of A_G. **Right Panel:** Distribution of A_G values for the members of the Orion relic filament.

Name	colour	mean(ϖ [mas])	age [Myr]
1d-1	magenta	2.3 ± 0.2	2.0 ± 0.6
1d-2	yellow	2.3 ± 0.2	2.4 ± 0.6
1c-1	gold	2.6 ± 0.3	6.2 ± 0.5
1b	dark-red	2.5 ± 0.3	5.2 ± 1.5
1a-1	green	2.4 ± 0.3	10.2 ± 0.6
1a-2	cyan	2.8 ± 0.3	10.0 ± 1.1
1a-3	purple	2.9 ± 0.3	9.8 ± 2.8
1a-4	olive	2.8 ± 0.2	12.6 ± 1.1
NGC2067	red	2.8 ± 0.3	1.2 ± 0.4
Orion relic filament	black (arrows)	2.4 ± 0.3	16.8 ± 2.5

Table 5.2: List of representative groups in the OSFR, as shown in Fig. 5.5 in the indicated colour, with their mean parallax and mean age, and their associated range. We link each group to the OSFR division by Bally (2008) (the first column of this table). In case we found several sub-structures to one of Bally's group, we indicate this.

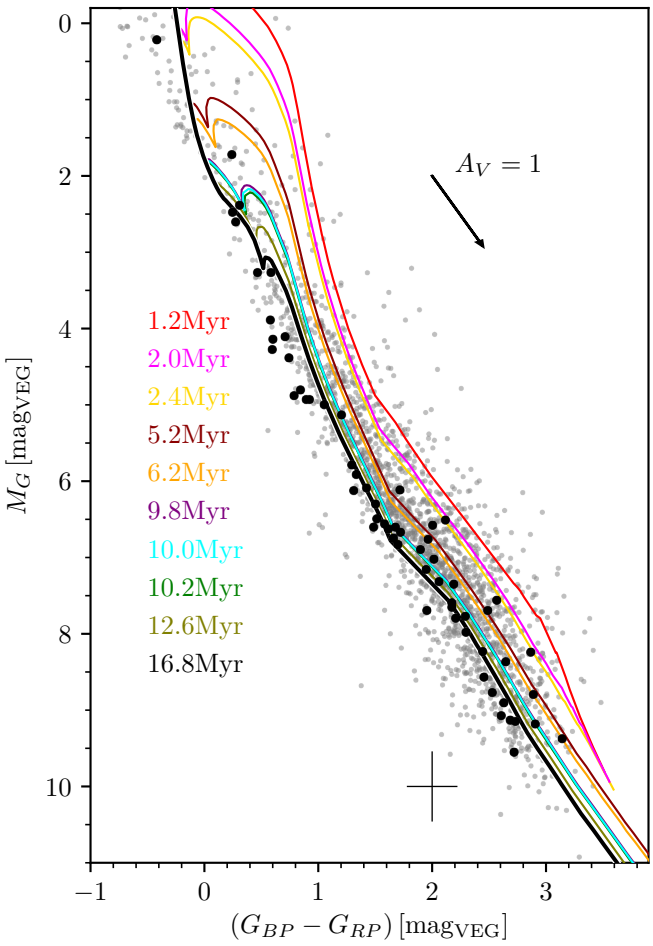

Figure 5.8: The colour-absolute magnitude diagramme showing all the identified members of the OSFR in gray and the members of the Orion relic filament in black. The error bars for the black points combine the photometric uncertainties, the parallax uncertainties used to compute absolute magnitudes and the uncertainty given by the correction for the extinction: their representative value is only shown by the cross in the left bottom corner in order to increase the clarity of the plot. We do not show the error bars for the gray points. The plotted isochrones correspond to the relic filament (black) and to the other identified structures in the OSFR. Tab. 5.2 lists each age with the corresponding color, while the ages are also shown directly in this Figure.

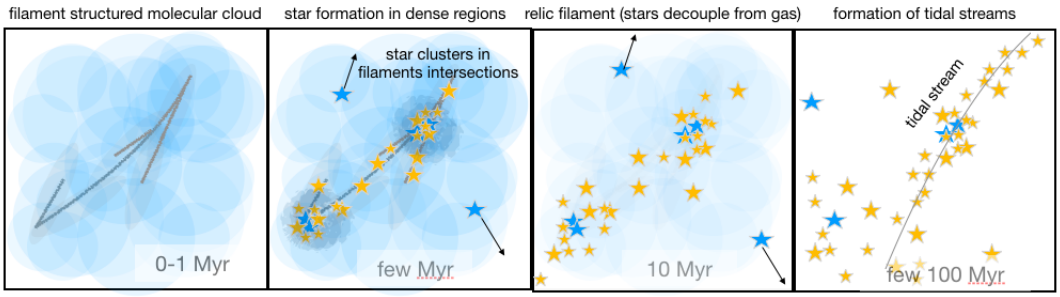

Figure 5.9: Sketch of filament star formation. From left to right we show different evolutionary stages starting from a molecular cloud with filament substructure. Stars then form in the densest parts (in the filaments, but mainly in the intersection of sub-filaments of fibres which form embedded clusters). After few Myr the stars decouple from the gas as the residual gas disperses. Some of the embedded clusters will survive, some dissolve after the dispersal of the residual gas. This evolutionary stage is the *relic filament*, i.e., the original molecular cloud filament remains evident in the freshly hatched stellar population. After a couple of 100 Myr the surviving star clusters can start to develop tidal tailes. At later stages and after one to a few Galactic orbits (0.2-few Gyr) the relic filament disperses into the Galactic field due to tides and shears.

5.4 Physical origin of the Orion Relic Filament

The Orion relic filament is an approximately 90 pc-long structure that is coeval, with an age of $\approx$ 17Myr. To understand the physical origin of such a structure, its absolute age plays a critical role and can help us to distinguish between different possible formation scenarios.

A natural scenario for the formation of such a coeval and elongated structure would be that it originated in one star cluster, that was disrupted by removal of the residual gas and further extended by Galactic tides up to the present day size (see discussion in Kroupa, Aarseth, and Hurley, 2001; Kroupa, 2005). This is clearly a viable scenario for formation of stellar streams. However, this process acts on a time scale proportional to the Galactic rotation period (200 Myr), and thus cannot be responsible for the formation of the discovered structure.

In principle, gas removal could trigger the expansion of a star cluster. For a 17 Myr-old structure spread over 100 pc, this would imply an expansion velocity of approximately $5 - 10$ km/s. We do not find evidence of such an expansion. Moreover, the dispersion of the stellar motions are ≈ 0.5 km/s and hence too low (by an order of magnitude) with respect to what would be needed to form such elongated structure. In addition, considering the low number of observed stars, the likely initial stellar mass of the putative star cluster is small ($<< 1000\ M_{\odot}$). For such star clusters, the expected expansion velocities are ≈ 0.5 km/s (e.g. Brinkmann, Banerjee, Motwani, and Kroupa, 2017), as also recently confirmed by Gaia DR2 data (Kuhn, Hillenbrand, Sills, Feigelson, and Getman, 2019b; Kuhn, Hillenbrand, Sills, Feigelson, and Getman, 2019a).

Another possible explanation is that the Orion relic filament is the relic of star formation in a molecular cloud filament structure. We show in Fig 5.9 an explanatory sketch of the possible formation scenario. As emphasised by André, Di Francesco,

Ward-Thompson, Inutsuka, Pudritz, and Pineda (2014) it is generally accepted that stars and more specifically pre-stellar cores form in regions of the molecular clouds characterized by high mass density (first two panels from the left of Fig. 5.9). André, Di Francesco, Ward-Thompson, Inutsuka, Pudritz, and Pineda (2014) demonstrate that, together with pre-stellar cores, filaments play a critical role in the star formation process as star formation proceeds in them. Moreover, filament intersections can provide column densities and pressures (Myers, 2009; Myers, 2011) high enough to trigger the formation of massive stars and embedded star sub-clusters (Joncour, Duchêne, Moraux and, and Motte, 2018; Hill, Motte, Didelon, et al., 2011; Hennemann, Motte, Schneider, et al., 2012; Schneider, Csengeri, Hennemann, et al., 2012).

Based on high resolution observations of nearby star-forming regions (Orion, NGC 1333) obtained with the Atacama Large Millimeter/submillimeter Array (ALMA), Hacar, Alves, Tafalla, and Goicoechea (2017) and Hacar, Tafalla, and Alves (2017) provide new strong observational evidence in support of a scenario in which pre-stellar cores forms in high-density filaments while embedded star clusters and high-mass stars reside in the intersection of filaments, hubs and ridges (Hacar, Tafalla, Forbrich, et al., 2018). Such filaments can be as large as a few hundred pc in size (Li, Urquhart, Leurini, et al., 2016; Mattern, Kauffmann, Csengeri, et al., 2018; Großschedl, Alves, Meingast, et al., 2018). Moreover, ALMA observations of the merging Antennae galaxies indicate the detection of proto-globular clusters (GC) and suggest that the extreme values of pressure detected in the observed regions may be produced by ram pressure from the collision of filaments (Finn, Johnson, Brogan, et al., 2019).

The OSFR is a complex star forming region where multiple burst of star formation have been happening over the last 10 to 12 Myr (Bally, 2008). While Orion A is a 90pc-large star forming region (Großschedl, Alves, Meingast, et al., 2018), filamenary structures with ongoing star formations in the vicinity of the Trapezium region have been recently observed with ALMA by Hacar, Alves, Tafalla, and Goicoechea (2017). In this context, the 17 Myr coeval filament of stars found in this paper can be interpreted as the relic filamentary structure of one of (if not the) oldest start formation event in OSFR. In other words, the Orion relic filament might bear witness to a filament-driven star formation event that occurred approximately 17 Myr ago in the OSFR and is decoupled from its natal gaseous filament. As shown by Padoan, Haugbølle, Nordlund, and Frimann (2017), the gaseous filaments are expected to survive ≈ 10 Myr (see also Egusa, Sofue, and Nakanishi, 2004; Egusa, Kohno, Sofue, Nakanishi, and Komugi, 2009; Fukui and Kawamura, 2010; Meidt, Hughes, Dobbs, et al., 2015; Padoan, Pan, Haugbølle, and Nordlund, 2016) while the stars have lost association with their birth clouds after a few Myr (Grasha, Calzetti, Adamo, et al., 2019). This scenario is described in the third panel from the left of Fig. 5.9.

Using Hipparcos, Bouy and Alves (2015) report the discovery of a number of large-scale (≈ 100 pc in length) stellar streams in the Solar neighbourhood, Scorpius-Centaurus, Vela and Orion. Their detection was later confirmed by Zari, Hashemi, Brown, Jardine, and de Zeeuw (2018) using Gaia DR2 data. Given the definition above, we suppose that these streams might be too young to be tidal streams and thus are most likely the same kind of objects as the Orion relic filament.

Strong efforts have been made (e.g., Federrath, 2016; Vázquez-Semadeni, González-Samaniego, and Colín, 2017) to perform hydrodynamical simulations capable of repro-

ducing the collapse of the gas into a sequence of filaments of initially turbulent self-gravitating molecular clouds. While such simulations provide theoretical insights into filamentary star formation, they are limited by the lack of spatial resolution needed to explore the physics of star formation in filamentary structures at the sub-parsec scale.

Our observations provide unique observational evidence that filamentary star formation is producing large scale co-eval structures, that were likely sub-clustered in the past, but did not merge. Hence, observations of relic filaments present a very valuable asset to our understanding of star formation in general.

5.5 Conclusions

We report the discovery of the oldest stellar population linked to the Orion star forming region. The structure is clustered in proper motions, is located at a distance of ≈ 430 pc from us, has a filament-like shape on the sky of length of ≈ 90 pc and is coeval with an age of ≈ 17 Myr. We measure radial velocities (RV) of 13 proper motion-selected candidate members using the high-resolution spectrograph Hermes at the 1.2m Mercator telescope at La Palma. The distribution of the RVs, complemented with a few measurements available from Gaia DR2, peaks at 26.1 ± 4.7 km/s, indicating that the group of stars share a common bulk motion.

We interpret the discovered the 17 Myr-old structure, which we refer to as the *Orion relic filament*, to be a relic of star formation in a molecular cloud filament. This may represent a short-lived evolutionary phase after gas removal and prior to the dispersion of the structure due to shears and tides. The formation of tidal tails and streams should occur later, if at all, on a time-scale of hundreds of Myr and only for the surviving (i.e., massive and compact enough) star clusters. The following evolutionary stages thus seem to occur: i) dust/gas filaments and fibres, ii) filament star formation emerging in the densest parts of the molecular cloud filaments, iii) phase of relic filament after the stars decouple from the gas, iv) tidal/shear disruptions and tidal streams development. We present a descriptive sketch in Fig. 5.9 as a summary.

Therefore this discovery puts additional constraints on filamentary star formation that happens on large scales and should be systematically searched for and quantified. Any simulations describing star formation should aim to be able to reproduce these structures that are lacking evidence of hierarchical large-scale merging. This suggest that molecular clouds are not initially gravitationally bound, but produce large scale structures built from filaments that host nests of stars and star clusters at their intersections (e.g., Joncour, Duchêne, Moraux and, and Motte, 2018).

Acknowledgements: *We thank Laurent Eyer and Jiri Zak for carrying out the Hermes observations as well as the Mercator team for providing support. This research is based on observations made with the Mercator Telescope, operated on the island of La Palma by the Flemish Community, at the Spanish Observatorio del Roque de los Muchachos of the Instituto de Astrofísica de Canarias. Hermes is supported by the Fund for Scientific Research of Flanders (FWO), Belgium, the Research Council of K.U. Leuven, Belgium, the Fonds National de la Recherche Scientifique (F.R.S.-FNRS), Belgium, the Royal Observatory of Belgium, the Observatoire de Geneève, Switzerland, and the Thuüringer Landessternwarte, Tautenburg, Germany. This re-*

search was made possible through the use of the AAVSO Photometric All-Sky Survey (APASS), funded by the Robert Martin Ayers Sciences Fund. C.F.M. acknowledges the ESA Research Fellowship. This work has made use of data from the European Space Agency (ESA) mission Gaia (https://www.cosmos.esa.int/gaia), processed by the Gaia Data Processing and Analysis Consortium (DPAC, https://www.cosmos.esa.int/web/gaia/dpac/consortium). Funding for the DPAC has been provided by national institutions, in particular the institutions participating in the Gaia Multilateral Agreement. This research has made use of the SIMBAD database, operated at CDS, Strasbourg, France.

5.6 Appendix: Extra material

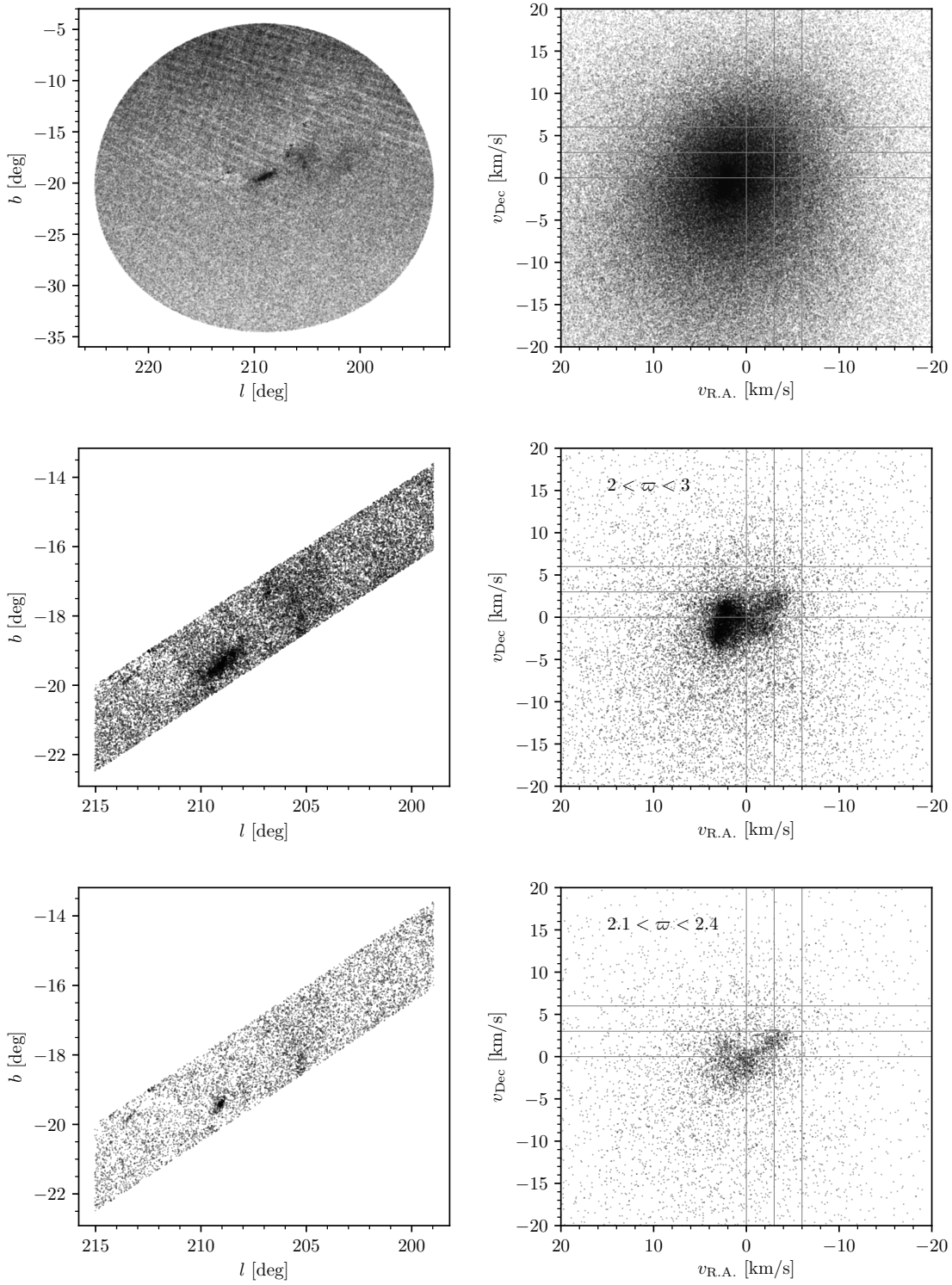

Figure 5.A1: **Top panels:** (left) The 15deg catalogue in l and b coordinates and (right) in proper motion space (in km/s) in R.A. and Dec. **Middle panels:** (left) Same as above with parallax cut between 2 to 3 mas and the cut in l and b applied. (right) Proper motions corresponding to middle left panel data selection. **Bottom panels:** Same as the middle panels above, albeit with a stricter cuts on parallax, showing only objects with parallax between 2.1 and 2.4 mas.

Chapter 6

Building bridges between stars and galaxies

This chapter summarises results from several publications for which the author provided significant/major contributions, while not being the leading author. These contributions are highlighted through the following text, and at the same time this chapter also emphasizes their relevance to multi-scale star-formation and stellar populations. *Bellow we list the publications which inspired this chapter. The text presented here is an original summary based on them. With the permission of the first author of the publication Kroupa,* ***Jerabkova****, Dinnbier, Becarri and Yan (2018, A&A) we used some parts of the text from it which were written by the author of this thesis.*

- Chruslinska, **Jerabkova**, Nelemans, and Yan (A&A, 2020): "The effect of the environment-dependent IMF on the formation and metallicities of stars over the cosmic history",
  In connection to Chapter 3,
  Contribution: project/idea shaping, numerical computations of part of the results, contribution to making plots, to the text and science.

- Kroupa, **Jerabkova**, Dinnbier, Becarri and Yan (2018, A&A): "Evidence for feedback and stellar-dynamically regulated bursty star cluster formation: the case of the Orion Nebula Cluster",
  In connection to Chapter 4,
  Contribution: numerical computations of the majority of the results, majority of the plots, contribution to the text and science.

- Yan, **Jerabkova**, Kroupa and Vazdekis (2019, A&A): "Chemical evolution of elliptical galaxies with a variable IMF",
  In connection to Chapter 3,
  Contribution: Code development tests and consultations, contribution to the text, structuring/content and science.

- Bekki, **Jerabkova** and Kroupa (2017, MNRAS): "The origin of discrete multiple stellar populations in globular clusters",
  In connection to Chapter 3,
  Contribution: project/idea shaping, numerical computations of part of the results, contribution to making plots.

- Yan, **Jerabkova** and Kroupa (2017, A&A): "The optimally sampled galaxy-wide stellar initial mass function. Observational tests and the publicly available GalIMF code",

In connection to Chapter 3,
Contribution: Code development tests and consultations, contribution to the text, structuring/content and science.

- Watts, Meurer, Lagos, Bruzzese, Kroupa, and **Jerabkova** (2018, MNRAS): "Star formation in the outskirts of DDO 154: a top-light IMF in a nearly dormant disc",
In connection to Chapter 3,
Contribution: numerical computations of part of the results, contribution to making plots.

The complexity of star-formation challenges boundaries of technical feasibility in numerical simulations, as it requires sub-pc resolution while simultaneously accounting for kpc-scale galactic tides and shears and for processes also happening at different time-scales. To avoid this problem, one viable approach allowing to link stellar populations on large (>100 pc) scales with their properties as resulting from small-scale (<1 pc) physics of star-formation, *is to rely on observations and empirical relations.*

The foundations of the idea to build up composite (large-scale/galactic) stellar populations from smaller building blocks originates in Kroupa (2002a) and Kroupa and Weidner (2003b). The theory arising from these publications, named the Integrated Galactic Initial Mass Function (IGIMF) theory, is able to compute various galaxy-wide properties and in particular the stellar initial mass function (among other applications) from embedded star-clusters as the building blocks (Kroupa, Weidner, Pflamm-Altenburg, et al., 2013). The IGIMF theory is in detail formulated in Chapter 3 with underlying axioms and needed relations and equations and is also addressed in the introduction Chapter 1.

In this chapter the focus is on showing how the IGIMF theory can be used to start building bridges between individual star-forming regions and galaxy-wide stellar populations. It discusses what advancements have been made in this field (on both small and large scales) during the author's PhD work, and comments on the development of computational means and its applications.

The following subsections are based on the author's contribution to the above-listed publications.

6.1 The IGIMF theory as a bridging tool

As this thesis presents and combines research of stellar populations from individual star clusters to cosmic scales in this section the IGIMF theory is presented as a bridging tool able to link various scales, while providing constraints and insights to physics of star-formation.

6.1.1 The GalIMF modular code

While the first studies building up galaxy-wide stellar populations from small building blocks are dated back to 2002 (Kroupa, 2002a; Kroupa and Weidner, 2003b), there was no publicly available tool allowing to perform such computation and to easily update input empirical relations that might be modified as observational data improve.

The need for having a publicly available modular code was satisfied with the GalIMF Python package developed by Yan, Jerabkova, and Kroupa (2017). This first version of the code was able to calculate galaxy-wide stellar and cluster population based on two input parameters, the galaxy-wide SFR and the galaxy's metallicity (Jeřábková, Hasani Zonoozi, Kroupa, et al., 2018). One specific ability of the code to highlight is its ability to provide stellar populations in the most common integrated form, but it can also treat them on a star by star basis with implemented optimal sampling [1] of individual stars from their mass function. The GalIMF code is written in the Python3 language and the up-to-date version is available on Github https://github.com/Azeret/galIMF. The following updates of the code in Yan, Jerabkova, Kroupa, and Vazdekis (2019) and Yan, Jerabkova, and Kroupa (2019) allow, in addition, for self-consistent treatment of chemical evolution. The general structure of the code is shown as a flow chart Fig. 6.1.

Having this tool at hand not only means complete reproducibility and transparency of any research done using the GalIMF code, but also allows for easy access to any computations related to stellar populations and chemical evolution.

6.1.2 The IGIMF theory as an operator

While the equations and basic assumptions underlying the GalIMF code and that are defining the IGIMF theory are described in detail in Chap. 3 above, this subsection provides a short summary highlighting the new conceptual developments and notations.

The fundamental insight underlying the IGIMF theory is that the systematic variation of the gwIMF, which appears to correlate with galactic SFR and metallicity, has its origin in the variation of the IMF on a sub-pc (embedded star cluster) scale. In other words, the physics driving star-formation and consequently as well the shape of the IMF function is driven by small scale processes (feedback, self-gravity) and couple to the galaxy-wide properties by the galactic gravitational potential, its tides and shears.

One of the main developments in this field is the interpretation of the IGIMF theory as being a computational framework – it is neither a single function, nor a set of fixed equations. It is rather a mathematical operator or procedure that allows the computation of composite stellar populations from their building blocks, as shown in Fig. 6.2. This very general formulation allows for many possible assumptions within it, and thus the modular structure of the GalIMF code is important. In the work presented in this thesis the original empirically-constrained IGIMF theory is followed. This means, as shown in Fig. 6.2, that we used star-forming structures (embedded star-clusters) as building blocks and their empirically derived properties as an input into the IGIMF theory. Different IGIMF formulations have been tested and possible

[1] Optimal sampling was introduced by Kroupa, Weidner, Pflamm-Altenburg, et al. (2013) to account for the apparent lack of variation in observed young stellar populations. Optimal sampling constitutes an extreme assumption such that Poisson dispersion in a stellar population is entirely absent, as opposed to random sampling from the IMF (or any distribution function). Its physical interpretation is that the formation of the stellar population in an embedded cluster is perfectly self-regulated through a balance of inflowing molecular gas versus the feedback of the emerging stellar population. Optimal sampling has, as the input parameters, the mass of the young population, $M_{\rm ecl}$, and the shape of the IMF, and it returns a precise sequence of individual stellar masses which only depends on $M_{\rm ecl}$. This accounts for the lack of dispersion seen in the shapes of measured IMFs and in the most-massive-star vs $M_{\rm ecl}$ relation, and it accounts also for this relation. An improved mathematical formulation of optimal sampling has been published by Schulz, Pflamm-Altenburg, and Kroupa (2015).

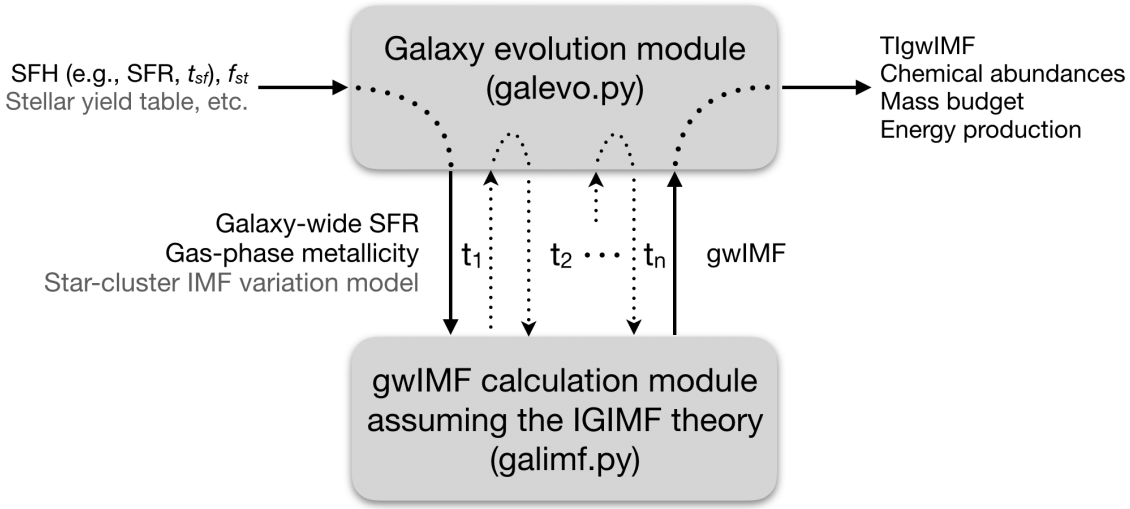

Figure 6.1: Figure taken from Yan, Jerabkova, Kroupa, and Vazdekis (2019). It shows the schematic implementation of the chemical/galaxy evolution module (Yan, Jerabkova, Kroupa, and Vazdekis, 2019, galevo.py) and its interaction with the stellar populations gwIMF module (Yan, Jerabkova, and Kroupa, 2017, galimf.py). The main input parameters to the chemical evolution module are the star formation history, SFH, and the star transformation fraction, $f_{\rm st}$. The star formation timescale, $t_{\rm sf}$, is one of the most important parameters for chemical evolution. The galaxy evolution module computes chemical evolution at each step, t_i. The updated value of gas-phase metallicity and the galaxy-wide SFR is then used by the gwIMF calculation module to compute the newly formed stellar population (the galaxy-wide IMF, gwIMF). This procedure allows for chemically self-consistent build up of stellar population in galaxies. TIgwIMF is the time-integrated galaxy-wide IMF.

improvements of the empirical relations have been suggested (e.g. Jeřábková, Hasani Zonoozi, Kroupa, et al., 2018). In this publication the need for clearly distinguishing and defining the stellar IMF is emphasized. In addition, to make as clear as possible the operator-like nature of the IGIMF description, a new terminology has been established in the form of having the IGIMF operator acting on a series of assumptions (A_i), that is $IGIMF(A_1, A_2, ...)$. This notation was first used by Yan, Jerabkova, and Kroupa (2020).

6.2 Stellar populations in star-clusters

The GalIMF theory and the GalIMF code has been used in several publications by the author in order to compute stellar populations in individual star-clusters. In the following subsections the works of Bekki, **Jerabkova** and Kroupa (2017, MNRAS) and Kroupa, **Jerabkova**, Dinnbier, Becarri and Yan (2018, A&A) are described.

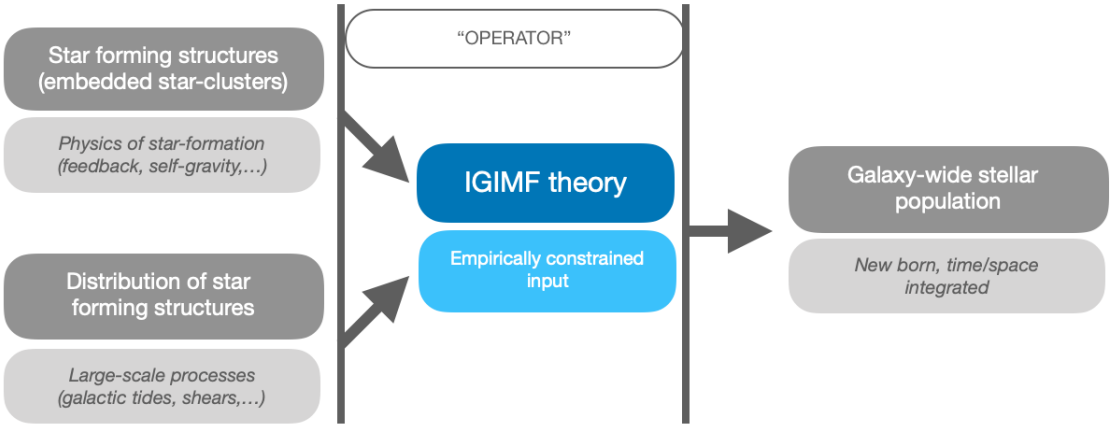

Figure 6.2

6.2.1 The origin of discrete multiple stellar populations in globular clusters

Bekki, Jerabkova, and Kroupa (2017) addressed the origin of discrete multiple stellar populations in globular clusters (GCs). It is now well established that Galactic GCs host multiple stellar populations that are most prominently manifested by observed anticorrelations between chemical abundances of light elements (Carretta, Bragaglia, Gratton, et al., 2009, e.g.). The stars enhanced in [Na/Fe], [Al/Fe] and depleted in [O/Fe], [Mg/Fe] along the Na-O anticorrelation are assumed to have formed from enriched material possibly from the first generation of stars (having element abundances similar to stars in the Galactic halo). Interestingly, for some clusters the distribution of stars along the [Mg/Fe]–[A/Fe] is not continuous, but it is instead clumped into several distinct groups (Carretta, 2014, study of GCs NGC2808).

Motivated by these observations, we constructed a new one-zone GC formation model, reproducing the observed clumpiness in the distribution of light elements. The model can be summarised as follows: 1) The first population of stars forms, further star formation being truncated by SNeII explosions. 2) Approximately after 30-50 Myr, after the majority of SNeII have exploded, the second stellar population can be formed from the material ejected by asymptotic giant branch stars. As for the first population, the formation of the second one is truncated in 10-20 Myr due to the newly formed SNeII. This cycle of star formation followed by its truncation through SNeII can continue until all AGB ejecta is removed by some physical process. The schematic sketch explaining the proposed scenario for the formation of discrete populations in GCs is shown in Fig. 6.3, it emphasizes that the stellar populations are formed clustered within the GC.

The most massive stars forming in each stellar generation are important, as they regulate the star-formation by their feedback. The author's contribution to this work was to quantify the numbers and life-time spans of newly born stars assuming a certain value of the SFR predicted by the one-zone cluster formation calculations. The stellar masses followed an invariant or universal canonical IMF and the empirically motivated IMF compute with the GalIMF code withing the IGIMF theory. Both IMF assumptions

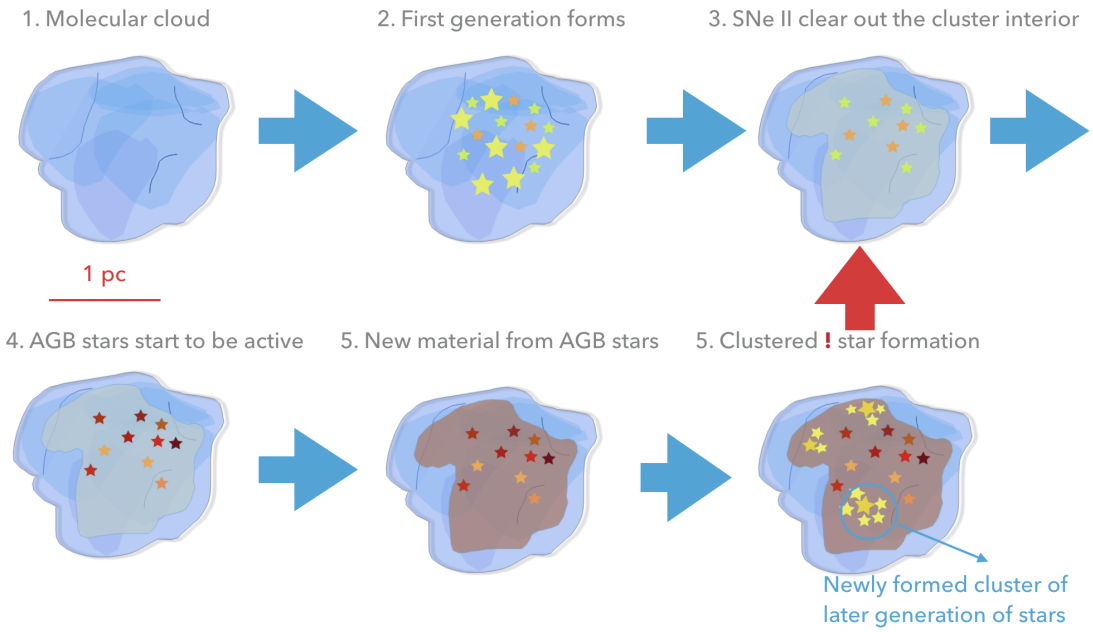

Figure 6.3: Schematic visualisation of the formation of chemically discrete multiple populations in GCs.

are able to produce discrete multiple populations within a GC. The main difference between the two is the stellar masses produced in a stellar population. While in the canonical IMF scenario stars with masses larger than 20-30$M_{\odot}$ can form at a low SFR, this is not the case in the IGIMF theory. One of the central constrains implemented in the IGIMF theory is the empirical correlation between the most massive star formed and the total mass of the stellar population in an embedded cluster (Yan, Jerabkova, and Kroupa, 2017). Due to this the IGIMF-based model produces more extended episodes of star-formation and reproduces the observations better. The presented model also predicts that low mass GCs are unlike to have discrete multiple stellar populations, while still hosting multiple stellar populations. This is because the most massive star forming in these clusters does not reach the SNeII progenitor mass and thus star-formation would not be truncated.

Another example of using the IGIMF theory to populate star-clusters is closely related to Chapter 4. The next subsection is devoted to its description.

6.2.2 Evidence for feedback and stellar-dynamically regulated bursty star cluster formation: the case of the Orion Nebula Cluster

Some parts of the following text are adapted from the publication by Kroupa, Jerabkova, Dinnbier, Beccari, and Yan (2018), however all the used material has been produced by the author of this thesis and is used here with the permission of the first author of the manuscript.

The presence of multiple bursts of star-formation each lasting < 1 Myr and separaterd by $\approx 1 Myr$ in the ONC challenges our understanding of star-cluster formation

(see Chapter 4 for more details). The main reason of the challenge is, in a simplistic way, that star formation in a star cluster should be shut off due to the feedback from massive stars once these form. That is why star clusters were thought to be formed in a single burst of star formation (e.g. the ONC, Kroupa, Aarseth, and Hurley, 2001).

As the author summarized in the IAU proceedings Jerabkova (2020), Kroupa, Jerabkova, Dinnbier, Beccari, and Yan (2018) present a scenario for the formation of multiple coeval populations separated in age by about 1 Myr as observed in the ONC. The scenario is explained in the schematic sketch, Fig. 6.4. It is based on a converging inflow from a molecular gaseous filament that is building up a first stellar population. Once (and if) massive O stars are formed they ionise the inflow and suppress star formation in the cluster. However, the O stars can eject each on a short time scale (< 1 Myr) – before the converging filament is destroyed by their feedback. The inflow of molecular gas onto the cluster can then resume and a second stellar population can start forming. We show that for an ONC-like star cluster this process is realistic, because massive stars are formed as multiple systems at the centre (potential minimum) of the embedded cluster, and thus can eject each other rapidly enough and can therewith reproduce the observed three stellar populations. The mass-inflow history is constrained using this model and the number of OB stars ejected from each population is estimated for verification using Gaia data. Subsequent Nbody simulations by Wang, Kroupa, and Jerabkova (2018) verify this process to be viable. As a further consequence of the proposed model, the three runaway O star systems, AE Aur, μ Col and η Ori, are considered as significant observational evidence for the stellar-dynamical ejections of massive stars from the oldest population in the ONC.

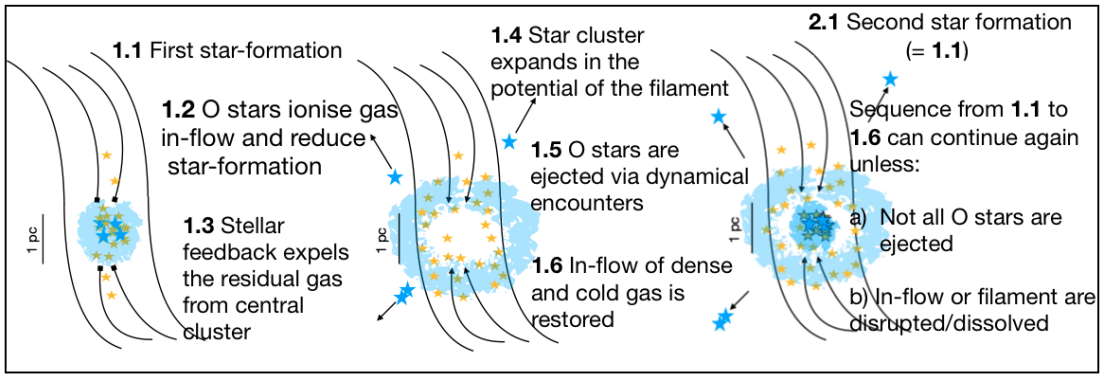

Figure 6.4: Schematic visualisation of the evolution of the molecular cloud filament, shown by the black curves, through the process of inflow, the monolithic formation of the first embedded cluster and termination of the inflow (left panel), the expansion of the first population due to gas expulsion and the ejection of the OB stars and resumption of gas inflow (middle panel), the monolithic formation of the second embedded cluster (right panel). Taken with modifications from Kroupa, Jeřábková, Dinnbier, Beccari, and Yan (2018).

One aspect to be considered is the amount of ionizing radiation produced by massive stars - is it enough to truncate star-formation, but not to destroy the whole filament at the same time? For a given mass of a stellar population one can estimate the masses of the ionising (O, B) stars, once the IMF and sampling method (random or optimal, see footnote 1 on page 121) is assumed. Since the past inflow history is not known, the

masses of the populations are estimated from the observed population numbers. Given an estimate of the population's mass, the IMF allows a quantification of the number of ionising stars. The IMF in nearby star forming regions can be well described by an invariant canonical IMF (Kroupa, 2001). The canonical IMF can be conveniently represented by two power-law segments, $dN/dm \propto m^{-\alpha_{1,2}}$, where $\alpha_1 = 1.3$ for $0.08 \leq m/M_\odot < 0.5$ and $\alpha_2 = 2.3$ (the Salpeter value) for $0.5 \leq m/M_\odot < m_{\rm max}$. Here, dN is the infinitesimal number of stars in the infinitesimal stellar-mass interval $m, m + dm$, and $m_{\rm max}$ is the most massive star in the population, this being empirically a function of the embedded cluster's stellar mass (Weidner, Kroupa, Pflamm-Altenburg, and Vazdekis, 2013; Kroupa, Weidner, Pflamm-Altenburg, et al., 2013; Megeath, Gutermuth, Muzerolle, et al., 2016; Ramírez Alegría, Borissova, Chené, et al., 2016; Stephens, Gouliermis, Looney, et al., 2017; Yan, Jerabkova, and Kroupa, 2017).

To sample stellar populations, two approaches are employed:

1. Mass-constrained random sampling: the IMF is sampled randomly until the desired population mass is achieved within a tolerance of $0.09\,M_\odot$, rejecting stars until the population mass is reached with a deviation of up to this amount).

2. Optimal sampling, with the most massive star being constrained by the total mass of the stellar population. This sampling method leads naturally to the observed $m_{\rm max} - M_{\rm ecl}$ relation, (Weidner, Kroupa, Pflamm-Altenburg, and Vazdekis, 2013; Kroupa, Weidner, Pflamm-Altenburg, et al., 2013; Megeath, Gutermuth, Muzerolle, et al., 2016; Ramírez Alegría, Borissova, Chené, et al., 2016; Stephens, Gouliermis, Looney, et al., 2017). The mathematical procedure of optimal sampling (see footnote 1 on page 121) may be interpret physically as reflecting perfect self-regulation of the forming stars and star cluster (Kroupa, Weidner, Pflamm-Altenburg, et al., 2013). It has been suggested that the available data appear to prefer optimal over random sampling (e.g. Yan, Jerabkova, and Kroupa 2017 and footnote 1).

Since random sampling gives Poison scatter to the final stellar population, each of the four populations is sampled 1000 times and the mean values and $1-\sigma$ dispersions are listed in Tab. 6.1. To sample stars optimally the GalIMF module from Yan, Jerabkova, and Kroupa (2017) is employed[2]. For all computations it is assumed that the total stellar mass of the ONC is $M_{\rm ONC} \approx 1500\,M_\odot$. This allows an estimation of the stellar masses of the individual stellar populations (Table 6.1), given that Beccari, Petr-Gotzens, Boffin, et al., 2017 provide measurements of the relative fractions of the first three of these. The mass of the fourth (currently forming) population is calculated assuming the ionising stellar binary in the current Trapezium, θ1C Ori, is comprised of a primary star which is the most massive star with a mass of $27\,M_\odot$ (Kraus, Weigelt, Balega, et al., 2009). Assuming optimal sampling (see footnote 1 on page 121), this allows a calculation of the total mass of this stellar population. This gives a mass of the fourth population of $650\,M_\odot$, which then allows the calculation of the individual stellar masses listed in Table 6.2, using optimal sampling.

[2]The source code is freely available on the github repository. The GalIMF version 1.0.0 with associated programs is available at https://github.com/Azeret/galIMF

		$\#\star : m_\star > 19 M_\odot$	$\#\star : m_\star > 5 M_\odot$
$1^{\rm st}$ pop.	RS	3 ± 2	18 ± 3
$886 M_\odot$	OS	2	18
$2^{\rm nd}$ pop.	RS	2 ± 1	10 ± 3
$486 M_\odot$	OS	1	10
$3^{\rm rd}$ pop.	RS	0 ± 1	3 ± 1
$128 M_\odot$	OS	0	2
$4^{\rm th}$ pop.	RS	2 ± 1	13 ± 3
$650 M_\odot$	OS	1	13

Table 6.1: Estimated mass in each of the four populations (left column), the associated number of O stars (central column) and of the number of all stars more massive than $5\,M_\odot$ (right column). "RS" and "OS" refers to random sampling and optimal sampling, respectively (see footnote 1 on page 121).

It is to be noted that the sequences of masses given here depends on the population masses and should therefore be taken to be illustrative rather than definitive. Nevertheless, the masses of individual stars are in agreement with the observational data. For example, the three most massive stars in the first (oldest) population appear to be similar to the three runaway O stars ejected from the ONC about 2.5Myr ago (see above). The first and second most massive star ($18.6\,M_\odot$) of the fourth (now forming) population combined, corresponds very closely to the mass of the binary system $\theta 1$ C Ori (Kraus, Weigelt, Balega, et al., 2009). The number of stars in the fourth population more massive than $5\,M_\odot$ is in agreement between model and the observed ONC, which currently has 10 of these (Pflamm-Altenburg and Kroupa, 2006). Note that Pflamm-Altenburg and Kroupa (2006) assumed a population mass of $1600\,M_\odot$ for the ONC such that it must have ejected 30 stars more massive than $5\,M_\odot$. The model here now solves this top-light IMF problem of the ONC naturally by having it being made up of four populations. With optimal sampling, the overall ONC now becomes very consistent with the IMF (see footnote 1 on page 121).

6.2.2.1 Halting star formation

Having specified the stellar populations, the question addressed now is whether the populations can ionise the inner region of the embedded cluster while not destroying the entire cloud within more than a pc radius, *before* the ionising stars eject each other out of the forming embedded cluster.

Once we have an O star in the cluster-forming cloud core, the ionising flux of the O star creates a plasma around it. The radius of this plasma can be estimated using the Strömgren sphere around the star, taking into account that the molecular gas is inflowing with the observed velocity (Raga, 1986). This is only a rough, but for the present purposes sufficient approximation in that the details are highly complex (e.g. Wood and Churchwell 1989; O'Dell, Henney, Abel, Ferland, and Arthur 2009).

The radius of the ionised gas bubble (the Strömgren radius) around the star is established rapidly (Wood and Churchwell, 1989) when the rate of emissions of ionising photons and the rate of recombinations in the plasma balance, assuming the density

1^{st}, $886 M_\odot$	2^{nd}, $486 M_\odot$	3^{rd}, $128 M_\odot$	4^{th}, $650 M_\odot$
$[M_\odot]$	$[M_\odot]$	$[M_\odot]$	$[M_\odot]$
32.9	22.3	9.0	27.0
22.9	15.3	6.0	18.6
18.0	11.8	–	14.5
15.0	9.8	–	12.0
13.0	8.4	–	10.4
11.4	7.4	–	9.1
10.2	6.7	–	8.2
9.3	6.1	–	7.5
8.6	5.6	–	6.9
8.0	5.2	–	6.4
7.4	–	–	5.9
7.0	–	–	5.6
6.6	–	–	5.3
6.2	–	–	–
5.9	–	–	–
5.7	–	–	–
5.4	–	–	–
5.2	–	–	–

Table 6.2: The exact model stellar populations assuming optimal sampling, a canonical IMF and the masses of the four populations as described in the text.

of the plasma remains unchanged during the photo-ionisation process. Within the Strömgren radius, the gas temperature increases from about 10 K to 10^4 K. This gas, still at the same density, is like a bomb, as it is in significant overpressure compared to the surrounding cold cloud. So it erupts by whichever way the gas can find a way out, the cloud never being homogeneous. When the density of ionised gas has fallen because it is flowing out with about the sound-speed of the plasma, 10 km/s, the radius of the ionised region grows, because now more ionising photons are left over. It grows with about 10 km/s, i.e. on the time scale with which the 10^4 K gas is flowing out. Indeed, measurements of the growth rate of UCHII regions show that they increase their radii by $5 - 35$ km/s (Kawamura and Masson, 1998; Acord, Churchwell, and Wood, 1998). The evolution from this ultra-compact HII (UCHII) region to the young HII region takes about 0.1 Myr (Kawamura and Masson, 1998).

Thus, once an O star is present, the evolution is explosive and most of the gas not in stars is evacuated and the molecular cloud is destroyed (Lada, 2010). That more than 60 per cent of the gas is not in stars in very young embedded clusters is affirmed by observations (Lada and Lada, 2003; Megeath, Gutermuth, Muzerolle, et al., 2016). High-resolution magnetohydrodynamical simulations of proto-stellar formation also imply that a large fraction of the accreting gas is channeled outwards into outflows (Machida and Matsumoto, 2012; Banerjee, 2014; Bate, 2014). These numbers (the life-time of UCHII regions and the blow-out of the gas and thus growth of the HII region with about 10 km/s) are in noteworthy agrement with independently obtained stellar-

dynamical results. According to these, the density and velocity profiles of observed very young clusters (ONC, NGC3603 and R136) are well reproduced if 67 per cent of the total mass is removed as gas with a velocity of 10 km/s and after a delay time of 0.6 Myr (Banerjee and Kroupa, 2018) and the expansion of embedded clusters to become open clusters (Banerjee and Kroupa, 2017). There is therefore a well-founded overall theoretical and empirical understanding of the early evolution of embedded clusters.

For a given stellar population, computed values of ionising fluxes from Sternberg, Hoffmann, and Pauldrach (2003) are used assuming luminosity class V stars (their table 1). The fluxes are interpolated and linearly extrapolated, based on the last two points, to be able to sum contributions from all stars. The values of ionising fluxes are plotted in Fig. 6.5 on the x-axis.

To estimate which effect the computed ionising flux has on the gas filaments inflowing into the ONC we consider the physical values as deduced from observations by Hacar, Alves, Tafalla, and Goicoechea (2017), i.e. a density of $\varrho \approx 10^4 - 10^5 cm^{-3}$ and an inflow velocity of $v_{\rm inflow} \approx 2\,{\rm kms}^{-1}$. It is not our aim to characterise the exact effect of the ionising photons on the surrounding region here, because the full problem including ionisation species and stellar winds is computationally highly involved (for a discussion of the observational situation see O'Dell, Henney, Abel, Ferland, and Arthur 2009). Thus, the aim here is to estimate the damage done to the filaments on a time scale of about 10^5 yr due to the photo-ionising radiation from the O stars in the formed populations. To estimate the evolution of the distance, R_S, at which the inflowing molecular filament is ionised we apply eq. 4 in Raga (1986) finding that it is indistinguishable to the Strömgren radius (eq. 6 in Raga 1986). This distance is plotted in Fig. 6.5 for the three stellar populations quantified above.

Once the UCHII region has formed, after a few 10^5 yr after the onset of the formation of the embedded cluster and the appearance of the O star(s) the plasma erupts outwards, forming a champagne flow (Tenorio-Tagle, 1979) and the density of the plasma decreases. The time-scale of this process can be approximated by the plasma flowing out with 10 km/s. A maximum effect is obtained if all plasma has been lost and all ionising photons can reach the ionisation front which separates the HI region from the molecular cloud. The front will therefore expand into the molecular cloud, the new plasma flowing out through the opening(s) of the cloud. Such flows are observed in the ONC (O'Dell, Henney, Abel, Ferland, and Arthur, 2009). This leads to an estimate of this distance, $R_S(t)$, at a time $t = 10^5$ Myr (Fig. 6.5) being about 1 pc for all populations. This estimate thus demonstrates that the O stars which most likely formed with the three previous populations were not able to destroy the molecular cloud filaments within about 0.1 Myr, but that they did ionise these within the innermost few 0.1pc region. This is indeed observed to be the case in the presently forming fourth population (O'Dell, Henney, Abel, Ferland, and Arthur, 2009).

6.2.2.2 A possible history of mass accretion, and the IMFs

In an attempt to perform such a re-creation of the inflow history, the masses of the four populations are corrected for a SFE of 33 per cent and divided by the 1-sigma and 5–95 per cent age time-intervals for each of the first, second and third population

(table 1 in Beccari, Petr-Gotzens, Boffin, et al. 2017). For the presently forming one it is assumed it formed over a time interval of 1 Myr. The so estimated mass-inflow rates are compared to the currently observed rate in Fig. 6.6.

Given that Beccari, Petr-Gotzens, Boffin, et al. (2017) have now the means to separate the populations in the ONC in the colour-magnitude diagramme, it has become possible to observationally estimate their individual IMFs, by performing the complex transformation of luminosities to stellar masses for pre-main sequence stars, taking into account that a large fraction of these are in unresolved multiple systems (Kroupa, Weidner, Pflamm-Altenburg, et al., 2013). Within the present model, it is possible to calculate the IMFs of the four populations, as shown in Fig. 6.7.

To summarize, this work present a viable formation scenario of the recent discovery of the ONC being composed of three stellar population formed in three short bursts of star-formation. Worth emphasizing is the fact that the presented scenario considers previously done numerical simulations and points out that the observations of Beccari, Petr-Gotzens, Boffin, et al. (2017) and Jerabkova, Beccari, Boffin, et al. (2019) can be naturally explained by the interplay of dynamical interactions of stars in star clusters and stellar feedback.

6.3 Stellar populations in galaxies

Another possible application of the GalIMF code and the IGIMF theory in general is to compute stellar populations in galaxies. Watts, Meurer, Lagos, Bruzzese, Kroupa, and Jerabkova (2018) investigated star-formation in the outskirts of the dwarf irregular galaxy DDO 154 using Hubble Space Telescope (HST) Advanced Camera for Surveys (ACS)/ Wide Field Camera (WFC) data. The HST data allow to study resolved stellar populations in the outer parts of the disc of DDO 154. Interestingly, the outer regions of the galactic disk contain almost none of the young stellar populations. Instead, the majority of young stars are found to be clustered near the main stellar component of the galaxy. It was also possible to explore the stellar mass function of the young populations and thus put constraints on the stellar IMF assuming a single power-law shape and a constant star-formation history over the galactic dynamical time-scale. The best fitting IMF power-;aw is found to be $\alpha = 2.45$ which is top-light in comparison to the universal canonical IMF. This means that the young stellar population in DDO 145 is deficient in high mass stars. The observational constraint on the upper mass limit is $M_U = 16\,M_\odot$, assuming a constant SFH over the dynamical timescale without clustering in space or time. (Watts, Meurer, Lagos, Bruzzese, Kroupa, and Jerabkova, 2018) did not compute a formal uncertainty to the upper mass limit estimate, the $M_U = 16\,M_\odot$ representing the best fitting model from a grid with an upper mass limit step of $4M_\odot$.

This galaxy, in which stars are forming in a low-density environment at a small star formation rate, presents a useful test case for the IGIMF theory. This test comparison was done by the author of the thesis as a contribution to the manuscript. As input parameters needed for computing the stellar population expected within the IGIMF theory we adopted a metallicity of $Z = 0.1Z_\odot$ (Kennicutt and Skillman, 2001) and a star-formation rate, $SFR = 4.65 \times 10^{-4} M_\odot/\mathrm{yr}$, derived using the best fitting IMF in

the HST/ACS field of view.

The final comparison of the empirically derived results and the predictions from the IGIMF theory can be seen in Fig. 6.8. Remarkably, the best-fit single power-law IMF is very close to the prediction from the IGIMF theory and the upper mass limits are basically identical.

6.4 The effect of the environment-dependent IMF on the formation and metallicities of stars over the cosmic history

Chruślińska, Jeřábková, Nelemans, and Yan (2020) present a first application of the IGIMF theory on cosmic scales. The work is built-up on two pillar publications, 1) Chruslinska and Nelemans (2019) who found the observation-based cosmic star-formation rate density (however, assuming the invariant canonical IMF, Kroupa 2001), and 2) Jeřábková, Hasani Zonoozi, Kroupa, et al. (2018) who formulated the SFR and metallicity-dependent IGIMF model and corrections for observationally inferred SFRs assuming a variable versus invariant canonical IMF. These two works allowed to quantify, for the first time, the stellar-populations over cosmic history using an environment-dependent IMF.

The cosmic star-formation is not only important for a general understanding of the cosmic baryonic cycle and the physics of star-formation under different conditions occurring at high redshifts, but also to quantify any stellar/binary evolution phenomena as for example stellar mergers, supernova Ia and II events, and gravitational wave progenitors.

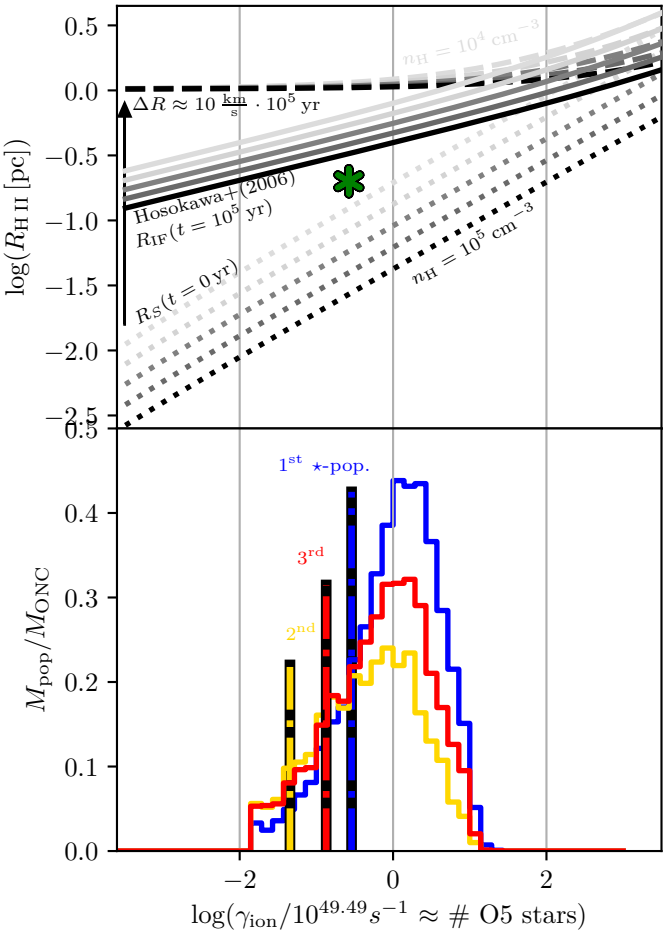

Figure 6.5: The distance, R_S, to the radial molecular cloud filament within which the gas is ionised in dependence of the number of ionising photons whereby one O5V star emits $10^{49.49}$ ionising photons/s. The shaded regions show the range of values obtained for the random sampling cases, and the thick vertical bars refer to the optimal sampling cases which have no Poisson spread. The height of the population is proportional to the mass of the population. The color code is the same as in Tab. 6.1. The dotted lines show R_S for different values of the density of the cloud, $n_{\rm H}$, assuming no change in density within the UCHII region compared to the surrounding molecular cloud. The solid lines indicate R_S assuming the density of the gas is zero up until the ionisation front. This front expands with 10 km/s such that at 10^5 yr $R_s \approx 1$ pc for $\gamma_{\rm ion} < 10^{49.49}$ photons/s, being progressively larger for larger photon fluxes. For example, the first (oldest, blue) population, once its few O5V stars begin to emit ionising radiation, would have produced an UCHII region with $R_S \approx 10^{-1.2}$ pc. It expands within about 0.1 Myr to $R_S \approx 1$ pc and that $10^5\,{\rm cm}^{-3} = 4.3\,M_\odot{\rm pc}^{-3}$. Note that the mass of an O5 star is $\approx 60\,M_\odot$.

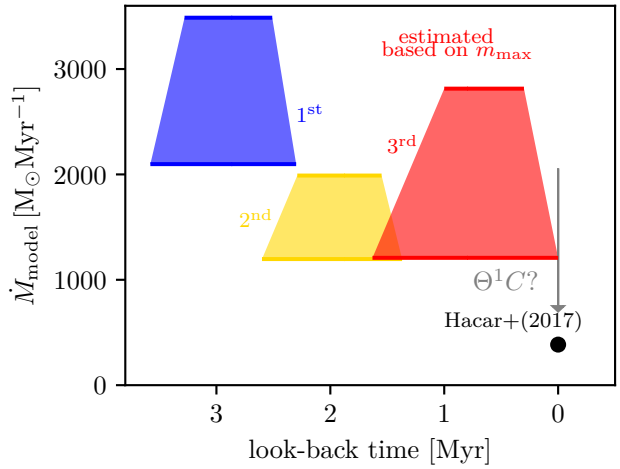

Figure 6.6: The estimated mass inflow rates, $\dot{M}_{\rm g,flow}$, which may have occurred during the successive built-up of the stellar population of the ONC. Inflow began about 3 Myr ago when the molecular-cloud filament, at present in the shape of an integral, established itself. This formed the first (blue) population. The presently on-going inflow, shown as a black point, has been forming the fourth (present-day) population and is larger than the directly measured value by (Hacar, Alves, Tafalla, and Goicoechea, 2017) which may be a sign of on-going photo-ionisation of the inflow through the star θ1 C Ori.

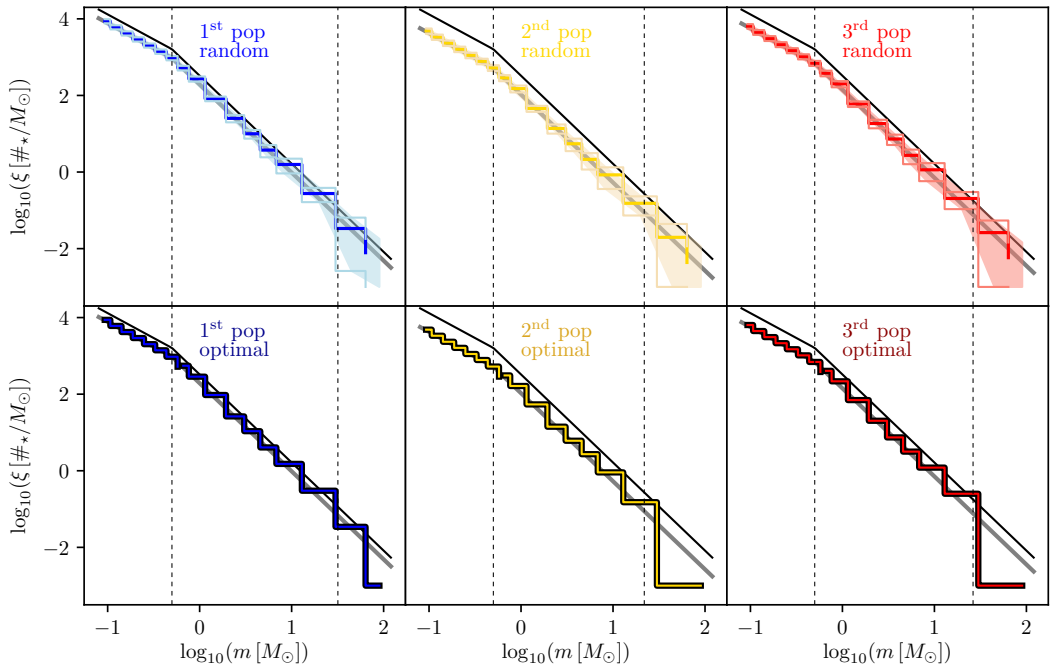

Figure 6.7: The model IMFs of the four populations, colour coded as in Table 6.1. The upper row depicts the IMFs assuming random sampling. The shaded regions indicate the minimum and maximum values for 1000 realisations. The lower row shows the IMFs assuming nature follows optimal sampling. These have no uncertainties. The solid lines are the canonical IMF, and the dashed vertical lines denote $m_{\rm max}$.

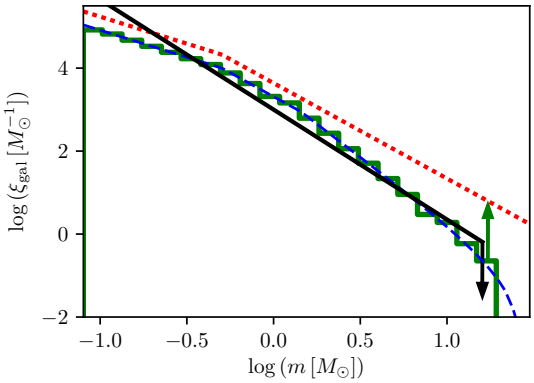

Figure 6.8: Plot computed by the author for Watts, Meurer, Lagos, Bruzzese, Kroupa, and Jerabkova (2018). It shows the best fitting single-power law IMF to the data (black), the canonical Kroupa IMF (red, offset +0.5 dex), the prediction from the IGIMF theory (blue, dashed), and the optimally sampled IGIMF result (green). The upper mass limit found by (Watts, Meurer, Lagos, Bruzzese, Kroupa, and Jerabkova, 2018), $M_U = 16\,M_\odot$, is indicated by the down pointing black arrow. The upper mass limit predicted by the optimally sampled IGIMF theory, $m = 15\,M_\odot$, is indicated by the green up pointing arrow.

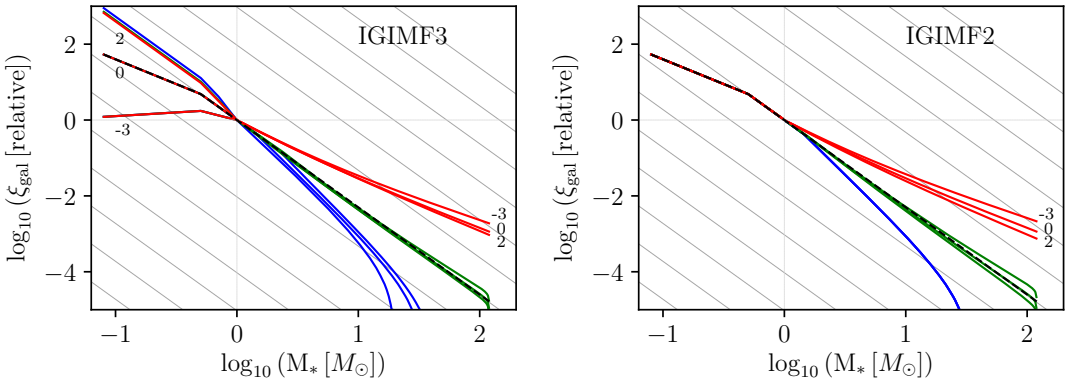

Figure 6.9: From Chruślińska, Jeřábková, Nelemans, and Yan (2020), produced by the author of the thesis. **Left:** Galaxy-wide IMFs computed using IGIMF3 as a function of stellar mass plotted for several values of SFRs (10^{-3} – blue, 1.0 – green, 10^{3} – red $M_{\odot}$/yr) and [Fe/H] (-3, 0 2). The galaxy-wide IMFs are normalised by their values at 1 $M_{\odot}$ to show the slope changes. The universal Kroupa, 2001 IMF is plotted as a black dashed line. **Right:** Galaxy-wide IMFs computed using IGIMF2 as a function of stellar mass plotted for several values of SFRs (10^{-3}, 1.0, 10^{3} $M_{\odot}$/yr) and metallicities (-3, 0 2). The galaxy-wide IMFs are normalised by their values for 1 $M_{\odot}$ to show the slope changes. Note the main difference between the IGIMF2 and IGIMF3 models is the variation for the low-mass part of the galaxy-wide IMF.

Chapter 7

Conclusions and future directions

This thesis presents research on star-formation and stellar populations in the form of four original papers published in refereed journals that are led by the author of this thesis and, in addition, a complementary Chapter 6 based on of six refereed publications to which the author contributed significantly.

In the introduction Chapter 1 the fundamental importance of the need for understanding star-formation and stellar-populations is emphasized. These processes manifest themselves and are coupled to an enormous span in spatial and mass dimensions. They are difficult and challenging to study because the environment in which stars are born is so different from any conditions on Earth. For example, the dense parts of molecular clouds would be considered an excellent vacuum in any laboratory and, yet on top of that, self-gravity adds to the complexity. All this contributes to the challenge to comprehend the physics of star-formation and results in the continuous large research focus on this field. While in general there is unambiguous progress, many questions still remain unanswered.

Interestingly, the two possibly main pillars of the theories of star formation – ISM turbulence and the filamentary structure of molecular clouds – have been described in the literature decades before being widely studied by the science community. Possibly due to the above mentioned reasons, this field is largely driven by astronomical observations and, at least based on the historical record, it is hard to trace progress in real time. *This thesis is addresing the complex multi-scale stellar populations with a multi-scale research program combining theory and observations.*

The content of the thesis can be broadly divided into two areas: 1) Resolved star-formation in the Milky Way (MW) and 2) Stellar-populations in galaxies.

7.1 Resolved star-formation in the MW with OmegaCAM and Gaia and by means of Nbody simulations

In a series of papers between 2018-2019 I have been studying nearby star-forming regions with a focus on the Orion star-forming region and the area around γ^2 Vel, both located $\approx$ 400 pc from the Sun.

Using Gaia DR2 data we confirmed in Jerabkova, Beccari, Boffin, et al. (2019) the presence of multiple bursts of star-formation each lasting < 1 Myr in the Orion Nebula Cluster (ONC), as first proposed by Beccari, Petr-Gotzens, Boffin, et al. (2017). Later in Kroupa, Jeřábková, Dinnbier, Beccari, and Yan (2018), we developed a theoretical model that accounts for these observations by truncating star cluster formation via stellar feedback and then allowing for re-accretion of new molecular (star-forming) gas into the cluster after the dynamical ejection of the massive ionizing stars.This we later

confirmed to be possible using high-precision N-body computations (Wang, Kroupa, and Jerabkova, 2019).

The discovery of short bursts of star-formation questions our understanding of star cluster formation. The ONC is considered to be a benchmark for cluster formation studies and was thought to have formed in a single star-formation event. This motivates the question: Do the observed bursts of star-formation in the ONC represent a characteristic way in which stars form?

Another piece of the puzzle on the nature of star-formation emerged from two discoveries. (i) In Jerabkova, Boffin, Beccari, and Anderson (2019) we report a long (90pc) thin (about 10pc) co-eval stellar structure in the Orion star-forming region. The stellar structure is compact in proper motion space and partly offset from the proper motions of the rest of the stellar population in the region. The structure is too young to be of tidal origin, and the presence of dust/gaseous filaments as sites of star formation had been established (André, Di Francesco, Ward-Thompson, Inutsuka, Pudritz, and Pineda, 2014; Mattern, Kauffmann, Csengeri, et al., 2018; Li, Urquhart, Leurini, et al., 2016). Thus I deduced that the coeval filament is likely a relic of star formation in a molecular cloud filament, naming it the *Orion relic filament.* (ii) In Beccari, Boffin, and Jerabkova (2020), we report an even longer (260pc) co-eval structure in the Gamma Velorum region.

The unexpected existence of relic filaments must be taken into account when trying to understand the nature of star-formation and how it relates to the phase-space properties of stellar populations in a galaxy. In view of these discoveries the following questions need to be addressed: How can stars from so co-eval over a > 100 *pc long structure, and what is their kinematics and life-time/dispersal rate?*

7.2 Stellar populations in galaxies and high redshift predictions for the JWST

In a series of papers (Yan, Jerabkova, and Kroupa, 2017; Jeřábková, Hasani Zonoozi, Kroupa, et al., 2018; Yan, Jerabkova, Kroupa, and Vazdekis, 2019), we have developed the publicly available code GalIMF [1] allowing the computation of stellar populations of star clusters and galaxies based on the physical parameters such as the star-formation rate and metallicity, including self-consistent chemical evolution.

In Jeřábková, Hasani Zonoozi, Kroupa, et al. (2018) we explored the effect of a varying metallicity and star-formation rate on galactic stellar populations assuming empirical relations for the formation of stars and star-clusters mainly obtained from resolved studies in the MW. The stellar initial mass function (IMF) in each (embedded) star cluster is parametrized by its metallicty and density as given by a previously empirically derived parametrisation. The galaxy-wide star-formation rate (SFR) then ensures that the embedded cluster mass function is fully sampled over the star-formation time scale. Remarkably, the Milky-Way galaxy-wide IMF for solar metallicty and a SFR$=1 M_{\odot}$/yr is approximately the canonical IMF, as found observationally. This is an important test of self-consistency and realism of the IGIMF theory. For low metallicies and high SFRs the galaxy-wide IMF becomes top-heavy, for super-solar

[1] https://github.com/Azeret/galIMF

metallicities it becomes bottom-heavy and for low SFRs top-light. The initial mass function of embedded star clusters is described by a power-law function with a power-law index -2 for the Milky Way and has a mild dependency on the star-formation rate of the galaxy. The stellar initial mass function within individual embedded star clusters is described by a three-part power-law function that depends on metallicity and initial gas density (Marks and Kroupa, 2012). For MW-like conditions it resembles the canonical/standard IMF. However it becomes top-heavy for low metallicity conditions and high-densities and bottom-heavy for super-solar metallicity. Our results are in good agreement with recent independent observations suggesting the presence of an over-abundance of massive stars (top-heavy galaxy-wide IMF) in starburst galaxies (Romano, Matteucci, Zhang, Papadopoulos, and Ivison, 2017; Zhang, Romano, Ivison, Papadopoulos, and Matteucci, 2018). Using such observations as empirical constraints on the IMF, in Jeřábková, Kroupa, Dabringhausen, Hilker, and Bekki (2017) we predict, for testing with the JWST, that the most-massive star clusters (as possibly also progenitors of ultra-compact dwarf galaxies) forming at a very high redshift should appear as quasar-like objects given their photometric quantities. If this were confirmed, some very high redshift quasars may not be accreting super-massive black holes (SMBHs) but extreme starburst clusters, which may, with time, evolve to SMBHs, possibly lessening the formation time-scale problem for SMBHs.

In addition in the work Chruślińska, Jeřábková, Nelemans, and Yan (2020) we used the results on the environment variable IMF from Jeřábková, Hasani Zonoozi, Kroupa, et al. (2018) to study the cosmic star-formation and differences and implications of the variable versus the canonical universal IMF, for the first time.

To summarize, the research presented in this thesis addresses stellar populations in star-forming regions, star clusters, galaxies and reaches up to cosmic scales as cartooned in Fig. 7.1. This thesis is making the important and necessary initial steps in bridging the studies of resolved stellar systems and of stellar populations at cosmic distances by combining observations and theory. The GalIMF code, co-developed within this thesis, introduces an innovative way forward in the study of the formation and evolution of stellar systems.

7.3 Towards a synthesis of star formation over cosmic time

The above summarized projects focus on studies of resolved star-formation and, as well, on stellar populations in galaxies. Usually these are considered as separate research fields. This thesis, however, starts building up connections between the fields. In order to better understand how galaxy-wide properties influence the star formation events in individual molecular cloud cores and thus the galaxy's emergent stellar population, this approach is likely essential. The future continuation of the very recent research on stellar relic filaments, as pioneered with this thesis work, constitutes, a completely new field of research with a potentially large impact on our understanding of star formation. It is going to flourish with the upcoming ESA's Gaia data releases, other surveys as the ESO's 4MOST and as well as with the James Webb Space telescope.

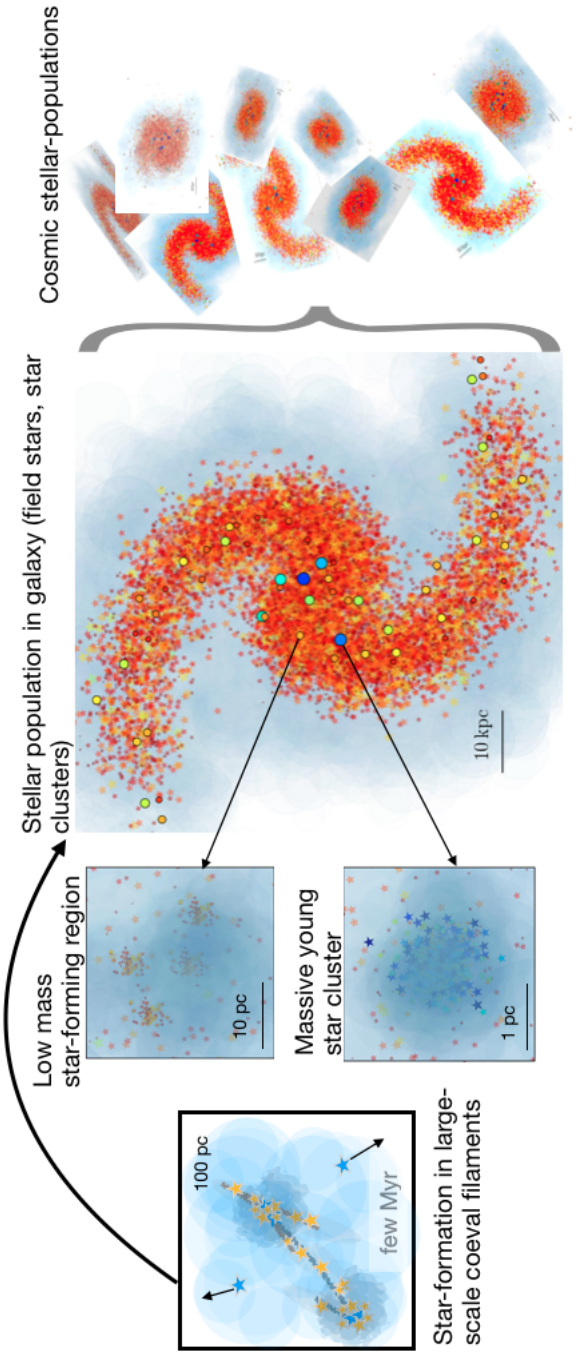

Figure 7.1: Sketch based on Jeřábková, Hasani Zonoozi, Kroupa, et al. (2018) showing the complexity of star-formation in space and time.

Bibliography

Acord, J. M., E. Churchwell, and D. O. S. Wood (Mar. 1998). "The Expansion Rate of and Distance to G5.89-0.39". In: *ApJ* 495, pp. L107–L110. DOI: 10.1086/311230.

Adams, F. C. and M. Fatuzzo (June 1996). "A Theory of the Initial Mass Function for Star Formation in Molecular Clouds". In: *ApJ* 464, p. 256. DOI: 10.1086/177318. eprint: astro-ph/9601139.

Adams, F. C. and G. Laughlin (Sept. 1996). "Implications of White Dwarf Galactic Halos". In: *ApJ* 468, p. 586. DOI: 10.1086/177717. eprint: astro-ph/9602006.

Ahn, Christopher P, Anil C Seth, Mark den Brok, et al. (Apr. 2017). "Detection of Supermassive Black Holes in Two Virgo Ultracompact Dwarf Galaxies". In: *The Astrophysical Journal* 839.2, p. 72.

Alves, J. and H. Bouy (Nov. 2012). "Orion revisited. I. The massive cluster in front of the Orion nebula cluster". In: *A&A* 547, A97, A97. DOI: 10.1051/0004-6361/201220119. arXiv: 1209.3787 [astro-ph.GA].

Anderson, J. P., S. M. Habergham, and P. A. James (Sept. 2011). "On the multiple supernova population of Arp 299: constraints on progenitor properties and host galaxy star formation characteristics". In: *MNRAS* 416, pp. 567–579. DOI: 10.1111/j.1365-2966.2011.19080.x. arXiv: 1105.2837.

André, P., J. Di Francesco, D. Ward-Thompson, S.-I. Inutsuka, R. E. Pudritz, and J. E. Pineda (2014). "From Filamentary Networks to Dense Cores in Molecular Clouds: Toward a New Paradigm for Star Formation". In: *Protostars and Planets VI*, pp. 27–51. DOI: 10.2458/azu_uapress_9780816531240-ch002. arXiv: 1312.6232.

André, P., V. Revéret, V. Könyves, et al. (July 2016). "Characterizing filaments in regions of high-mass star formation: High-resolution submilimeter imaging of the massive star-forming complex NGC 6334 with ArTéMiS". In: *A&A* 592, A54, A54. DOI: 10.1051/0004-6361/201628378. arXiv: 1605.07434.

Arenou, F., X. Luri, C. Babusiaux, et al. (Apr. 2018). "Gaia Data Release 2: Catalogue validation". In: *ArXiv e-prints*. arXiv: 1804.09375.

Ascenso, J. (2018). "Embedded Clusters". In: *The Birth of Star Clusters*. Ed. by S. Stahler. Vol. 424. Astrophysics and Space Science Library, p. 1. DOI: 10.1007/978-3-319-22801-3_1. arXiv: 1801.09940.

Asplund, M., N. Grevesse, A. J. Sauval, and P. Scott (Sept. 2009). "The Chemical Composition of the Sun". In: *ARA&A* 47, pp. 481–522. DOI: 10.1146/annurev.astro.46.060407.145222. arXiv: 0909.0948 [astro-ph.SR].

Balbinot, Eduardo and Mark Gieles (Feb. 2017). "The devil is in the tails: the role of globular cluster mass evolution on stream properties". In: *arXiv.org*, arXiv:1702.02543. arXiv: 1702.02543 [1702].

Ballesteros-Paredes, J, R S Klessen, M M Mac Low, and E Vazquez-Semadeni (2007). "Molecular Cloud Turbulence and Star Formation". In: *Protostars and Planets V*, pp. 63–80.

Bally, J. (Dec. 2008). "Overview of the Orion Complex". In: *Handbook of Star Forming Regions, Volume I*. Ed. by B. Reipurth, p. 459.

Bally, J., W. D. Langer, A. A. Stark, and R. W. Wilson (Jan. 1987). "Filamentary structure in the Orion molecular cloud". In: *ApJ* 312, pp. L45–L49. DOI: 10.1086/184817.

Balog, Zoltan, Nick Siegler, G H Rieke, et al. (Nov. 2016). "Protoplanetary and Transitional Disks in the Open Stellar Cluster IC 2395". In: *The Astrophysical Journal* 832.1, p. 87.

Banerjee, R. (Sept. 2014). "Star formation efficiency in turbulent clouds". In: *ArXiv e-prints*. arXiv: 1409.7584.

Banerjee, S. (May 2017). "Stellar-mass black holes in young massive and open stellar clusters and their role in gravitational-wave generation". In: *MNRAS* 467, pp. 524–539. DOI: 10.1093/mnras/stw3392. arXiv: 1611.09357 [astro-ph.HE].

Banerjee, S. and P. Kroupa (Jan. 2017). "How can young massive clusters reach their present-day sizes?" In: *A&A* 597, A28, A28. DOI: 10.1051/0004-6361/201526928. arXiv: 1510.04293.

— (2018). "Formation of Very Young Massive Clusters and Implications for Globular Clusters". In: *The Birth of Star Clusters*. Ed. by S. Stahler. Vol. 424. Astrophysics and Space Science Library, p. 143. DOI: 10.1007/978-3-319-22801-3_6.

Banerjee, S., P. Kroupa, and S. Oh (Oct. 2012). "The emergence of super-canonical stars in R136-type starburst clusters". In: *MNRAS* 426, pp. 1416–1426. DOI: 10.1111/j.1365-2966.2012.21672.x. arXiv: 1208.0826 [astro-ph.SR].

Banerjee, Sambaran and Pavel Kroupa (Feb. 2013). "Did the Infant R136 and NGC 3603 Clusters Undergo Residual Gas Expulsion?" In: *ApJ* 764.1, p. 29.

— (June 2014). "A Perfect Starburst Cluster made in One Go: The NGC 3603 Young Cluster". In: *ApJ* 787.2, p. 158.

— (Feb. 2015). "The formation of NGC 3603 young starburst cluster: 'prompt' hierarchical assembly or monolithic starburst?" In: *MNRAS* 447.1, pp. 728–746.

Baraffe, I, G Chabrier, and J Gallardo (Sept. 2009). "Episodic Accretion at Early Stages of Evolution of Low-Mass Stars and Brown Dwarfs: A Solution for the Observed Luminosity Spread in H-R Diagrams?" In: *The Astrophysical Journal Letters* 702.1, pp. L27–L31.

Barnard, Edward Emerson (1927). *Catalogue of 349 dark objects in the sky.*

Bastian, N., K. R. Covey, and M. R. Meyer (Sept. 2010). "A Universal Stellar Initial Mass Function? A Critical Look at Variations". In: *ARA&A* 48, pp. 339–389. DOI: 10.1146/annurev-astro-082708-101642. arXiv: 1001.2965.

Bastian, N. and J. Strader (Oct. 2014). "Constraining globular cluster formation through studies of young massive clusters - III. A lack of gas and dust in massive stellar clusters in the LMC and SMC". In: *MNRAS* 443, pp. 3594–3600. DOI: 10.1093/mnras/stu1407. arXiv: 1407.2726.

Bate, M. R. (July 2014). "The statistical properties of stars and their dependence on metallicity: the effects of opacity". In: *MNRAS* 442, pp. 285–313. DOI: 10.1093/mnras/stu795. arXiv: 1405.5583 [astro-ph.SR].

Baumgardt, H. and J. Makino (Mar. 2003). "Dynamical evolution of star clusters in tidal fields". In: *MNRAS* 340, pp. 227–246. DOI: 10.1046/j.1365-8711.2003.06286.x. eprint: astro-ph/0211471.

Baumgardt, H. and S. Sollima (Nov. 2017). "The global mass functions of 35 Galactic globular clusters - II. Clues on the initial mass function and black hole retention

fraction". In: *MNRAS* 472.1, pp. 744–750. DOI: 10.1093/mnras/stx2036. arXiv: 1708.09530 [astro-ph.GA].

Beccari, Giacomo, Henri M. J. Boffin, and Tereza Jerabkova (Jan. 2020). "Uncovering a 260 pc wide, 35-Myr-old filamentary relic of star formation". In: *MNRAS* 491.2, pp. 2205–2216. DOI: 10.1093/mnras/stz3195. arXiv: 1911.05709 [astro-ph.SR].

Beccari, Giacomo, Henri M. J. Boffin, Tereza **Jerabkova, et al.** (Nov. 2018). "A sextet of clusters in the Vela OB2 region revealed by Gaia". In: *MNRAS* 481.1, pp. L11–L15. DOI: 10.1093/mnrasl/sly144. arXiv: 1807.07073 [astro-ph.SR].

Beccari, Giacomo, Henri M. J. Boffin, and Tereza **Jerabkova** (Jan. 2020). "Uncovering a 260 pc wide, 35-Myr-old filamentary relic of star formation". In: *MNRAS* 491.2, pp. 2205–2216. DOI: 10.1093/mnras/stz3195. arXiv: 1911.05709 [astro-ph.SR].

Beccari, Giacomo, M G Petr-Gotzens, Henri M J Boffin, et al. (July 2017). "A tale of three cities. OmegaCAM discovers multiple sequences in the color-magnitude diagram of the Orion Nebula Cluster". In: *Astronomy & Astrophysics* 604, A22.

Bekki, K. (Feb. 2010). "Dynamical friction of star clusters against disc field stars in galaxies: implications on stellar nucleus formation and globular cluster luminosity functions". In: *MNRAS* 401, pp. 2753–2762. DOI: 10.1111/j.1365-2966.2009.15874.x.

— (Dec. 2013). "Simulating galaxy evolution with a non-universal stellar initial mass function". In: *MNRAS* 436, pp. 2254–2275. DOI: 10.1093/mnras/stt1735. arXiv: 1309.3878.

Bekki, K., W. J. Couch, and M. J. Drinkwater (May 2001). "Galaxy Threshing and the Formation of Ultracompact Dwarf Galaxies". In: *ApJ* 552, pp. L105–L108. DOI: 10.1086/320339. eprint: astro-ph/0106402.

Bekki, K., W. J. Couch, M. J. Drinkwater, and Y. Shioya (Sept. 2003). "Galaxy threshing and the origin of ultra-compact dwarf galaxies in the Fornax cluster". In: *MNRAS* 344, pp. 399–411. DOI: 10.1046/j.1365-8711.2003.06916.x. eprint: astro-ph/0308243.

Bekki, K., T. Jerabkova, and P. Kroupa (Oct. 2017). "The origin of discrete multiple stellar populations in globular clusters". In: *MNRAS* 471.2, pp. 2242–2253. DOI: 10.1093/mnras/stx1609. arXiv: 1706.06787 [astro-ph.GA].

Bekki, K., T. **Jerabkova**, and P. Kroupa (2017). "The origin of discrete multiple stellar populations in globular clusters". In: *MNRAS* 471.2, pp. 2242–2253. DOI: 10.1093/mnras/stx1609. arXiv: 1706.06787 [astro-ph.GA].

Bell, Cameron P M, Tim Naylor, N J Mayne, R D Jeffries, and S P Littlefair (Sept. 2013). "Pre-main-sequence isochrones - II. Revising star and planet formation timescales". In: *Monthly Notices of the Royal Astronomical Society* 434.1, pp. 806–831.

Bertelli Motta, C., P. C. Clark, S. C. O. Glover, R. S. Klessen, and A. Pasquali (Nov. 2016). "The IMF as a function of supersonic turbulence". In: *MNRAS* 462, pp. 4171–4182. DOI: 10.1093/mnras/stw1921. arXiv: 1608.01306.

Jerabkova, Tereza, Henri M. J. Boffin, Giacomo Beccari, and Richard I. Anderson (2019). "A stellar relic filament in the Orion star-forming region". In: *MNRAS* 489.3, pp. 4418–4428. DOI: 10.1093/mnras/stz2315. arXiv: 1909.04056 [astro-ph.SR].

Binney, J. and S. Tremaine (1987). *Galactic dynamics*.

Boquien, M., V. Buat, and V. Perret (Nov. 2014). "Impact of star formation history on the measurement of star formation rates". In: *A&A* 571, A72, A72. DOI: 10.1051/0004-6361/201424441. arXiv: 1409.5792.

Bouy, H. and J. Alves (Dec. 2015). "Cosmography of OB stars in the solar neighbourhood". In: *A&A* 584, A26, A26. DOI: 10.1051/0004-6361/201527058.

Bressan, A., P. Marigo, L. Girardi, et al. (Nov. 2012). "PARSEC: stellar tracks and isochrones with the PAdova and TRieste Stellar Evolution Code". In: *MNRAS* 427, pp. 127–145. DOI: 10.1111/j.1365-2966.2012.21948.x. arXiv: 1208.4498 [astro-ph.SR].

Bressert, E, N Bastian, R Gutermuth, et al. (Nov. 2010). "The spatial distribution of star formation in the solar neighbourhood: do all stars form in dense clusters?" In: *MNRAS: Letters* 409.1, pp. L54–L58.

Brinkmann, Nina, Sambaran Banerjee, Bhawna Motwani, and Pavel Kroupa (Apr. 2017). "The bound fraction of young star clusters". In: *Astronomy & Astrophysics* 600, A49.

Brodie, J. P., A. J. Romanowsky, J. Strader, and D. A. Forbes (Dec. 2011). "The Relationships among Compact Stellar Systems: A Fresh View of Ultracompact Dwarfs". In: *AJ* 142, 199, p. 199. DOI: 10.1088/0004-6256/142/6/199. arXiv: 1109.5696.

Brüns, R. C., P. Kroupa, M. Fellhauer, M. Metz, and P. Assmann (May 2011). "A parametric study on the formation of extended star clusters and ultra-compact dwarf galaxies". In: *A&A* 529, A138, A138. DOI: 10.1051/0004-6361/201016220. arXiv: 1103.4857.

Calzetti, D. (Oct. 2013). "Star Formation Rate Indicators". In: *Secular Evolution of Galaxies*. Ed. by J. Falcón-Barroso and J. H. Knapen, p. 419.

Cardelli, J. A., G. C. Clayton, and J. S. Mathis (Oct. 1989). "The relationship between infrared, optical, and ultraviolet extinction". In: *ApJ* 345, pp. 245–256. DOI: 10.1086/167900.

Cargile, P A and D J James (Sept. 2010). "Employing a New, BVIc Photometric Survey of IC 4665 to Investigate the Age of This Young Open Cluster". In: *The Astronomical Journal* 140.3, pp. 677–691.

Carretta, E. (Nov. 2014). "Three Discrete Groups with Homogeneous Chemistry along the Red Giant Branch in the Globular Cluster NGC 2808". In: *ApJ* 795.2, L28, p. L28. DOI: 10.1088/2041-8205/795/2/L28. arXiv: 1410.3476 [astro-ph.SR].

Carretta, E., A. Bragaglia, R. G. Gratton, et al. (Oct. 2009). "Na-O anticorrelation and HB. VII. The chemical composition of first and second-generation stars in 15 globular clusters from GIRAFFE spectra". In: *A&A* 505.1, pp. 117–138. DOI: 10.1051/0004-6361/200912096. arXiv: 0909.2938 [astro-ph.GA].

Castelli, F. and R. L. Kurucz (2003). "New Grids of ATLAS9 Model Atmospheres". In: *Modelling of Stellar Atmospheres*. Ed. by N. Piskunov, W. W. Weiss, and D. F. Gray. Vol. 210. IAU Symposium, 20P.

Chabrier, G. (July 2003). "Galactic Stellar and Substellar Initial Mass Function". In: *PASP* 115, pp. 763–795. DOI: 10.1086/376392. eprint: astro-ph/0304382.

Chabrier, G., P. Hennebelle, and S. Charlot (Dec. 2014). "Variations of the Stellar Initial Mass Function in the Progenitors of Massive Early-type Galaxies and in Extreme Starburst Environments". In: *ApJ* 796, 75, p. 75. DOI: 10.1088/0004-637X/796/2/75. arXiv: 1409.8466.

Chen, Yang, Alessandro Bressan, Léo Girardi, Paola Marigo, Xu Kong, and Antonio Lanza (2015). "PARSEC evolutionary tracks of massive stars up to 350 $M_\odot$ at metallicities $0.0001 \leq Z \leq 0.04$". In: *MNRAS* 452.1, pp. 1068–1080. DOI: 10.1093/mnras/stv1281. arXiv: 1506.01681 [astro-ph.SR].

Chen, Yang, Léo Girardi, Alessandro Bressan, Paola Marigo, Mauro Barbieri, and Xu Kong (2014). "Improving PARSEC models for very low mass stars". In: *MNRAS* 444.3, pp. 2525–2543. DOI: 10.1093/mnras/stu1605. arXiv: 1409.0322 [astro-ph.SR].

Chiboucas, K., R. B. Tully, R. O. Marzke, et al. (Aug. 2011). "Ultra-compact Dwarfs in the Coma Cluster". In: *ApJ* 737, 86, p. 86. DOI: 10.1088/0004-637X/737/2/86. arXiv: 1106.5828.

Chilingarian, I. V., V. Cayatte, and G. Bergond (Nov. 2008). "Stellar population constraints on the dark matter content and origin of ultra-compact dwarf galaxies". In: *MNRAS* 390, pp. 906–912. DOI: 10.1111/j.1365-2966.2008.13845.x. arXiv: 0808.0320.

Chruślińska, M., T. **Jeřábková**, G. Nelemans, and Z. Yan (Apr. 2020). "The effect of the environment-dependent IMF on the formation and metallicities of stars over the cosmic history". In: *A&A* 636, A10, A10. DOI: 10.1051/0004-6361/202037688. arXiv: 2002.11122 [astro-ph.GA].

Chruślińska, M., T. Jeřábková, G. Nelemans, and Z. Yan (Apr. 2020). "The effect of the environment-dependent IMF on the formation and metallicities of stars over the cosmic history". In: *A&A* 636, A10, A10. DOI: 10.1051/0004-6361/202037688. arXiv: 2002.11122 [astro-ph.GA].

Chruslinska, Martyna and Gijs Nelemans (Oct. 2019). "Metallicity of stars formed throughout the cosmic history based on the observational properties of star-forming galaxies". In: *MNRAS* 488.4, pp. 5300–5326. DOI: 10.1093/mnras/stz2057. arXiv: 1907.11243 [astro-ph.GA].

Cignoni, M, M Tosi, E Sabbi, et al. (Mar. 2010). "Pre-main-sequence Turn-On as a Chronometer for Young Clusters: NGC 346 as a Benchmark". In: *The Astrophysical Journal Letters* 712.1, pp. L63–L68.

Conroy, C., P. G. van Dokkum, and A. Villaume (Mar. 2017). "The Stellar Initial Mass Function in Early-type Galaxies from Absorption Line Spectroscopy. IV. A Super-Salpeter IMF in the Center of NGC 1407 from Non-parametric Models". In: *ApJ* 837, 166, p. 166. DOI: 10.3847/1538-4357/aa6190. arXiv: 1612.00013.

Côté, P., S. Piatek, L. Ferrarese, et al. (July 2006). "The ACS Virgo Cluster Survey. VIII. The Nuclei of Early-Type Galaxies". In: *ApJS* 165, pp. 57–94. DOI: 10.1086/504042. eprint: astro-ph/0603252.

Da Rio, N, M Robberto, D R Soderblom, et al. (Oct. 2010). "A Multi-color Optical Survey of the Orion Nebula Cluster. II. The H-R Diagram". In: *The Astrophysical Journal* 722.2, pp. 1092–1114.

Da Rio, N., J. C. Tan, K. R. Covey, et al. (Feb. 2016). "IN-SYNC. IV. The Young Stellar Population in the Orion A Molecular Cloud". In: *ApJ* 818, 59, p. 59. DOI: 10.3847/0004-637X/818/1/59. arXiv: 1511.04147.

da Silva, R. L., M. Fumagalli, and M. Krumholz (Feb. 2012). "SLUG – Stochastically Lighting Up Galaxies. I. Methods and Validating Tests". In: *ApJ* 745, 145, p. 145. DOI: 10.1088/0004-637X/745/2/145. arXiv: 1106.3072 [astro-ph.IM].

Dabringhausen, J., M. Fellhauer, and P. Kroupa (Apr. 2010). "Mass loss and expansion of ultra compact dwarf galaxies through gas expulsion and stellar evolution for top-heavy stellar initial mass functions". In: *MNRAS* 403, pp. 1054–1071. DOI: 10.1111/j.1365-2966.2009.16189.x. arXiv: 0912.2998.

Dabringhausen, J., M. Hilker, and P. Kroupa (May 2008). "From star clusters to dwarf galaxies: the properties of dynamically hot stellar systems". In: *MNRAS* 386, pp. 864–886. DOI: 10.1111/j.1365-2966.2008.13065.x. arXiv: 0802.0703.

Dabringhausen, J., P. Kroupa, and H. Baumgardt (2009). "A top-heavy stellar initial mass function in starbursts as an explanation for the. high mass-to-light ratios of ultra-compact dwarf galaxies". en. In: *Monthly Notices of the Royal Astronomical Society* 394.3, pp. 1529–1543. ISSN: 00358711. DOI: 10.1111/j.1365-2966.2009.14425.x. URL: http://adslabs.org/adsabs/abs/2009MNRAS.394.1529D/.

Dabringhausen, J., P. Kroupa, J. Pflamm-Altenburg, and S. Mieske (Mar. 2012). "Low-mass X-Ray Binaries Indicate a Top-heavy Stellar Initial Mass Function in Ultra-compact Dwarf Galaxies". In: *ApJ* 747, 72, p. 72. DOI: 10.1088/0004-637X/747/1/72. arXiv: 1110.2779.

De Masi, C., F. Matteucci, and F. Vincenzo (Mar. 2018). "The effects of the initial mass function on the chemical evolution of elliptical galaxies". In: *MNRAS* 474, pp. 5259–5271. DOI: 10.1093/mnras/stx3044. arXiv: 1710.04439.

de Zeeuw, P. T., R. Hoogerwerf, J. H. J. de Bruijne, A. G. A. Brown, and A. Blaauw (Jan. 1999). "A HIPPARCOS Census of the Nearby OB Associations". In: *AJ* 117, pp. 354–399. DOI: 10.1086/300682. eprint: astro-ph/9809227.

Dib, Sami, Jongsoo Kim, and Mohsen Shadmehri (Oct. 2007). "The origin of the Arches stellar cluster mass function". In: *Monthly Notices of the Royal Astronomical Society: Letters* 381.1, pp. L40–L44.

Disney, M. J. and P. B. Hopper (1975). "The alignment of interstellar dust clouds and the differential z-field of the Galaxy." In: *MNRAS* 170, pp. 177–184. DOI: 10.1093/mnras/170.1.177.

Dobbs, C L, A Burkert, and J E Pringle (June 2011). "Why are most molecular clouds not gravitationally bound?" In: *MNRAS* 413.4, pp. 2935–2942.

Drinkwater, M. J., M. D. Gregg, W. J. Couch, et al. (2004). "Ultra-Compact Dwarf Galaxies in Galaxy Clusters". In: *PASA* 21, pp. 375–378. DOI: 10.1071/AS04048.

Drinkwater, M. J., M. D. Gregg, M. Hilker, et al. (May 2003). "A class of compact dwarf galaxies from disruptive processes in galaxy clusters". In: *Nature* 423, pp. 519–521. DOI: 10.1038/nature01666. eprint: astro-ph/0306026.

Drinkwater, M. J., J. B. Jones, M. D. Gregg, and S. Phillipps (Dec. 2000). "Compact Stellar Systems in the Fornax Cluster: Super-massive Star Clusters or Extremely Compact Dwarf Galaxies?" In: *PASA* 17, pp. 227–233. DOI: 10.1071/AS00034. eprint: astro-ph/0002003.

Duarte-Cabral, A., S. Bontemps, F. Motte, M. Hennemann, N. Schneider, and P. André (Oct. 2013). "CO outflows from high-mass Class 0 protostars in Cygnus-X". In: *A&A* 558, A125, A125. DOI: 10.1051/0004-6361/201321393. arXiv: 1308.6490.

Duchêne, G., S. Lacour, E. Moraux, S. Goodwin, and J. Bouvier (May 2018). "Is stellar multiplicity universal? Tight stellar binaries in the Orion Nebula Cluster". In: *MNRAS*. DOI: 10.1093/mnras/sty1180. arXiv: 1805.00965 [astro-ph.SR].

Dunlop, J. S., R. J. McLure, M. J. Kukula, S. A. Baum, C. P. O'Dea, and D. H. Hughes (Apr. 2003). "Quasars, their host galaxies and their central black holes". In: *MNRAS* 340, pp. 1095–1135. DOI: 10.1046/j.1365-8711.2003.06333.x. eprint: astro-ph/0108397.

Dunlop, J. S., G. L. Taylor, D. H. Hughes, and E. I. Robson (Sept. 1993). "Infrared Imaging of the Host Galaxies of Radio-Loud and Radio-Quiet Quasars". In: *MNRAS* 264, p. 455. DOI: 10.1093/mnras/264.2.455.

Duquennoy, A. and M. Mayor (Aug. 1991). "Multiplicity among solar-type stars in the solar neighbourhood. II - Distribution of the orbital elements in an unbiased sample". In: *A&A* 248, pp. 485–524.

Egusa, Fumi, Kotaro Kohno, Yoshiaki Sofue, Hiroyuki Nakanishi, and Shinya Komugi (June 2009). "Determining Star Formation Timescale and Pattern Speed in Nearby Spiral Galaxies". In: *ApJ* 697.2, pp. 1870–1891.

Egusa, Fumi, Yoshiaki Sofue, and Hiroyuki Nakanishi (Dec. 2004). "Offsets between Hα and CO Arms of a Spiral Galaxy, NGC 4254: A New Method for Determining the Pattern Speed of Spiral Galaxies". In: *Publications of the Astronomical Society of Japan* 56, pp. L45–L48.

Elmegreen, B. G. (Oct. 2004). "Variability in the stellar initial mass function at low and high mass: three-component IMF models". In: *MNRAS* 354, pp. 367–374. DOI: 10.1111/j.1365-2966.2004.08187.x. eprint: astro-ph/0408231.

Elmegreen, Bruce G (Sept. 2002). "Star Formation from Galaxies to Globules". In: *ApJ* 577.1, pp. 206–220.

— (Oct. 2007). "On the Rapid Collapse and Evolution of Molecular Clouds". In: *ApJ* 668.2, pp. 1064–1082.

Elmegreen, Bruce G. and Debra Meloy Elmegreen (Nov. 2019). "Highly Embedded 8 μm cores of Star Formation in the Spiral Arms and Filaments of 15 Nearby Disk Galaxies". In: *ApJS* 245.1, 14, p. 14. DOI: 10.3847/1538-4365/ab4903. arXiv: 1910.02535 [astro-ph.GA].

Elmegreen, Bruce G., Debra Meloy Elmegreen, and Yuri N. Efremov (Aug. 2018). "Regularly Spaced Infrared Peaks in the Dusty Spirals of Messier 100". In: *ApJ* 863.1, 59, p. 59. DOI: 10.3847/1538-4357/aacf9a. arXiv: 1806.08957 [astro-ph.GA].

Elmegreen, Bruce G. and John Scalo (Sept. 2004). "Interstellar Turbulence I: Observations and Processes". In: *ARA&A* 42.1, pp. 211–273. DOI: 10.1146/annurev.astro.41.011802.094859. arXiv: astro-ph/0404451 [astro-ph].

Emsellem, Eric, Remco F. J. van der Burg, Jérémy Fensch, et al. (**incl. Jerabkova, 2019**). "The ultra-diffuse galaxy NGC 1052-DF2 with MUSE. I. Kinematics of the stellar body". In: *A&A* 625, A76, A76. DOI: 10.1051/0004-6361/201834909. arXiv: 1812.07345 [astro-ph.GA].

Ester, Martin, Hans-Peter Kriegel, Jorg Sander, and Xiaowei Xu (1996). "A density-based algorithm for discovering clusters in large spatial databases with noise". In: AAAI Press, pp. 226–231.

Evans, D. W., M. Riello, F. De Angeli, et al. (Aug. 2018). "Gaia Data Release 2. Photometric content and validation". In: *A&A* 616, A4, A4. DOI: 10.1051/0004-6361/201832756. arXiv: 1804.09368 [astro-ph.IM].

Evstigneeva, E. A., M. J. Drinkwater, C. Y. Peng, et al. (July 2008). "Structural Properties of Ultra-Compact Dwarf Galaxies in the Fornax and Virgo Clusters". In: *AJ* 136, pp. 461–478. DOI: 10.1088/0004-6256/136/1/461. arXiv: 0804.4353.

Famaey, B. and S. S. McGaugh (Sept. 2012). "Modified Newtonian Dynamics (MOND): Observational Phenomenology and Relativistic Extensions". In: *Living Reviews in Relativity* 15, 10, p. 10. DOI: 10.12942/lrr-2012-10. arXiv: 1112.3960.

Fasano, G. and A. Franceschini (Mar. 1987). "A multidimensional version of the Kolmogorov-Smirnov test". In: *MNRAS* 225, pp. 155–170. DOI: 10.1093/mnras/225.1.155.

Federrath, Christoph (July 2015). "Inefficient star formation through turbulence, magnetic fields and feedback". In: *MNRAS* 450.4, pp. 4035–4042.

— (Mar. 2016). "On the universality of interstellar filaments: theory meets simulations and observations". In: *MNRAS* 457.1, pp. 375–388.

Federrath, Christoph, Martin Schrön, Robi Banerjee, and Ralf S. Klessen (2014). "Modeling Jet and Outflow Feedback during Star Cluster Formation". In: *ApJ* 790.2, 128, p. 128. DOI: 10.1088/0004-637X/790/2/128. arXiv: 1406.3625 [astro-ph.SR].

Fellhauer, M. and P. Kroupa (July 2002a). "Merging Massive Star Clusters as Building Blocks of Dwarf Galaxies?" In: *Ap&SS* 281, pp. 355–358. DOI: 10.1023/A:1019551203852. eprint: astro-ph/0112109.

— (Mar. 2002b). "The formation of ultracompact dwarf galaxies". In: *MNRAS* 330, pp. 642–650. DOI: 10.1046/j.1365-8711.2002.05087.x. eprint: astro-ph/0110621.

Fensch, Jérémy, Remco F. J. van der Burg, Tereza **Jerabkova, et al.** (2019). "The ultra-diffuse galaxy NGC 1052-DF2 with MUSE. II. The population of DF2: stars, clusters, and planetary nebulae". In: *A&A* 625, A77, A77. DOI: 10.1051/0004-6361/201834911. arXiv: 1812.07346 [astro-ph.GA].

Ferrarese, L. and D. Merritt (June 2002). "Supermassive Black Holes". In: *Phys. World* 15N6, pp. 41–46.

Ferreras, I., F. La Barbera, I. G. de la Rosa, et al. (Feb. 2013). "Systematic variation of the stellar initial mass function with velocity dispersion in early-type galaxies". In: *MNRAS* 429, pp. L15–L19. DOI: 10.1093/mnrasl/sls014. arXiv: 1206.1594.

Ferreras, I., C. Weidner, A. Vazdekis, and F. La Barbera (Mar. 2015). "Further evidence for a time-dependent initial mass function in massive early-type galaxies". In: *MNRAS* 448, pp. L82–L86. DOI: 10.1093/mnrasl/slv003. arXiv: 1501.01636.

Figer, D. F. (Mar. 2005). "An upper limit to the masses of stars". In: *Nature* 434, pp. 192–194. DOI: 10.1038/nature03293. eprint: astro-ph/0503193.

Finn, M. K., K. E. Johnson, C. L. Brogan, et al. (Apr. 2019). "New Insights into the Physical Conditions and Internal Structure of a Candidate Proto-globular Cluster". In: *ApJ* 874, 120, p. 120. DOI: 10.3847/1538-4357/ab0d1e. arXiv: 1903.08669.

Fioc, M., D. Le Borgne, and B. Rocca-Volmerange (Aug. 2011). *PÉGASE: Metallicity-consistent Spectral Evolution Model of Galaxies*. Astrophysics Source Code Library. ascl: 1108.007.

Fioc, M. and B. Rocca-Volmerange (Oct. 1997). "PEGASE: a UV to NIR spectral evolution model of galaxies. Application to the calibration of bright galaxy counts." In: *A&A* 326, pp. 950–962. eprint: astro-ph/9707017.

— (Dec. 1999). "PEGASE.2, a metallicity-consistent spectral evolution model of galaxies: the documentation and the code". In: *ArXiv Astrophysics e-prints*. code description, only astro-ph version: astro-ph/9912179. eprint: astro-ph/9912179.

Fontanot, F., G. De Lucia, M. Hirschmann, G. Bruzual, S. Charlot, and S. Zibetti (Feb. 2017). "Variations of the stellar initial mass function in semi-analytical models: implications for the mass assembly and the chemical enrichment of galaxies in the GAEA model". In: *MNRAS* 464, pp. 3812–3824. DOI: 10.1093/mnras/stw2612. arXiv: 1606.01908.

Fontanot, F., G. De Lucia, L. Xie, M. Hirschmann, G. Bruzual, and S. Charlot (Apr. 2018). "Variations of the stellar initial mass function in semi-analytical models - II. The impact of cosmic ray regulation". In: *MNRAS* 475, pp. 2467–2479. DOI: 10.1093/mnras/stx3323. arXiv: 1801.02631.

Fontanot, F., F. La Barbera, G. De Lucia, A. Pasquali, and A. Vazdekis (Oct. 2018). "On the shape and evolution of a cosmic-ray-regulated galaxy-wide stellar initial mass function". In: *MNRAS* 479, pp. 5678–5685. DOI: 10.1093/mnras/sty1768. arXiv: 1807.01319.

Forbes, D. A., P. Lasky, A. W. Graham, and L. Spitler (Oct. 2008). "Uniting old stellar systems: from globular clusters to giant ellipticals". In: *MNRAS* 389, pp. 1924–1936. DOI: 10.1111/j.1365-2966.2008.13739.x. arXiv: 0806.1090.

Frank, M. J., M. Hilker, S. Mieske, H. Baumgardt, E. K. Grebel, and L. Infante (June 2011). "Spatially resolved kinematics of an ultracompact dwarf galaxy". In: *MNRAS* 414, pp. L70–L74. DOI: 10.1111/j.1745-3933.2011.01058.x. arXiv: 1104.2593.

Fukui, Yasuo and Akiko Kawamura (Sept. 2010). "Molecular Clouds in Nearby Galaxies". In: *ARA&A* 48, pp. 547–580.

Gaia Collaboration, A. G. A. Brown, A. Vallenari, et al. (Apr. 2018). "Gaia Data Release 2. Summary of the contents and survey properties". In: *ArXiv e-prints*. arXiv: 1804.09365.

Gaia Collaboration, T. Prusti, J. H. J. de Bruijne, et al. (Nov. 2016a). "The Gaia mission". In: *A&A* 595, A1, A1. DOI: 10.1051/0004-6361/201629272. arXiv: 1609.04153 [astro-ph.IM].

Gaia Collaboration, T. Prusti, J. H. J. de Bruijne, et al. (2016b). "The Gaia mission". In: *A&A* 595, A1, A1. DOI: 10.1051/0004-6361/201629272. arXiv: 1609.04153 [astro-ph.IM].

Gal-Yam, A. (Aug. 2012). "Luminous Supernovae". In: *Science* 337, p. 927. DOI: 10.1126/science.1203601. arXiv: 1208.3217.

Geha, M., T. M. Brown, J. Tumlinson, et al. (July 2013). "The Stellar Initial Mass Function of Ultra-faint Dwarf Galaxies: Evidence for IMF Variations with Galactic Environment". In: *ApJ* 771, 29, p. 29. DOI: 10.1088/0004-637X/771/1/29. arXiv: 1304.7769.

Gennaro, M., M. Geha, K. Tchernyshyov, et al. (Aug. 2018). "The Initial Mass Function in the Coma Berenices Dwarf Galaxy from Deep Near-infrared HST Observations". In: *ApJ* 863, 38, p. 38. DOI: 10.3847/1538-4357/aaceff. arXiv: 1806.08380.

Gennaro, M., K. Tchernyshyov, T. M. Brown, et al. (Mar. 2018). "Evidence of a Non-universal Stellar Initial Mass Function. Insights from HST Optical Imaging of Six Ultra-faint Dwarf Milky Way Satellites". In: *ApJ* 855, 20, p. 20. DOI: 10.3847/1538-4357/aaa973. arXiv: 1801.06195.

Getman, K V, E D Feigelson, M A Kuhn, M R Bate, P S Broos, and G P Garmire (May 2018). "Intracluster age gradients in numerous young stellar clusters". In: *Monthly Notices of the Royal Astronomical Society* 476.1, pp. 1213–1223.

Getman, K V, M A Kuhn, E D Feigelson, P S Broos, M R Bate, and G P Garmire (Feb. 2018). "Young Star Clusters In Nearby Molecular Clouds". In: *Monthly Notices of the Royal Astronomical Society* 477.1, pp. 298–324.

Gieles, M., N. Moeckel, and C. J. Clarke (Oct. 2012). "Do all stars in the solar neighbourhood form in clusters? A cautionary note on the use of the distribution of surface densities". In: *MNRAS* 426, pp. L11–L15. DOI: 10.1111/j.1745-3933.2012.01312.x. arXiv: 1207.2059.

Giersz, M, N Leigh, A Hypki, N Lützgendorf, and A Askar (Dec. 2015). "MOCCA Code for Star Cluster Simulations - IV. A new Scenario for Intermediate Mass Black Hole Formation in Globular Clusters". In: *MNRAS* 454, pp. 3150–3165. DOI: 10.1093/mnras/stv2162. arXiv: 1506.05234v2 [astro-ph.GA].

Ginsburg, Adam, Thomas Robitaille, Madhura Parikh, et al. (2013). *Astroquery v0.1*. DOI: 10.6084/m9.figshare.805208.v2. URL: https://figshare.com/articles/Astroquery_v0_1/805208/2.

Giovanelli, Riccardo, Martha P Haynes, Elizabeth A K Adams, et al. (July 2013). "ALFALFA Discovery of the Nearby Gas-rich Dwarf Galaxy Leo P. I. H I Observations". In: *AJ* 146.1, p. 15.

Girardi, L., G. Bertelli, A. Bressan, et al. (Aug. 2002). "Theoretical isochrones in several photometric systems. I. Johnson-Cousins-Glass, HST/WFPC2, HST/NICMOS, Washington, and ESO Imaging Survey filter sets". In: *A&A* 391, pp. 195–212. DOI: 10.1051/0004-6361:20020612. eprint: astro-ph/0205080.

Gladwin, P. P., S. Kitsionas, H. M. J. Boffin, and A. P. Whitworth (Jan. 1999). "The structure of young star clusters". In: *MNRAS* 302, pp. 305–313. DOI: 10.1046/j.1365-8711.1999.02136.x.

Glazebrook, Karl, Corentin Schreiber, Ivo Labbé, et al. (Apr. 2017). "A massive, quiescent galaxy at a redshift of 3.717". In: *Nature* 544.7, pp. 71–74.

Goerdt, T., B. Moore, S. Kazantzidis, T. Kaufmann, A. V. Macciò, and J. Stadel (Apr. 2008). "The formation of ultra-compact dwarf galaxies and nucleated dwarf galaxies". In: *MNRAS* 385, pp. 2136–2142. DOI: 10.1111/j.1365-2966.2008.12982.x. arXiv: 0711.1162.

Gong, Y., G. X. Li, R. Q. Mao, et al. (Nov. 2018). "The Serpens filament at the onset of slightly supercritical collapse". In: *A&A* 620, A62, A62. DOI: 10.1051/0004-6361/201833583. arXiv: 1809.07598 [astro-ph.GA].

Graham, A. W. and L. R. Spitler (Aug. 2009). "Quantifying the coexistence of massive black holes and dense nuclear star clusters". In: *MNRAS* 397, pp. 2148–2162. DOI: 10.1111/j.1365-2966.2009.15118.x. arXiv: 0907.5250.

Grasha, K., D. Calzetti, A. Adamo, et al. (Mar. 2019). "The spatial relation between young star clusters and molecular clouds in M51 with LEGUS". In: *MNRAS* 483, pp. 4707–4723. DOI: 10.1093/mnras/sty3424. arXiv: 1812.06109.

Greggio, L. and A. Renzini (Feb. 1983). "The binary model for type I supernovae - Theoretical rates". In: *A&A* 118, pp. 217–222.

Großschedl, J. E., J. Alves, S. Meingast, et al. (Nov. 2018). "3D shape of Orion A from Gaia DR2". In: *A&A* 619, A106, A106. DOI: 10.1051/0004-6361/201833901. arXiv: 1808.05952.

Gunawardhana, M. L. P., A. M. Hopkins, S. Sharp R. G. and. Brough, et al. (Aug. 2011). "Galaxy and Mass Assembly (GAMA): the star formation rate dependence of the stellar initial mass function". In: *MNRAS* 415, pp. 1647–1662. DOI: 10.1111/j.1365-2966.2011.18800.x. arXiv: 1104.2379.

Gustafsson, B., B. Edvardsson, K. Eriksson, U. G. Jørgensen, Å. Nordlund, and B. Plez (Aug. 2008). "A grid of MARCS model atmospheres for late-type stars. I. Methods and general properties". In: *A&A* 486, pp. 951–970. DOI: 10.1051/0004-6361:200809724. arXiv: 0805.0554.

Hacar, A., J. Alves, M. Tafalla, and J. R. Goicoechea (June 2017). "Gravitational collapse of the OMC-1 region". In: *A&A* 602, L2, p. L2. DOI: 10.1051/0004-6361/201730732. arXiv: 1703.03464.

Hacar, A., M. Tafalla, and J. Alves (Oct. 2017). "Fibers in the NGC 1333 protocluster". In: *A&A* 606, A123, A123. DOI: 10.1051/0004-6361/201630348. arXiv: 1703.07029.

Hacar, A., M. Tafalla, J. Forbrich, et al. (Mar. 2018). "An ALMA study of the Orion Integral Filament. I. Evidence for narrow fibers in a massive cloud". In: *A&A* 610. DOI: 10.1051/0004-6361/201731894.

Haghi, H., A. H. Zonoozi, P. Kroupa, S. Banerjee, and H. Baumgardt (Dec. 2015). "Possible smoking-gun evidence for initial mass segregation in re-virialized post-gas expulsion globular clusters". In: *MNRAS* 454, pp. 3872–3885. DOI: 10.1093/mnras/stv2207. arXiv: 1509.07119.

Haghi, Hosein, Pouria Khalaj, Akram Hasani Zonoozi, and Pavel Kroupa (2017). "A Possible Solution for the M/L-[Fe/H] Relation of Globular Clusters in M31. II. The Age-Metallicity Relation". In: *ApJ* 839.1, 60, p. 60. DOI: 10.3847/1538-4357/aa6719. arXiv: 1703.04635 [astro-ph.GA].

Hansen, C. E., R. I. Klein, C. F. McKee, and R. T. Fisher (Mar. 2012). "Feedback Effects on Low-mass Star Formation". In: *ApJ* 747, 22, p. 22. DOI: 10.1088/0004-637X/747/1/22. arXiv: 1201.2751 [astro-ph.SR].

Hartmann, Lee, Javier Ballesteros-Paredes, and Edwin A Bergin (Dec. 2001). "Rapid Formation of Molecular Clouds and Stars in the Solar Neighborhood". In: *ApJ* 562.2, pp. 852–868.

Hasani Zonoozi, A., H. Mahani, and P. Kroupa (Sept. 2018). "Was the Milky Way a chain galaxy? Using the IGIMF theory to constrain the thin-disk star formation history and mass". In: *ArXiv e-prints:1810.00034*. accepted by MNRAS. arXiv: 1810.00034.

Heggie, D. and P. Hut (Feb. 2003). *The Gravitational Million-Body Problem: A Multidisciplinary Approach to Star Cluster Dynamics*.

Hennemann, M., F. Motte, N. Schneider, et al. (July 2012). "The spine of the swan: a Herschel study of the DR21 ridge and filaments in Cygnus X". In: *A&A* 543, L3, p. L3. DOI: 10.1051/0004-6361/201219429. arXiv: 1206.1243.

Hilker, M. (2009). "UCDs - A Mixed Bag of Objects". In: *Globular Clusters - Guides to Galaxies*. Ed. by T. Richtler and S. Larsen, p. 51. DOI: 10.1007/978-3-540-76961-3_14.

Hilker, M., L. Infante, G. Vieira, M. Kissler-Patig, and T. Richtler (Jan. 1999). "The central region of the Fornax cluster. II. Spectroscopy and radial velocities of member and background galaxies". In: *A&AS* 134, pp. 75–86. DOI: 10.1051/aas:1999434. eprint: astro-ph/9807144.

Hill, T., F. Motte, P. Didelon, et al. (Sept. 2011). "Filaments and ridges in Vela C revealed by Herschel: from low-mass to high-mass star-forming sites". In: *A&A* 533, A94, A94. DOI: 10.1051/0004-6361/201117315. arXiv: 1108.0941.

Hillenbrand, L. A. (May 1997a). "On the Stellar Population and Star-Forming History of the Orion Nebula Cluster". In: *AJ* 113, pp. 1733–1768. DOI: 10.1086/118389.

— (May 1997b). "On the Stellar Population and Star-Forming History of the Orion Nebula Cluster". In: *AJ* 113, pp. 1733–1768. DOI: 10.1086/118389.

Hopkins, A. M. (July 2018). "The Dawes Review 8: Measuring the Stellar Initial Mass Function". In: *ArXiv e-prints*. Accepted for publication in PASA. arXiv: 1807.09949.

Hsu, W.-H., L. Hartmann, L. Allen, et al. (June 2012). "The Low-mass Stellar Population in L1641: Evidence for Environmental Dependence of the Stellar Initial Mass Function". In: *ApJ* 752, 59, p. 59. DOI: 10.1088/0004-637X/752/1/59. arXiv: 1204.3704 [astro-ph.SR].

Hsu, W.-H., L. Hartmann, L. Allen, et al. (Feb. 2013). "Evidence for Environmental Dependence of the Upper Stellar Initial Mass Function in Orion A". In: *ApJ* 764, 114, p. 114. DOI: 10.1088/0004-637X/764/2/114. arXiv: 1212.1171 [astro-ph.SR].

Janz, J., D. A. Forbes, M. A. Norris, et al. (May 2015). "How elevated is the dynamical-to-stellar mass ratio of the ultracompact dwarf S999?" In: *MNRAS* 449, pp. 1716–1730. DOI: 10.1093/mnras/stv389. arXiv: 1502.06598.

Jeffries, R D, S P Littlefair, Tim Naylor, and N J Mayne (Dec. 2011). "No wide spread of stellar ages in the Orion Nebula Cluster". In: *Monthly Notices of the Royal Astronomical Society* 418.3, pp. 1948–1958.

Jerabkova, T., A. Hasani Zonoozi, P. Kroupa, et al. (2018). "Impact of metallicity and star formation rate on the time-dependent, galaxy-wide stellar initial mass function". In: *A&A* 620, A39, A39. DOI: 10.1051/0004-6361/201833055. arXiv: 1809.04603 [astro-ph.GA].

Jerabkova, T., D. Korčáková, A. Miroshnichenko, et al. (2016). "Time-dependent spectral-feature variations of stars displaying the B[e] phenomenon. III. HD 50138". In: *A&A* 586, A116, A116. DOI: 10.1051/0004-6361/201526290. arXiv: 1512.02506 [astro-ph.SR].

Jerabkova, T., P. Kroupa, J. Dabringhausen, M. Hilker, and K. Bekki (2017). "The formation of ultra compact dwarf galaxies and massive globular clusters. Quasar-like objects to test for a variable stellar initial mass function". In: *A&A* 608, A53, A53. DOI: 10.1051/0004-6361/201731240. arXiv: 1708.07127 [astro-ph.GA].

Jerabkova, Tereza (Jan. 2020). "Multiple bursts of star formation in young star clusters: The case of the Orion Nebula Cluster". In: *IAU Symposium*. Ed. by Angela Bragaglia, Melvyn Davies, Alison Sills, and Enrico Vesperini. Vol. 351. IAU Symposium, pp. 200–203. DOI: 10.1017/S1743921319007713. arXiv: 1909.07397 [astro-ph.SR].

Jerabkova, Tereza, Giacomo Beccari, Henri M. J. Boffin, et al. (2019). "When the tale comes true: multiple populations and wide binaries in the Orion Nebula Cluster".

In: *A&A* 627, A57, A57. DOI: 10.1051/0004-6361/201935016. arXiv: 1905.06974 [astro-ph.SR].

Jerabkova, Tereza, Giacomo Beccari, Henri M. J. Boffin, et al. (2019). "When the tale comes true: multiple populations and wide binaries in the Orion Nebula Cluster". In: *A&A* 627, A57, A57. DOI: 10.1051/0004-6361/201935016. arXiv: 1905.06974 [astro-ph.SR].

Jerabkova, Tereza, Henri M. J. Boffin, Giacomo Beccari, and Richard I. Anderson (2019). "A stellar relic filament in the Orion star-forming region". In: *MNRAS* 489.3, pp. 4418–4428. DOI: 10.1093/mnras/stz2315. arXiv: 1909.04056 [astro-ph.SR].

Jeřábková, T., A. Hasani Zonoozi, P. Kroupa, et al. (2018). "Impact of metallicity and star formation rate on the time-dependent, galaxy-wide stellar initial mass function". In: *A&A* 620, A39, A39. DOI: 10.1051/0004-6361/201833055. arXiv: 1809.04603 [astro-ph.GA].

Jeřábková, T., P. Kroupa, J. Dabringhausen, M. Hilker, and K. Bekki (2017). "The formation of ultra compact dwarf galaxies and massive globular clusters. Quasar-like objects to test for a variable stellar initial mass function". In: *A&A* 608, A53, A53. DOI: 10.1051/0004-6361/201731240. arXiv: 1708.07127 [astro-ph.GA].

Johnson, L Clifton, Anil C Seth, Julianne J Dalcanton, et al. (Apr. 2017). "Panchromatic Hubble Andromeda Treasury. XVIII. The High-mass Truncation of the Star Cluster Mass Function". In: *ApJ* 839.2, p. 78.

Joncour, I., G. Duchêne, E. Moraux and, and F. Motte (Sept. 2018). "Multiplicity and clustering in Taurus star forming region. II. From ultra-wide pairs to dense NESTs". In: *ArXiv e-prints*. Accepted to A&A. arXiv: 1809.02380 [astro-ph.SR].

Joseph, R. D. and G. S. Wright (May 1985). "Recent star formation in interacting galaxies. II - Super starburst in merging galaxies". In: *MNRAS* 214, pp. 87–95. DOI: 10.1093/mnras/214.2.87.

Kalari, V. M., G. Carraro, C. J. Evans, and M. Rubio (Apr. 2018). "The Magellanic Bridge Cluster NGC 796: Deep Optical AO Imaging Reveals the Stellar Content and Initial Mass Function of a Massive Open Cluster". In: *ApJ* 857, 132, p. 132. DOI: 10.3847/1538-4357/aab609. arXiv: 1801.01490 [astro-ph.SR].

Kawamura, J. H. and C. R. Masson (Dec. 1998). "Expansion of W3(OH)". In: *ApJ* 509, pp. 270–282. DOI: 10.1086/306472. eprint: astro-ph/9808056.

Kennicutt, R. C. and N. J. Evans (Sept. 2012). "Star Formation in the Milky Way and Nearby Galaxies". In: *ARA&A* 50, pp. 531–608. DOI: 10.1146/annurev-astro-081811-125610. arXiv: 1204.3552.

Kennicutt, Robert C Jr (1998). "Star Formation in Galaxies Along the Hubble Sequence". In: *ARA&A* 36.1, pp. 189–232.

Kennicutt, Robert C. Jr. and Evan D. Skillman (2001). "H [CSC]ii[/CSC] Regions and Abundances in the "Dark Galaxy" DDO 154 and the Chemical Evolution of Dwarf Irregular Galaxies". In: *The Astronomical Journal* 121.3, pp. 1461–1472. DOI: 10.1086/319424. URL: https://doi.org/10.1086%2F319424.

Kirk, H. and P. C. Myers (Feb. 2011). "Young Stellar Groups and Their Most Massive Stars". In: *ApJ* 727, 64, p. 64. DOI: 10.1088/0004-637X/727/2/64. arXiv: 1011.1416.

Kirk, H. and P. C. Myers (Feb. 2012). "Variations in the Mass Functions of Clustered and Isolated Young Stellar Objects". In: *ApJ* 745, 131, p. 131. DOI: 10.1088/0004-637X/745/2/131. arXiv: 1110.4032.

Klassen, Mikhail, Ralph E Pudritz, and Helen Kirk (Feb. 2017). "Filamentary flow and magnetic geometry in evolving cluster-forming molecular cloud clumps". In: *Monthly Notices of the Royal Astronomical Society* 465.2, pp. 2254–2276.

Koen, C. (Jan. 2006). "On the upper limit on stellar masses in the Large Magellanic Cloud cluster R136". In: *MNRAS* 365, pp. 590–594. DOI: 10.1111/j.1365-2966.2005.09739.x.

Kounkel, M., K. Covey, G. Suárez, et al. (Sept. 2018). "The APOGEE-2 Survey of the Orion Star-forming Complex. II. Six-dimensional Structure". In: *AJ* 156, 84, p. 84. DOI: 10.3847/1538-3881/aad1f1. arXiv: 1805.04649 [astro-ph.SR].

Kraus, S., G. Weigelt, Y. Y. Balega, et al. (Apr. 2009). "Tracing the young massive high-eccentricity binary system θ^1 Orionis C through periastron passage". In: *A&A* 497, pp. 195–207. DOI: 10.1051/0004-6361/200810368. arXiv: 0902.0365 [astro-ph.SR].

Kroupa, P. (Dec. 1995a). "Star cluster evolution, dynamical age estimation and the kinematical signature of star formation". In: *MNRAS* 277. DOI: 10.1093/mnras/277.4.1522. eprint: astro-ph/9507017.

— (Oct. 1998). "The dynamical evolution of stellar superclusters". In: *MNRAS* 300, pp. 200–204. DOI: 10.1046/j.1365-8711.1998.01892.x. eprint: astro-ph/9806206.

— (Apr. 2001). "On the variation of the initial mass function". In: *MNRAS* 322, pp. 231–246. DOI: 10.1046/j.1365-8711.2001.04022.x. eprint: astro-ph/0009005.

— (Jan. 2002a). "The Initial Mass Function of Stars: Evidence for Uniformity in Variable Systems". In: *Science* 295, pp. 82–91. DOI: 10.1126/science.1067524. eprint: astro-ph/0201098.

— (Jan. 2005). "The Fundamental Building Blocks of Galaxies". In: *The Three-Dimensional Universe with Gaia*. Ed. by C. Turon, K. S. O'Flaherty, and M. A. C. Perryman. Vol. 576. ESA Special Publication, p. 629. eprint: astro-ph/0412069.

Kroupa, P. and C. M. Boily (Nov. 2002). "On the mass function of star clusters". In: *MNRAS* 336, pp. 1188–1194. DOI: 10.1046/j.1365-8711.2002.05848.x. eprint: astro-ph/0207514.

Kroupa, P. and J. Bouvier (Dec. 2003). "On the origin of brown dwarfs and free-floating planetary-mass objects". In: *MNRAS* 346, pp. 369–380. DOI: 10.1046/j.1365-2966.2003.07224.x. eprint: astro-ph/0309645.

Kroupa, P., T. Jeřábková, F. Dinnbier, G. Beccari, and Z. Yan (Apr. 2018). "Evidence for feedback and stellar-dynamically regulated bursty star cluster formation: the case of the Orion Nebula Cluster". In: *A&A* 612, A74, A74. DOI: 10.1051/0004-6361/201732151. arXiv: 1801.03095.

Kroupa, P., M. G. Petr, and M. J. McCaughrean (Dec. 1999). "Binary stars in young clusters: models versus observations of the Trapezium Cluster". In: *New A* 4, pp. 495–519. DOI: 10.1016/S1384-1076(99)00038-X. eprint: astro-ph/9906460.

Kroupa, P., C. A. Tout, and G. Gilmore (July 1991). "The effects of unresolved binary stars on the determination of the stellar mass function." In: *MNRAS* 251, pp. 293–302. DOI: 10.1093/mnras/251.2.293.

— (June 1993). "The distribution of low-mass stars in the Galactic disc". In: *MNRAS* 262, pp. 545–587. DOI: 10.1093/mnras/262.3.545.

Kroupa, P. and C. Weidner (Dec. 2003a). "Galactic-Field Initial Mass Functions of Massive Stars". In: *ApJ* 598, pp. 1076–1078. DOI: 10.1086/379105. eprint: astro-ph/0308356.

Kroupa, P., C. Weidner, J. Pflamm-Altenburg, et al. (2013). "The Stellar and Sub-Stellar Initial Mass Function of Simple and Composite Populations". In: *Planets, Stars and Stellar Systems. Volume 5: Galactic Structure and Stellar Populations*, p. 115. DOI: 10.1007/978-94-007-5612-0_4.

Kroupa, Pavel (Dec. 1995b). "Inverse dynamical population synthesis and star formation". In: *MNRAS* 277, p. 1491. DOI: 10.1093/mnras/277.4.1491. arXiv: astro-ph/9508117 [astro-ph].

— (Mar. 2002b). "Thickening of galactic discs through clustered star formation". In: *MNRAS* 330.3, pp. 707–718. DOI: 10.1046/j.1365-8711.2002.05128.x. arXiv: astro-ph/0111175 [astro-ph].

— (Apr. 2011). "The universality hypothesis: binary and stellar populations in star clusters and galaxies". In: *Computational Star Formation*. Ed. by João. Alves, Bruce G. Elmegreen, Josep M. Girart, and Virginia Trimble. Vol. 270. IAU Symposium, pp. 141–149. DOI: 10.1017/S1743921311000305. arXiv: 1012.1596 [astro-ph.GA].

Kroupa, Pavel (Feb. 2015). "Galaxies as simple dynamical systems: observational data disfavor dark matter and stochastic star formation". In: *Canadian Journal of Physics* 93, pp. 169–202.

Kroupa, Pavel, Sverre Aarseth, and Jarrod Hurley (Mar. 2001). "The formation of a bound star cluster: from the Orion nebula cluster to the Pleiades". In: *MNRAS* 321.4, pp. 699–712.

Kroupa, Pavel, Sverre Aarseth, and Jarrod Hurley (2001). "The formation of a bound star cluster: from the Orion nebula cluster to the Pleiades". In: *MNRAS* 321.4, pp. 699–712. DOI: 10.1046/j.1365-8711.2001.04050.x. arXiv: astro-ph/0009470 [astro-ph].

Kroupa, Pavel and Tereza Jerabkova (2018). "The Impact of Binaries on the Stellar Initial Mass Function". In: *Cambridge University Press, 2019*, arXiv:1806.10605. DOI: https://doi.org/10.1017/9781108553070. arXiv: 1806.10605 [astro-ph.GA].

Kroupa, Pavel and Tereza **Jerabkova** (2018). "The Impact of Binaries on the Stellar Initial Mass Function". In: *Cambridge University Press, 2019*, arXiv:1806.10605. DOI: https://doi.org/10.1017/9781108553070. arXiv: 1806.10605 [astro-ph.GA].

Kroupa, Pavel and Tereza Jerabkova (2019). "The Salpeter IMF and its descendants". In: *Nature Astronomy* 3, pp. 482–484. DOI: 10.1038/s41550-019-0793-0.

Kroupa, Pavel, Tereza Jerabkova, František Dinnbier, Giacomo Beccari, and Zhiqiang Yan (2018). "Evidence for feedback and stellar-dynamically regulated bursty star cluster formation: the case of the Orion Nebula Cluster". In: *A&A* 612, A74, A74. DOI: 10.1051/0004-6361/201732151. arXiv: 1801.03095 [astro-ph.GA].

Kroupa, Pavel, Tereza **Jerabkova**, František Dinnbier, Giacomo Beccari, and Zhiqiang Yan (2018). "Evidence for feedback and stellar-dynamically regulated bursty star cluster formation: the case of the Orion Nebula Cluster". In: *A&A* 612, A74, A74. DOI: 10.1051/0004-6361/201732151. arXiv: 1801.03095 [astro-ph.GA].

Kroupa, Pavel, Ladislav Subr, Tereza **Jerabkova**, and Long Wang (Aug. 2020). "Very high redshift quasars and the rapid emergence of super-massive black holes". In: *MNRAS*. DOI: 10.1093/mnras/staa2276. arXiv: 2007.14402 [astro-ph.GA].

Kroupa, Pavel, Christopher A. Tout, and Gerard Gilmore (May 1990). "The low-luminosity stellar mass function." In: *MNRAS* 244, pp. 76–85.

Kroupa, Pavel and Carsten Weidner (Dec. 2003b). "Galactic-Field Initial Mass Functions of Massive Stars". In: *ApJ* 598.2, pp. 1076–1078. DOI: 10.1086/379105. arXiv: astro-ph/0308356 [astro-ph].

Kuhn, M. A., L. A. Hillenbrand, A. Sills, E. D. Feigelson, and K. V. Getman (July 2018). "Kinematics in Young Star Clusters and Associations with Gaia DR2". In: *ArXiv e-prints*. arXiv version: 1807.02115, AAS Journals submitted. arXiv: 1807.02115.

Kuhn, Michael A., Lynne Hillenbrand, Alison Sills, Eric Feigelson, and Konstantin V. Getman (2019a). "Gaia's View of the Assembly and Dissolution of Young Star Clusters and Associations". In: *American Astronomical Society Meeting Abstracts #233*. Vol. 233. American Astronomical Society Meeting Abstracts, p. 342.07.

Kuhn, Michael A., Lynne A. Hillenbrand, Alison Sills, Eric D. Feigelson, and Konstantin V. Getman (2019b). "Kinematics in Young Star Clusters and Associations with Gaia DR2". In: *ApJ* 870.1, 32, p. 32. DOI: 10.3847/1538-4357/aaef8c. arXiv: 1807.02115 [astro-ph.GA].

Kuijken, K. (2011). "OmegaCAM: ESO's Newest Imager". In: *The Messenger* 146, pp. 8–11.

La Barbera, F., I. Ferreras, A. Vazdekis, et al. (Aug. 2013). "SPIDER VIII - constraints on the stellar initial mass function of early-type galaxies from a variety of spectral features". In: *MNRAS* 433, pp. 3017–3047. DOI: 10.1093/mnras/stt943. arXiv: 1305.2273.

Lada, C. J. (Jan. 2010). "The physics and modes of star cluster formation: observations". In: *Philosophical Transactions of the Royal Society of London Series A* 368, pp. 713–731. DOI: 10.1098/rsta.2009.0264. arXiv: 0911.0779.

Lada, C. J. and E. A. Lada (2003). "Embedded Clusters in Molecular Clouds". In: *ARA&A* 41, pp. 57–115. DOI: 10.1146/annurev.astro.41.011802.094844. eprint: astro-ph/0301540.

Lamers, H. J. G. L. M., M. Gieles, N. Bastian, H. Baumgardt, N. V. Kharchenko, and S. Portegies Zwart (Oct. 2005). "An analytical description of the disruption of star clusters in tidal fields with an application to Galactic open clusters". In: *A&A* 441, pp. 117–129. DOI: 10.1051/0004-6361:20042241. eprint: astro-ph/0505558.

Larson, R. B. (Mar. 1981). "Turbulence and star formation in molecular clouds." In: *MNRAS* 194, pp. 809–826. DOI: 10.1093/mnras/194.4.809.

— (Jan. 1995). "Star formation in groups". In: *MNRAS* 272, pp. 213–220. DOI: 10.1093/mnras/272.1.213.

— (Dec. 1998). "Early star formation and the evolution of the stellar initial mass function in galaxies". In: *MNRAS* 301, pp. 569–581. DOI: 10.1046/j.1365-8711.1998.02045.x. eprint: astro-ph/9808145.

Larson, Richard B (Oct. 2003). "The physics of star formation". In: *Reports on Progress in Physics* 66.1, pp. 1651–1697.

Lee, J. C., A. Gil de Paz, C. Tremonti, et al. (Nov. 2009). "Comparison of Hα and UV Star Formation Rates in the Local Volume: Systematic Discrepancies for Dwarf Galaxies". In: *ApJ* 706, 599-613, pp. 599–613. DOI: 10.1088/0004-637X/706/1/599. arXiv: 0909.5205 [astro-ph.CO].

Lee, Janice C, John J Salzer, Chris Impey, Trinh X Thuan, and Caryl Gronwall (Dec. 2002). "H I Properties of Low-Luminosity Star-forming Galaxies in the KPNO International Spectroscopic Survey". In: *AJ* 124.6, pp. 3088–3117.

Leisawitz, D (Sept. 1989). "Physical Properties of the Molecular Clouds Found in a CO Survey of Regions Around 34 Open Clusters". In: *BAAS* 21, pp. 1189–.

Leitherer, C., D. Schaerer, J. D. Goldader, et al. (July 1999). "Starburst99: Synthesis Models for Galaxies with Active Star Formation". In: *ApJS* 123, pp. 3–40. DOI: 10.1086/313233. eprint: astro-ph/9902334.

Lelli, F., S. S. McGaugh, and J. M. Schombert (Jan. 2016). "The Small Scatter of the Baryonic Tully-Fisher Relation". In: *ApJ* 816, L14, p. L14. DOI: 10.3847/2041-8205/816/1/L14. arXiv: 1512.04543.

Lesh, J. R. (Dec. 1968). "The Kinematics of the Gould Belt: an Expanding Group?" In: *ApJS* 17, p. 371. DOI: 10.1086/190179.

Li, Guang-Xing, James S. Urquhart, Silvia Leurini, et al. (2016). "ATLASGAL: A Galaxy-wide sample of dense filamentary structures". In: *A&A* 591, A5, A5. DOI: 10.1051/0004-6361/201527468. arXiv: 1604.00544 [astro-ph.SR].

Li, Guang-Xing, Friedrich Wyrowski, Karl Menten, and Arnaud Belloche (Nov. 2013). "A 500 pc filamentary gas wisp in the disk of the Milky Way". In: *A&A* 559, A34, A34. DOI: 10.1051/0004-6361/201322411. arXiv: 1310.3267 [astro-ph.GA].

Li, Hui, Oleg Y Gnedin, Nickolay Y Gnedin, Xi Meng, Vadim A Semenov, and Andrey V Kravtsov (Jan. 2017). "Star Cluster Formation in Cosmological Simulations. I. Properties of Young Clusters". In: *The Astrophysical Journal* 834.1, p. 69.

Lieberz, P and P Kroupa (Mar. 2017). "On the origin of the Schechter-like mass function of young star clusters in disc galaxies". In: *MNRAS* 465.4, pp. 3775–3783.

Lim, B., H. Sung, M. S. Bessell, et al. (June 2018). "Kinematic evidence for feedback-driven star formation in NGC 1893". In: *MNRAS* 477, pp. 1993–2003. DOI: 10.1093/mnras/sty713. arXiv: 1803.05978 [astro-ph.SR].

Lindblad, P. O., K. Grape, A. Sandqvist, and J. Schober (Apr. 1973). "On the kinematics of a local component of the interstellar hydrogen gas possibly related to Gould's Belt." In: *A&A* 24, pp. 309–312.

Lindegren, L., J. Hernández, A. Bombrun, et al. (2018). "Gaia Data Release 2. The astrometric solution". In: *A&A* 616, A2, A2. DOI: 10.1051/0004-6361/201832727. arXiv: 1804.09366 [astro-ph.IM].

Liptai, D., D. J. Price, J. Wurster, and M. R. Bate (Feb. 2017). "Does turbulence determine the initial mass function?" In: *MNRAS* 465, pp. 105–110. DOI: 10.1093/mnras/stw2770. arXiv: 1610.07619.

Longmore, S. N. (Mar. 2015). "Heart of darkness: dust obscuration of the central stellar component in globular clusters younger than 100 Myr in multiple stellar population models". In: *MNRAS* 448, pp. L62–L66. DOI: 10.1093/mnrasl/slu203. arXiv: 1501.01216.

Lonsdale, C. J., P. J. Diamond, H. Thrall, H. E. Smith, and C. J. Lonsdale (Aug. 2006). "VLBI Images of 49 Radio Supernovae in Arp 220". In: *ApJ* 647, pp. 185–193. DOI: 10.1086/505193. eprint: astro-ph/0604570.

Lu, X., Q. Zhang, H. B. Liu, et al. (Mar. 2018). "Filamentary Fragmentation and Accretion in High-mass Star-forming Molecular Clouds". In: *ApJ* 855, 9, p. 9. DOI: 10.3847/1538-4357/aaad11. arXiv: 1801.05955.

Lucas, W. E., M. Rybak, I. A. Bonnell, and M. Gieles (Mar. 2018). "A clustered origin for isolated massive stars". In: *MNRAS* 474, pp. 3582–3592. DOI: 10.1093/mnras/stx2997. arXiv: 1711.09927.

Lyman, J D, D Bersier, P A James, et al. (Mar. 2016). "Bolometric light curves and explosion parameters of 38 stripped-envelope core-collapse supernovae". In: *Monthly Notices of the Royal Astronomical Society* 457.1, pp. 328–350.

Lynds, Beverly T. (1962). "Catalogue of Dark Nebulae." In: *ApJS* 7, p. 1. DOI: 10.1086/190072.

Machida, Masahiro N and Tomoaki Matsumoto (Mar. 2012). "Impact of protostellar outflow on star formation: effects of the initial cloud mass". In: *MNRAS* 421.1, pp. 588–607.

Maíz Apellániz, J., N. R. Walborn, N. I. Morrell, V. S. Niemela, and E. P. Nelan (May 2007). "Pismis 24-1: The Stellar Upper Mass Limit Preserved". In: *ApJ* 660, pp. 1480–1485. DOI: 10.1086/513098. eprint: astro-ph/0612012.

Manara, C. F., G. Beccari, N. Da Rio, et al. (Oct. 2013). "Accurate determination of accretion and photospheric parameters in young stellar objects: The case of two candidate old disks in the Orion Nebula Cluster". In: *A&A* 558, A114, A114. DOI: 10.1051/0004-6361/201321866. arXiv: 1307.8118 [astro-ph.SR].

Manara, C. F., T. Prusti, F. Comeron, et al. (**incl. Jerabkova,2018**). "Gaia DR2 view of the Lupus V-VI clouds: The candidate diskless young stellar objects are mainly background contaminants". In: *A&A* 615, L1, p. L1. DOI: 10.1051/0004-6361/201833383. arXiv: 1806.04943 [astro-ph.SR].

Maoz, D. (Feb. 2008). "On the fraction of intermediate-mass close binaries that explode as Type Ia supernovae". In: *MNRAS* 384, pp. 267–277. DOI: 10.1111/j.1365-2966.2007.12697.x. arXiv: 0707.4598.

Marks, M. and P. Kroupa (July 2012). "Inverse dynamical population synthesis. Constraining the initial conditions of young stellar clusters by studying their binary populations". In: *A&A* 543, A8, A8. DOI: 10.1051/0004-6361/201118231. arXiv: 1205.1508.

Marks, M., P. Kroupa, J. Dabringhausen, and M. S. Pawlowski (May 2012). "Evidence for top-heavy stellar initial mass functions with increasing density and decreasing metallicity". In: *MNRAS* 422, pp. 2246–2254. DOI: 10.1111/j.1365-2966.2012.20767.x. arXiv: 1202.4755.

— (Aug. 2014). "Erratum: Evidence for top-heavy stellar initial mass functions with increasing density and decreasing metallicity". In: *MNRAS* 442, pp. 3315–3315. DOI: 10.1093/mnras/stu1083.

Marks, M., P. Kroupa, and S. Oh (Nov. 2011). "An analytical description of the evolution of binary orbital-parameter distributions in N-body computations of star clusters". In: *MNRAS* 417, pp. 1684–1701. DOI: 10.1111/j.1365-2966.2011.19257.x. arXiv: 1106.5050.

Marks, Michael and Pavel Kroupa (Nov. 2011). "Dynamical population synthesis: constructing the stellar single and binary contents of galactic field populations". In: *MNRAS* 417.3, pp. 1702–1714. DOI: 10.1111/j.1365-2966.2011.19519.x. arXiv: 1109.2896 [astro-ph.GA].

Martín-Navarro, I. (Feb. 2016). "Revisiting the classics: is [Mg/Fe] a good proxy for galaxy formation time-scales?" In: *MNRAS* 456, pp. L104–L108. DOI: 10.1093/mnrasl/slv181. arXiv: 1511.03284.

Massey, Philip (2003). "MASSIVE STARS IN THE LOCAL GROUP: Implications for Stellar Evolution and Star Formation". In: *ARA&A* 41, pp. 15–56.

Massey, Philip, Kelsey E. Johnson, and Kathleen Degioia-Eastwood (Nov. 1995). "The Initial Mass Function and Massive Star Evolution in the OB Associations of the Northern Milky Way". In: *ApJ* 454, p. 151. DOI: 10.1086/176474.

Mattern, M., J. Kauffmann, T. Csengeri, et al. (2018). "SEDIGISM: the kinematics of ATLASGAL filaments". In: *A&A* 619, A166, A166. DOI: 10.1051/0004-6361/201833406. arXiv: 1808.07499 [astro-ph.GA].

Matteucci, F. (Aug. 1994). "Abundance ratios in ellipticals and galaxy formation". In: *A&A* 288, pp. 57–64.

Matteucci, F. and L. Greggio (Jan. 1986). "Relative roles of type I and II supernovae in the chemical enrichment of the interstellar gas". In: *A&A* 154, pp. 279–287.

McCaughrean, M. J. and J. R. Stauffer (Oct. 1994). "High resolution near-infrared imaging of the trapezium: A stellar census". In: *AJ* 108, pp. 1382–1397. DOI: 10.1086/117160.

McConnell, N. J., J. R. Lu, and A. W. Mann (Apr. 2016). "Radial Trends in IMF-sensitive Absorption Features in Two Early-type Galaxies: Evidence for Abundance-driven Gradients". In: *ApJ* 821, 39, p. 39. DOI: 10.3847/0004-637X/821/1/39. arXiv: 1506.07880.

McGaugh, S. S., J. M. Schombert, G. D. Bothun, and W. J. G. de Blok (Apr. 2000). "The Baryonic Tully-Fisher Relation". In: *ApJ* 533, pp. L99–L102. DOI: 10.1086/312628. eprint: astro-ph/0003001.

McKee, Christopher F. and Eve C. Ostriker (Sept. 2007). "Theory of Star Formation". In: *Annu. Rev. Astron. Astrophys.* 45.1. arXiv: 0707.3514, pp. 565–687. ISSN: 0066-4146, 1545-4282. DOI: 10.1146/annurev.astro.45.051806.110602. URL: http://arxiv.org/abs/0707.3514 (visited on 01/30/2020).

McQuinn, Kristen B W, Evan D Skillman, Andrew Dolphin, et al. (Oct. 2015). "Leo P: An Unquenched Very Low-mass Galaxy". In: *ApJ* 812.2, p. 158.

Megeath, S. T., R. Gutermuth, J. Muzerolle, et al. (Jan. 2016). "The Spitzer Space Telescope Survey of the Orion A and B Molecular Clouds. II. The Spatial Distribution and Demographics of Dusty Young Stellar Objects". In: *AJ* 151, 5, p. 5. DOI: 10.3847/0004-6256/151/1/5. arXiv: 1511.01202.

Meidt, Sharon E, Annie Hughes, Clare L Dobbs, et al. (June 2015). "Short GMC Lifetimes: An Observational Estimate with the PdBI Arcsecond Whirlpool Survey (PAWS)". In: *ApJ* 806.1, p. 72.

Menten, K. M., M. J. Reid, J. Forbrich, and A. Brunthaler (Nov. 2007). "The distance to the Orion Nebula". In: *A&A* 474, pp. 515–520. DOI: 10.1051/0004-6361:20078247. arXiv: 0709.0485.

Meurer, G. R., O. I. Wong, J. H. Kim, et al. (Apr. 2009). "Evidence for a Nonuniform Initial Mass Function in the Local Universe". In: *ApJ* 695, pp. 765–780. DOI: 10.1088/0004-637X/695/1/765. arXiv: 0902.0384 [astro-ph.GA].

Michalik, Daniel, Lennart Lindegren, David Hobbs, and Uwe Lammers (2014). "Joint astrometric solution of HIPPARCOS and Gaia. A recipe for the Hundred Thousand Proper Motions project". In: *A&A* 571, A85, A85. DOI: 10.1051/0004-6361/201424606. arXiv: 1407.4025 [astro-ph.IM].

Mieske, S., J. Dabringhausen, P. Kroupa, M. Hilker, and H. Baumgardt (Dec. 2008). "High M/L ratios of UCDs: A variation of the IMF?" In: *Astronomische Nachrichten* 329, p. 964. DOI: 10.1002/asna.200811073. arXiv: 0808.3213.

Mieske, S., M. J. Frank, H. Baumgardt, N. Lützgendorf, N. Neumayer, and M. Hilker (Oct. 2013). "On central black holes in ultra-compact dwarf galaxies". In: *A&A* 558, A14, A14. DOI: 10.1051/0004-6361/201322167. arXiv: 1308.1398.

Mieske, S., M. Hilker, and L. Infante (Mar. 2002). "Ultra compact objects in the Fornax cluster of galaxies: Globular clusters or dwarf galaxies?" In: *A&A* 383, pp. 823–837. DOI: 10.1051/0004-6361:20011833. eprint: astro-ph/0201011.

Mieske, S., M. Hilker, A. Jordán, L. Infante, and M. Kissler-Patig (Sept. 2007). "A search for ultra-compact dwarf galaxies in the Centaurus galaxy cluster". In: *A&A* 472, pp. 111–119. DOI: 10.1051/0004-6361:20077631. arXiv: 0706.2724.

Mieske, S., M. Hilker, and I. Misgeld (Jan. 2012). "The specific frequencies of ultra-compact dwarf galaxies". In: *A&A* 537, A3, A3. DOI: 10.1051/0004-6361/201117634. arXiv: 1112.4475.

Mieske, S. and P. Kroupa (Apr. 2008). "An Extreme IMF as an Explanation for High M/L Ratios in UCDs? The CO Index as a Tracer of Bottom-heavy IMFs". In: *ApJ* 677, 276-282, pp. 276–282. DOI: 10.1086/528739. arXiv: 0712.1821.

Milgrom, M. (July 1983). "A modification of the Newtonian dynamics as a possible alternative to the hidden mass hypothesis". In: *ApJ* 270, pp. 365–370. DOI: 10.1086/161130.

Miller, G. E. and J. M. Scalo (Nov. 1979). "The initial mass function and stellar birthrate in the solar neighborhood". In: *ApJS* 41, pp. 513–547. DOI: 10.1086/190629.

Misgeld, I., S. Mieske, M. Hilker, T. Richtler, I. Y. Georgiev, and Y. Schuberth (July 2011). "A large population of ultra-compact dwarf galaxies in the Hydra I cluster". In: *A&A* 531, A4, A4. DOI: 10.1051/0004-6361/201116728. arXiv: 1103.5463.

Mor, R., A. C. Robin, F. Figueras, and T. Antoja (Sept. 2018). "BGM FASt: Besan\c{c}on Galaxy Model for Big Data. Simultaneous inference of the IMF, SFH and density in the Solar Neighbourhood". In: *ArXiv e-prints*. Accepted to A&A. arXiv: 1809.03511.

Mor, R., A. C. Robin, F. Figueras, and B. Lemasle (Mar. 2017). "Constraining the thin disc initial mass function using Galactic classical Cepheids". In: *A&A* 599, A17, A17. DOI: 10.1051/0004-6361/201629464. arXiv: 1610.08520.

Mortlock, Daniel J, Stephen J Warren, Bram P Venemans, et al. (June 2011). "A luminous quasar at a redshift of z = 7.085". In: *Nature* 474.7, pp. 616–619.

Murray, N. (Feb. 2009). "The Sizes and Luminosities of Massive Star Clusters". In: *ApJ* 691, pp. 946–962. DOI: 10.1088/0004-637X/691/2/946. arXiv: 0809.4320.

Myers, P. C. (Aug. 2009). "Filamentary Structure of Star-forming Complexes". In: *ApJ* 700, pp. 1609–1625. DOI: 10.1088/0004-637X/700/2/1609. arXiv: 0906.2005 [astro-ph.GA].

— (July 2011). "Filamentary Condensations in a Young Cluster". In: *ApJ* 735, 82, p. 82. DOI: 10.1088/0004-637X/735/2/82. arXiv: 1105.0688.

Neuhäuser, R., S. Frink, S. R. Röser, et al. (1998). "Spatial distribution and kinematics of T Tauri stars discovered with ROSAT". In: *Acta Historica Astronomiae* 3, p. 206.

Norman, C. A. (May 1987). "Star formation and dynamics in starburst nuclei". In: *NASA Conference Publication*. Ed. by C. J. Lonsdale Persson. Vol. 2466. NASA Conference Publication.

O'Dell, C. R., W. J. Henney, N. P. Abel, G. J. Ferland, and S. J. Arthur (Jan. 2009). "The Three-Dimensional Dynamic Structure of the Inner Orion Nebula". In: *AJ* 137, pp. 367–382. DOI: 10.1088/0004-6256/137/1/367. arXiv: 0810.4375.

Oey, M. S. and C. J. Clarke (Feb. 2005). "Statistical Confirmation of a Stellar Upper Mass Limit". In: *ApJ* 620, pp. L43–L46. DOI: 10.1086/428396. eprint: astro-ph/0501135.

Offner, S. S. R., P. C. Clark, P. Hennebelle, et al. (2014). "The Origin and Universality of the Stellar Initial Mass Function". In: *Protostars and Planets VI*, pp. 53–75. DOI: 10.2458/azu_uapress_9780816531240-ch003. arXiv: 1312.5326 [astro-ph.SR].

Oh, K. S., D. N. C. Lin, and S. J. Aarseth (Mar. 1995). "On the tidal disruption of dwarf spheroidal galaxies around the galaxy". In: *ApJ* 442, pp. 142–158. DOI: 10.1086/175429.

Oh, S. and P. Kroupa (July 2012). "The influence of stellar dynamical ejections and collisions on the relation between the maximum stellar and star cluster mass". In: *MNRAS* 424, pp. 65–79. DOI: 10.1111/j.1365-2966.2012.21152.x. arXiv: 1204.5474.

— (May 2016a). "Dynamical ejections of massive stars from young star clusters under diverse initial conditions". In: *A&A* 590, A107, A107. DOI: 10.1051/0004-6361/201628233. arXiv: 1604.00006.

— (May 2016b). "Dynamical ejections of massive stars from young star clusters under diverse initial conditions". In: *A&A* 590, A107, A107. DOI: 10.1051/0004-6361/201628233. arXiv: 1604.00006.

Oh, S., P. Kroupa, and J. Pflamm-Altenburg (June 2015a). "Dependency of Dynamical Ejections of O Stars on the Masses of Very Young Star Clusters". In: *ApJ* 805, 92, p. 92. DOI: 10.1088/0004-637X/805/2/92. arXiv: 1503.08827.

— (June 2015b). "Dependency of Dynamical Ejections of O Stars on the Masses of Very Young Star Clusters". In: *ApJ* 805, 92, p. 92. DOI: 10.1088/0004-637X/805/2/92. arXiv: 1503.08827.

Padoan, P., T. Haugbølle, Å. Nordlund, and S. Frimann (May 2017). "Supernova Driving. IV. The Star-formation Rate of Molecular Clouds". In: *ApJ* 840, 48, p. 48. DOI: 10.3847/1538-4357/aa6afa. arXiv: 1702.07270.

Padoan, P., L. Pan, T. Haugbølle, and Å. Nordlund (May 2016). "Supernova Driving. I. The Origin of Molecular Cloud Turbulence". In: *ApJ* 822, 11, p. 11. DOI: 10.3847/0004-637X/822/1/11. arXiv: 1509.04663.

Palla, F. and S. W. Stahler (Sept. 2000). "Accelerating Star Formation in Clusters and Associations". In: *ApJ* 540, pp. 255–270. DOI: 10.1086/309312.

Papadopoulos, P. P. (Sept. 2010). "A Cosmic-ray-dominated Interstellar Medium in Ultra Luminous Infrared Galaxies: New Initial Conditions for Star Formation". In: *ApJ* 720, pp. 226–232. DOI: 10.1088/0004-637X/720/1/226. arXiv: 1009.1134.

Pavlík, Václav, Tereza **Jerabkova**, Pavel Kroupa, and Holger Baumgardt (2018). "The black hole retention fraction in star clusters". In: *A&A* 617, A69, A69. DOI: 10.1051/0004-6361/201832919. arXiv: 1806.05192 [astro-ph.GA].

Peacock, J. A. (Feb. 1983). "Two-dimensional goodness-of-fit testing in astronomy". In: *MNRAS* 202, pp. 615–627. DOI: 10.1093/mnras/202.3.615.

Pejcha, O. and T. A. Thompson (Mar. 2015). "The Landscape of the Neutrino Mechanism of Core-collapse Supernovae: Neutron Star and Black Hole Mass Functions, Explosion Energies, and Nickel Yields". In: *ApJ* 801, 90, p. 90. DOI: 10.1088/0004-637X/801/2/90. arXiv: 1409.0540 [astro-ph.HE].

Penny, S. J., D. A. Forbes, and C. J. Conselice (May 2012). "Hubble Space Telescope survey of the Perseus cluster - IV. Compact stellar systems in the Perseus cluster core and ultracompact dwarf formation in star-forming filaments". In: *MNRAS* 422, pp. 885–901. DOI: 10.1111/j.1365-2966.2012.20669.x. arXiv: 1202.2623.

Peuten, M., A. Zocchi, M. Gieles, A. Gualandris, and V. Hénault-Brunet (Nov. 2016). "A stellar-mass black hole population in the globular cluster NGC 6101?" In: *MNRAS* 462, pp. 2333–2342. DOI: 10.1093/mnras/stw1726. arXiv: 1609.01720.

Pfalzner, S (Dec. 2011). "Formation and dissolution of leaky clusters". In: *Astronomy & Astrophysics* 536, A90.

Pfeffer, J. and H. Baumgardt (Aug. 2013). "Ultra-compact dwarf galaxy formation by tidal stripping of nucleated dwarf galaxies". In: *MNRAS* 433, pp. 1997–2005. DOI: 10.1093/mnras/stt867. arXiv: 1305.3656.

Pfeffer, J., B. F. Griffen, H. Baumgardt, and M. Hilker (Nov. 2014). "Contribution of stripped nuclear clusters to globular cluster and ultracompact dwarf galaxy populations". In: *MNRAS* 444, pp. 3670–3683. DOI: 10.1093/mnras/stu1705. arXiv: 1408.4467.

Pfeffer, J., M. Hilker, H. Baumgardt, and B. F. Griffen (May 2016). "Constraining ultracompact dwarf galaxy formation with galaxy clusters in the local universe". In: *MNRAS* 458, pp. 2492–2508. DOI: 10.1093/mnras/stw498. arXiv: 1603.00032.

Pflamm-Altenburg, J., R. A. González-López lira, and P. Kroupa (Nov. 2013a). "The galactocentric radius dependent upper mass limit of young star clusters:. stochastic star formation ruled out". In: *MNRAS* 435, pp. 2604–2609. DOI: 10.1093/mnras/stt1474. arXiv: 1310.0012.

— (Nov. 2013b). "The galactocentric radius dependent upper mass limit of young star clusters: stochastic star formation ruled out". In: *MNRAS* 435, pp. 2604–2609. DOI: 10.1093/mnras/stt1474. arXiv: 1310.0012.

Pflamm-Altenburg, J. and P. Kroupa (Nov. 2006). "A highly abnormal massive star mass function in the Orion Nebula cluster and the dynamical decay of trapezium systems". In: *MNRAS* 373, pp. 295–304. DOI: 10.1111/j.1365-2966.2006.11028.x. eprint: astro-ph/0610230.

— (Oct. 2008a). "Clustered star formation as a natural explanation for the Hα cut-off in disk galaxies". In: *Nature* 455, pp. 641–643. DOI: 10.1038/nature07266. arXiv: 0905.0898 [astro-ph.GA].

— (Oct. 2008b). "Clustered star formation as a natural explanation for the Hα cut-off in disk galaxies". In: *Nature* 455, pp. 641–643. DOI: 10.1038/nature07266. arXiv: 0905.0898 [astro-ph.GA].
— (July 2009a). "Recurrent gas accretion by massive star clusters, multiple stellar populations and mass thresholds for spheroidal stellar systems". In: *MNRAS* 397, pp. 488–494. DOI: 10.1111/j.1365-2966.2009.14954.x. arXiv: 0904.4476.
— (Nov. 2009b). "The Fundamental Gas Depletion and Stellar-Mass Buildup Times of Star-Forming Galaxies". In: *ApJ* 706, pp. 516–524. DOI: 10.1088/0004-637X/706/1/516. arXiv: 0910.1089.
Pflamm-Altenburg, J., C. Weidner, and P. Kroupa (May 2009). "Diverging UV and Hα fluxes of star-forming galaxies predicted by the IGIMF theory". In: *MNRAS* 395, pp. 394–400. DOI: 10.1111/j.1365-2966.2009.14522.x. arXiv: 0901.4335 [astro-ph.GA].
— (June 2011). "Applications of the IGIMF Theory to the Astrophysics of Galaxies". In: *UP2010: Have Observations Revealed a Variable Upper End of the Initial Mass Function?* Ed. by M. Treyer, T. Wyder, J. Neill, M. Seibert, and J. Lee. Vol. 440. Astronomical Society of the Pacific Conference Series, p. 269. arXiv: 1011.2200 [astro-ph.CO].
Pflamm-Altenburg, Jan, Carsten Weidner, and Pavel Kroupa (Dec. 2007). "Converting Hα Luminosities into Star Formation Rates". In: *ApJ* 671.2, pp. 1550–1558.
Planck Collaboration, R. Adam, N. Aghanim, et al. (Dec. 2016). "Planck intermediate results. XLVII. Planck constraints on reionization history". In: *A&A* 596, A108, A108. DOI: 10.1051/0004-6361/201628897. arXiv: 1605.03507.
Planck Collaboration, P. A. R. Ade, N. Aghanim, et al. (Sept. 2016). "Planck 2015 results. XIII. Cosmological parameters". In: *A&A* 594, A13, A13. DOI: 10.1051/0004-6361/201525830. arXiv: 1502.01589.
Ploeckinger, S., G. Hensler, S. Recchi, N. Mitchell, and P. Kroupa (Feb. 2014). "Chemodynamical evolution of tidal dwarf galaxies. I. Method and IMF dependence". In: *MNRAS* 437, pp. 3980–3993. DOI: 10.1093/mnras/stt2211. arXiv: 1311.2932.
Plunkett, A. L., M. Fernández-López, H. G. Arce, G. Busquet, D. Mardones, and M. M. Dunham (July 2018). "Distribution of Serpens South protostars revealed with ALMA". In: *A&A* 615, A9, A9. DOI: 10.1051/0004-6361/201732372. arXiv: 1804.02405 [astro-ph.SR].
Press, William H., Saul A. Teukolsky, William T. Vetterling, and Brian P. Flannery (2007). *Numerical Recipes 3rd Edition: The Art of Scientific Computing*. 3rd ed. section 14.8. New York, NY, USA: Cambridge University Press. ISBN: 0521880688, 9780521880688.
Price, J., S. Phillipps, A. Huxor, et al. (Aug. 2009). "The HST/ACS Coma Cluster Survey - V. Compact stellar systems in the Coma Cluster". In: *MNRAS* 397, pp. 1816–1835. DOI: 10.1111/j.1365-2966.2009.15122.x. arXiv: 0906.1123.
Prosser, C. F., J. R. Stauffer, L. Hartmann, et al. (Feb. 1994). "HST photometry of the trapezium cluster". In: *ApJ* 421, pp. 517–541. DOI: 10.1086/173668.
Qiu, K., Q. Zhang, H. Beuther, and J. Yang (Jan. 2007). "High-Resolution Imaging of Molecular Outflows in Massive Young Stars". In: *ApJ* 654, pp. 361–372. DOI: 10.1086/509069. eprint: astro-ph/0609285.

Qiu, K., Q. Zhang, S. T. Megeath, et al. (Oct. 2008). "Spitzer IRAC and MIPS Imaging of Clusters and Outflows in Nine High-Mass Star Forming Regions". In: *ApJ* 685, pp. 1005–1025. DOI: 10.1086/591044. arXiv: 0806.2488.

Qiu, K., Q. Zhang, and K. M. Menten (Feb. 2011). "Outflows, Accretion, and Clustered Protostellar Cores Around a Forming O Star". In: *ApJ* 728, 6, p. 6. DOI: 10.1088/0004-637X/728/1/6. arXiv: 1011.5990.

Raga, A. C. (Jan. 1986). "'Stromgren region' analysis of cometary H II regions". In: *ApJ* 300, pp. 745–748. DOI: 10.1086/163849.

Ramírez Alegría, S., J. Borissova, A.-N. Chené, et al. (Apr. 2016). "Massive open star clusters using the VVV survey. V. Young clusters with an OB stellar population". In: *A&A* 588, A40, A40. DOI: 10.1051/0004-6361/201526618. arXiv: 1602.04898 [astro-ph.SR].

Randich, S., E. Tognelli, R. Jackson, et al. (May 2018). "The Gaia-ESO Survey: open clusters in Gaia-DR1 . A way forward to stellar age calibration". In: *A&A* 612, A99, A99. DOI: 10.1051/0004-6361/201731738. arXiv: 1711.07699 [astro-ph.SR].

Randriamanakoto, Z., A. Escala, P. Väisänen, et al. (Oct. 2013). "Near-infrared Adaptive Optics Imaging of Infrared Luminous Galaxies: The Brightest Cluster Magnitude-Star Formation Rate Relation". In: *ApJ* 775, L38, p. L38. DOI: 10.1088/2041-8205/775/2/L38. arXiv: 1308.6293.

Raskin, G., H. van Winckel, H. Hensberge, et al. (Feb. 2011). "HERMES: a high-resolution fibre-fed spectrograph for the Mercator telescope". In: *A&A* 526, A69, A69. DOI: 10.1051/0004-6361/201015435. arXiv: 1011.0258 [astro-ph.IM].

Recchi, S., F. Calura, and P. Kroupa (June 2009). "The chemical evolution of galaxies within the IGIMF theory: the [α/Fe] ratios and downsizing". In: *A&A* 499, pp. 711–722. DOI: 10.1051/0004-6361/200811472. arXiv: 0903.2395.

Recchi, S. and P. Kroupa (Feb. 2015). "The chemical evolution of galaxies with a variable integrated galactic initial mass function". In: *MNRAS* 446, pp. 4168–4175. DOI: 10.1093/mnras/stu2338. arXiv: 1411.0318.

Reggiani, M, M Robberto, N Da Rio, M R Meyer, D R Soderblom, and L Ricci (Oct. 2011). "Quantitative evidence of an intrinsic luminosity spread in the Orion nebula cluster". In: *Astronomy & Astrophysics* 534, A83.

Reipurth, B., M. M. Guimarães, M. S. Connelley, and J. Bally (Dec. 2007). "Visual Binaries in the Orion Nebula Cluster". In: *AJ* 134, pp. 2272–2285. DOI: 10.1086/523596. arXiv: 0709.3824.

Renaud, F., F. Bournaud, and P.-A. Duc (Jan. 2015). "A parsec-resolution simulation of the Antennae galaxies: formation of star clusters during the merger". In: *MNRAS* 446, pp. 2038–2054. DOI: 10.1093/mnras/stu2208. arXiv: 1410.5754.

Renaud, Florent, Benoit Famaey, and Pavel Kroupa (Dec. 2016). "Star formation triggered by galaxy interactions in modified gravity". In: *MNRAS* 463.4, pp. 3637–3652.

Renzini, A., F. D'Antona, S. Cassisi, et al. (2015). "The Hubble Space Telescope UV Legacy Survey of Galactic Globular Clusters – V. Constraints on formation scenarios". en. In: *Monthly Notices of the Royal Astronomical Society* 454.4, pp. 4197–4207. ISSN: 0035-8711. DOI: 10.1093/mnras/stv2268. URL: http://adslabs.org/adsabs/abs/2015MNRAS.454.4197R/.

Renzini, Alvio (July 2017). "Finding forming globular clusters at high redshifts". In: *Monthly Notices of the Royal Astronomical Society: Letters* 469.1, pp. L63–L67.

Riccio, G., M. Brescia, S. Cavuoti, A. Mercurio, A. M. di Giorgio, and S. Molinari (Feb. 2017). "C ^{3}, A Command-line Catalog Cross-match Tool for Large Astrophysical Catalogs". In: *PASP* 129.2, p. 024005. DOI: 10.1088/1538-3873/129/972/024005. arXiv: 1611.04431 [astro-ph.IM].

Riello, M., F. De Angeli, D. W. Evans, et al. (2018). "Gaia Data Release 2. Processing of the photometric data". In: *A&A* 616, A3, A3. DOI: 10.1051/0004-6361/201832712. arXiv: 1804.09367 [astro-ph.IM].

Romano, D, F Matteucci, Z Y Zhang, P P Papadopoulos, and R J Ivison (Sept. 2017). "The evolution of CNO isotopes: a new window on cosmic star formation history and the stellar IMF in the age of ALMA". In: *Monthly Notices of the Royal Astronomical Society* 470.1, pp. 401–415.

Salpeter, E. E. (Jan. 1955). "The Luminosity Function and Stellar Evolution." In: *ApJ* 121, p. 161. DOI: 10.1086/145971.

Scally, A., C. Clarke, and M. J. McCaughrean (June 1999). "Wide binaries in the Orion nebula cluster". In: *MNRAS* 306, pp. 253–256. DOI: 10.1046/j.1365-8711.1999.02513.x. eprint: astro-ph/9902156.

Scalo, J. M. (May 1986). "The stellar initial mass function". In: *Fund. Cosmic Phys.* 11, pp. 1–278.

Schneider, F. R. N., H. Sana, C. J. Evans, et al. (Jan. 2018). "An excess of massive stars in the local 30 Doradus starburst". In: *Science* 359, pp. 69–71. DOI: 10.1126/science.aan0106. arXiv: 1801.03107 [astro-ph.SR].

Schneider, N., T. Csengeri, M. Hennemann, et al. (Apr. 2012). "Cluster-formation in the Rosette molecular cloud at the junctions of filaments". In: *A&A* 540, L11, p. L11. DOI: 10.1051/0004-6361/201118566. arXiv: 1203.6472.

Schneider, S. and B. G. Elmegreen (1979). "A catalog of dark globular filaments." In: *ApJS* 41, pp. 87–95. DOI: 10.1086/190609.

Scholz, F. W. and M. A. Stephens (1987). "K-Sample Anderson–Darling Tests". In: *Journal of the American Statistical Association* 82.399, pp. 918–924. DOI: 10.1080/01621459.1987.10478517. eprint: https://doi.org/10.1080/01621459.1987.10478517. URL: https://doi.org/10.1080/01621459.1987.10478517.

Schulz, C., M. Hilker, P. Kroupa, and J. Pflamm-Altenburg (Oct. 2016). "Distribution of star formation rates during the rapid assembly of NGC 1399 as deduced from its globular cluster system". In: *A&A* 594, A119, A119. DOI: 10.1051/0004-6361/201628927. arXiv: 1607.06443.

Schulz, C., J. Pflamm-Altenburg, and P. Kroupa (Oct. 2015). "Mass distributions of star clusters for different star formation histories in a galaxy cluster environment". In: *A&A* 582, A93, A93. DOI: 10.1051/0004-6361/201425296. arXiv: 1507.00860.

Sedaghati, E., H. M. J. Boffin, T. **Jerabkova, et al.** (2016). "Potassium detection in the clear atmosphere of a hot-Jupiter. FORS2 transmission spectroscopy of WASP-17b". In: *A&A* 596, A47, A47. DOI: 10.1051/0004-6361/201629090. arXiv: 1609.03906 [astro-ph.EP].

Selman, F. J. and J. Melnick (Dec. 2008). "The Scale-Free Character of the Cluster Mass Function and the Universality of the Stellar Initial Mass Function". In: *ApJ* 689, 816-824, pp. 816–824. DOI: 10.1086/590481. arXiv: 0805.2443.

Seth, A. C., R. van den Bosch, S. Mieske, et al. (Sept. 2014). "A supermassive black hole in an ultra-compact dwarf galaxy". In: *Nature* 513, pp. 398–400. DOI: 10.1038/nature13762. arXiv: 1409.4769.

Shu, Frank H., Fred C. Adams, and Susana Lizano (1987). "Star formation in molecular clouds: observation and theory." In: *ARA&A* 25, pp. 23–81. DOI: 10.1146/annurev.aa.25.090187.000323.

Silva, Robert L da, Michele Fumagalli, and Mark R Krumholz (Nov. 2014). "SLUG - Stochastically Lighting Up Galaxies - II. Quantifying the effects of stochasticity on star formation rate indicators". In: *MNRAS* 444.4, pp. 3275–3287.

Simon, M. (June 1997). "Clustering of Young Stars in Taurus, Ophiuchus, and the Orion Trapezium". In: *ApJ* 482, pp. L81–L84. DOI: 10.1086/310678.

Smith, N., K. G. Stassun, and J. Bally (Feb. 2005). "Opening the Treasure Chest: A Newborn Star Cluster Emerges from Its Dust Pillar in Carina". In: *AJ* 129, pp. 888–899. DOI: 10.1086/427249. eprint: astro-ph/0411178.

Smith, R. J. and J. R. Lucey (Sept. 2013). "A giant elliptical galaxy with a lightweight initial mass function". In: *MNRAS* 434, pp. 1964–1977. DOI: 10.1093/mnras/stt1141. arXiv: 1306.4983.

Souchay, J., A. H. Andrei, C. Barache, et al. (Nov. 2015). "The third release of the Large Quasar Astrometric Catalog (LQAC-3): a compilation of 321 957 objects". In: *A&A* 583, A75, A75. DOI: 10.1051/0004-6361/201526092.

Speagle, J. S., C. L. Steinhardt, P. L. Capak, and J. D. Silverman (Oct. 2014). "A Highly Consistent Framework for the Evolution of the Star-Forming "Main Sequence" from z ˜ 0-6". In: *ApJS* 214, 15, p. 15. DOI: 10.1088/0067-0049/214/2/15. arXiv: 1405.2041.

Stanway, E. R., J. J. Eldridge, and G. D. Becker (Feb. 2016). "Stellar population effects on the inferred photon density at reionization". In: *MNRAS* 456, pp. 485–499. DOI: 10.1093/mnras/stv2661. arXiv: 1511.03268.

Stephens, I. W., D. Gouliermis, L. W. Looney, et al. (Jan. 2017). "Stellar Clusterings around "Isolated" Massive YSOs in the LMC". In: *ApJ* 834, 94, p. 94. DOI: 10.3847/1538-4357/834/1/94. arXiv: 1609.04399.

Sternberg, Amiel, Tadziu L Hoffmann, and A W A Pauldrach (Dec. 2003). "Ionizing Photon Emission Rates from O- and Early B-Type Stars and Clusters". In: *The Astrophysical Journal* 599.2, pp. 1333–1343.

Stolte, A., B. Hußmann, M. R. Morris, et al. (July 2014). "The Orbital Motion of the Quintuplet Cluster: A Common Origin for the Arches and Quintuplet Clusters?" In: *ApJ* 789, 115, p. 115. DOI: 10.1088/0004-637X/789/2/115. arXiv: 1407.1854 [astro-ph.SR].

Tafalla, M., P. C. Myers, P. Caselli, C. M. Walmsley, and C. Comito (Apr. 2002). "Systematic Molecular Differentiation in Starless Cores". In: *ApJ* 569, pp. 815–835. DOI: 10.1086/339321. eprint: astro-ph/0112487.

Tang, Jing, Alessandro Bressan, Philip Rosenfield, et al. (2014). "New PARSEC evolutionary tracks of massive stars at low metallicity: testing canonical stellar evolution in nearby star-forming dwarf galaxies". In: *MNRAS* 445.4, pp. 4287–4305. DOI: 10.1093/mnras/stu2029. arXiv: 1410.1745 [astro-ph.SR].

Tenorio-Tagle, G. (Jan. 1979). "The gas dynamics of H II regions. I - The champagne model". In: *A&A* 71, pp. 59–65.

Terlevich, R. J. and B. J. Boyle (May 1993). "Young ellipticals at high redshift". In: *MNRAS* 262, pp. 491–498. DOI: 10.1093/mnras/262.2.491.

Thielemann, F.-K., K. Nomoto, and K. Yokoi (Apr. 1986). "Explosive nucleosynthesis in carbon deflagration models of Type I supernovae". In: *A&A* 158, pp. 17–33.

Thies, Ingo, Jan Pflamm-Altenburg, Pavel Kroupa, and Michael Marks (2015). "Characterizing the Brown Dwarf Formation Channels from the Initial Mass Function and Binary-star Dynamics". In: *The Astrophysical Journal* 800.1, p. 72. URL: http://stacks.iop.org/0004-637X/800/i=1/a=72.

Thomas, P. A., M. J. Drinkwater, and E. Evstigneeva (Sept. 2008). "Formation of ultra-compact dwarf galaxies: tests of the galaxy threshing scenario in Fornax". In: *MNRAS* 389, pp. 102–112. DOI: 10.1111/j.1365-2966.2008.13543.x. arXiv: 0801.4840.

Tobin, John J., Lee Hartmann, Gabor Furesz, Mario Mateo, and S. Tom Megeath (June 2009). "Kinematics of the Orion Nebula Cluster: Velocity Substructure and Spectroscopic Binaries". In: *ApJ* 697, pp. 1103–1118. DOI: 10.1088/0004-637X/697/2/1103. arXiv: 0903.2775.

Tognelli, E., S. Degl'Innocenti, and P. G. Prada Moroni (Dec. 2012). "^{7}Li surface abundance in pre-main sequence stars. Testing theory against clusters and binary systems". In: *A&A* 548, A41, A41. DOI: 10.1051/0004-6361/201219111. arXiv: 1210.4134 [astro-ph.SR].

Tognelli, E., P. G. Prada Moroni, and S. Degl'Innocenti (Sept. 2011). "The Pisa pre-main sequence tracks and isochrones. A database covering a wide range of Z, Y, mass, and age values". In: *A&A* 533, A109, A109. DOI: 10.1051/0004-6361/200913913. arXiv: 1107.2318 [astro-ph.SR].

— (May 2018). "Theoretical uncertainties on the radius of low- and very-low-mass stars". In: *MNRAS* 476, pp. 27–42. DOI: 10.1093/mnras/sty195. arXiv: 1802.04550 [astro-ph.SR].

Valle, G., M. Dell'Omodarme, P. G. Prada Moroni, and S. Degl'Innocenti (Apr. 2017). "Statistical errors and systematic biases in the calibration of the convective core overshooting with eclipsing binaries. A case study: TZ Fornacis". In: *A&A* 600, A41, A41. DOI: 10.1051/0004-6361/201628240. arXiv: 1612.07066 [astro-ph.SR].

van Dokkum, P. G. and C. Conroy (Dec. 2010). "A substantial population of low-mass stars in luminous elliptical galaxies". In: *Nature* 468, pp. 940–942. DOI: 10.1038/nature09578. arXiv: 1009.5992.

Vanbeveren, D. (Nov. 1982). "On the difference between the initial mass function of single stars and of primaries of binaries". In: *A&A* 115, pp. 65–68.

Vanzella, E, F Calura, M Meneghetti, et al. (June 2017). "Paving the way for the JWST: witnessing globular cluster formation at z $>$ 3". In: *Monthly Notices of the Royal Astronomical Society* 467.4, pp. 4304–4321.

Vazdekis, A., R. F. Peletier, J. E. Beckman, and E. Casuso (July 1997). "A New Chemo-evolutionary Population Synthesis Model for Early-Type Galaxies. II. Observations and Results". In: *ApJS* 111, pp. 203–232. DOI: 10.1086/313008. eprint: astro-ph/9701036.

Vázquez-Semadeni, E., A. González-Samaniego, and P. Colín (May 2017). "Hierarchical star cluster assembly in globally collapsing molecular clouds". In: *MNRAS* 467, pp. 1313–1328. DOI: 10.1093/mnras/stw3229. arXiv: 1611.00088.

von Weizsäcker, C. F. (Sept. 1951). "The Evolution of Galaxies and Stars." In: *ApJ* 114, p. 165. DOI: 10.1086/145462.

Wang, L., P. Kroupa, and T. Jerabkova (Aug. 2018). "Complete ejection of OB stars from very young star clusters and the formation of multiple populations". In: *MNRAS*. DOI: 10.1093/mnras/sty2232.

Wang, Long, Pavel Kroupa, and Tereza Jerabkova (2019). "Complete ejection of OB stars from very young star clusters and the formation of multiple populations". In: *MNRAS* 484.2, pp. 1843–1851. DOI: 10.1093/mnras/sty2232. arXiv: 1810.07697 [astro-ph.SR].

Wang, Long, Pavel Kroupa, and Tereza **Jerabkova** (2019). "Complete ejection of OB stars from very young star clusters and the formation of multiple populations". In: *MNRAS* 484.2, pp. 1843–1851. DOI: 10.1093/mnras/sty2232. arXiv: 1810.07697 [astro-ph.SR].

Wang, Long, Pavel Kroupa, Koh Takahashi, and Tereza **Jerabkova** (2020). "The possible role of stellar mergers for the formation of multiple stellar populations in globular clusters". In: *MNRAS* 491.1, pp. 440–454. DOI: 10.1093/mnras/stz3033. arXiv: 1910.14040 [astro-ph.SR].

Watts, A. B., G. R. Meurer, C. D. P. Lagos, S. M. Bruzzese, P. Kroupa, and T. Jerabkova (July 2018). "Star formation in the outskirts of DDO 154: a top-light IMF in a nearly dormant disc". In: *MNRAS* 477. in press, pp. 5554–5567. DOI: 10.1093/mnras/sty1006. arXiv: 1804.07072.

Watts, Adam B., Gerhardt R. Meurer, Claudia D. P. Lagos, Sarah M. Bruzzese, Pavel Kroupa, and Tereza **Jerabkova** (2018). "Star formation in the outskirts of DDO 154: a top-light IMF in a nearly dormant disc". In: *MNRAS* 477.4, pp. 5554–5567. DOI: 10.1093/mnras/sty1006. arXiv: 1804.07072 [astro-ph.GA].

Weidner, C., I. Ferreras, A. Vazdekis, and F. La Barbera (Nov. 2013). "The (galaxy-wide) IMF in giant elliptical galaxies: from top to bottom". In: *MNRAS* 435, pp. 2274–2280. DOI: 10.1093/mnras/stt1445. arXiv: 1306.6332.

Weidner, C. and P. Kroupa (Feb. 2004). "Evidence for a fundamental stellar upper mass limit from clustered star formation". In: *MNRAS* 348, pp. 187–191. DOI: 10.1111/j.1365-2966.2004.07340.x. eprint: astro-ph/0310860.

— (June 2005). "The Variation of Integrated Star Initial Mass Functions among Galaxies". In: *ApJ* 625, pp. 754–762. DOI: 10.1086/429867. eprint: astro-ph/0502525.

— (Feb. 2006). "The maximum stellar mass, star-cluster formation and composite stellar populations". In: *MNRAS* 365, pp. 1333–1347. DOI: 10.1111/j.1365-2966.2005.09824.x. eprint: astro-ph/0511331.

Weidner, C., P. Kroupa, and I. A. D. Bonnell (Jan. 2010). "The relation between the most-massive star and its parental star cluster mass". In: *MNRAS* 401, pp. 275–293. DOI: 10.1111/j.1365-2966.2009.15633.x. arXiv: 0909.1555 [astro-ph.SR].

Weidner, C., P. Kroupa, and S. S. Larsen (June 2004). "Implications for the formation of star clusters from extragalactic star formation rates". In: *MNRAS* 350, pp. 1503–1510. DOI: 10.1111/j.1365-2966.2004.07758.x. eprint: astro-ph/0402631.

Weidner, C., P. Kroupa, and J. Pflamm-Altenburg (Sept. 2013). "The m_{max}-M_{ecl} relation, the IMF and IGIMF: probabilistically sampled functions". In: *MNRAS* 434, pp. 84–101. DOI: 10.1093/mnras/stt1002. arXiv: 1306.1229.

Weidner, C., P. Kroupa, J. Pflamm-Altenburg, and A. Vazdekis (Dec. 2013). "The galaxy-wide initial mass function of dwarf late-type to massive early-type galaxies". In: *MNRAS* 436, pp. 3309–3320. DOI: 10.1093/mnras/stt1806. arXiv: 1309.6634.

Whitmore, B. C., Q. Zhang, C. Leitherer, S. M. Fall, F. Schweizer, and B. W. Miller (Oct. 1999). "The Luminosity Function of Young Star Clusters in "the Antennae" Galaxies (NGC 4038-4039)". In: *AJ* 118, pp. 1551–1576. DOI: 10.1086/301041. eprint: astro-ph/9907430.

Wood, D. O. S. and E. Churchwell (Apr. 1989). "The morphologies and physical properties of ultracompact H II regions". In: *ApJS* 69, pp. 831–895. DOI: 10.1086/191329.

Wright, G. S., R. D. Joseph, P. A. Robertson N. A. and. James, and W. P. S. Meikle (July 1988). "Recent star formation in interacting galaxies. III - Evidence from mid-infrared photometry". In: *MNRAS* 233, pp. 1–23. DOI: 10.1093/mnras/233.1.1.

Wright, N. J. and E. E. Mamajek (May 2018). "The kinematics of the Scorpius-Centaurus OB association from Gaia DR1". In: *MNRAS* 476, pp. 381–398. DOI: 10.1093/mnras/sty207. arXiv: 1801.08540 [astro-ph.SR].

Wu, J., N. J. Evans II, Y. L. Shirley, and C. Knez (June 2010). "The Properties of Massive, Dense Clumps: Mapping Surveys of HCN and CS". In: *ApJS* 188, pp. 313–357. DOI: 10.1088/0067-0049/188/2/313. arXiv: 1004.0398.

Wuchterl, G. and W. M. Tscharnuter (Feb. 2003). "From clouds to stars. Protostellar collapse and the evolution to the pre-main sequence I. Equations and evolution in the Hertzsprung-Russell diagram". In: *A&A* 398, pp. 1081–1090. DOI: 10.1051/0004-6361:20021707.

Yan, Z, T Jerabkova, and P Kroupa (July 2017). "The optimally-sampled galaxy-wide stellar initial mass function - Observational tests and the publicly available GalIMF code". In: *arXiv.org*, arXiv:1707.04260. arXiv: 1707.04260 [1707].

Yan, Zhiqiang, Tereza **Jerabkova**, and Pavel Kroupa (2017). "The optimally sampled galaxy-wide stellar initial mass function. Observational tests and the publicly available GalIMF code". In: *A&A* 607, A126, A126. DOI: 10.1051/0004-6361/201730987. arXiv: 1707.04260 [astro-ph.GA].

Yan, Zhiqiang, Tereza Jerabkova, and Pavel Kroupa (2019). *GalIMF: Galaxy-wide Initial Mass Function*. ascl: 1903.010.

— (Mar. 2020). "Chemical evolution of ultra-faint dwarf galaxies in the self-consistently calculated IGIMF theory". In: *arXiv e-prints*, arXiv:2003.11029, arXiv:2003.11029. arXiv: 2003.11029 [astro-ph.GA].

Yan, Zhiqiang, Tereza **Jerabkova**, and Pavel Kroupa (Mar. 2020). "Chemical evolution of ultra-faint dwarf galaxies in the self-consistently calculated IGIMF theory". In: *arXiv e-prints, A&A accepted*, arXiv:2003.11029, arXiv:2003.11029. arXiv: 2003.11029 [astro-ph.GA].

Yan, Zhiqiang, Tereza Jerabkova, Pavel Kroupa, and Alejandro Vazdekis (2019). "Chemical evolution of elliptical galaxies with a variable IMF. A publicly available code". In: *A&A* 629, A93, A93. DOI: 10.1051/0004-6361/201936029. arXiv: 1907.10614 [astro-ph.GA].

Yan, Zhiqiang, Tereza **Jerabkova**, Pavel Kroupa, and Alejandro Vazdekis (2019). "Chemical evolution of elliptical galaxies with a variable IMF. A publicly available code". In: *A&A* 629, A93, A93. DOI: 10.1051/0004-6361/201936029. arXiv: 1907.10614 [astro-ph.GA].

Yan, Zhiqiang, Tereza **Jerabkova**, and Pavel Kroupa (2019). "The star formation timescale of elliptical galaxies. Fitting [Mg/Fe] and total metallicity simultaneously". In: *A&A* 632, A110, A110. DOI: 10.1051/0004-6361/201936636. arXiv: 1911.02568 [astro-ph.GA].

Zari, E., A. G. A. Brown, and P. T. de Zeeuw (2019). "Structure, kinematics, and ages of the young stellar populations in the Orion region". In: *A&A* 628, A123, A123. DOI: 10.1051/0004-6361/201935781. arXiv: 1906.07002 [astro-ph.SR].

Zari, E., H. Hashemi, A. G. A. Brown, K. Jardine, and P. T. de Zeeuw (Dec. 2018). "3D mapping of young stars in the solar neighbourhood with Gaia DR2". In: *A&A* 620, A172, A172. DOI: 10.1051/0004-6361/201834150. arXiv: 1810.09819 [astro-ph.SR].

Zhang, Q., S. M. Fall, and B. C. Whitmore (Nov. 2001). "A Multiwavelength Study of the Young Star Clusters and Interstellar Medium in the Antennae Galaxies". In: *ApJ* 561, pp. 727–750. DOI: 10.1086/322278. eprint: astro-ph/0105174.

Zhang, Y. and E. F. Bell (Jan. 2017). "M32 Analogs? A Population of Massive Ultracompact Dwarf and Compact Elliptical Galaxies in Intermediate-redshift Clusters". In: *ApJ* 835, L2, p. L2. DOI: 10.3847/2041-8213/835/1/L2. arXiv: 1610.06174.

Zhang, Z.-Y., D. Romano, R. J. Ivison, P. P. Papadopoulos, and F. Matteucci (June 2018). "Stellar populations dominated by massive stars in dusty starburst galaxies across cosmic time". In: *Nature* 558, pp. 260–263. DOI: 10.1038/s41586-018-0196-x. arXiv: 1806.01280.

Ziegler, C., N. M. Law, C. Baranec, et al. (June 2018). "Measuring the Recoverability of Close Binaries in Gaia DR2 with the Robo-AO Kepler Survey". In: *ArXiv e-prints*. Submitted to AAS Journals. arXiv: 1806.10142 [astro-ph.EP].

Zinnecker, H. (Sept. 1984). "Star formation from hierarchical cloud fragmentation - A statistical theory of the log-normal Initial Mass Function". In: *MNRAS* 210, pp. 43–56. DOI: 10.1093/mnras/210.1.43.

— (Jan. 1991). "A Binary Star Formation Mechanism Through the Fragmentation of Prolate Dense Cores Rotating End Over End". In: *Fragmentation of Molecular Clouds and Star Formation*. Ed. by Edith Falgarone, F. Boulanger, and G. Duvert. Vol. 147. IAU Symposium, p. 526.

Zinnecker, H., M. J. McCaughrean, and B. A. Wilking (1993). "The initial stellar population". In: *Protostars and Planets III*. Ed. by E. H. Levy and J. I. Lunine, pp. 429–495.

Zinnecker, Hans and Harold W. Yorke (Sept. 2007). "Toward Understanding Massive Star Formation". In: *ARA&A* 45.1, pp. 481–563. DOI: 10.1146/annurev.astro.44.051905.092549. arXiv: 0707.1279 [astro-ph].

Zonoozi, A. H., H. Haghi, and P. Kroupa (July 2016). "A Possible Solution for the M/L-[Fe/H] Relation of Globular Clusters in M3. I. A Metallicity- and Density-dependent Top-heavy IMF". In: *ApJ* 826, 89, p. 89. DOI: 10.3847/0004-637X/826/1/89.

Appendices

Appendix A

Curriculum Vitae (CV)

---

name:	Tereza Jeřábková
nationality:	Czech Republic
date of birth:	21.05.1991
e-mail:	tjerabkova@gmail.com
web page:	https://sites.google.com/view/tereza-jerabkova/

University Education

Nov'16 – now	**PhD** Astronomy/Astrophysics, University of Bonn, Germany *title: Stellar populations and dynamics of self-gravitating systems* *superviors:* Prof. Dr. Pavel Kroupa, Prof Dr. Karl Menten
Sep'13 – Jun'16	**Mgr** Astronomy/Astrophysics, Charles University in Prague, Czech Republic *title: Supernova driven super star cluster winds* *grade: excellent, with distinction*
Sep'10 – Jun'13	**Bc** General Physics, Charles University in Prague, Czech Republic *title: Spectral analysis of the B[e] star V743 Mon* *grade: excellent*

Employment History

Sep'19-now	ERASMUS+ GTC studentship, CALP, Spain *GranTeCan support astronomer trainee*
Sep'17-Aug'19	ESO Studentship, ESO, Germany *Study of star forming regions using OmegaCAM and Gaia data*
Aug'15	DAAD student, DLR, Berlin *Reduction and analysis of photometric and spectroscopic data*
Aug-Oct'14	Undergraduate internship, ESO, Chile *Optimization of transmission spectroscopy of exoplanet*
Jul-Aug'12	Internship, Stellar Department, CZ *observations, data reduction and analysis - Perek 2m telescope*
Jul-Aug'10	Internship, Stellar Department, CZ (while still at high-school) *spectroscopic observations and data reduction - Perek 2m telescope*

Additional Research Experience

01 Nov – 17 Nov'18	Observational training at APEX, *Chile*
19 Feb – 02 Mar'18	ESO/NEON La Silla Summer School, *Chile*
01 Mar – 06 Apr'17	Visit at ICRAR, UWA, *Australia*
14 Oct – 27 Oct'16	Visit at IAC, La Laguna, Tenerife, *Spain*
01 Sep – 11 Sep'15	ESO/OPTICON Summer School *Czech Republic*

Honors, awards, grants

2019–2020	Erasmus+ GTC studentship at La Palma
2017–2019	ESO studentship in Garching
2018	ESO 2018 annual overview student highlight, ESO annual report 2018
2019	Deans prize for significant publishing activity (Charles University in Prague)
2016	Master degree with honours (Charles University in Prague)

Community work

Workshops/conferences organization

2019	LOC chair	Artificial Intelligence in Astronomy, ESO/Germany
2018	LOC	Take a closer Look, ESO/Germany
2017	LOC	The Impact of Binaries on Stellar Evolution, ESO/Germany

inside-institute organization/duties

2019-now	founder	Journal Club (GTC/ING/NOT telescopes), La Palma/ Spain
2018-2019	representative	i.e. contact person for students, ESO/Germany
2017,2019	sci. assistant	Observing Committee meeting (OPC),ESO/Germany
2017-2019	organizer	Journal Club, ESO/Germany

selection committees

2019	committee	ESO summer research program,ESO/Germany

co-supervision/mentoring

2017-now	co-supervision	PhD Student Zhiqian Yan, Charles University, CZ
2018	mentoring	PhD Student Vaclav Pavlik, Charles University, CZ

teaching experience

Aug' 2017	lecturer	Summer School on Exoplanets - IRAF/PYRAF course, CZ
2015,2016	lecturer	Introduction to Python (2h), Charles University, CZ
2011-2014	organizer	Camps of Physics and Mathematics (smf.mff.cuni.cz), CZ

outreach

2018-2019	ESO/ambassador	Charles University and Astronomical Institute, CZ
2018	tour guide	Delegation from Slovakia at ESO Supernova Centre, Germany
2018	invited talk	Star cluster formation, Senec Observatory, Slovakia
2019	workshop	IAU 100 initiative , Senec Observatory, Slovakia
2019	article	Outreach astronomy journal - *Astropis*
2019-2020	online blog	Blog about my GTC duties within the ERASMUS+ stay, online link: http://erasmus.asu.cas.cz/blog,

Observing Experience

Observing nights:
GTC/OSIRIS,EMIR,MEGARA • APEX/SEPIA,PI230,FLASH • NTT/EFOSC2 • Danish 1.54m/DFOSC • Perek 2m

Data reduction:
VLT/MUSE • Perek 2m • WHT/LIRIS • NTT/EFOSC2 • Danish 1.54m/DFOSC

Approved proposals:
39.6 hours of observing time at VLT (XSHOOTER,MUSE) and 189 hours VST (OmegaCAM)

Publications

24 refereed publications, 5 first author, 14 second/third author, h-index = 12

1. Pavel Kroupa, Ladislav Subr, Tereza **Jerabkova**, and Long Wang (Aug. 2020). "Very high redshift quasars and the rapid emergence of super-massive black holes". In: *MNRAS*. DOI: 10.1093/mnras/staa2276. arXiv: 2007.14402 [astro-ph.GA]

2. Zhiqiang Yan, Tereza **Jerabkova**, and Pavel Kroupa (Mar. 2020). "Chemical evolution of ultra-faint dwarf galaxies in the self-consistently calculated IGIMF theory". In: *arXiv e-prints, A&A accepted*, arXiv:2003.11029, arXiv:2003.11029. arXiv: 2003.11029 [astro-ph.GA]

3. M. Chruślińska, T. **Jeřábková**, G. Nelemans, and Z. Yan (Apr. 2020). "The effect of the environment-dependent IMF on the formation and metallicities of stars over the cosmic history". In: *A&A* 636, A10, A10. DOI: 10.1051/0004-6361/202037688. arXiv: 2002.11122 [astro-ph.GA]

4. Giacomo Beccari, Henri M. J. Boffin, and Tereza **Jerabkova** (Jan. 2020). "Uncovering a 260 pc wide, 35-Myr-old filamentary relic of star formation". In: *MNRAS* 491.2, pp. 2205–2216. DOI: 10.1093/mnras/stz3195. arXiv: 1911.05709 [astro-ph.SR]

5. Long Wang, Pavel Kroupa, Koh Takahashi, and Tereza **Jerabkova** (2020). "The possible role of stellar mergers for the formation of multiple stellar populations in globular clusters". In: *MNRAS* 491.1, pp. 440–454. DOI: 10.1093/mnras/stz3033. arXiv: 1910.14040 [astro-ph.SR]

6. Zhiqiang Yan, Tereza **Jerabkova**, and Pavel Kroupa (2019). "The star formation timescale of elliptical galaxies. Fitting [Mg/Fe] and total metallicity simultaneously". In: *A&A* 632, A110, A110. DOI: 10.1051/0004-6361/201936636. arXiv: 1911.02568 [astro-ph.GA]

7. Tereza **Jerabkova**, Henri M. J. Boffin, Giacomo Beccari, and Richard I. Anderson (2019). "A stellar relic filament in the Orion star-forming region". In: *MNRAS* 489.3, pp. 4418–4428. DOI: 10.1093/mnras/stz2315. arXiv: 1909.04056 [astro-ph.SR]

8. Zhiqiang Yan, Tereza **Jerabkova**, Pavel Kroupa, and Alejandro Vazdekis (2019). "Chemical evolution of elliptical galaxies with a variable IMF. A publicly available code". In: *A&A* 629, A93, A93. DOI: 10.1051/0004-6361/201936029. arXiv: 1907.10614 [astro-ph.GA]

9. Tereza **Jerabkova**, Giacomo Beccari, Henri M. J. Boffin, et al. (2019). "When the tale comes true: multiple populations and wide binaries in the Orion Nebula Cluster". In: *A&A* 627, A57, A57. DOI: 10.1051/0004-6361/201935016. arXiv: 1905.06974 [astro-ph.SR]

10. Jérémy Fensch, Remco F. J. van der Burg, Tereza **Jerabkova, et al.** (2019). "The ultra-diffuse galaxy NGC 1052-DF2 with MUSE. II. The population of

DF2: stars, clusters, and planetary nebulae". In: *A&A* 625, A77, A77. DOI: 10.1051/0004-6361/201834911. arXiv: 1812.07346 [astro-ph.GA]

11. Eric Emsellem, Remco F. J. van der Burg, Jérémy Fensch, et al. (**incl. Jerabkova, 2019**). "The ultra-diffuse galaxy NGC 1052-DF2 with MUSE. I. Kinematics of the stellar body". In: *A&A* 625, A76, A76. DOI: 10.1051/0004-6361/201834909. arXiv: 1812.07345 [astro-ph.GA]

12. Long Wang, Pavel Kroupa, and Tereza **Jerabkova** (2019). "Complete ejection of OB stars from very young star clusters and the formation of multiple populations". In: *MNRAS* 484.2, pp. 1843–1851. DOI: 10.1093/mnras/sty2232. arXiv: 1810.07697 [astro-ph.SR]

13. T. **Jerabkova**, A. Hasani Zonoozi, P. Kroupa, et al. (2018). "Impact of metallicity and star formation rate on the time-dependent, galaxy-wide stellar initial mass function". In: *A&A* 620, A39, A39. DOI: 10.1051/0004-6361/201833055. arXiv: 1809.04603 [astro-ph.GA]

14. Giacomo Beccari, Henri M. J. Boffin, Tereza **Jerabkova, et al.** (Nov. 2018). "A sextet of clusters in the Vela OB2 region revealed by Gaia". In: *MNRAS* 481.1, pp. L11–L15. DOI: 10.1093/mnrasl/sly144. arXiv: 1807.07073 [astro-ph.SR]

15. Václav Pavlík, Tereza **Jerabkova**, Pavel Kroupa, and Holger Baumgardt (2018). "The black hole retention fraction in star clusters". In: *A&A* 617, A69, A69. DOI: 10.1051/0004-6361/201832919. arXiv: 1806.05192 [astro-ph.GA]

16. Adam B. Watts, Gerhardt R. Meurer, Claudia D. P. Lagos, Sarah M. Bruzzese, Pavel Kroupa, and Tereza **Jerabkova** (2018). "Star formation in the outskirts of DDO 154: a top-light IMF in a nearly dormant disc". In: *MNRAS* 477.4, pp. 5554–5567. DOI: 10.1093/mnras/sty1006. arXiv: 1804.07072 [astro-ph.GA]

17. C. F. Manara, T. Prusti, F. Comeron, et al. (**incl. Jerabkova,2018**). "Gaia DR2 view of the Lupus V-VI clouds: The candidate diskless young stellar objects are mainly background contaminants". In: *A&A* 615, L1, p. L1. DOI: 10.1051/0004-6361/201833383. arXiv: 1806.04943 [astro-ph.SR]

18. Pavel Kroupa and Tereza **Jerabkova** (2018). "The Impact of Binaries on the Stellar Initial Mass Function". In: *Cambridge University Press, 2019*, arXiv:1806.10605. DOI: https://doi.org/10.1017/9781108553070. arXiv: 1806.10605 [astro-ph.GA]

19. Pavel Kroupa, Tereza **Jerabkova**, František Dinnbier, Giacomo Beccari, and Zhiqiang Yan (2018). "Evidence for feedback and stellar-dynamically regulated bursty star cluster formation: the case of the Orion Nebula Cluster". In: *A&A* 612, A74, A74. DOI: 10.1051/0004-6361/201732151. arXiv: 1801.03095 [astro-ph.GA]

20. T. **Jerabkova**, P. Kroupa, J. Dabringhausen, M. Hilker, and K. Bekki (2017). "The formation of ultra compact dwarf galaxies and massive globular clusters.

Quasar-like objects to test for a variable stellar initial mass function". In: *A&A* 608, A53, A53. DOI: 10.1051/0004-6361/201731240. arXiv: 1708.07127 [astro-ph.GA]

21. Zhiqiang Yan, Tereza **Jerabkova**, and Pavel Kroupa (2017). "The optimally sampled galaxy-wide stellar initial mass function. Observational tests and the publicly available GalIMF code". In: *A&A* 607, A126, A126. DOI: 10.1051/0004-6361/201730987. arXiv: 1707.04260 [astro-ph.GA]

22. K. Bekki, T. **Jerabkova**, and P. Kroupa (2017). "The origin of discrete multiple stellar populations in globular clusters". In: *MNRAS* 471.2, pp. 2242–2253. DOI: 10.1093/mnras/stx1609. arXiv: 1706.06787 [astro-ph.GA]

23. E. Sedaghati, H. M. J. Boffin, T. **Jerabkova, et al.** (2016). "Potassium detection in the clear atmosphere of a hot-Jupiter. FORS2 transmission spectroscopy of WASP-17b". In: *A&A* 596, A47, A47. DOI: 10.1051/0004-6361/201629090. arXiv: 1609.03906 [astro-ph.EP]

24. T. **Jerabkova**, D. Korčáková, A. Miroshnichenko, et al. (2016). "Time-dependent spectral-feature variations of stars displaying the B[e] phenomenon. III. HD 50138". In: *A&A* 586, A116, A116. DOI: 10.1051/0004-6361/201526290. arXiv: 1512.02506 [astro-ph.SR]